UNIVERSITY OF LIVERPOOL

Doctoral Thesis

Lithosphere extension at magma-poor rifted margins: extensional fault contribution, geometric evolution and orogenic reactivation

Thesis submitted in accordance with the requirements of the University of Liverpool for the degree of Doctor in Philosophy by

Júlia Gómez-Romeu

May 2019

a la meva mare, pare i germà

I now understand that…

"*Education is not the learning of facts, but the training of the mind to think*"

(Albert Einstein 1879 – 1955)

and that…

"*Questions are always more important than answers*"

(Nick Kusznir)

Abstract

Magma-poor rifted margins are formed by brittle fault deformation within the upper lithosphere with distributed pure-shear deformation below. In this thesis, I investigate extensional faulting at magma-poor rifted margins and how these faults reactivate during orogeny.

An important question is how does the amount of fault extension compares with that of the continental crust and lithosphere at the scale of a whole conjugate pair of rifted margins. To investigate this, I use the Iberia-Newfoundland conjugate margins example to determine; (i) continental crust extension using gravity anomaly inversion, (ii) continental lithosphere extension using subsidence analysis and (iii) extension from observed fault heave summation. Fault population analysis indicates that up to 35% of fault extension may be beneath seismic resolution and, when this is included, extension by brittle faulting is comparable with that measured for continental crust and lithosphere extension which is approximately 181 km. Uncertainties in fault heave summation arise due to ambiguities in fault geometry interpretation and polyphase faulting.

The difficulty of interpreting present-day fault geometries is clearer when the geometric evolution of these structures is considered particularly within distal magma-poor rifted margins. To investigate this problem, I use; (i) first-order seismic observations of the distal western Iberia margin and (ii) a lithosphere deformation model (RIFTER) that includes the flexural isostatic response to both extensional and compressional tectonics producing isostatically compensated as well as balanced lithosphere cross-sections. Modelling results show that to understand extensional faulting within distal rifted margins it is important to consider the flexural isostatic rotation of faults. Flexural isostatic rotation produces present-day sub-horizontal inactive faults; (i) beneath the hyperthinned continental crust extended by low offset faults and (ii) at the sea-bed within the exhumed mantle domain due to a rolling-hinge fault overlie by allochthon blocks. Modelling shows that a distal ridge between the transition of the hyperthinned and exhumed mantle domains must be formed by out-of-sequence faulting.

Understanding extensional faulting at magma-poor rifted margins is important not only to better comprehend lithosphere deformation during extensional processes but also to better understand orogen formation. To examine this, the Western Pyrenees are used as a case-study where evidence exists for a reactivated hyper-extended basin that preserves the earlier rift history. The RIFTER model is used to investigate the formation of this orogen which can only be understood by including both the extensional and compressional histories. The compressional stage is characterized by the inversion of the hyper-extended rift system reactivating extensional structures followed by crustal shortening of the proximal rift domain. Modelling results show how rift-related faults may be reactivated and incorporated into the present-day Western Pyrenees architecture.

Acknowledgments

Science can be defined as a way of thinking focused on understanding the objective reality based on evidence. This is what you learn throughout a PhD and thus you develop the capacity of questioning apparently well understood concepts which might give you, occasionally, the feeling that you do not know anything. As a consequence you might feel somehow lost, but you realize that this is part of the journey and therefore it is nothing to be afraid of. Finally, you end up understanding the beauty of science that consists of a continuing learning process which never ends. To become a scientist, it is essential to establish discussions with other scientists and indeed, this is what you learn as a PhD student.

This section is to acknowledge everyone who has been involved with this amazing and unique experience and have made me feel comfortable in an enjoyable atmosphere where I have been able to freely develop myself professionally and personally.

With no doubt, the first person who I want to thank for having given me the opportunity to undertake this journey is **Nick Kusznir**, my first PhD supervisor. Nick, I would have to write up another thesis to express all what I have learned from you and how grateful and pleased I am having had the chance to be one of your many PhD students. As you always say, it is important to communicate the message as simple and as short as possible; Nick, thank you so much for having shared with me your infinite enthusiasm and passion for science.

Secondly, I would like to thank **Gianreto Manatschal** for having believed in me from the beginning, and together with Nick, having given me the chance to investigate rifted margins using both geological and geophysical approaches. Receiving this combined training is such a privilege for which I will always be grateful for. Gianreto, many thanks for your supervision, support, discussions and outstanding fieldtrips over the Alps.

I also would like to thank **Alan Roberts** who has always given me brilliant advice and support. Alan, thanks for all the numerous discussions we have had throughout all my PhD and for your superb feedback, which has enormously helped me to get to the end.

I want to thank **Rebecca E. Bell** and **Pablo J. González** for agreeing to be my PhD examiners as well as for sharing three hours of stimulating discussion which resulted in new questions and suggestions.

I would like to acknowledge the **MM4** (Margin Modelling Phase 4) industry partners (BP, Conoco Phillips, Statoil, Petrobras, Total, Shell, BHP-Billiton, and BG) for the PhD funding and for fruitful discussions. I also would like to thank **Badley Geoscience** for allowing me to use Stretch and FlexDecomp.

I had the great opportunity to work together with **Emmanuel Masini** by modelling the Western Pyrenees. Manu, many thanks for being the best RIFTER player I could have had on my team, it was tricky but we finally won. Thank you so much for all and for making science good fun.

I would like to thank **Julie Tugend** for having been a member of the Western Pyrenees modelling experience. Julie, thank you for being a pillar of this work and for all your support, advice and good moments we have shared over these years. **Maxime Ducoux** thanks for sharing the Arzacq Basin, a crucial piece of our modelling experiment.

This journey started in some part thanks to **Geoffroy Mohn**. Geoffroy, thanks so much for having believed in me and gave me the chance to meet a bunch of great people as well as scientists. Thank you for all your support, advice and discussions, that with no doubt, have been essential for my professional development. I hope to keep learning from you.

I would like to thank **Caroline Harkin** for having shared this journey together. Caroline, you have been an amazing support throughout all my PhD and would like to thank you so much for having helped me on (literally) everything. It is such a pleasure to have experienced this with you, we have shared many memorable times that I will always remember and miss so much!!

I want to thank all the former and current MM4 researchers I have met and shared discussions, fieldtrips over the Alps, conferences and workshops with; **Geoffroy**, **Julie**, **Michael, Leanne**, **Ludovic**, **Mila** and **Caroline** thanks to you all for having spent unforgettable times together. I also would like to thank **Patricia, Rodolphe**, **Jordi, Oriol**, **Simon** and **Marie-Eva** who helped make conferences and fieldtrips a great experience with guaranteed fun.

I want to thank **Anthony Lamur** for having taught me Matlab. Anthony, many thanks for your time and collaboration on the development of the code.

Liverpool has been my host city where I got to meet many beautiful people. First of all I want to thank **Joe** and **John** for always have been there, you guys are super "*culos*". And many other people from the department; **Joe**, **Catalina**, **Mike**, **Becky**, **Anthony**, **Stephan**, **Arthur**, **James**, **Caroline, Simon, Sergio, Eugenio, Amy, Louise, Jenny**, **Josh**, **Yael**, **Paul**, **Louisa** … thank you for all the chats, beers, football games, nights out, frisbee games, BBQ… that we have shared together. All of these have definitely been essential throughout my PhD and I will always have the lovely memories. Thank you so much guys!!

També vull donar les gràcies als meus amics de Reus, Barcelona i altres terres catalanes que m'han donat suport i distracció sempre quan he baixat.

I finalment vull agraïr la meva **família** per sempre estar al meu costat i donar-me tot el suport del món. Mare, pare i Igor gràcies a tots tres per ser únics i perquè cadascú de vosaltres a la vostra més entranyable manera sempre m'ho heu donat tot i més, la qual cosa us ho agraeixo infinitament. Moltes gràcies per ser naturals i autèntics, és a dir, per ser vosaltres.

Moltes gràcies a tothom qui ha compartit aquesta experiència amb mi.

Muchas gracias a todos/as quién han compartido esta experiencia conmigo.

Thank you very much to everyone who has shared this experience with me.

Table of Contents

CHAPTER 1:

Introduction

CHAPTER 2:

Measurements of the extension required for continental breakup on the magma-poor Iberia-Newfoundland conjugate margins

CHAPTER 3:

The geometry and evolution of extensional faults within hyperthinned continental crust leading to mantle exhumation at magma-poor rifted margins

CHAPTER 4:

Role of rift structural inheritance in orogeny highlighted by the Western Pyrenees case-study

CHAPTER 5:

Discussion-Conclusions

APPENDICES :

CHAPTER 1
INTRODUCTION

1. Background

Rifted margins are formed by extensional tectonic processes by which continental lithosphere stretches and thins until its breakup is achieved. They correspond to a transition from thick continental crust (30 - 40 km) and thinner oceanic crust (~7 km). The boundary between new oceanic lithosphere and continental lithosphere at rifted margins corresponds to a divergent tectonic plate. Continental lithosphere breakup followed by sea-floor spreading leads to the formation of a conjugate pair of rifted margins and new oceanic crust between them (Figure 1). In contrast when oceanic lithosphere and continental lithosphere converge with each other, the boundary between them corresponds to a convergent tectonic plate boundary.

The outer shell of the Earth is divided into a number of thin and rigid plates that are in relative motion with respect to each other above a hot solid mantle which behaves as a fluid deforming by solid-state creep processes (Turcotte and Schubert, 2002). This dynamic process is explained by the plate tectonics theory developed from concepts first proposed by Wegener (1912) and further developed between the fifties and the seventies (e.g. Vine and Matthews, 1963; Bullard, 1965; Morgan, 1968; Le Pichon, 1968). One of the most important concepts of the plate tectonics theory is the Wilson cycle (Wilson, 1966). This hypothesis describes how continental rifting first forms two tectonic plates with new oceanic lithosphere between them, and then evolves into a convergence that leads to the collision of the two tectonic plates, the closure of the ocean previously formed and the collision of two rifted margins.

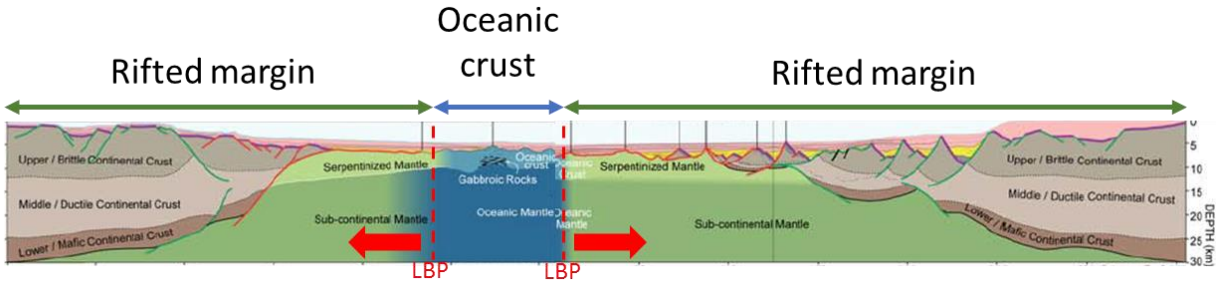

Figure 1: Present-day architecture of a conjugate pair of rifted margins and new oceanic crust formed between them (modified from Sutra et al., 2013). LBP = Lithospheric breakup point. Red arrows indicate the extension direction by which continental lithosphere has been thinned and stretched.

In this thesis I focus on the study of how continents rift apart and form rifted margins, and also how these margins collide and reactivate during continent collision leading to orogens formation. The study of rifted margins is important for understanding one of the most important tectonics and geodynamic processes on Earth as well as the formation and evolution of oceans. The investigation of rifted margins is also important for deepwater natural resource exploration (oil and gas) and to determine marine territorial boundaries.

1.1. Architecture of magma-poor rifted margins

Rifted margins are extensively distributed worldwide (Figure 2). Based on a number of morphological features they are typically classified as magma-poor and magma-rich margins (e.g. Sawyer et al., 2007; Reston, 2009; Reston and Manatschal, 2011; Franke, 2013; Doré and Lundin, 2015). This classification results from observations about the magmatic budget during the formation of rifted margins leading to continental lithospheric breakup. However, recent studies (e.g. Davis and Lavier et al., 2017; Tugend et al., 2018; Harkin et al., 2019) have shown that despite the different amount of magmatism associated with the formation of rifted margins, the lithospheric breakup mechanism by which both magma-poor and magma-rich rifted margins are formed can be compared. Another type of passive continental margins (Figure 2), formed by continental lithospheric breakup but not directly through rifting processes, are transform margins (e.g. Edwards et al., 1997). These are usually associated with low magmatism and marked by an abrupt change in crustal thickness (Reston, 2009). The focus of this thesis is to better understand the tectonic formation and evolution of rifted margins. To achieve this, I study magma-poor rifted margins to avoid the complexities of magma-rich margins due to magmatic additions modifying crustal thickness as well as obscuring tectonic structures.

It has been proposed that magma-poor rifted margins architecture consists of a set of structural rift domains (Figure 3). From continent to ocean these are (i) proximal domain, (ii) necking domain, (iii) hyperthinned domain, (iv) exhumed mantle domain and (v) oceanic domain (Mohn et al., 2012; Tugend et al., 2015). This thesis examines the processes responsible for the evolution of all of these domains.

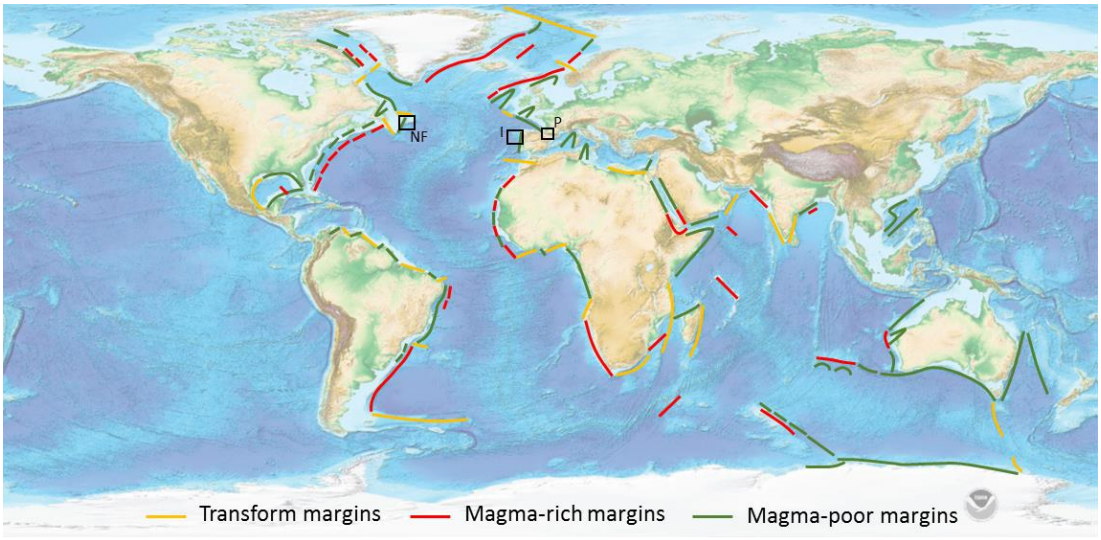

Figure 2: Bathymetric global map showing passive margins formed by continental lithospheric breakup (from Haupert et al., 2015 and using the map from the National Geophysical Data Centre). These margins are; magma-poor, magma-rich and transform. Black squares show the study-cases of this thesis (NF = Newfoundland margin, I = Iberia margin, P = Pyrenees).

Proximal domain

The proximal domain is characterized by low continental lithosphere thinning and stretching leading to the formation of intra-continental rift basins, consisting of grabens and half-grabens separated by extensional faults leading to a typical accommodation space up to 5 km. The thickness of continental crust within this domain ranges between 35 and 20 km (Marsden et al., 1990).

Necking domain

Within the necking domain, the thickness of continental crust strongly varies along the margin from 25 km to 10 km thick. In this region the crust undergoes an intense stretching and thinning (Péron-Pinvidic and Manatschal, 2009; Mohn et al., 2010). The architecture of this domain consists of tilted crustal blocks that decrease in size oceanwards (Ranero and Pérez-Gussinyé, 2010). There is a deepening of the top basement oceanwards which coincides with the ascending of the Moho topography defining a taper geometry (Osmundsen and Redfield, 2011; Sutra and Manatschal, 2012; Nirrengarten et al., 2017).

Hyperthinned domain

Within the proximal hyperthinned domain, the continental crust is already very thinned (~10 km) (Péron-Pinvidic et al., 2013) but the crustal stretching and thinning continues

until continental crust ruptures and separates. The distal boundary of this domain is characterized by the continental crust breakup point.

Exhumed mantle domain

The exhumed mantle domain is characterized by the presence of serpentinized mantle rather than continental crust. However, continental crust may be locally present in the form of triangular isolated pieces (i.e. allochthon blocks) above the exhumed mantle. This domain is part of the Ocean Continent Transition (OCT) (Tugend et al., 2015).

Oceanic domain

The oceanic domain is characterized by undisputable oceanic crust (5-7 km thick). This is formed when decompression melting occurs and thus focuses the extensional deformation into a narrow region less than ~20 km wide, forming the ocean ridge axis and continental lithospheric breakup. The creation of first oceanic crust results from a competition between dying tectonic and emerging magmatic processes (Gillard et al., 2017).

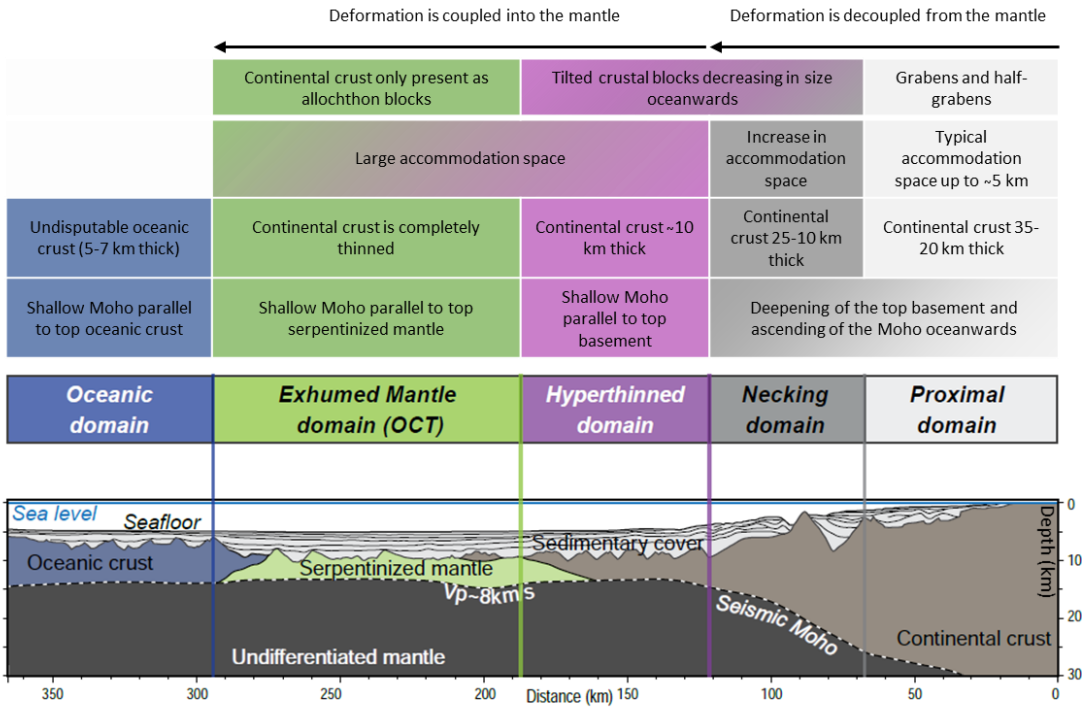

Figure 3: Top: Table summarizing the criteria to define rift domains along a rifted margin based on and modified from Tugend et al., (2014b); Péron-Pinvidic and Osmundsen (2016). Bottom: Simplified architecture of a magma-poor rifted margin showing rift domains (Tugend et al., 2014a and references therein).

1.2. Lithospheric deformation models: from continental rifting to slow spreading ocean ridges

Continental rifting and slow spreading ocean ridges are the two end-member stages of rifted margin formation (Figure 4a). Specific lithospheric deformation models have

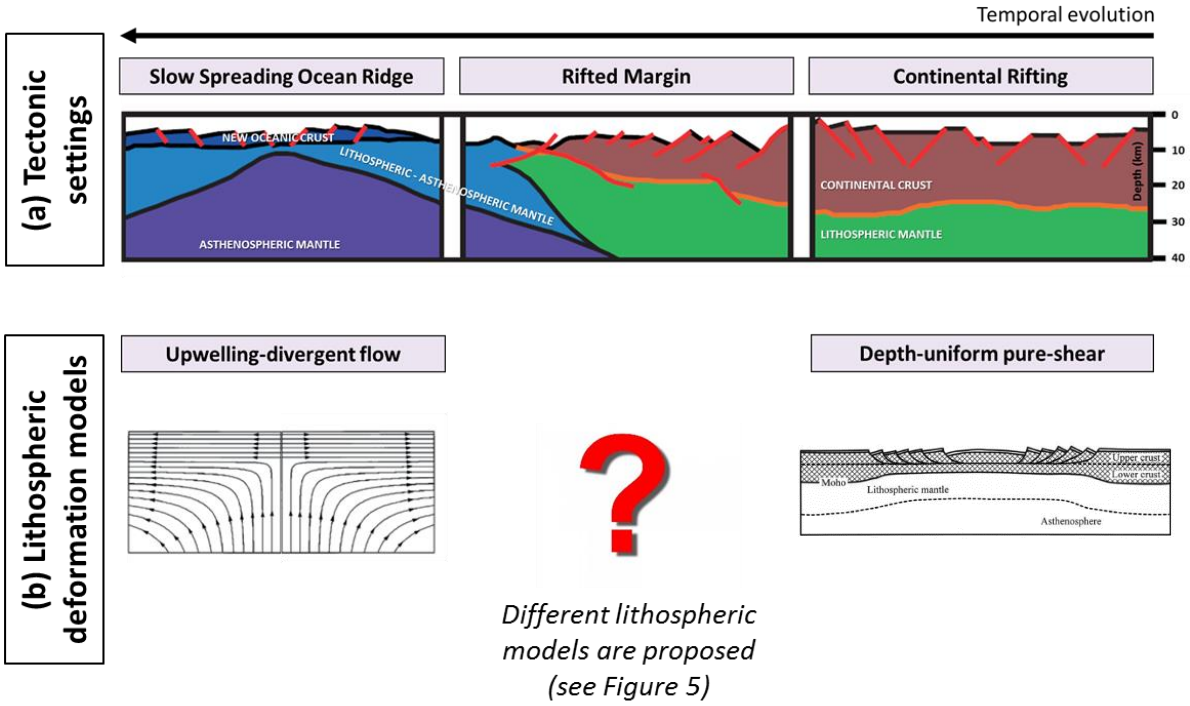

Figure 4: **(a)** Schematic cartoon showing the main architecture of continental rifting, rifted margin and slow spreading ocean ridges. **(b)** Lithospheric deformation model of continental rifting depth-uniform pure-shear of McKenzie (1978) (from Davis and Kusznir, 2004) and an upwelling-divergent flow describing slow spreading ocean ridges lithosphere deformation (modified after Morgan, 1987).

been described for these two end-members (see following section). In contrast, how the continental lithosphere deforms between these end-members during magma-poor rifted margins formation is still controversial (Figure 4b).

1.2.1. Continental rifting and ocean ridges lithospheric models

Pure-shear stretching and thinning of continental lithosphere beneath a brittle seismogenic layer is accepted to be a good description of the process by which continental rifting leading to continental rift basins formation occurs (McKenzie, 1978). This model assumes that the magnitude of stretching and thinning, accommodated by both upper and lower continental lithosphere, is uniform with depth (Figure 4b). In contrast, the extensional deformation at ocean ridges has been

classically described by an upwelling-divergent flow (Figure 4b) (Morgan, 1987). Ocean ridges form when two continental plates break apart and as a consequence lithospheric and asthenospheric mantle rise upwards leading to the formation of new oceanic crust. This process is driven by an extensional rate corresponding to the divergence between the two plates and a vertical axial rate corresponding to the upwelling of active (buoyancy enhanced upwelling) or passive (without buoyancy) fluid flow (Batchelor, 2000; Braun et al., 2000).

1.2.2. Key observations at magma-poor rifted margins

Two key observations have been reported at magma-poor rifted margins which are strongly influenced by the lithosphere deformation mode (Kusznir and Karner, 2007; Fletcher et al., 2009). One of these is a wide zone of exhumed serpentinized continental mantle between continental crust and unequivocal oceanic crust (e.g. Boillot et al., 1987; Boillot et al., 1989; Chian et al., 1995; Pickup et al., 1996; Manatschal and Bernoulli, 1999; Whitmarsh et al., 2001; Jammes et al., 2009; Gillard et al., 2015; Harkin et al., 2019) and the other is lithospheric Depth-Dependent Stretching and Thinning (DDST) consisting of the upper lithosphere being less extended than that of the whole lithosphere (e.g. Roberts et al., 1997; Driscoll and Karner 1998; Baxter et al., 1999; Davis and Kusznir, 2004; Kusznir and Karner, 2007). Examples of DDST obtained to date have usually been based on observations primarily within the proximal and necking domains (e.g. Roberts et al., 1997; Driscoll and Karner, 1998; Baxter et al., 1999; Davis and Kusznir, 2004; Kusznir et al., 2004; Reston, 2007). The suggestion of DDST has led to an intense debate based on whether it is a real observation (Davis and Kusznir, 2004; Kusznir and Karner, 2007) or is due to the limitations of seismic imaging (Reston, 2007; Reston and McDermott, 2014). Despite this ongoing discussion, an interesting related question is whether the upper lithosphere is less extended than that of the whole lithosphere in the distal domain of a conjugate rifted margin system.

Therefore, any robust lithospheric extensional model used to model rifted margins formation must be able to reproduce both exhumed continental mantle and DDST (e.g. Huismans and Beaumont et al., 2014).

1.2.3. Lithosphere deformation modes during rifted margin formation

Two end-member models of continental lithosphere extension have been classically proposed; the pure-shear stretching model of McKenzie (1978) in which lithosphere stretching is uniform with depth (Figure 5a) and the simple-shear model of Wernicke (1985) in which lithosphere extension is controlled by a low-angle lithosphere scale extensional fault (Figures 5b). DDST observed at rifted margins is not consistent with the pure-shear (uniform) lithosphere extension model (McKenzie, 1978). In contrast, DDST can be predicted by the simple-shear lithosphere extensional model (Wernicke, 1985). However, while Wernicke (1985) suggests that lithosphere extension is controlled by a low-angle lithosphere scale extensional fault, no lithosphere-scale dip-slip fault or shear zone cross-cutting continuously from the surface down into the upper mantle has been observed on any deep seismic section (Kusznir and Matthews, 1988). Major basement faults imaged on deep seismic data appear to be restricted to the topmost part of the lithosphere corresponding to the brittle seismogenic layer (10-15 km thick) (Kusznir et al., 1991). Neither the pure-shear (McKenzie, 1978) or the simple-shear models (Wernicke, 1985) can individually explain lithosphere deformation during rifted margin formation, which suggests that other lithosphere-scale deformation processes may play an important role (Fletcher et al., 2009).

An upwelling-divergent flow (Figure 5c) has been suggested as a possible deformation mechanism to explain lithosphere thinning leading to lithospheric breakup and seafloor spreading initiation (Kusznir et al., 2005; Kusznir and Karner, 2007). This lithospheric deformation mode predicts both DDST and exhumation of continental mantle prior to melt initiation (Kusznir et al., 2005; Kusznir and Karner, 2007; Fletcher et al., 2009). However, a unique lithospheric deformation mode driven by an upwelling-divergent flow cannot explain complex rifted margins architecture (Jeanniot et al., 2016). Jeanniot et al., (2016) explored a combination of two lithosphere deformation modes consisting of; (i) pure-shear together with an upwelling divergent passive flow and (ii) pure-shear together with an upwelling divergent active flow (Figure 5d). They showed that both deformation modes are required to explain lithosphere deformation during rifted margins formation when calibrated by observed crustal thinning, water-loaded subsidence, melt initiation timing and mantle exhumation.

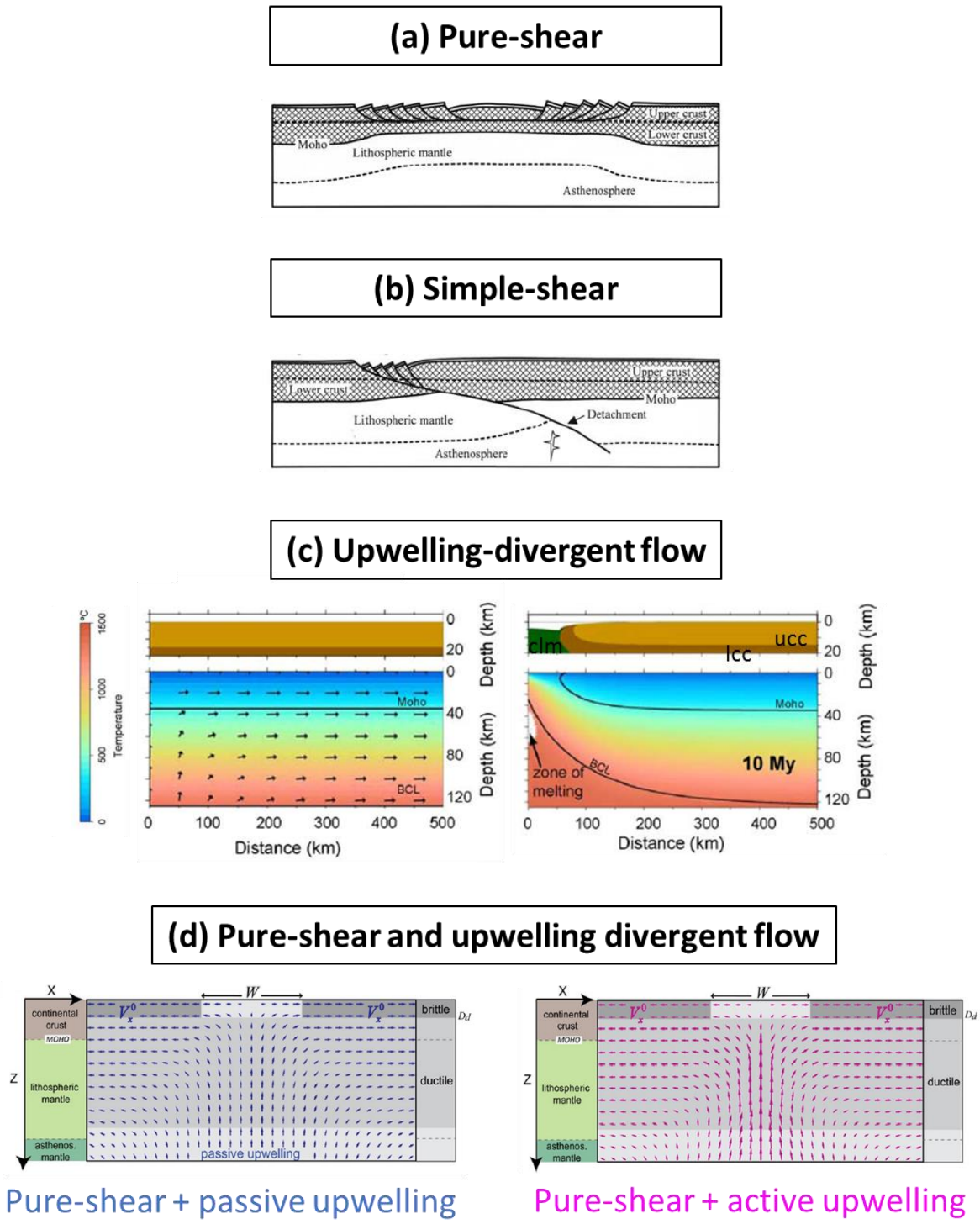

Figure 5: Deformation modes used to explain lithosphere deformation during rifted margin formation. **(a)** Pure-shear model of McKenzie (1978) (from Davis and Kusznir, 2004). **(b)** Simple-shear model of Wernicke (1985) (from Davis and Kusznir, 2004). **(c)** An upwelling-divergent flow. ucc: upper continental crust, lcc: lower continental crust; clm: continental lithospheric mantle (modified from Fletcher et al., 2009). **(d)** Combination of pure-shear and an upwelling divergent flow. Two possible models; pure-shear with a passive upwelling or pure-shear with an active upwelling (from Jeanniot et al., 2016).

1.3. Fault geometry: from continental rifting to slow spreading ocean ridges

If rifted margins record the transitional evolution from continental rifting to slow spreading ocean ridges (Figure 4a), then extensional fault geometries characteristic of both continental rifting and slow spreading ocean ridges are expected to be involved in the lithosphere extension during rifted margins formation. However, fault geometry at rifted margins is still highly debated, especially within the distal domains (i.e. necking and hyperthinned domains).

1.3.1. Continental rifting fault geometry

Observations from earthquake seismology, geodesy and geophysical field data suggest that faults are planar rather than listric during early continental rifting (Stein and Barrientos, 1985; Jackson, 1987). These extensional structures are restricted to the seismogenic upper crustal layer (less than 15 km depth) which corresponds to the cool brittle upper lithosphere (Stein and Barrientos, 1985; Jackson, 1987; Kusznir et al., 1991). A recent study, tested whether geological observations of the Corinth rift are best reproduced by low-angle normal faults or high-angle planar faults (Bell et al., 2017). They showed that high-angle faults are able to reproduce the uplift and subsidence patterns observed in the area while low-angle normal faults cannot. This allowed them to suggest that high-angle planar faults are the dominant accommodation mechanism in the upper crust during early continental rifting (Bell et al., 2017) consistent with Stein and Barrientos (1985), Jackson (1987) and Kusznir et al., (1991).

1.3.2. Slow spreading ocean ridges fault geometry

Seismic refraction, microearthquake, drilling and dredging data at slow spreading ocean ridges (e.g. Tucholke et al., 1998; deMartin et al., 2007; Schroeder et al., 2007) suggest that brittle lithosphere extension is mostly achieved by rolling-hinge extensional faults (Buck, 1988). These consist of an active steep dipping fault (70°) penetrating down to depths of 7 km or greater below the seafloor. These faults have large heaves which lead to the flexural isostatic rotation of the footwall block giving a sub-horizontal exhumed footwall at the sea-bed (Buck, 1988; deMartin, et al., 2007). Schroeder et al., (2007) suggested that secondary high-angle faults characterized by

low-displacement may be also present and cross-cut the exhumed footwall block of rolling-hinge faults.

1.3.3. Fault geometry at rifted margins

During magma-poor rifted margin formation, lithosphere undergoes a progression of different extensional deformation phases. Each of them are believed to be associated with a particular fault geometry (Figures 6 and 7). These distinct phases have been interpreted using seismic observations (e.g. Gillard et al., 2015; Péron-Pinvidic and Manatschal, 2009; Sutra and Manatschal, 2012), field analogues (e.g. Manatschal, 2004; Mohn et al., 2012; Masini et al., 2013; Beltrando et al., 2014) and numerical models (e.g. Lavier and Manatschal, 2006; Brune et al., 2014; Huismans and Beaumont, 2014).

Distributed lithosphere stretching and thinning

During continental rifting, distributed stretching and thinning is characterized by high-angle planar extensional faults (e.g. Bell et al., 2017) soling out at mid-crustal levels with distributed deformation below within the lower crust and mantle (Stein and Barrientos, 1985; Jackson, 1987). Continental rifting leads to the formation of the proximal rift domain characterized by horsts, grabens and half-grabens bounded by high-angle planar faults (Figure 6a and 7a). Continental rifting occurs over a broad region that may range between 50 and 100 km wide (Brun and Chourkoune, 1983; Kusznir and Ziegler, 1992) leading to lithosphere stretching and thinning typically with $\beta < 1.3$.

Localised lithosphere stretching and thinning

Localised stretching and thinning occurs in the advanced stages of continental rifting during necking, hyper-thinning and mantle exhumation. Extensional fault activity and the deeper lithosphere deformation become localized within a narrower area (~50 km, Chenin et al., 2017) compared with that during earlier distributed stretching and thinning (Figure 6b). During this advanced stage of continental rifting, the formation of the necking rift domain is characterized by strong crustal thinning leading to crustal thicknesses ranging from 25 km thick continentwards to less than 10 km thick oceanwards (Manatschal et al., 2001). Despite the deformation being localized within

a narrower area, the extensional faults are still decoupled from the mantle and sole out at mid or lower crustal levels (Pérez-Gussinyé et al., 2001; Sutra et al., 2013).

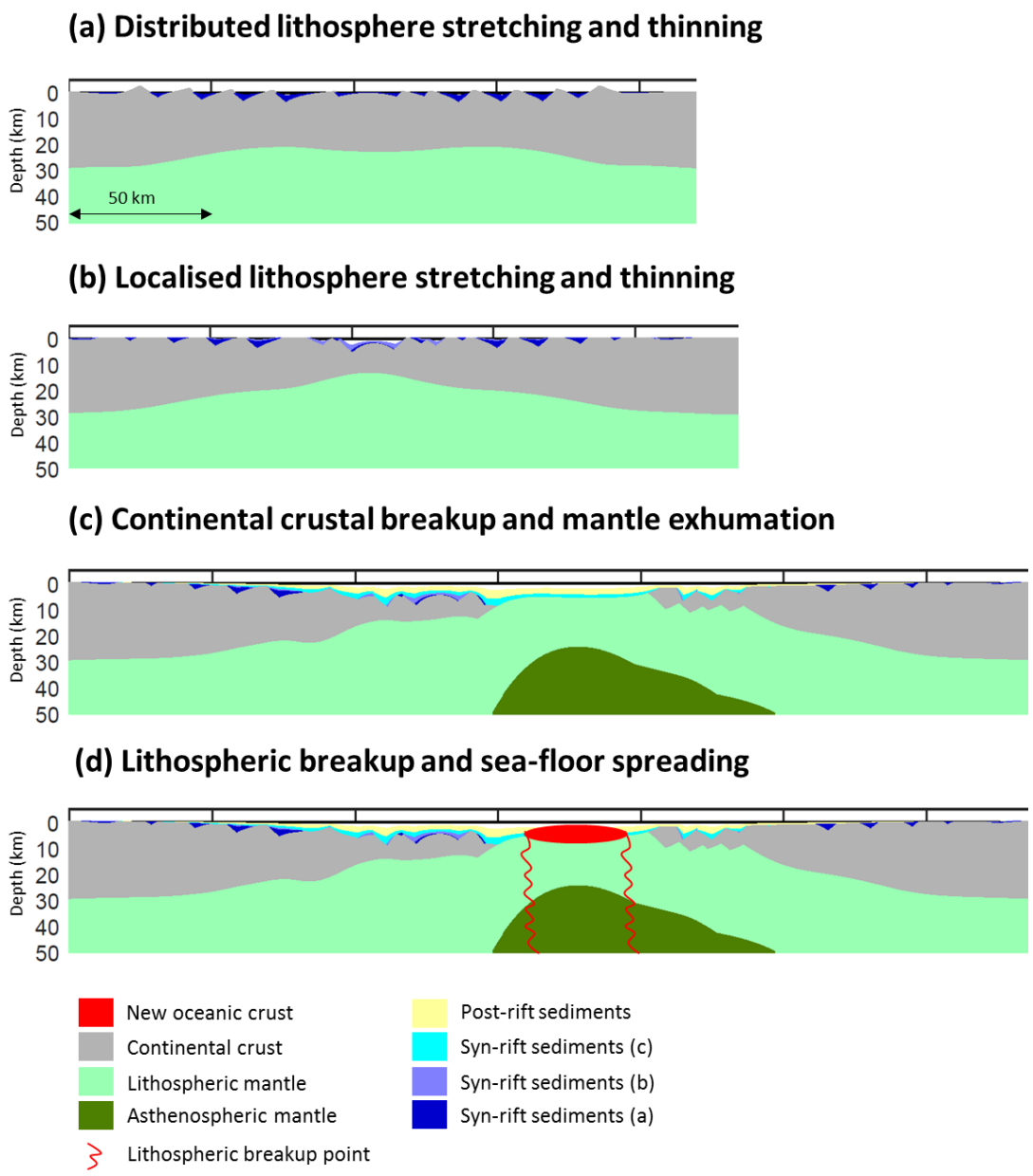

Figure 6: An isostatic numerical model (RIFTER) showing the lithospheric extensional deformation phases during magma-poor rifted margin formation (based on and modified from Péron-Pinvidic and Manatschal, 2009).

It has been suggested that at the end of this deformation stage, a keystone corresponding to the residual thinned continental block is formed (Péron-Pinvidic and Manatschal, 2009; Mohn et al., 2012; Sutra et al., 2013). However, the formation of this thinned keystone cannot explain how continental crust is able to thin to less than 15 km across the necking domain. The extensional mechanism by which continental

crust thins as well as the characteristic and expected faults geometries within the necking domain are still debated topics.

Continental crustal breakup and mantle exhumation

This deformation phase is characterized by the last stage of crustal stretching and thinning leading to continental crustal breakup and mantle exhumation (Figure 6c). The formation of the exhumed mantle domain occurs if decompression melting is not generated and extracted prior to crustal breakup to form an oceanic crust (e.g. Boillot et al., 1987; Jagoutz et al., 2007; Bronner et al., 2011). Continental crustal breakup is achieved by an advanced stage of continental rifting leading to the formation of the hyperthinned domain where continental crust ranges from less than 10 km until its disappearance (Manatschal et al., 2001). Within this domain extensional faults are directly coupled into the mantle because no ductile continental crust remains (Pérez-Gussinyé et al., 2001; Sutra et al., 2013). Planar, rolling-hinge, listric and low-angle faults (Figure 7) have been proposed within the hyperthinned domain (e.g. Manatschal et al., 2001; Péron-Pinvidic et al., 2007; Reston and McDermott, 2011; Pérez-Gussinyé, 2013; Epin and Manatschal, 2018). Despite the fault mechanical theory indicates that faults slip at high angles, examples of low-angle faults were first recognized in the Basin and Range province (Longwell, 1945; Anderson, 1971; Armstrong, 1972; Crittenden et al., 1980; Wernicke, 1981) and subsequently worldwide (e.g. Snake River). In addition, some recent work in the northern North Sea rift has shown high reflectivity zones throughout the crust which have been interpreted as low-angle faults (e.g. Fazlikhani et al., 2017).

It is still controversial whether the present-day fault geometries within the hyperthinned domain are the same as when faults were active. This is a very important remaining question that needs to be addressed to better understand how the hyperthinned domain leading to mantle exhumation at rifted margins is formed. To answer this question, it is crucial to investigate the geometric evolution of extensional faults within the hyperthinned continental crust leading to exhumed mantle initiation.

The transition between “true” oceanic crust and either exhumed mantle or hyperthinned continental crust is characterized by in- and out-of-sequence stepping extensional faults (Gillard et al., 2016). These extensional faults (i.e. rolling-hinge

faults) are active at high-angles and, due to their high offsets, the footwall block strongly rotates and leads to a sub-horizontal sea-bed (Figure 7b) (Buck, 1988).

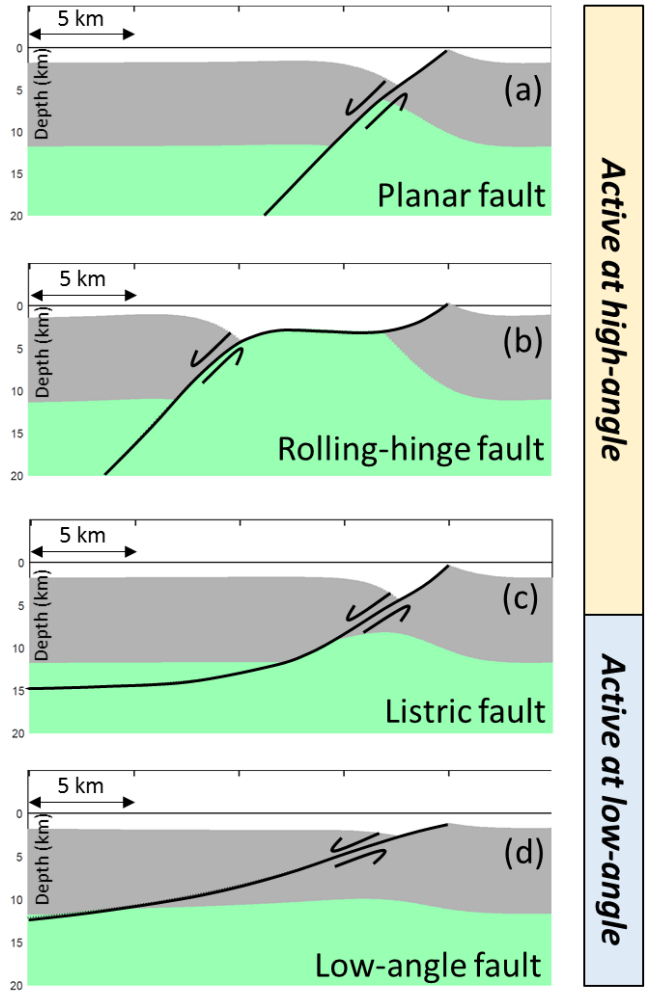

Figure 7: An isostatic numerical model (RIFTER) showing extensional fault geometries. **(a)** Active fault at 60° and 5 km of extension, **(b)** Active fault at 60° and 20 km of extension (Buck, 1988), **(c)** Top fault active at 60° while the deeper fault active at low-angle and 5 km of extension and **(d)** Active fault at 30° and 5 km of extension. Grey and green represent two different stratigraphic units.

Lithospheric breakup and sea-floor spreading

Eventually decompression melting produces magmatic rocks and focuses the deformation into a narrow region leading to the creation of a new divergent plate boundary. It is at this point that lithospheric breakup occurs and a slow-spreading ocean ridge is formed producing new oceanic crust (Figure 6d). At slow spreading ocean ridges (i.e. within the oceanic domain of rifted margins) typical active fault

geometries are steep and planar (~70°) penetrating to depths greater than 7 km (Cannat, 1996) below seafloor and at large extension lead to an exhumed sub-horizontal footwall (e.g. deMartin et al., 2007). These observations are consistent with the rolling-hinge model of Buck (1988) (Figure 7b).

1.4. Rift inheritance in orogeny

The Wilson cycle represents one of the most important concepts of the plate tectonic theory and one of its key implications is that mountain belts are built on the former site of continental rifted margins (Wilson, 1966). This implies that present-day orogens are formed by the closure of precursor rift basins or rifted margins. Indeed, several studies have shown that remnants of distal rifted margins are present within the internal parts of orogens (e.g. in the Alps: Lemoine et al., 1987; Manatschal, 2004; Mohn et al., 2010; Masini et al., 2012, Beltrando et al., 2014 and Epin et al., 2017, in the Pyrenees: Lagabrielle and Bodinier, 2008; Jammes et al., 2009; Lagrabrielle et al., 2010; Clerc et al., 2012, 2014, Masini et al., 2014, Tugend et al., 2014, Mouthereau et al., 2014, Teixell et al., 2016, and in the Caledonies: Andersen et al., 2012). Therefore, to better understand orogen formation it is important to investigate the earlier extensional rift history.

Several scientific contributions have focused on aspects related to the pre-collision history such as earlier rift-related thinning and the role of rift inheritances during orogen formation (e.g. Jammes et al., 2009, 2014; Roca et al., 2011; Masini et al., 2014; Mohn et al., 2014; Mouthereau et al., 2014; Tugend et al., 2014; Teixell et al., 2016, 2018; Chenin et al., 2017; Epin et al., 2017). In particular, the work by Tugend et al., (2014) centred on the Western Pyrenees emphasized the importance of understanding not only how rift domains are formed but also how they evolve during orogen formation. They suggested that to reproduce the present-day architecture of the Pyrenees, rift domains must have been reactivated sequentially. A more recent study by Teixell et al., (2018) indicated that earlier extensional faults were subsequently reactivated during collision and by doing so allow mantle and crustal rocks to be brought into the internal parts of the orogen. However, why some relics of rifted margins (e.g. exhumed mantle) found within mountain belts are preserved from tectonic reworking is unknown (Jourdon et al., 2019). Jourdon et al., (2019) suggested that the upper mantle and surrounding units are never reactivated during collision due

to crustal strain localization. They also emphasized the important role that pre-collisional rift domains play in controlling strain distribution in the orogenic wedge.

Despite recent increased understanding of how rift domains reactivate during collision, key questions remain. The earlier extensional history prior to orogen formation has recently been included using palinspastically restored cross-sections (e.g. Tugend et al., 2014; Mouthereau et al., 2014; Teixell et al., 2016, 2018), however these have not included the isostatic compensation of the lithosphere resulting from both extensional and compressional tectonics. An additional poorly constrained aspect is the evolution of deep fault geometry during collision and whether they are coupled or decoupled from the mantle.

2. Thesis questions and aims

Magma-poor rifted margins are formed by progressive lithosphere stretching and thinning leading to lithospheric breakup. This is achieved by brittle fault deformation within the upper lithosphere with distributed pure-shear deformation below. In this thesis I investigate; (i) extensional faulting during magma-poor rifted margin formation leading to mantle exhumation and (ii) how extensional structures formed during rifted margin formation are reactivated during orogeny.

Extensional faults at rifted margins have been studied by direct observations using seismic data and field observations. In contrast, the deeper distributed pure-shear deformation is not directly observed and as a consequence numerical models are required to simulate it. On this basis, it has been often assumed that extensional faults are the most important means by which continental lithosphere extends simply because they are visible. To conserve area and volume, the thinning and stretching of the upper continental crust (i.e. extensional faulting) is assumed to be the same as the whole continental crust (i.e. extensional faulting and deeper distributed pure-shear deformation must balance). Contradicting this assumption, depth-dependent stretching and thinning (i.e. the upper lithosphere being less extended than that of the whole lithosphere) has been observed within the proximal and necking domains of rifted margins. An important and still unknown question is the amount by which continental crust is extended by brittle faulting during the formation of a conjugate pair of rifted margins.

The kinematic and geometric evolution of extensional faults at rifted margins are studied by examining present-day datasets (e.g. seismic and field data) which provide the post-extensional structural configuration. Therefore, these datasets do not directly indicate the initial and active fault geometry. This has led to an ongoing debate about how faults form and evolve especially within the distal part of rifted margins. To address this problem, it is essential to consider the physical response of the lithosphere due to fault displacement, in particular the flexural isostatic response, as it strongly controls the geometric evolution of faults as well as syn-rift accommodation space for sediments.

Investigating how extensional faults lead to the different rift domains at rifted margins is crucial not only to better comprehend lithosphere deformation during extensional processes but also to better understand orogen formation. It has been suggested that present-day orogens cannot be explained without including the sequential reactivation of rift domains (Tugend et al., 2014). However, it has not been tested whether this hypothesis is coherent from an isostatic compensation viewpoint. Understanding how rift domains reactivate during collision may give insights on how extensional faults geometrically reactivate and evolve during orogeny.

The aim of this thesis is to bring insights that contribute to answering these questions and thus to better understand extensional faulting at magma-poor rifted margins and the reactivation of rift domains and rift-related faults during collision. The aims of my PhD can be split into addressing four questions:

A. How much extension is required to produce continental crustal breakup? (*Chapter 2*)

B. How does extension by faulting compare with extension from crustal and lithosphere thinning at conjugate rifted margins? (*Chapter 2*)

C. What is the geometric evolution of extensional faults within distal magma-poor rifted margins? (*Chapter 3*)

D. How do rift domains and their extensional structures reactivate during compression leading to orogen formation? (*Chapter 4*)

3. Data and methods

To achieve the aims of my PhD previously described, I use the Iberia-Newfoundland conjugate rifted margins, the distal Iberia margin and the Western Pyrenees as natural laboratories (Figure 2). The Iberia-Newfoundland rifted margins are an ideal natural laboratory because they are both magma- and sediment-starved and are among the best studied rifted margin systems worldwide. Thus, this conjugate pair of margins are an ideal example to investigate how much extension is required to produce continental crustal breakup. The distal Iberia margin shows a sub-horizontal seismic reflector and a set of topographic highs that have led to a number of studies focused on fault geometries (e.g. Reston et al., 1996; Péron-Pinvidic et al., 2007; Reston and McDermott, 2011 and references therein), therefore, this is an excellent area to investigate the geometric evolution of extensional faults. In the Western Pyrenees evidences for a reactivated hyper-extended basin that preserves the earlier rift history have been shown (e.g. Masini et al., 2014; Tugend et al., 2014) which makes this as a perfect case-study to investigate the reactivation of rift domains as well as rift-related faults during collision.

To approach the scientific questions proposed in this thesis, I use seismic data, two quantitative techniques and a numerical kinematic model (RIFTER).

3.1. Seismic data

I use the SCREECH1 – ISE01 (Funck et al., 2003; Zelt et al., 2003) and SCREECH2 – TGS/LG12 (Beslier, 1996; Shillington et al., 2008; Sutra and Manatschal, 2012) published seismic profiles across the Iberia-Newfoundland conjugate margins. I geo-reference these four lines against public domain bathymetry (Smith and Sandwell, 1997) as well as converting the sea-bed horizon and sediment thickness into the depth domain. This is achieved by using a water velocity of 1.5 km/s and Vz = Vo + kz where Vo is 1.75 km/s and 0.4 is the depth gradient used to convert the sediment thickness time into depth. In Chapter 2, I use the SCREECH1 – ISE01 and SCREECH2 – TGS/LG12 seismic lines while in Chapter 3, I only use the first-order seismic features of the distal TGS profile.

3.2. Quantitative techniques

A gravity anomaly inversion method and a subsidence analysis technique are used to determine continental crustal thinning and continental lithosphere thinning respectively along SCREECH1 – ISE01 and SCREECH2 – TGS/LG12 seismic profiles. Results obtained from the application of these two techniques are shown and discussed in Chapter 2. The gravity anomaly inversion and subsidence analysis methods are described within Chapter 2 and in more detail in Appendix 1 and 2 respectively.

3.3. Numerical kinematic model (RIFTER)

I use a numerical kinematic model (RIFTER) developed by Nick Kusznir to investigate the geometric evolution of faults within the distal domain of rifted margins (Chapter 3) and the reactivation of rift domains and their rift-related faults during collision and orogen formation (Chapter 4).

RIFTER is a kinematic forward lithosphere deformation model that provides flexural isostatically compensated as well as balanced cross-sections. Within RIFTER, lithosphere is deformed by faulting in the upper crust with underlying distributed pure-shear deformation in the lower crust and mantle. A key attribute of RIFTER is that it incorporates the flexural isostatic response to extensional and/or compressional faulting, crustal thinning and/or thickening, lithosphere thermal loads, sedimentation and erosion. RIFTER can be used to model the structural and stratigraphic development of both extensional and compressional tectonic settings. The model is kinematically controlled with fault geometry and displacement, pure-shear distribution and the amount of sedimentation and erosion given as model inputs. Lithosphere flexural strength, parameterised as lithosphere effective elastic thickness, is also defined. Thus, RIFTER provides for the isostatic testing of palinspastic cross-sections and can also be used to explore different kinematic scenarios.

To understand the response of the lithosphere to deformation, numerical modelling is often used which may be kinematic or dynamic. Dynamic models are thermo-mechanically self-consistent and driven by boundary conditions (e.g. Huismans & Beaumont, 2014; Brune et al. 2014). These models show a complex evolution

determined by the initial rheological properties of continental crust and mantle, however, they cannot be used to model particular observed cross-sections and therefore cannot be calibrated against real data. In contrast, kinematic models, while omitting lithosphere rheology and its control of how lithosphere deformation evolves, can be used to model specific cross-sections and can be quantitatively calibrated.

I have written, in collaboration with Anthony Lamur, a new Matlab code which is used to display the graphics of all RIFTER models presented in this thesis. The numerical formulation of RIFTER is described in Appendix 3.

4. Thesis structure

Chapter 1 of this thesis is this chapter which introduces the subjects and identifies major scientific questions addressed in the following chapters.

The scientific chapters (Chapters 2-4) are the core of this thesis and show the main results in a format of journal manuscripts either published or in preparation. As a consequence, some duplicate information may exist between these chapters.

Chapter 2 is a manuscript in preparation for a special issue on Marine and Petroleum Geology entitled: "Continental margins unleashed: From early inception to continental breakup". The manuscript in preparation is entitled "*Measurements of the extension required for continental breakup on the magma-poor Iberia-Newfoundland conjugate margins*". Gravity anomaly inversion, subsidence analysis and seismic observations are used to determine whole continental crust extension, whole continental lithosphere extension and observed cumulative fault heave respectively for two conjugate margin profiles. These measurements are obtained between the proximal continental crust and its distal edge providing estimates of how much extension is required to produce continental crustal breakup.

Chapter 3 is presented in a paper format suitable for a scientific publication and is entitled "*The geometry and evolution of extensional faults within hyperthinned continental crust leading to mantle exhumation at magma-poor rifted margins*". RIFTER model is used to carry out a set of numerical experiments to explore the development of hyperthinned continental crust leading to mantle exhumation. This examines the geometric evolution of extensional faults and the form by which continental crustal breakup may occur.

Chapter 4 is a draft manuscript published in a special issue on Tectonophysics in June 2019 entitled: "Style of deformation and tectono-sedimentary evolution of fold-and-thrust belts and foreland basins: from nature to models". The manuscript is entitled "*Role of rift structural inheritance in orogeny highlighted by the Western Pyrenees case-study*". RIFTER is used to model first the rift extensional tectonic history of the Western Pyrenees at the propagating tip of the Bay of Biscay, and then the reactivation of those rift domains leading to the formation of the present-day Western Pyrenees.

Chapter 5 is a discussion that summarizes the main findings of this thesis bringing answers to the questions presented within the introduction (Chapter 1). In addition, the results of the three scientific chapters are discussed altogether providing new insights on extensional faulting at magma-poor rifted margins and how extensional faults reactivate during orogeny. Lastly the main conclusions of this thesis are given.

REFERENCES

Andersen, T.B., Corfu, F., Labrousse, L., Osmundsen, P.-T., 2012. Evidence for hyperextension along the pre-Caledonian margin of Baltica. J. Geol. Soc. London. 169, 601–612. https://doi.org/10.1144/0016-76492012-011.

Anderson, R.E., 1971. Thin skin dstension in Tertiary rocks of southeastern Nevada. Geol. Soc. Am. Bull. 82, 43–58.

Armstrong, R.L., 1972. Low-angle (denudation) faults, hinterland of the Sevier orogenic belt, eastern Nevada and western Utah. Geol. Soc. Am. Bull. 83, 1729–1754.Batchelor, G.K., 2000. An introduction to Fluid Dynamics. Cambridge Univ. Press.

Baxter, K., Cooper, G.T., Hill, K.C., O'Brien, G.W., 1999. Late Jurassic subsidence and passive margin evolution in the Vulcan Sub-basin, north-west Australia: Constraints from basin modelling. Basin Res. 11, 97–111. https://doi.org/10.1046/j.1365-2117.1999.00088.

Bell, R.E., Duclaux, G., Nixon, C.W., Gawthorpe, R.L., McNeill, L.C., 2017. High-angle, not low-angle, normal faults dominate early rift extension in the Corinth Rift, central Greece. Geology 46, 115–118. https://doi.org/10.1130/g39560.1.

Beltrando, M., Manatschal, G., Mohn, G., Dal Piaz, G.V., Vitale Brovarone, A., Masini, E., 2014. Recognizing remnants of magma-poor rifted margins in high-pressure orogenic belts: The Alpine case study. Earth-Science Rev. 131, 88–115. https://doi.org/10.1016/j.earscirev.2014.01.001.

Beslier, M.O., 1996. 48. Data report: Seismic line LG12 in the Iberia Abyssal Plain in Whitmarsh, R.B., Sawyer, D.S., Klaus, A., and Masson, D.G. (Eds.). Proc. Ocean Drill. Program, Sci. Results 149, 737–739.

Boillot, G., Recq, M., Winterer, E.L., Meyer, A.W., Applegate, J., Baltuck, M., Bergen, J.A., Comas, M.C., Davies, T.A., Dunham, K., Evans, C.A., Girardeau, J., Goldberg, G., Haggerty, J., Jansa, L.F., Johnson, J.A., Kasahara, J., Loreau, J.P., Luna-Sierra, E., Moullade, M., Ogg, J., Sarti, M., Thurow, J., Williamson, M., 1987. Tectonic denudation of the upper mantle along passive margins: a model based on drilling results (ODP leg 103, western Galicia margin, Spain).

Tectonophysics 132, 335–342. https://doi.org/10.1016/0040-1951(87)90352-0.

Boillot, G., Féraud, G., Girardeau, J., 1989. Undercrusting by serpentinite beneath rifted margins. Nature 341, 523–525.

Braun, M.G., Hirth, G., Parmentier, E.M., 2000. The effects of deep damp melting on mantle flow and melt generation beneath mid-ocean ridges. Earth Planet. Sci. Lett. 176, 339–356. https://doi.org/10.1016/S0012-821X(00)00015-7.

Bronner, A., Sauter, D., Manatschal, G., Péron-Pinvidic, G., Munschy, M., 2011. Magmatic breakup as an explanation for magnetic anomalies at magma-poor rifted margins. Nat. Geosci. 4, 461–461. https://doi.org/DOI:10.1038/NGEO1201.

Brun, J., Choukroune, P., 1983. Normal faulting, block tilting, and décollement in a stretched crust. Tectonics 2, 345–356.

Brune, S., Heine, C., Pérez-Gussinyé, M., Sobolev, S. V, 2014. Rift migration explains continental margin asymmetry and crustal hyper-extension. Nat. Commun. 5, 4014. https://doi.org/10.1038/ncomms5014.

Buck, W.R., 1988. Flexural Rotation of Normal Faults. Tectonics 7, 959–973.

Bullard, E., 1965. Concluding remarks, Philosophical Transactions of the Royal Society of London, Series A, Mathematical and Physical Sciences. A Symp. Cont. Drift (Oct. 28th, 1965) 258, 322–323.

Cannat, M., 1996. How thick is the magmatic crust at slow spreading oceanic ridges? J. Geophys. Res. 101, 2847–2857. https://doi.org/10.1029/95JB03116.

Chenin, P., Manatschal, G., Picazo, S., Müntener, O., Karner, G., Johnson, C., Ulrich, M., 2017. Influence of the architecture of magma-poor hyperextended rifted margins on orogens produced by the closure of narrow versus wide oceans. Geosphere 13, 559–576. https://doi.org/10.1130/GES01363.1.

Chian, D., Louden, K.E., Reid, I., 1995. Crustal structure of the Labrador Sea conjugate margin and implications for the formation of nonvolcanic continental margins. J. Geophys. Res. 100, 24239–24253. https://doi.org/10.1029/95jb02162.

Clerc, C., Lagabrielle, Y., Neumaier, M., Reynaud, J.-Y., de Saint Blanquat, M., 2012. Exhumation of subcontinental mantle rocks: evidence from ultramafic-bearing clastic deposits nearby the Lherz peridotite body, French Pyrenees. Bull. la Soc. Geol. Fr. 183, 443–459. https://doi.org/10.2113/gssgfbull.183.5.443.

Clerc, C., Lagabrielle, Y., 2014. Thermal control on the modes of crustal thinning leading to mantle exhumation: Insights from the cretaceous pyrenean hot paleomargins. Tectonics 33. https://doi.org/10.1002/2013TC003471.

Crittenden, M.D., Coney, P.J., Davis, G.H., 1980. Cordilleran metamorphic core complexes. Geol. Soc. Am. Bull.

Davis, M., Kusznir, N., 2004. Depth-dependent lithospheric stretching at rifted continental margins. In: Karner, G.D. (ed). Proc. NSF Rift. Margins Theor. Institute. Columbia Univ. Press. New York 92–136. https://doi.org/10.7312/karn12738-005.

Davis, J.K., Lavier, L.L., 2017. Influences on the development of volcanic and magma-poor morphologies during passive continental rifting. Geosphere 13, 1524–1540. https://doi.org/10.1130/GES01538.1.

deMartin, B.J., Sohn, R.A., Canales, J.P., Humphris, S.E., 2007. Kinematics and geometry of active detachment faulting beneath the Trans-Atlantic geotraverse (TAG) hydrothermal field on the Mid-Atlantic Ridge. Geology 35, 711–714. https://doi.org/10.1130/G23718A.1.

Doré, T., Lundin, E., 2015. Hyperextended continental margins — Knowns and unknowns. Geology 43, 95–96. https://doi.org/10.1016/0040.

Driscoll, N.W., Karner, G.D., 1998. Lower crustal extension across the Northern Carnarvon basin, Australia: Evidence for an eastward dipping detachment. J. Geophys. Res. 103, 4975–4991.

Edwards, R.A., Whitmarsh, R.B., Scrutton, R.A., 1997. The crustal structure across the transform continental margin off Ghana, eastern equatorial Atlantic. J. Geophys. Res. 102, 747–772. https://doi.org/10.1029/96jb02098.

Epin, M., Manatschal, G., Amann, M., 2017. Defining diagnostic criteria to describe the role of rift inheritance in collisional orogens : the case of the Err-Platta nappes

(Switzerland). Swiss J Geosci. https://doi.org/10.1007/s00015-017-0271-6.

Epin, M.E., Manatschal, G., 2018. Three-Dimensional Architecture, Structural Evolution, and Role of Inheritance Controlling Detachment Faulting at a Hyperextended Distal Margin: The Example of the Err Detachment System (SE Switzerland). Tectonics 37, 4494–4514. https://doi.org/10.1029/2018TC005125.

Fazlikhani, H., Fossen, H., Gawthorpe, R.L., Inge Faleide, J., Bell, R.E., 2017. Basement structure and its in fl uence on the structural con fi guration of the northern North Sea rift. Tectonics 36. https://doi.org/10.1002/2017TC004514.

Fletcher, R., Kusznir, N., Cheadle, M., 2009. Melt initiation and mantle exhumation at the Iberian rifted margin: Comparison of pure-shear and upwelling-divergent flow models of continental breakup. C.R. Geosci. 341, 394–405. https://doi.org/10.1016/j.crte.2008.12.008.

Franke, D., 2013. Rifting, lithosphere breakup and volcanism: Comparison of magma-poor and volcanic rifted margins. Mar. Pet. Geol. 43, 63–87. https://doi.org/10.1016/j.marpetgeo.2012.11.003.

Funck, T., Hopper, J.R., Larsen, H.C., Louden, K.E., Tucholke, B.E., Holbrook, W.S., 2003. Crustal structure of the ocean-continent transition at Flemish Cap : Seismic refraction results. J. Geophys. Res. 108, 2531. https://doi.org/10.1029/2003JB002434.

Gillard, M., Autin, J., Manatschal, G., Sauter, D., Munschy, M., Schaming, M., 2015. Tetconomagmatic evolution of the final stages of rifting along the deep conjugate Australian-Antarctic magma-poor rifted margins: Constraints from seismic observations. Tectonics 34, 753–783. https://doi.org/10.1002/2015TC003850.

Gillard, M., Autin, J., Manatschal, G., 2016. Fault systems at hyper-extended rifted margins and embryonic oceanic crust: Structural style, evolution and relation to magma. Mar. Pet. Geol. https://doi.org/10.1016/j.marpetgeo.2016.05.013.

Gillard, M., Sauter, D., Tugend, J., Tomasi, S., Epin, M.-E., Manatschal, G., 2017. Birth of an oceanic spreading center at a magma-poor rift system. Sci. Rep. 7. https://doi.org/10.1038/s41598-017-15522-2.

Harkin, C., Kusznir, N., Tugend, J., Manatschal, G., McDermott, K., 2019. Evaluating

magmatic additions at a magma-poor rifted margin: An East Indian case study. Geophys. J. Int. 217, 25–40. https://doi.org/10.1093/gji/ggz007.

Haupert, I., Manatschal, G., Decarlis, A., Unternehr, P., 2016. Upper-plate magma-poor rifted margins: Stratigraphic architecture and structural evolution. Mar. Pet. Geol. 69, 241–261. https://doi.org/10.1016/j.marpetgeo.2015.10.020.

Huismans, R.S., Beaumont, C., 2014. Rifted continental margins: The case for depth-dependent extension. Earth Planet. Sci. Lett. 407, 148–162. https://doi.org/10.1016/j.epsl.2014.09.032.

Jackson, J. a., 1987. Active normal faulting and crustal extension. Geol. Soc. London, Spec. Publ. 28, 3–17. https://doi.org/10.1144/GSL.SP.1987.028.01.02.

Jagoutz, O., Müntener, O., Manatschal, G., Rubatto, D., Péron-Pinvidic, G., Turrin, B.D., Villa, I.M., 2007. The rift-to-drift transition in the North Altantic: A stuttering start of the MORB machine? Geology 35, 1087–1090. https://doi.org/10.1130/G23613A.1.

Jammes, S., Manatschal, G., Lavier, L., Masini, E., 2009. Tectonosedimentary evolution related to extreme crustal thinning ahead of a propagating ocean: Example of the western Pyrenees. Tectonics 28. https://doi.org/10.1029/2008TC002406.

Jammes, S., Huismans, R.S., Muñoz, J.A., 2014. Lateral variation in structural style of mountain building: Controls of rheological and rift inheritance. Terra Nov. 26, 201–207. https://doi.org/10.1111/ter.12087.

Jeanniot, L., Kusznir, N., Mohn, G., Manatschal, G., Cowie, L., 2016. Constraining lithosphere deformation modes during continental breakup for the Iberia-Newfoundland conjugate rifted margins. Tectonophysics 680, 28–49. https://doi.org/10.1016/j.tecto.2016.05.006.

Jourdon, A., Le Pourhiet, L., Mouthereau, F., Masini, E., 2019. Role of rift maturity on the architecture and shortening distribution in mountain belts. Earth Planet. Sci. Lett. 512, 89–99. https://doi.org/S0012821X19300937.

Kusznir, N.J., Marsden, G., Egan, S.S., 1991. A flexural-cantilever simple-shear/pure-shear model of continental lithosphere extension: applications to the Jeanne d'Arc

Basin, Grand Banks and Viking Graben, North Sea. Geol. Soc. London, Spec. Publ. 56, 41–60. https://doi.org/10.1144/gsl.sp.1991.056.01.04.

Kusznir, N.J., Ziegler, P.A., 1992. The mechanics of continental extension and sedimentary basin formation : A simple-shear / pure-shear flexural cantilever model. Tectonophysics 215, 117–131.

Kusznir, N.J., Matthews, D.H., 1988. Deep seismic reflections and the deformational mechanics of the continental lithosphere. J. Petrol. Special_Vo, 63–87. https://doi.org/10.1093/petrology/Special_Volume.1.63.

Kusznir, N.J., Hunsdale, R., Roberts, A.M., 2004. Timing of depth-dependent lithosphere stretching on the S. Lofoten rifted margin offshore mid-Norway: Pre-breakup or post-breakup? Basin Res. 16, 279–296. https://doi.org/10.1111/j.1365-2117.2004.00233.

Kusznir, N.J., Hunsdale, R., Roberts, A.M., Team, I., 2005. Timing and magnitude of depth-dependent lithosphere stretching on the southern Lofoten and northern Vøring continental margins offshore mid-Norway: implications for subsidence and hydrocarbon maturation at volcanic rifted margins in Doré, A.G. & Vining, B. Proc. 6th Pet. Geol. Conf. Geol. Soc. London 767–783.

Kusznir, N.J., Karner, G.D., 2007. Continental lithospheric thinning and breakup in response to upwelling divergent mantle flow: application to the Woodlark, Newfoundland and Iberia margins. Geol. Soc. London, Spec. Publ. 282, 389–419. https://doi.org/10.1144/SP282.16.

Lagabrielle, Y., Bodinier, J., 2008. Submarine reworking of exhumed subcontinental mantle rocks : field evidence from the Lherz peridotites , French Pyrenees. Terra Nov. 20, 11–21. https://doi.org/10.1111/j.1365-3121.2007.00781.

Lagabrielle, Y., Labaume, P., Blanquat, M.D. Saint, 2010. Mantle exhumation , crustal denudation , and gravity tectonics during Cretaceous rifting in the Pyrenean realm (SW Europe): Insights from the geological setting of the lherzolite bodies. Tectonics 29. https://doi.org/10.1029/2009TC002588.

Lavier, L.L., Manatschal, G., 2006. A mechanism to thin the continental lithosphere at magma-poor margins. Nature 440, 324–328.

https://doi.org/10.1038/nature04608.

Le Pichon, X., 1968. Sea-floor spreading and continental drift. J. Geophys. Res. 73, 3661–3697. https://doi.org/10.1029/jb073i012p03661.

Lemoine, M., Tricart, P., Boillot, G., 1987. Ultramafic and gabbroic ocean floow of the Ligurian Tethys (Alps, Corsica, Apennines): In searhc of a genetic model. Geology 15, 622–625.

Longwell, C.R., 1945. Low-angle normal faults in the Basin and Range province. Am. Geophiscal Union, Washington, DC 26, 107–118.

Manatschal, G., Bernoulli, D., 1999. Architecture and tectonic evolution of nonvolcanic margins: Present-day Galicia and ancient Adria. Tectonics 18, 1099–1119. https://doi.org/10.1029/1999TC900041.

Manatschal, G., Froitzheim, N., Rubenach, M., Turrin, B.., 2001. The role of detachment faulting in the formation of an ocean-continent transition: insights from the Iberia Abyssal Plain from: Wilson, R.C.L., Whitmarsh, R.B., Taylor, B. & Froitzheim, N. Non-Volcaninc Rifting of Continental Margins: A Comparison of Evid. Geol. Soc. London, Spec. Publ. 187, 405–428. https://doi.org/0305-8719/01/1500.

Manatschal, G., 2004. New models for evolution of magma-poor rifted margins based on a review of data and concepts from West Iberia and the Alps. Int. J. Earth Sci. 93, 432–466. https://doi.org/10.1007/s00531-004-0394-7.

Marsden, G., Yielding, G., Roberts, A.., Kusznir, N.., 1990. Application of a flexural cantilever simple-shear/pure-shear model of continental lithosphere extension to the formation of the northern North Sea basin. In: D.J. Blundell and A.D. Gibbs (Editors), Tectonic Evolution of the North Sea Rifts. Oxford Univ, Press 236–257.

Masini, E., Manatschal, G., Mohn, G., Unternehr, P., 2012. Anatomy and tectono-sedimentary evolution of a rift-related detachment system : The example of the Err detachment (central Alps , SE Switzerland). GSA Bull. 1535–1551. https://doi.org/10.1130/B30557.1.

Masini, E., Manatschal, G., Mohn, G., 2013. The Alpine Tethys rifted margins:

Reconciling old and new ideas to understand the stratigraphic architecture of magma-poor rifted margins. Sedimentology 60, 174–196. https://doi.org/10.1111/sed.12017.

Masini, E., Manatschal, G., Tugend, J., Mohn, G., Marie, J., 2014. The tectono‐sedimentary evolution of a hyper‐extended rift basin : the example of the Arzacq – Mauléon rift system (Western Pyrenees , SW France). Int J Earth Sci. https://doi.org/10.1007/s00531-014-1023-8.

Mckenzie, D., 1978. Some Remarks on Development of Sedimentary Basins. Earth Planet. Sci. Lett. 40, 25–32.

Mohn, G., Manatschal, G., Müntener, O., Beltrando, M., Masini, E., 2010. Unravelling the interaction between tectonic and sedimentary processes during lithospheric thinning in the Alpine Tethys margins. Int. J. Earth Sci. 99, 75–101. https://doi.org/10.1007/s00531-010-0566-6.

Mohn, G., Manatschal, G., Beltrando, M., Masini, E., Kusznir, N., 2012. Necking of continental crust in magma-poor rifted margins: Evidence from the fossil Alpine Tethys margins. Tectonics 31, 1–28. https://doi.org/10.1029/2011TC002961.

Mohn, G., Karner, G., Manatschal, G., Johnson, C., 2014. Structural and stratigraphic evolution of the Iberia and Newfoundland hyper-extended rifted margins: A quantitative modeling approach. Sediment. Basin Crustal Process. Cont. Margins From Mod. Hyper-extended Margins to Deform. Anc. Analog. 16, 9156. https://doi.org/10.1144/SP413.9.

Morgan, J.P., 1987. Melt migration beneath mid-ocean spreading centers. Geophys. Res. Lett. 14, 1238–1241. https://doi.org/10.1029/GL014i012p01238.

Morgan, W.J., 1968. Rises, trenches, great faults and crustal blocks. J. Geophys. Res.

Mouthereau, F., Filleaudeau, P.-Y., Vacherat, A., Pik, R., Lacombe, O., Guiditta-Fellin, M., Castelltort, S., Christophoul, F., Masini, E., 2014. Placing limits to shortening evolution in the Pyrenees: Role of margin architecture and implications for the Iberia/Europe convergence. Tectonics 2283–2314. https://doi.org/10.1002/2014TC003663.

Osmundsen, P.T., Redfield, T.F., 2011. Crustal taper and topography at passive

continental margins. Terra Nov. https://doi.org/10.1111/j.1365-3121.2011.01014.

Pérez-Gussinyé, M., Reston, T.J., Morgan, J.., 2001. Serpentinization and magmatism during extension at non-volcanic margins: the effect of initial lithospheric structure. Geol. Soc. London, Spec. Publ. 187, 551–576. https://doi.org/10.1144/GSL.SP.2001.187.01.27.

Pérez-Gussinyé, M., 2013. A tectonic model for hyperextension at magma-poor rifted margins: an example from the West Iberia – Newfoundland conjugate margins. Geol. Soc. London, Spec. Publ. 369, 403–427. https://doi.org/10.1144/SP369.19.

Péron-Pinvidic, G., Manatschal, G., Minshull, T.A., Sawyer, D.S., 2007. Tectonosedimentary evolution of the deep Iberia-Newfoundland margins: Evidence for a complex breakup history. Tectonics 26, 1–19. https://doi.org/10.1029/2006TC001970.

Péron-Pinvidic, G., Manatschal, G., 2009. The final rifting evolution at deep magma-poor passive margins from Iberia-Newfoundland : a new point of view. Int. J. Earth Sci. 98, 1581–1597. https://doi.org/10.1007/s00531-008-0337-9.

Péron-Pinvidic, G., Manatschal, G., Osmundsen, P.T., 2013. Structural comparison of archetypal Atlantic rifted margins: A review of observations and concepts. Mar. Pet. Geol. 43, 21–47. https://doi.org/10.1016/j.marpetgeo.2013.02.002.

Peron-Pinvidic, G., Osmundsen, P.T., 2016. Architecture of the distal and outer domains of the Mid-Norwegian rifted margin: insights from the Ran-Gjallar ridges system. Mar. Pet. Geol. 77, 280–299.

Pickup, S.L.B., Whitmarsh, R.B., Fowler, C.M.R., Reston, T.J., 1996. Insight into the nature of the ocean-continent transition Off West Iberia from a deep multichannel seismic reflection profile. Geology 24, 1079.

Ranero, C.R., Pérez-Gussinyé, M., 2010. Sequential faulting explains the asymmetry and extension discrepancy of conjugate margins. Nature 468, 294–299. https://doi.org/10.1038/nature09520.

Reston, T.J., 1996. The S reflector west of Galicia: The seismic signature of a detachment fault. Geophys. J. Int. 127, 230–244. https://doi.org/10.1111/j.1365-

246X.1996.tb01547.

Reston, T., 2007. Extension discrepancy at North Atlantic nonvolcanic rifted margins : Depth-dependent stretching or unrecognized faulting? Geology 367–370. https://doi.org/10.1130/G23213A.1.

Reston, T.J., 2009. The structure, evolution and symmetry of the magma-poor rifted margins of the North and Central Atlantic : A synthesis. Tectonophysics 468, 6–27. https://doi.org/10.1016/j.tecto.2008.09.002.

Reston, T., Manatschal, G., 2011. Rifted margins: building blocks of later collision, in: Arc-Continent Collision: Front. Earth Sci. Ed. by Brown, D. Ryan, P.D., Springer-Verlag. Berlin, 3-21.

Reston, T.J., McDermott, K.G., 2011. Successive detachment faults and mantle unroofing at magma-poor rifted margins. Geology 39, 1071–1074. https://doi.org/10.1130/G32428.1.

Reston, T., Mcdermott, K., 2014. An assessment of the cause of the "extension discrepancy" with reference to the west Galicia margin. Basin Res. 26, 135–153. https://doi.org/10.1111/bre.12042.

Roberts, A.M., Lundin, E.R., Kusznir, N.J., 1997. Subsidence of the Vøring Basin and the influence of the Atlantic continental margin. J. Geol. Soc. London 154, 551–557. https://doi.org/10.1144/gsjgs.154.3.0551.

Roca, E., Muñoz, J.A., Ferrer, O., Ellouz, N., 2011. The role of the Bay of Biscay Mesozoic extensional structure in the configuration of the Pyrenean orogen: Constraints from the MARCONI deep seismic reflection survey. Tectonics 30, 1–33. https://doi.org/10.1029/2010TC002735.

Sawyer, D.S., Coffin, M.F., Reston, T.J., Stock, J.M., Hopper, J.R., 2007. COBBOOM: The Continental Breakup and Birth of Oceans Mission. Work. Reports. Sci. Drill. 13–25. https://doi.org/10.2204/iodp.sd.5.02.2007.

Schroeder, T., Cheadle, M.J., Dick, H.J.B., Faul, U., Casey, J.F., Kelemen, P.B., 2007. Nonvolcanic seafloor spreading and corner-flow rotation accommodated by extensional faulting at 15°N on the Mid-Atlantic Ridge: A structural synthesis of ODP Leg 209. Geochemistry, Geophys. Geosystems 8.

https://doi.org/10.1029/2006GC001567.

Shillington, D.J., Hopper, J.R., Holbrook, W.S., 2008. Seismic signal penetration beneath postrift sills on the Newfoundland rifted margin. Geophysics 73.

Smith, W.H., Sandwell, D., 1997. Global sea floor topography from satellite altimetry and ship depth soundings. Science (80-.). 277, 1956–1962.

Stein, R.-S., Barrientos, S.-E., 1985. Planar High-Angle Faulting in the Basin and Range: Geodetic Analysis of the 1983 Borah Peak, Idaho, Earthquake. J. Geophys. Res. 90, 11,355-11,366.

Sutra, E., Manatschal, G., 2012. How does the continental crust thin in a hyperextended rifted margin? Insights from the iberia margin. Geology 40, 139–142. https://doi.org/10.1130/G32786.1.

Sutra, E., Manatschal, G., Mohn, G., Unternehr, P., 2013. Quantification and restoration of extensional deformation along the Western Iberia and Newfoundland rifted margins. Geochemistry, Geophys. Geosystems 14, 2575–2597. https://doi.org/10.1002/ggge.20135.

Teixell, A., Labaume, P., Lagabrielle, Y., 2016. The crustal evolution of the west-central Pyrenees revisited: Inferences from a new kinematic scenario. Comptes Rendus - Geosci. 348, 257–267. https://doi.org/10.1016/j.crte.2015.10.010.

Teixell, A., Labaume, P., Ayarza, P., Espurt, N., de Saint Blanquat, M., Lagabrielle, Y., 2018. Crustal structure and evolution of the Pyrenean-Cantabrian belt: A review and new interpretations from recent concepts and data. Tectonophysics 724–725, 146–170. https://doi.org/10.1016/j.tecto.2018.01.009.

Tucholke, B.E., Lin, J., Kleinrock, M.C., 1998. Megamullions and mullion structure defining oceanic metamorphic core complexes on the Mid-Atlantic Ridge. J. Geophys. Res. 103, 9857–9866. https://doi.org/10.1029/98JB00167.

Tugend, J., Manatschal, G., Kusznir, N.J., Masini, E., Mohn, G., Thinon, I., 2014. Formation and deformation of hyperextended rift systems: Insights from rift domain mapping in the Bay of Biscay-Pyrenees. Tectonics 33, 1239–1276. https://doi.org/10.1002/2014TC003529.

Tugend, J., Manatschal, G., Kusznir, N.J., Masini, E., 2015. Characterizing and

identifying structural domains at rifted continental margins: application to the Bay of Biscay margins and its Western Pyrenean fossil remnants. From Gibson, G.M, Roure, F. & Manatschal, G. (eds). Sedimentary basins and crustal processe. Geol. Soc. London, Spec. Publ. 413. https://doi.org/10.1144/SP413.3.

Tugend, J., Gillard, M., Manatschal, G., Nirrengarten, M., Harkin, C., Epin, M.-E., Sauter, D., Autin, J., Kusznir, N., McDermott, K., 2018. Reappraisal of the magma-rich versus magma-poor rifted margin archetypes. From: McClay, K.R. & Hammerstein, J.A. (eds) Passive Margins: Tectonics, Sedimentation and Magmatism. Geol. Soc. London, Spec. Publ. 476. https://doi.org/10.1144/sp476.9.

Turcotte, D.., Schubert, G., 2002. Geodynamics. Second Edition. Cambridge University Press.

Vine, F.J., Matthews, D.H., 1963. Magnetic anomalies over ocean ridges. Nature 947–949.

Wegener, A., 1912. Die entstehung der kontinente. Geol. Rundschau, 3(4) 276–292.

Wernicke, B., 1981. Low-angle normal faults in the Basin and Range Province: nappe tectonics in an extending orogen. Nature 291, 645–648. https://doi.org/10.1038/291645a0.

Wernicke, B., 1985. Uniform-sense normal simple shear of the continental lithosphere. Can. J. Earth Sci. 22(1), 108–125.

Whitmarsh, R.B., Manatschal, G., Minshull, T. a, 2001. Evolution of magma-poor continental margins from rifting to seafloor spreading. Nature 413, 150–154. https://doi.org/10.1038/35093085.

Wilson, J., 1966. Did the atlantic close and then reopen?. Nature 211, 286. https://doi.org/10.12789/geocanj.2016.43.109.

Zelt, C.A., Sain, K., Naumenko, J. V, Sawyer, D.S., 2003. Assessment of crustal velocity models using seismic refraction and reflection tomography. Geophys. J. Int. 609–626.

CHAPTER 2

Chapter 2: in preparation for a special issue on Marine and Petroleum Geology entitled: "Continental margins unleashed: From early inception to continental breakup"

Measurements of the extension required for continental breakup on the magma-poor Iberia-Newfoundland conjugate margins

Júlia Gómez-Romeu[1], Nick Kusznir[1,2], Alan Roberts[2] & Gianreto Manatschal[3]

[1]*Department of Earth, Ocean and Ecological Sciences, University of Liverpool, Liverpool, UK*

[2]*Badley Geoscience Ltd, Spilsby, UK*

[3]*Institut de Physique du Globe de Strasbourg-EOST, Université de Strasbourg-CNRS, France*

Abstract

Rifted margins have been extensively studied, however there are still many important unknowns related to their formation processes. We use the Iberia-Newfoundland conjugate rifted margins as a natural laboratory to investigate how much extension is required to produce continental crustal rupture and separation. To achieve our aim we use; (i) gravity anomaly inversion to measure continental crustal thinning, (ii) subsidence analysis to measure continental lithosphere thinning and (iii) fault heave summation from seismic observations to obtain brittle continental crust extension. Integration of thinning from gravity anomaly inversion and subsidence analysis is used to determine continental crust extension and continental lithosphere extension respectively. These measurements have been made between the proximal continental crust and the distal end of continental crust (COB) on the northern (Screech-1 and ISE-01) and the southern (Screech-2 and Lusigal-12/TGS) conjugate seismic profiles. Extension values determined from the integration of crustal and lithosphere thinning are very similar and suggest that on average continental lithosphere and continental crust are required to be extended by between 186 km and 176 km (181 km in average)

to produce continental crustal breakup. In contrast, measured extension from fault heave summation is less than 181 km which indicates an apparent extension discrepancy at the scale of the whole conjugate margin system when observed brittle continental crust is compared with lithosphere and crust extension.

A fault population analysis has been carried out to examine whether sub-seismic resolution faulting significantly contributes to an under-estimate of brittle crustal extension. Results of this analysis show that up to 35% of sub-seismic faulting may be present along the southern profiles while the northern profile analysis is inconclusive. Therefore, allowing for fault extension at sub-seismic resolution an extension discrepancy at the scale of the whole conjugate margin system does not appear to exist. In addition to sub-seismic faulting, fault geometries and the location of the distalmost continental crust are important issues that should be carefully considered when comparing fault heave summation and extension from crust and lithosphere thinning.

An extension discrepancy at the scale of a whole conjugate margin system should not be confused with depth-dependent stretching and thinning at a given location on the margin which is usually observed and expected within the proximal and necking domains of rifted continental margins.

1. Introduction

How much extension is required to produce continental crustal breakup is still poorly constrained. Continental crustal breakup occurs due to progressive continental lithosphere stretching and thinning achieved by two main processes, brittle faulting deformation within the upper crust with underlying more distributed deformation within the lower crust and upper mantle. Studies based on geometric restoration techniques (e.g. Sutra et al., 2013) or extension rate histories (e.g. Jeanniot et al., 2016) have been used to estimate the amount of crustal extension required to produce crustal breakup at the Iberia-Newfoundland conjugate rifted margins. However, no study exists to date that determines how much extension by brittle faulting is involved in continental crustal breakup and separation along the total length of a conjugate pair of rifted margins.

Extensional faults at rifted margins have been studied by direct observations using seismic data and field observations. In contrast the deeper distributed pure-shear deformation is not directly observed and as a consequence numerical models are required to simulate it. On this basis, it has been often assumed that extensional faults are the most important means by which continental lithosphere extends simply because they are visible. To conserve area and volume, the thinning and stretching of the upper continental crust (i.e. extensional faulting) is assumed to be the same as the whole continental crust (i.e. extensional faulting and deeper distributed pure-shear deformation must balance). Contradicting this assumption, depth-dependent stretching and thinning (i.e. the upper lithosphere being less extended than that of the whole lithosphere) has been observed within the proximal and necking domains of rifted margins (e.g. Driscoll and Karner 1998; Roberts et al., 1997; Baxter et al., 1999; Davis and Kusznir, 2004; Kusznir and Karner, 2007). An important and still unknown question is whether the amount by which continental crust is extended by brittle faulting is less than that of the whole continental crustal extension at the scale of a whole conjugate pair of rifted margins.

We investigate whether the observed brittle fault extension from seismic observations differs or equals the measured whole-lithosphere and whole-crust extension at the scale of a whole conjugate pair of rifted margins. To achieve our aim, we use the Iberia-Newfoundland conjugate rifted margins and apply a gravity anomaly inversion method to quantify continental crustal thinning and a subsidence analysis technique to measure continental lithosphere thinning. Integration of thinning from gravity anomaly inversion and subsidence analysis is used to determine continental crust extension and continental lithosphere extension respectively. In addition to that, we use seismic interpretation to measure brittle extension from fault heave summation. These three estimates have been made between the proximal and distalmost continental crust for the conjugate margins profiles examined in this study (although some of the proximal domain on the southern Iberia margin is not covered by available seismic data).

We also investigate the importance of sub-seismic resolution fault extension when comparing fault heave summation with lithosphere and crust extension. Failing to do

that may lead to an apparent extension discrepancy at the scale of the whole conjugate margin system.

2. The Iberia-Newfoundland conjugate rifted margins

The conjugate Iberia-Newfoundland rifted margins are an ideal natural laboratory because they are both sediment and magma starved and are among the best studied rifted margin systems worldwide. The Iberia-Newfoundland margins have undergone a polyphase evolution characterized by an earlier rift event during Late Triassic to

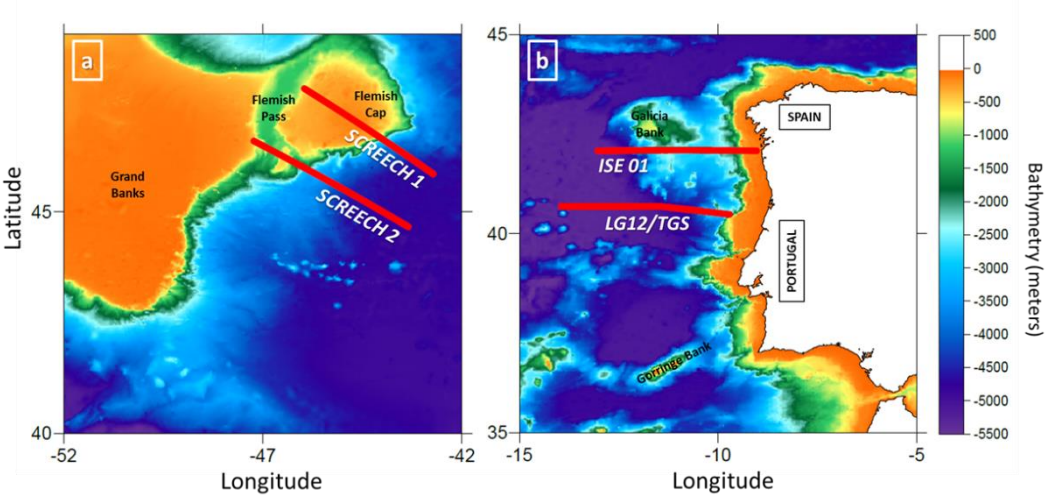

Figure 1: **a-b)** Bathymetric maps of Iberia and Newfoundland margins. Red lines show the position of SCREECH-1 and SCREECH-2 seismic profiles on Newfoundland and ISE-01 and TGS/LG12 seismic profiles on Iberia.

Early Jurassic followed by a later rift event during Middle-Late Jurassic to Early Cretaceous. The age of continental lithosphere breakup for these margins has been suggested to be between 112 Ma (Péron-Pinvidic et al., 2007) and 126 Ma (Russell and Whitmarsh, 2003; Manatschal, 2004). We focus on two pairs of conjugate seismic profiles along these margins; one across the Galicia Bank-Flemish Cap (i.e. northern profiles consisting of SCREECH1 – ISE01 seismic lines Funck et al., 2003; Zelt et al., 2003, Figure 1a) and the other one across the southern Iberia Abyssal Plain-Flemish Pass (i.e. southern profiles consisting of SCREECH2 – TGS/LG12 seismic lines, Beslier, 1996; Shillington et al., 2006; Sutra and Manatschal, 2012, Figure 1b).

3. Applying quantitative techniques

We use two quantitative techniques consisting of gravity anomaly inversion and subsidence analysis to measure continental crustal thinning and continental lithosphere thinning respectively. Integration of thinning from gravity anomaly inversion and subsidence analysis is used to determine total continental crust extension and total continental lithosphere extension across the length of the margin respectively. We apply both techniques to the northern and southern seismic profiles of the Iberia-Newfoundland conjugate rifted margins.

3.1. Gravity anomaly inversion

A gravity anomaly inversion has been used to determine the depth to the Moho, crustal thickness and continental crustal thinning (Greenhalgh and Kusznir, 2007; Alvey et al., 2008; Chappell and Kusznir, 2008; Roberts et al., 2013; Cowie et al., 2015; Kusznir et al., 2018). Inputs data used for the gravity anomaly inversion are; (i) satellite derived free-air gravity from Sandwell and Smith (2009) (V27.1), (ii) bathymetry data from Smith and Sandwell (1997) (V19.1), (iii) 2D sediment thickness obtained from both the northern (SCREECH1 – ISE01) and southern (SCREECH2 – TGS/LG12) seismic profiles of the Iberia and Newfoundland conjugate rifted margins and (iv) age of ocean isochrons are taken from Müller et al., (1997).

The gravity anomaly inversion method is carried out in a 3-D spectral domain using Smith's theorem (Smith, 1961) to provide a unique solution for the 3D Moho topography. We use constant crustal density of 2850 kg m^{-3} (averaged from Carlson and Herrick, 1990; Christensen and Mooney, 1995) and a mantle density of 3300 kg m^{-3} (Jordan and Anderson, 1974). Other global studies such as on the Equatorial Atlantic (Kusznir et al., 2018), Rockall Basin (Roberts et al., 2018), Levant Basin (Steinberg et al., 2018) and South China Sea (Gozzard et al., 2018) have made similar simplifying crustal and mantle density assumptions. The Moho topography is obtained from the mantle residual gravity anomaly using the scheme of Parker (1972). To determine Moho depth from gravity inversion, a reference Moho depth is needed and requires calibration against seismic refraction Moho depths (see Cowie et al., 2015 for a detailed discussion). We use a reference Moho depth of 40 km for the Iberia margin

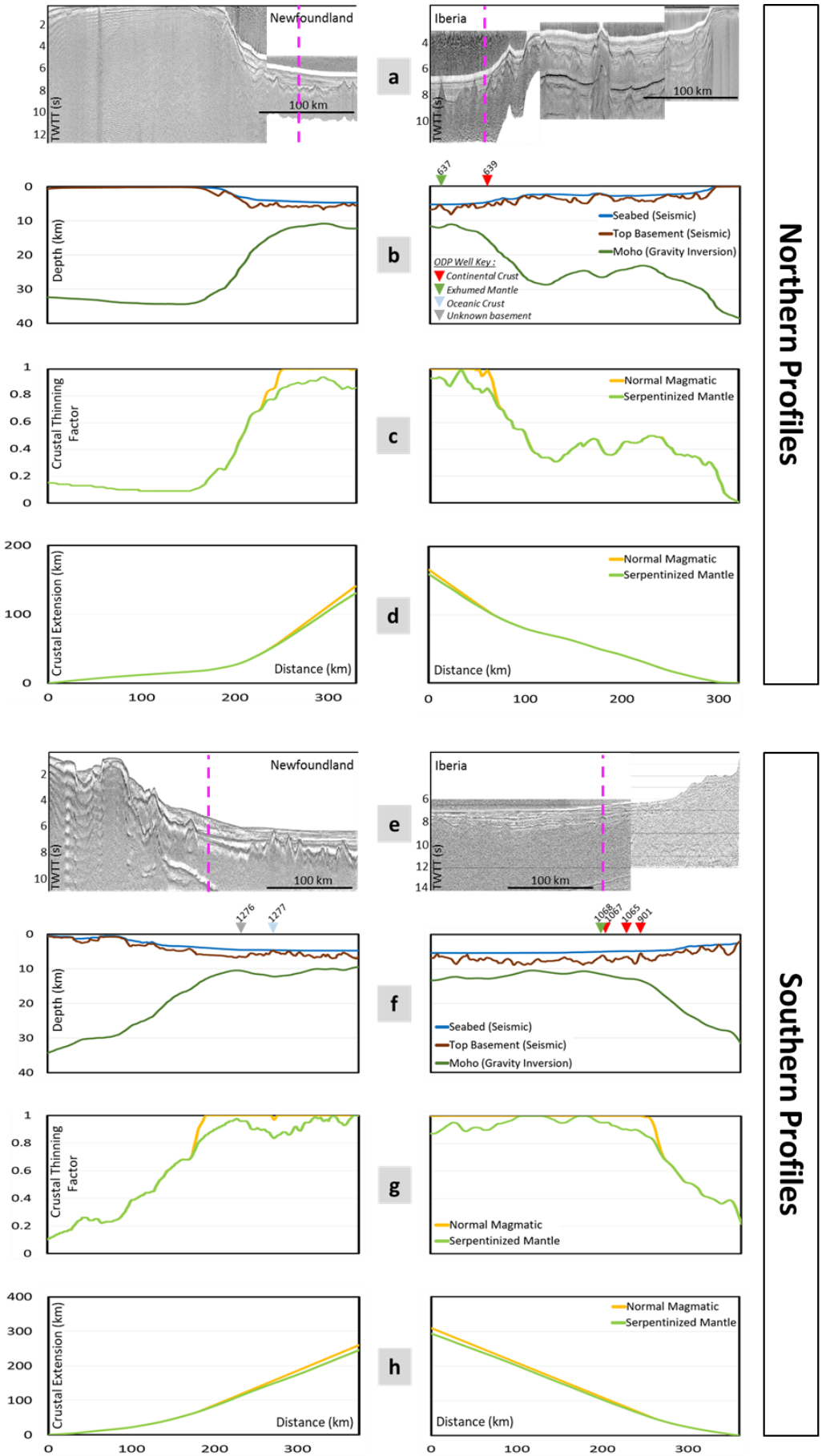
Newfoundland
Iberia
100 km
TWT (s)
a
b
c
d
e
f
g
h
Depth (km)
Crustal Thinning Factor
Crustal Extension (km)
Distance (km)
Seabed (Seismic)
Top Basement (Seismic)
Moho (Gravity Inversion)
ODP Well Key :
Continental Crust
Exhumed Mantle
Oceanic Crust
Unknown basement
Normal Magmatic
Serpentinized Mantle
637
639
1276
1277
1068
1067
1065
901
Northern Profiles
Southern Profiles

Figure 2: **a)** and **e)** The northern (SCREECH-1 and ISE-01, Funck et al., 2003; Zelt et al., 2003) and the southern (SCREECH-2 and TGS-LG12, Shillington et al., 2006; Sutra and Manatschal, 2012; Beslier, 1996) seismic profiles. Pink dashed lines show COB-1 location. **b)** and **f)** Present-day architecture of the Iberia and Newfoundland margins using sea-bed and top-basement from seismic and Moho depth from gravity anomaly inversion. Numbers and triangles indicate ODP wells (Sawyer et al., 1994; Whitmarsh et al., 1998; Funck et al., 2003). **c)** and **g)** Crustal thinning factor from gravity anomaly inversion. **d)** and **h)** Crustal extension from thinning factor integration.

(Cowie et al., 2015) while 37.5 km for the Newfoundland margin (Jeanniot et al., 2016). The depth to the Moho is obtained from the difference between the reference Moho depth and Moho topography. Continental crustal thickness is calculated using the depth to the Moho (Cowie et al., 2015).

Key to the success of the gravity anomaly inversion method is a correction for the lithosphere thermal gravity anomaly (Chappell and Kusznir, 2008) associated with the elevated geotherm resulting from rifting/breakup of the margin. Failure to include this correction leads to a substantial overestimate of Moho depth and crustal basement thickness and an underestimate of continental crustal thinning. The lithosphere thermal gravity anomaly is obtained from the gravity lithosphere thinning factor (γ) and the lithosphere thermal equilibration time (t). For ocean lithosphere $\gamma = 1$ while for continental lithosphere the γ is obtained from the stretching lithosphere factor defined by the difference between the initial crustal thickness respect to the present-day crustal thickness. A key assumption is that lithosphere thinning and crustal thinning are equivalent as depth-uniform stretching and thinning is supposed. For ocean lithosphere, the lithosphere thermal equilibration time (t) corresponds to the age of the lithosphere and is obtained from ocean isochrons (Müller et al., 1997) while for continental lithosphere the breakup age of the margin is used. In this study, a breakup age of 120 Ma is used which is consistent with Cowie et al., (2015).

During rifting and breakup there can be a significant amount of magmatic addition which contribute to the total thickness of the crust. The thickness of the crustal magmatic addition is estimated using a parametrization of the decompression melting model of White and McKenzie (1989) together with the continental lithosphere thinning factor (γ) obtained from the gravity anomaly inversion (further detail in Chappell and Kusznir, 2008 and references therein). Two parameterizations are used to estimate the thickness of magmatic addition and serpentinized mantle respectively at the Iberia and Newfoundland rifted margins; a “normal” magmatic solutionand a

serpentinized mantle solution. The critical thinning factor at which a "normal" decompression melting starts is 0.7 producing a maximum volcanic addition of 7 km at $\gamma = 1$ which corresponds to the maximum thickness of oceanic crust. The critical thinning factor at which the serpentinization of the mantle starts is 0.7 producing at $\gamma = 1.0$ serpentinized mantle with a mass deficiency with respect to mantle equivalent to a crustal basement 3 km thick (further detail in Cowie et al., 2015).

Figure 2 summarizes the results obtained from the gravity anomaly inversion applied along the northern (Figure 2a) and the southern (Figure 2e) profiles. Figures 2b and 2f show the present-day crustal architecture of the Iberia and Newfoundland margins consisting of sea-bed and top-basement interpreted on the seismic data and Moho depth obtained from the gravity anomaly inversion using a "normal" magmatic parameterization for decompression melting. The crustal thinning factor from gravity anomaly inversion using "normal" and serpentinized mantle parameterizations is shown in Figures 2c and 2g.We horizontally integrate the gravity crustal thinning factor from the proximal edge of continental crust until the end of the profile to determine crustal extension along the Iberia and Newfoundland rifted margins. Crustal extension estimates resulting from the integration of crustal thinning factor obtained using "normal" and serpentinized mantle solutions are shown in Figures 2d and 2h. Note that crustal extension results are not significantly dependent on the parameterization used to predict magmatic addition and serpentinized mantle.

3.2. Subsidence analysis

We use a subsidence analysis technique (e.g. for details see Roberts et al., 2013; Cowie et al., 2015) to obtain lithosphere thinning factor which we compare against the crustal thinning factor from gravity anomaly inversion. This technique involves converting water loaded subsidence into lithosphere thinning factor assuming a modified McKenzie (1978) model which incorporated magmatic addition. Flexural backstripping (Kusznir et al., 1995; Roberts et al., 1998) and decompaction assuming shaly-sand parameters (Sclater and Christie, 1980) is used to remove sedimentary layers and loading to the top of pre-rift sequence and top of oceanic crust. This gives a sediment-corrected bathymetry which we equate to water-loaded subsidence assuming that top of pre-rift sequence was at sea-level prior rifting. Backstripped water

loaded subsidence is considered to represent the sum of initial and thermal subsidence in the context of McKenzie (1978). We convert water-loaded subsidence into lithosphere thinning factor including a correction for magmatic addition from decompression melting and serpentinized mantle solution (White and McKenzie, 1989) which uses the same scheme as described in the gravity anomaly inversion section (see Roberts et al., 2013). A breakup age of 120 Ma, an initial crustal thickness of 37.5 km and a crustal density of 2.85 g cm^{-3} are used for the magmatic and serpentinized mantle solutions for the Iberia and Newfoundland margins. Note that in the subsidence analysis method, as with the gravity inversion, lithosphere thinning and crustal thinning are assumed to be the same (i.e. depth-uniform stretching and thinning is supposed). The detail of the subsidence analysis technique is described in Roberts et al., (2013) and Cowie et al., (2015).

Figure 3 summarizes the results obtained from the subsidence analysis applied along the northern and southern profiles of Iberia and Newfoundland. The sediment corrected bathymetry (i.e. water loaded subsidence) obtained from flexural backstripping, present-day top basement and sea-bed are shown in Figures 3a and 3d. The lithosphere thinning factor using "normal"and serpentinized mantle parameterizations obtained from the conversion of water-loaded subsidence is shown in Figures 3b and 3e. Note that the Newfoundland margin requires a correction for 500 m of present-day dynamic uplift due to convective circulation within the mantle (e.g. Crosby et al., 2008). To remove this effect, the water-loaded subsidence is deepened by 500 m prior to obtain the lithosphere thinning factor along the Newfoundland margin.

We horizontally integrate the continental lithosphere thinning factor derived from subsidence analysis from the proximal edge of continental crust until the distal end of the profile to determine lithosphere extension along Iberia and Newfoundland rifted margins. Lithosphere extension estimates resulting from the integration of lithosphere thinning factor obtained using "normal"and serpentinized mantle solutions are shown in Figures 3c and 3f. Note that lithosphere extension results are not significantly dependent of the parameterization used to predict magmatic addition and serpentinized mantle.

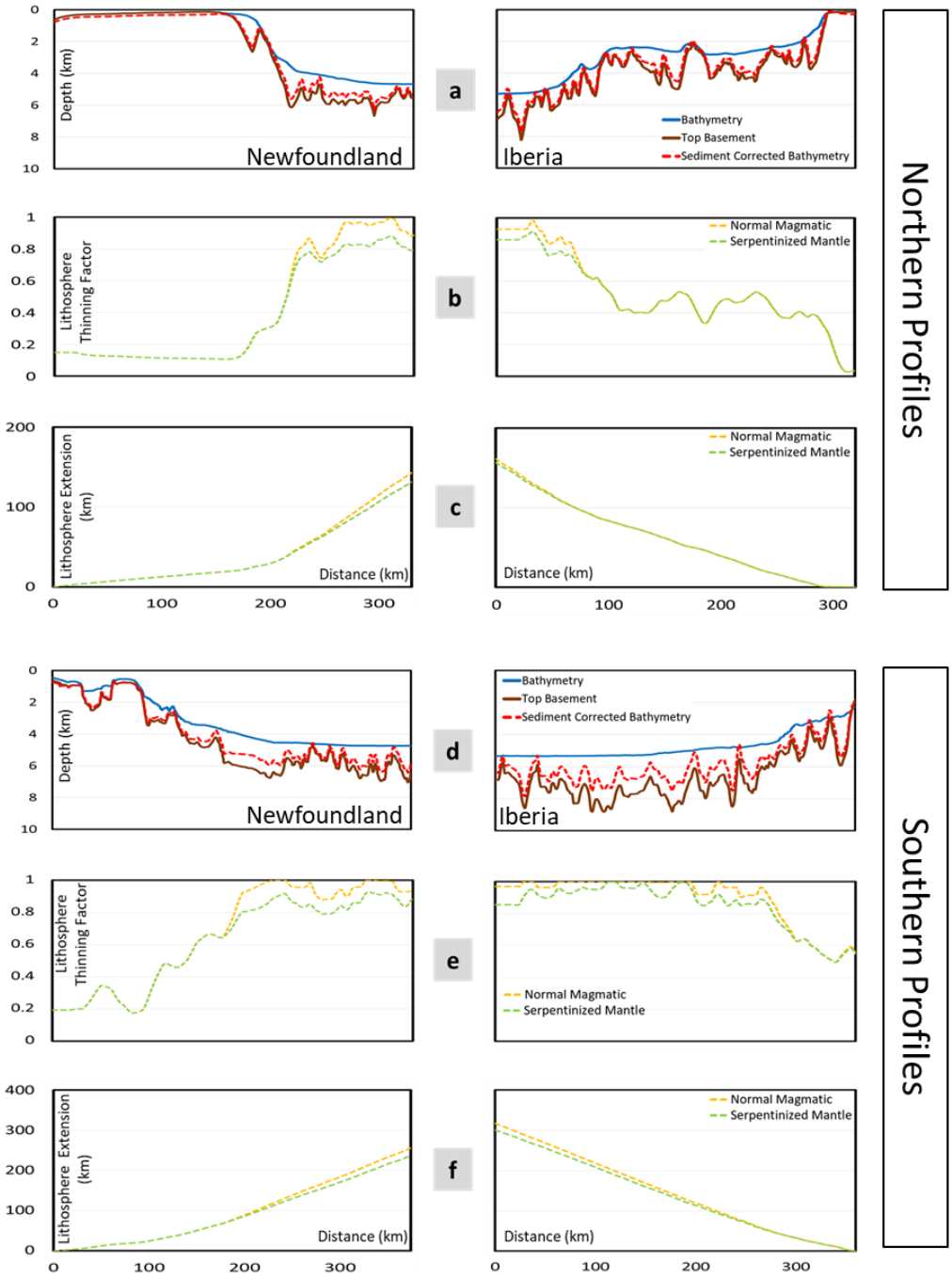

Figure 3: **a)** and **d)** Bathymetry and top-basement from seismic and sediment corrected bathymetry from flexural backstripping. **b)** and **e)** Lithosphere thinning factor from subsidence analysis. **c)** and **f)** Lithosphere extension from thinning factor integration.

4. Total-lithosphere and total-crust extension required for continental crustal breakup

The crustal breakup point has to be defined to determine the amount of total-lithosphere and total-crust extension needed to produce continental crustal breakup.

We identify the distal end of continental crust (COB) corresponding to the crustal breakup point along the northern (Figure 4) and the southern (Figure 5) profiles. Figures 4a-c and 5a-c summarizes the results from gravity anomaly inversion and subsidence analysis (Figures 2 and 3) applied along the northern and southern profiles respectively.

4.1. Distal end of continental crust (COB)

Cowie et al., (2015) carried out an integrated quantitative analysis on the Western Iberia margin to determine not only the COB location but also the ocean-continent structure. They successfully showed the importance of using quantitative techniques together with geological observations to determine the COB position along rifted margins. We use public domain ODP (Ocean Drilling Program) data to determine the distal end of continental crust (COB). However, when this data does not allow us to unequivocally identify the COB location, we use the thinning factor obtained from quantitative techniques together with published seismic interpretations. The thinning factor results from gravity anomaly inversion and subsidence analysis show the same pattern (Figures 4b and 5b), however we use the results from the gravity anomaly inversion as they show a clearer overall trend.

This approach is not robust enough to allow us to precisely define a unique distal limit of continental crust. To overcome this limitation, we suggest two possible COB locations; the inner (COB-1) and the outer (COB-2) that in turn define the boundaries of a zone within which the location of the COB could be placed anywhere.

Northern profiles

Along the SCREECH-1 seismic profile (Newfoundland margin) there is no ODP well information. Therefore, to define COB locations (Figure 4) we use the crustal thinning factor from gravity anomaly inversion (Figure 4b) together with the seismic interpretation suggested by Mohn et al., (2015). The COB-1 is defined where the "normal" magmatic thinning factor first reaches 1.0. This indicates that complete thinning of continental crust is achieved and thus either exhumed mantle or oceanic crust are present. The COB-2 is located more distally where the highest value of serpentinized mantle thinning factor occurs which indicates that mantle may be

exhumed and thus continental crust being completely thinned. COB-2 location is consistent with the Mohn et al., (2015) seismic interpretation.

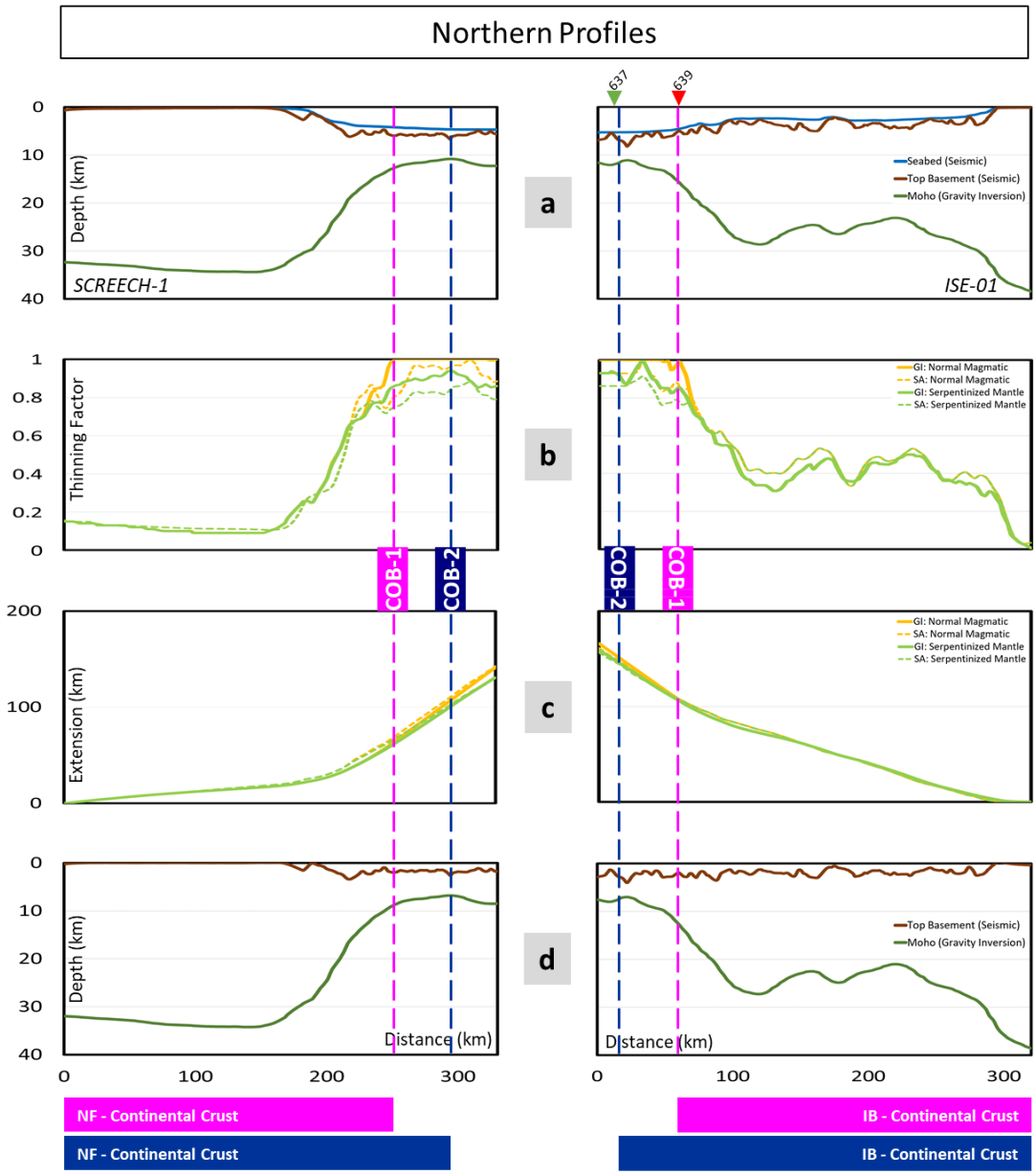

Figure 4: Pink and blue lines show the inner (COB-1) and outer (COB-2) distal end of continental curst. **a)** Present-day architecture of the margin (same as shown in Figure 2b). Numbers and triangles are ODP well data (see Figure 2 for legend). **b)** Thinning factor from gravity anomaly inversion (GI) and subsidence analysis (SA). **c)** Extension from thinning factor integration from gravity anomaly inversion (GI) and subsidence analysis (SA). **d)** Bathymetry and Moho depths for the Iberia and Newfoundland margins restored to the breakup time using a flexural backstripping model.

Along the ISE-01 seismic profile (Iberia margin) ODP well information is available (e.g. Sawyer et al., 1994; Whitmarsh et al., 1998). The 639 ODP well shows the presence of continental basement while the 637 ODP well shows serpentinized

peridotite (Figure 4a). The "normal" magmatic thinning factor from gravity anomaly inversion reaches first 1.0 at the western edge of the 639 ODP well (Figure 4b). This suggests that the distal limit of continental crust (our COB-1 location) may be placed at the western edge of 639 ODP well. In contrast, the COB-2 location is placed at the eastern edge of the 637 ODP well consistent with the Mohn et al., (2015) seismic interpretation and the Cowie et al., (2015) quantitative analysis.

Southern profiles

Along the SCREECH-2 seismic profile (Newfoundland margin), ODP well data is available (Figure 5a). The 1276 ODP well (Funck et al., 2003) was drilled in "transitional" crust between known continental crust and known oceanic crust.

This well shows sills above basement, however the nature of the basement is uncertain. In contrast, the 1277 ODP well (Funck et al., 2003) was drilled into a basement high that shows serpentinized peridotite with intrusive and extrusive mafic material interpreted as the onset of steady-state seafloor spreading (see Bronner et al., 2011 for a detailed description). The lack of ODP well information in the proximal margin gives a big uncertainty on where to place the distal limit of continental crust along this section. The COB-1 location is determined where "normal" magmatic thinning factor first reaches 1.0 (Figure 5b). This is consistent with the seismic interpretation by Mohn et al., (2015). We suggest that the COB-2 location may be placed at the western edge of 1276 ODP well and thus assuming that the known continental crust may be completely thinned before the "transitional" crust identified in this well.

Along the TGS/LG12 seismic profiles (Iberia margin) observations from several ODP drill wells are available (Figure 5a). The ODP site wells 1067 and 900 (Whitmarsh et al., 1998; Sawyer et al., 1994) show deep water turbidites over lower crustal rocks (Sutra and Manatschal, 2012; Cowie et al., 2015). In contrast, serpentinized peridotite was drilled in 1068 ODP well (Whitmarsh et al., 1998) which was interpreted as serpentinized exhumed mantle (Sutra and Manatschal, 2012; Cowie et al., 2015). Given the close proximity between the 1068 and 900 ODP wells (Figure 5a), we determine the COB between these two well positions. Note that we suggest only a single COB location along this section and thus this represents both the inner (COB-1) and the outer (COB-2) COB positions (Figure 5). The thinning factor from gravity

anomaly inversion (Figure 5b) can also be used to constrain COB location. The analysis by Cowie et al., (2015) along the TGS/LG12 seismic profiles showed that where "normal" magmatic solution of thinning factor first reaches 1.0 corresponds to hyper-extended crust which extends at least 50 km oceanwards. This is consistent with the COB location based on the ODP well data on the TGS/LG12 seismic profile.

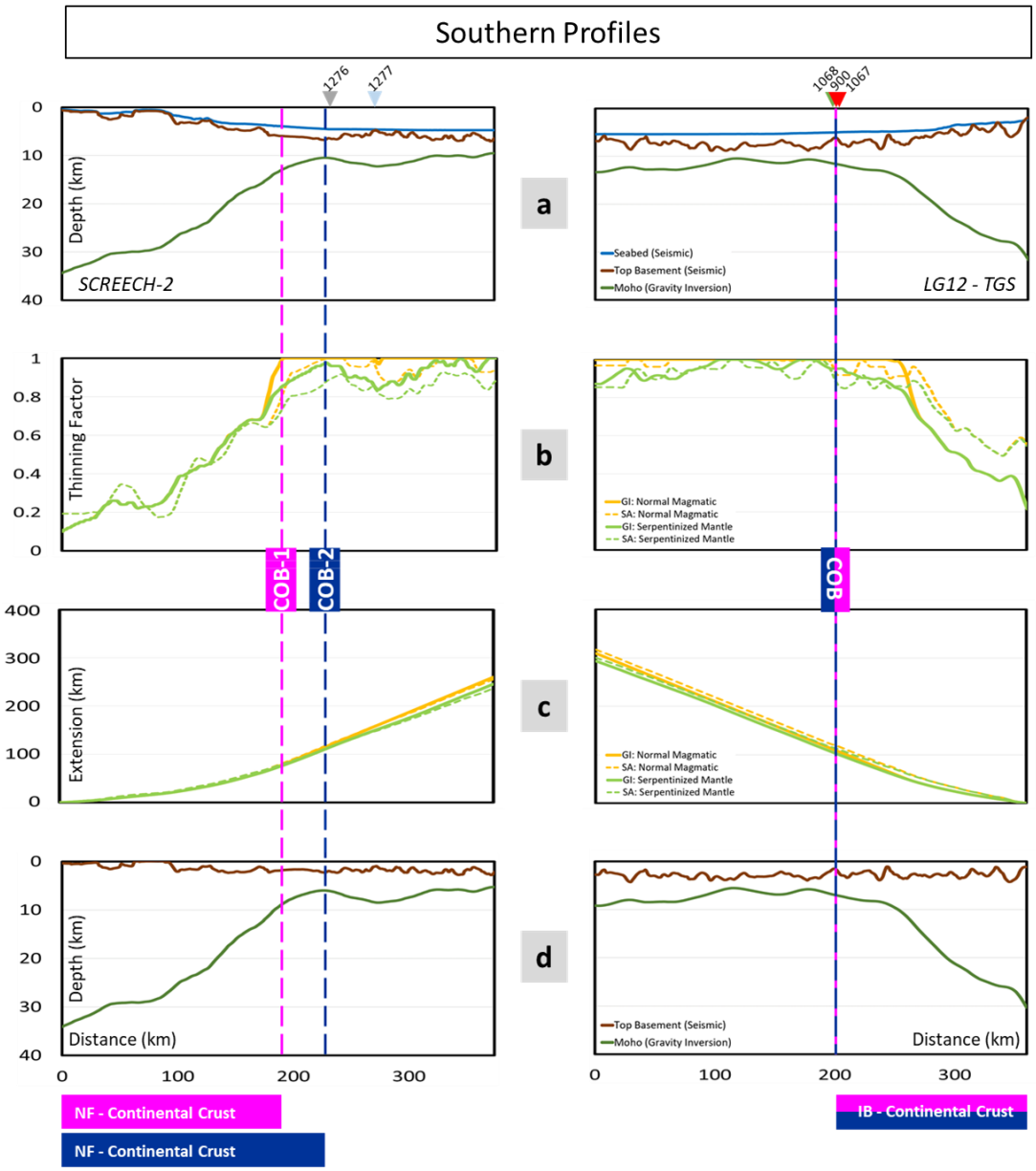

Figure 5: Pink and blue lines show the inner (COB-1) and outer (COB-2) distal end of continental curst. **a)-d)** Same as in Figure 4 but for the southern profiles.

4.2. Extension estimates from gravity anomaly inversion and subsidence analysis

Figures 4c and 5c summarize extension estimates along Iberia and Newfoundland conjugate margins obtained by the integration of thinning factor from gravity anomaly inversion and subsidence analysis previously shown in Figures 2 and 3. For completeness, we show the restored bathymetry and Moho depths for the Iberia and Newfoundland conjugate margins at breakup time for the northern (Figure 4d) and southern profiles (Figure 5d). This is achieved by the flexural backstripping of the sediment load, sediment decompaction and reverse post-rift thermal subsidence modelling (Kusznir et al., 1995; Roberts et al., 1998).

We use the inner and outer COB locations previously defined and produce two cross-sections showing the restored bathymetry of Iberia and Newfoundland margins at the breakup time along the northern (Figure 6) and the southern (Figure 7) profiles. To achieve this, we use the restored top basement and Moho horizons between the proximal edge of continental crust and the COB locations (Figure 4d and 5d).

Note that to remove the effect of post-breakup uplift on the Newfoundland margin (e.g. Crosby et al., 2008), both top-basement and Moho are deepened by 500 m prior to produce the restored bathymetry cross-sections at the time of breakup shown in Figures 6 and 7. A summary of the continental lithosphere (subsidence analysis) and continental crustal (gravity anomaly inversion) extension required to produce continental crustal breakup is shown in Figures 6 and 7. The amount of extension that continental lithosphere and continental crust have undergone depends on the COB location. The two extension values shown for each quantitative technique corresponds to the "normal" magmatic addition and the serpentinized mantle solution used to compute the thinning factor (see section 3.1 for further detail).The averaged values of total continental lithosphere extension and continental crust extension are also shown.

Our results for the northern profile using the COB-1 location show that continental crust was extended by 173 km whereas continental lithosphere 179 km (Figure 6a). In contrast,using the COB-2 location indicates that continental crust was extended by 250 km while continental lithosphere 252 km (Figure 6b). The results for the southern profile using a COB-1 location suggest that continental crust was extended by 179 km

while continental lithosphere 194 km (Figure 7a), while using the COB-2 location, continental crust was extended by 215 km and continental lithosphere 227 km (Figure 7b). Our preferred COB location is COB-1 on the basis of ODP data for the Iberia margin and evidenced from gravity inversion and subsidence analysis thinning factor profiles for the Newfoundland margin.

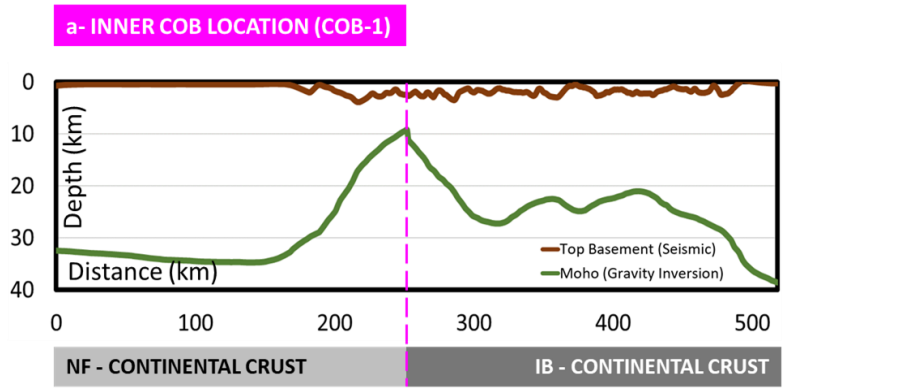

	Extension_SCREECH-1	Extension_ISE-01	*Total Extension (NF-IB)*
Continental crust (GI)	62 – 64 km	109 – 111 km	173 km
Continental lithosphere (SA)	67 – 69 km	111 – 111 km	179 km

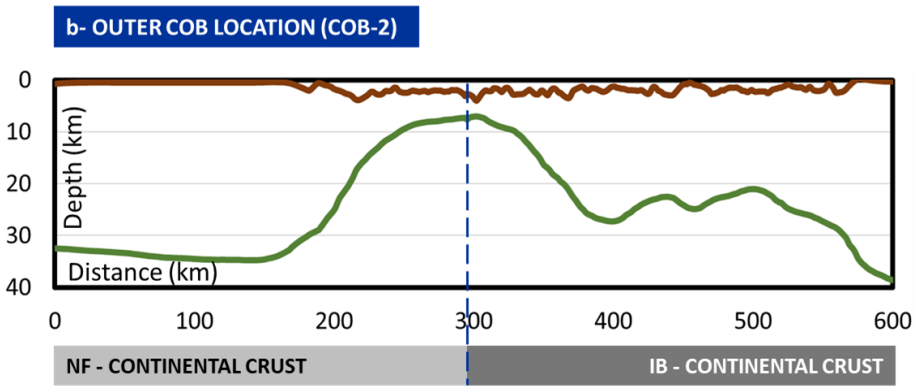

	Extension_SCREECH-1	Extension_ISE-01	*Total Extension (NF-IB)*
Continental crust (GI)	99 – 106 km	145 – 150 km	250 km
Continental lithosphere (SA)	101 – 109 km	145 – 148 km	252 km

Figure 6: **a-b)** Bathymetry and Moho depths for the northern Iberia and Newfoundland profiles restored to the breakup time (top). Continental crust extension (GI: Gravity Inversion) and continental lithosphere extension (SA: Subsidence Analysis) required to produce continental crustal breakup (bottom).

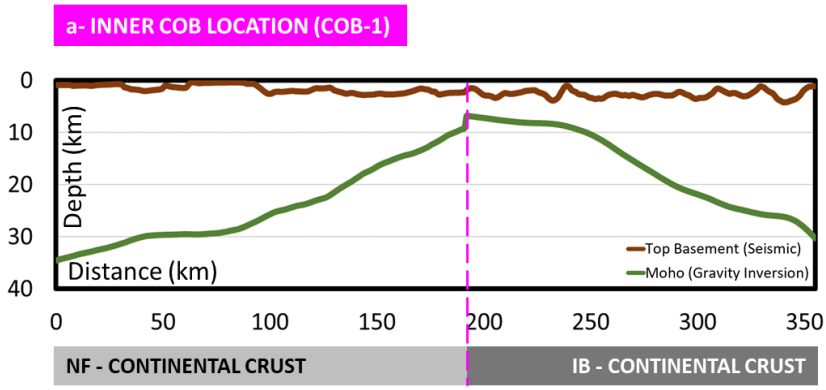

	Extension_SCREECH-2	Extension_TGS/LG12	*Total Extension (NF-IB)*
Continental crust (GI)	75 – 77 km	100 – 106 km	179 km
Continental lithosphere (SA)	79 – 81 km	111 – 117 km	194 km

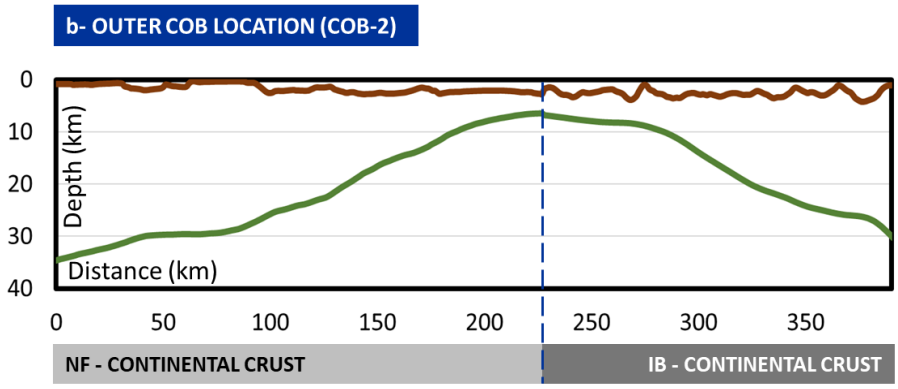

	Extension_SCREECH-2	Extension_TGS/LG12	*Total Extension (NF-IB)*
Continental crust (GI)	110 – 114 km	100 – 106 km	215 km
Continental lithosphere (SA)	110 – 116 km	111 – 117 km	227 km

Figure 7: Same as in Figure 6 but for the southern Iberia and Newfoundland profiles.

5. Observed brittle continental crust extension from seismic observations

We determine the observed brittle extension that continental crust has undergone between the proximal edge of continental crust and its distal end using the inner COB locations (COB-1) defined in section 4.1. To achieve this, we measure the horizontal displacement of the interpreted faults along the northern (Figure 8) and the southern (Figure 9) seismic profiles. Interpretation of seismic data is often non-unique and hence leads to more than one possible geological scenario.

Figure 8b shows the Northern Profiles Seismic Interpretation-1 (NPSI-1) while Figures 9b and 9c show the Southern Profiles Seismic Interpretation-1 (SPSI-1) and the Southern Profiles Seismic Interpretation-2 (SPSI-2) respectively. The NPSI-1 and SPSI-1 seismic interpretations are constrained using classic extensional faults (i.e. steep and planar faults) identified by the offset of the top pre-rift. The NPSI-1 seismic interpretation suggests that brittle continental crust extension of the Newfoundland margin is 36 km while for the Iberia margin it is 83 km (Table 1). In contrast, the SPSI-1 seismic interpretation indicates that brittle continental crust extension of the Newfoundland margin is 48 km while for the Iberia margin it is 68 km (Table 2).

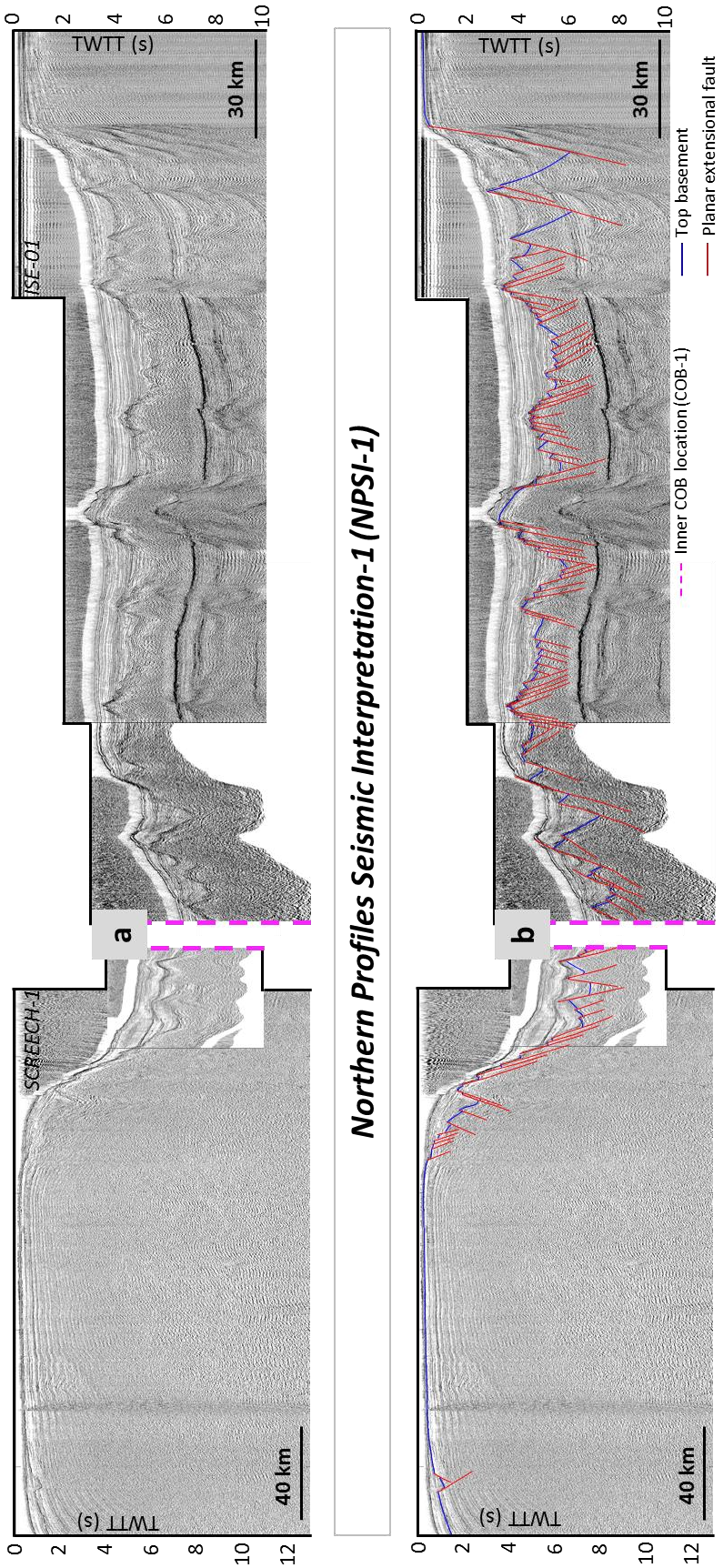

Figure 8: Northern seismic lines up to the inner-COB location (pink line) defined in this study. **a)** SCREECH-1 and ISE-01 seismic profiles (Funck et al., 2003; Zelt et al., 2003). **b)** Seismic interpretation (NPSI-1) of SCREECH-1 and ISE-01 (top basement and extensional faults are shown).

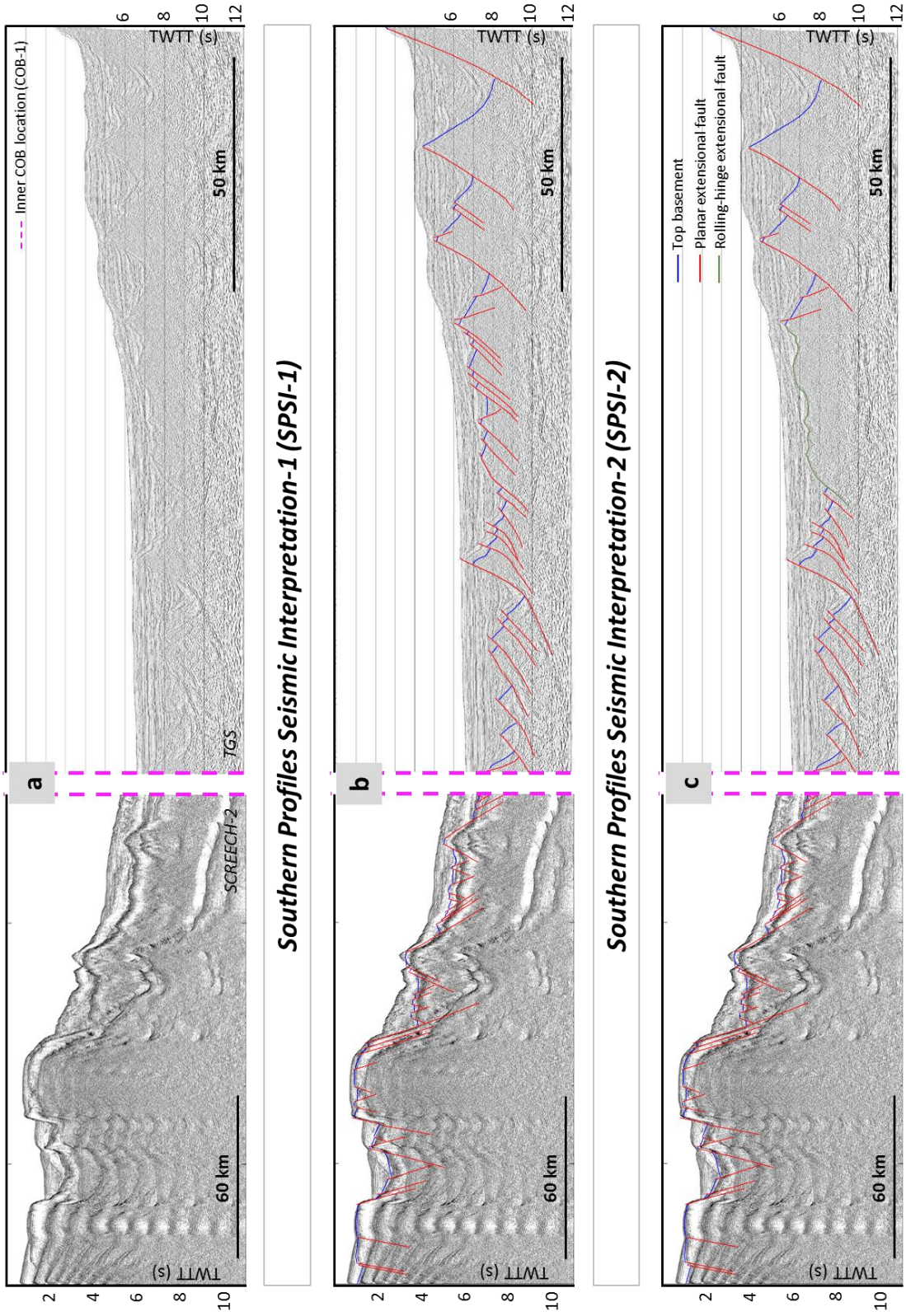

Figure 9: Southern seismic lines up to the inner-COB location (pink line) defined in this study. **a)** SCREECH-2 and TGS seismic profiles (Shillington et al., 2006; Sutra and Manatschal, 2012). **b)** Seismic interpretation (SPSI-1) of SCREECH-2 and TGS (top basement and extensional faults are shown). **c)** Seismic interpretation (SPSI-2) of SCREECH-2 and TGS (top basement and extensional faults are shown).

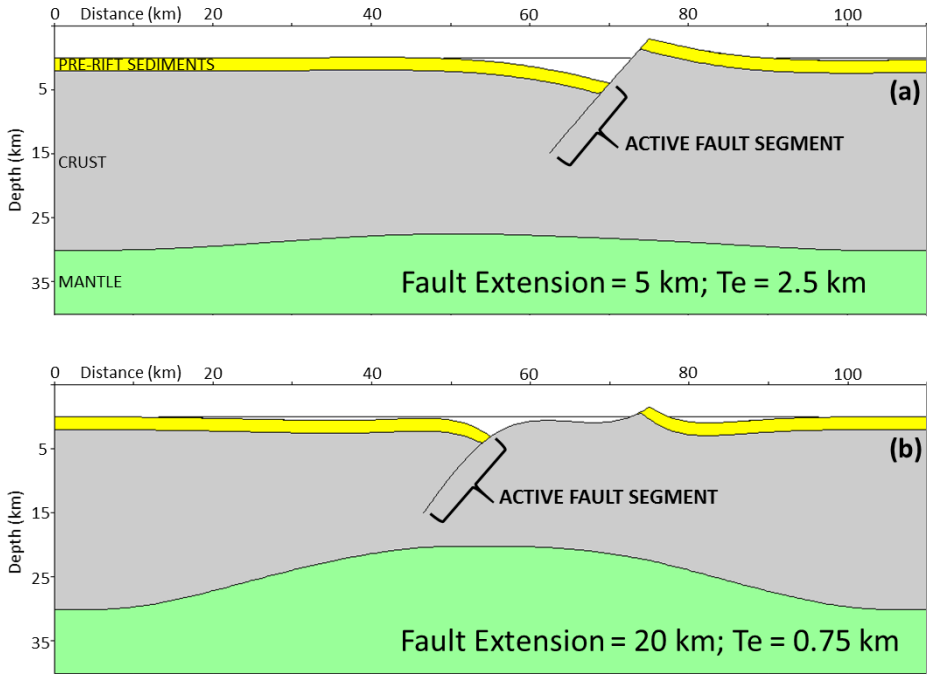

Figure 10: Stretch kinematic model showing the lithosphere isostatic response to extensional faulting and crustal thinning. **a)** Planar extensional fault. **b)** Rolling-hinge extensional fault. Fault extension and effective elastic thickness (Te) parameters vary for each fault type.

Figure 10a shows a classic extensional fault geometry which is typical of continental rifting settings (e.g. Stein and Barrientos, 1985; Jackson, 1987). Faults heaves are usually less than 10 km and the lithosphere effective elastic thickness is typically 1.5-3 km for continental rifting (Roberts et al., 1998; White, 1999; Roberts et al., 2019). The SPSI-2 seismic interpretation is similar to the SPSI-1 seismic interpretation except for part of the Iberia necking domain where a large extensional fault exhuming footwall that is subsequently re-faulted is used instead of steep and planar faults. The SPSI-2 seismic interpretation suggests that the brittle continental crust extension is 87 km for the Iberia margin while 48 km for the Newfoundland margin (Table 2). The large extensional fault within the Iberia necking domain is consistent with the rolling-hinge extensional-type faulting which requires large heaves (>10 km) and leads to extensive exhumation of their footwall block and a sub-horizontal sea-bed (Buck, 1988). Figure 10b shows a rolling-hinge extensional-type fault with 20 km of extension and a low lithosphere effective elastic thickness (0.75 km) typically required to form this type of structures.

Northern Profiles Seismic Interpretation-1 (Newfoundland)		
Faults numbers	Faults heaves (km)	Total extension (km)
1	1.9	36
2	1.6	
3	0.8	
4	0.3	
5	0.3	
6	0.6	
7	0.7	
8	0.8	
9	0.6	
10	2.2	
11	0.7	
12	1.9	
13	3.1	
14	2.1	
15	3.7	
16	0.8	
17	4.6	
18	0.8	
19	0.3	
20	1.9	
21	1.4	
22	1.5	
23	1.2	
24	1.3	
25	0.9	

Northern Profiles Seismic Interpretation-1 (Iberia)		
Faults numbers	Faults heaves (km)	Total extension (km)
1	7.7	83
2	0.4	
3	5.8	
4	1.4	
5	0.9	
6	1.5	
7	1.3	
8	0.3	
9	0.4	
10	1.8	
11	0.3	
12	0.3	
13	0.4	
14	0.6	
15	1.3	
16	1.0	
17	0.7	
18	0.7	
19	1.2	
20	0.3	
21	0.9	
22	1.2	
23	0.8	
24	0.6	
25	0.3	
26	0.4	
27	0.2	
28	0.1	
29	0.9	
30	0.7	
31	1.2	
32	0.9	
33	1.9	
34	0.7	
35	0.2	
36	1.4	
37	0.5	
38	1.0	
39	0.5	
40	0.8	
41	0.6	
42	0.4	
43	1.9	
44	0.5	
45	0.4	
46	0.5	
47	1.6	
48	0.5	
49	0.5	
50	0.3	
51	0.4	
52	0.4	
53	0.7	
54	0.9	
55	0.6	
56	0.9	
57	0.3	
58	0.4	
59	0.1	
60	0.4	
61	0.7	
62	0.4	
63	1.6	
64	0.8	
65	1.4	
66	3.8	
67	3.6	
68	0.9	
69	5.1	
70	0.5	
71	2.9	
72	0.9	
73	0.8	
74	4.3	

Table 1: Horizontal faults heaves for the northern profiles using the NPSI-1. Fault number 1 is the more proximal one.

The NPSI-1 seismic interpretation for the northern Iberia-Newfoundland profiles suggests that the continental crust has undergone 119 km of brittle extension. In contrast, the two seismic interpretations for the southern Iberia-Newfoundland profiles (SPSI-1 and SPSI-2) indicate 116 km and 135 km of brittle continental crust extension respectively.

Southern Profiles Seismic Interpretation-1 & 2 (Newfoundland)		
Faults numbers	Fault heaves (km)	Total extension (km)
1	0.5	48
2	0.4	
3	0.2	
4	2.4	
5	0.6	
6	0.7	
7	1.2	
8	0.4	
9	0.2	
10	2.1	
11	0.3	
12	0.7	
13	0.7	
14	0.3	
15	0.7	
16	0.7	
17	6.5	
18	0.9	
19	0.7	
20	0.4	
21	0.7	
22	0.7	
23	1.6	
24	1.0	
25	7.3	
26	1.7	
27	0.7	
28	0.9	
29	0.3	
30	0.3	
31	0.5	
32	0.4	
33	0.4	
34	2.0	
35	7.3	
36	0.6	
37	1.0	
38	0.4	

Southern Profiles Seismic Interpretation-1 (Iberia)		
Faults numbers	Faults heaves (km)	Total extension (km)
1	9.9	68
2	6.0	
3	0.3	
4	1.1	
5	0.4	
6	6.5	
7	0.2	
8	0.2	
9	1.3	
10	1.1	
11	0.9	
12	0.8	
13	1.2	
14	1.9	
15	0.5	
16	1.3	
17	0.6	
18	6.3	
19	1.5	
20	0.9	
21	0.4	
22	0.4	
23	0.3	
24	6.5	
25	0.5	
26	0.4	
27	1.4	
28	6.6	
29	4.5	
30	3.4	
31	0.4	

Southern Profiles Seismic Interpretation-2 (Iberia)		
Faults Numbers	Faults heaves (km)	Total extension (km)
1	9.9	87
2	6.0	
3	0.3	
4	1.1	
5	0.4	
6	6.5	
7	0.2	
8	0.2	
9	34.8	
10	1.5	
11	0.9	
12	0.4	
13	0.4	
14	0.3	
15	6.5	
16	0.5	
17	0.4	
18	1.4	
19	6.6	
20	4.5	
21	3.4	
22	0.4	

Table 2: Horizontal faults heaves for the southern profiles using the SPSI-1 and SPSI-2. Fault number 1 is the more proximal one.

6. Fault population analysis to explore sub-seismic faulting

We carry out a fault population analysis to explore whether there may be sub-seismic resolution faulting and if this may significantly contribute to an under-estimation of brittle crustal extension. This analysis determines the proportionof faults which have displacements too small to be imaged by seismic reflection data (e.g. Walsh et al., 1991; Marrett and Allmendinger, 1992;Gauthier and Lake, 1993; Pickering et al., 1997; Ackerman et al., 2001). Figure 11a shows a generalised example from Ackerman et al., (2001) illustrating the statistical expression of sampling artifacts and cumulative frequency analysis. The sampling artifacts consist of both data censoring because of the limited sampling area and data truncation because of non-imaged faults below the resolution of the seismic reflection data (Pickering et al., 1995). Two cumulative frequency curves are shown (Figure 11a); a power-law distribution that plots as a straight line in log-log space excluding the sampling artifacts and an exponential distribution that plots as a curved line in log-log space including the sampling artifacts. The idealised fault distribution shown by the cumulative frequency analysis consists of a central steep segment with negative gradient representing the average fault population. At large heaves it shows data censoring while for low heaves it shows data truncation (Walsh et al., 1991; Ackerman et al., 2001). The slope of a power-law distribution curve, gives the fractal dimension and is usually between -0.7 and -0.9 suggesting that a proportion of faults are not being seismically observed (Walsh et al., 1991) whereas an exponential distribution type indicates that the majority of faults are being seismically observed (e.g. Ackerman et al., 2001)

Our fault population analysis is carried out using the interpreted faults on the NPSI-1 (Figures 11b-c), SPSI-1 (Figures 11d-e) and SPSI-2 (Figures 11f-g) seismic interpretations to determine the amount of missing extension due to sub-seismic resolution faulting. The distribution of the sampled faults along the northern seismic profiles (NPSI-1 seismic interpretation) apparently fits with an exponential curve rather than a power-law relationship (Figure 11b-c). However, the relationship distribution between the sampled faults and the exponential curve does not show the same pattern as suggested by Ackerman et al., (2001). Our results show that the central data and truncation data fit perfectly well with the exponential curve while the censoring data is above the predicted frequency curve. The misfit between the data and

the exponential distribution curve suggests that a power-law frequency needs to be considered. However, a power-law relationship gives a fractal dimension higher than 1 which is a non-physical solution because the total extension would be greater than the length of the profile.

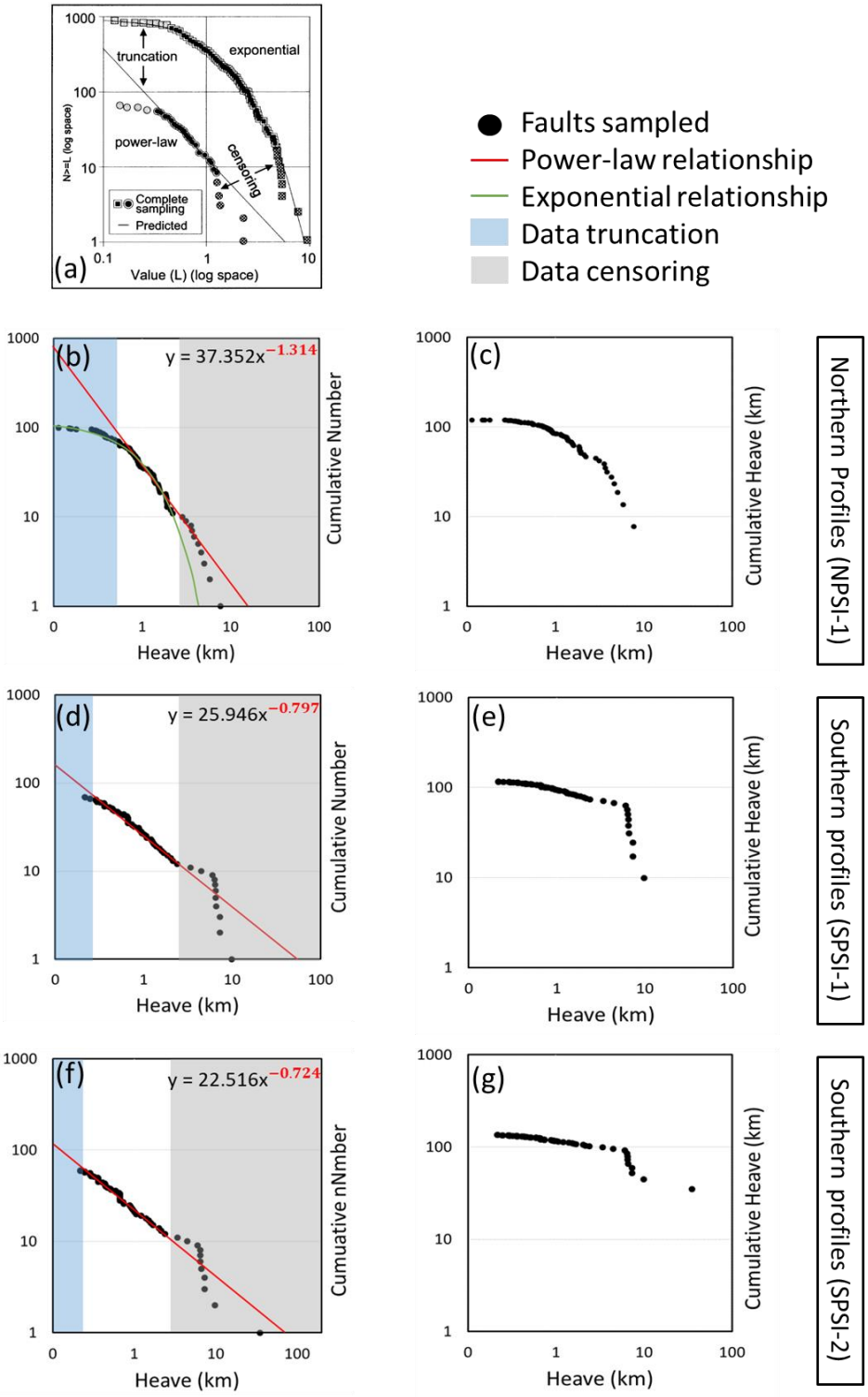

Figure 11: **a)** Exponential and power-law cumulative frequencies and sampling artifacts distribution from Ackermann et al., (2001). **b-g)** Results of the fault population analysis showing cumulative number versus faults heaves and cumulative heave respect to faults heaves. **b)** A power-law and an exponential frequency curves fitting the sampled faults using the NPSI-1. **d)** and **f)** A power-law frequency curve fitting the sampled faults using the SPSI-1 and SPSI-2 respectively. Equation for the power-law curve is shown for **b)**, **d)** and **f)** (red value is the fractal dimension).

The faults sampled along the northern profiles cannot be uniquely represented by either an exponential or power-law distribution frequency. A possible interpretation of the fault population analysis for the northern profiles is that there may be two distinct fault populations, possibly because the faulting within the Galicia Interior Basin has a different age to that of breakup (Jeanniot et al., 2016). Another possible explanation of the fault population analysis for the northern profiles is an imperfect interpretation on old seismic data. Regardless of the reason we are not able to reliably estimate the amount of sub-seismic relation faulting and we consider the northern profiles inconclusive for comparing fault extension with extension from crust and lithosphere thinning.

The sampled faults along the southern seismic profiles (SPSI-1 and SPSI-2 seismic interpretations) show a distribution that appears to match with a power-law frequency curve (Figures 11d-g). However, the data censoring segment at large heaves does not show the same pattern as suggested by Ackerman et al., (2001) instead the censored data plots above the extrapolated power-law curve. This may suggest that two distinct fault populations are also present for the southern profiles and/or it may indicate an imperfect interpretation on old seismic data. Despite this, the overall trend of fault data appears to fit with a power-law frequency curve which allows us to obtain the fractal dimension from which the contribution of sub-seismic fault resolution can be determined. Fractal dimension values for the SPSI-1 and SPSI-2 seismic interpretations are -0.8 and -0.7. Following Walsh et al., (1991), these values indicate that between 20-35% of faulting extension is not being seen on the seismic reflection data.

7. Discussion

In this section we summarise our results and discuss the amount of brittle crustal extension and total continental lithosphere and crust extension required to produce continental crustal breakup.

7.1. Extension estimates required for continental crustal breakup

Subsidence analysis, gravity inversion and fault heave summation from seismic observations have been used to determine total continental lithosphere extension, total continental crust extension and brittle continental crust extension respectively required to produce continental crustal breakup (Figure 12). These measurements have been made between the proximal continental crust and its distalmost edge (COB-1 location defined in this study) along the northern and the southern conjugate profiles of Iberia and Newfoundland margins.

Results from quantitative techniques suggest that continental lithosphere was extended by 179 km along the northern profiles and 194 km along the southern profiles while continental crust was extended by 173 km and 179 km along the northern and southern profiles respectively (Figures 12). These measurements from gravity inversion and subsidence analysis are very similar between them and indicate that continental lithosphere and continental crust are required to be extended 186 km and 176 km (~ 181 km in average), along the northern and southern profiles respectively, to produce continental crustal breakup. This is comparable with extension estimates obtained by Jeanniot et al., (2016) (~168 km) however, it is substantially lower than that suggested by Sutra et al., (2013) (~242 km).

Results from observed fault heave summation based on seismic observations indicate that the brittle continental crust was extended by 119 km using the NPSI-1 seismic interpretation along the northern profiles. For the southern profiles, observed fault extension is 116 km using the SPSI-1 seismic interpretation and 135 km using the SPSI-2 seismic interpretation (Figure 12). These results show that the observed fault extension is less than the calculated extension for the whole continental crust and lithosphere. If material is conserved then we would expect the thinning and stretching of the brittle continental crust by extensional faulting, and that of the whole continental

crust and lithosphere, by combined extensional faulting and deeper distributed pure-shear deformation, to be the same. Therefore, an apparent extension discrepancy at the scale of the whole conjugate margin system is observed when fault heave summation is compared with lithosphere and crust extension (Figure 12).

Figure 13 compares the cumulative extension from proximal to COB-1 location for extension derived from integrated crustal thinning and that from fault heave summation. It highlights the apparent extension discrepancy at the COB-1 location for the restored Iberia-Newfoundland margins to breakup. Along both the northern and the southern profiles, a similar cumulative extension pattern is observed between the proximal continental crust and the COB-1 location.

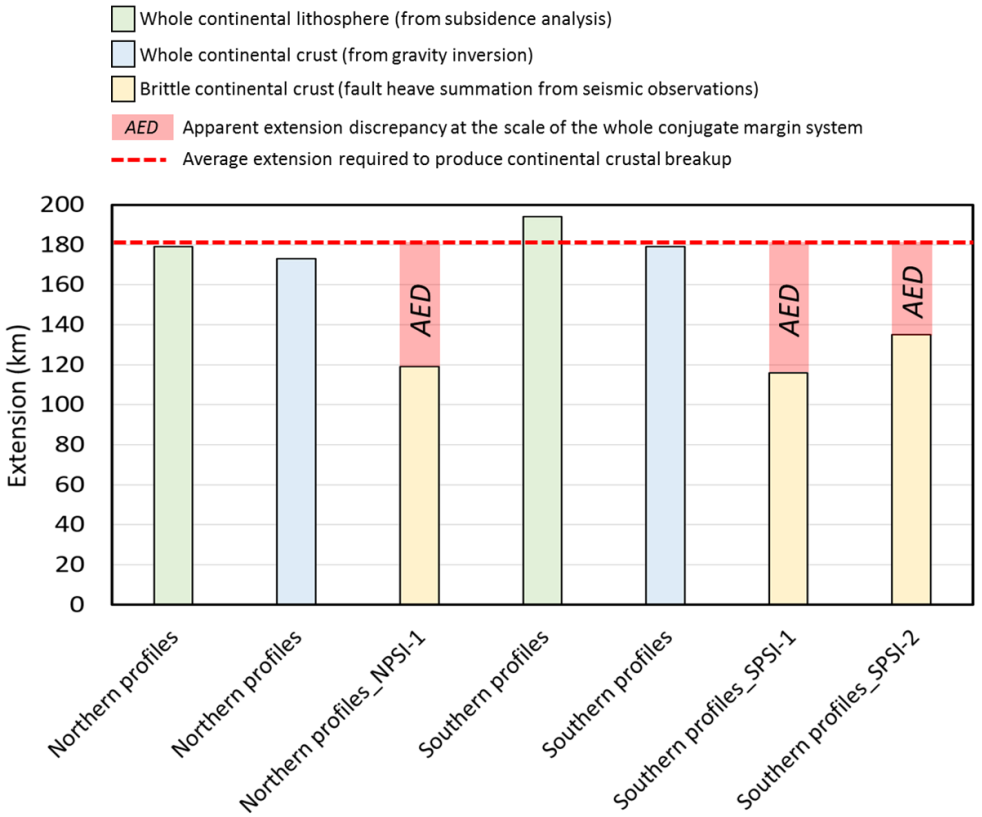

Figure 12: Summary of the extension estimates required to produce continental crustal breakup along the southern and northern profiles.

This is characterized by an increase of both whole continental crust extension and observed brittle continental crust extension towards the COB-1 location. Interestingly, the difference between the observed cumulative fault heave summation and the

integrated extension from crustal thinning decreases towards the COB-1 location (Figure 13).

Results from fault population analysis carried out in this study show that is important to include sub-seismic resolution fault extension when comparing fault heave summation with lithosphere and crust extension. Failing to do that, it may lead to an apparent extension discrepancy at the scale of the whole conjugate margin system. This is clearer for the southern profiles where the overall trend of faults sampled appear to fit with a power-law curve leading to a fractal dimension value between -0.8 and -0.7 which indicates that between 20-35% of faulting extension is not observed (e.g. Walsh et al., 1991; Ackermann et al., 2001). Extension from seismically observed fault heave summation along the southern profiles is between 116 km (using the SPSI-1 seismic interpretation) and 135 km (using the SPSI-2 seismic interpretation). Including both observed and sub-seismic resolution brittle faulting (estimated as 35%), the fault heave summation would increase to 157 and 182 km for the SPSI-1 and SPSI-2 seismic interpretations respectively. Our preferred seismic interpretation is SPSI-2 which is consistent with the result obtained from quantitative techniques and altogether suggests that, on average, continental lithosphere, continental crust and brittle continental crust are required to be extended by approximately 181 km to produce continental crustal breakup.

Therefore, allowing for fault extension at sub-seismic resolution an extension discrepancy at the scale of the whole conjugate margin system does not appear to exist.

7.2. Depth-dependent stretching and thinning

Comparing the cumulative extension from proximal to COB-1 derived from integrated crustal thinning and fault heave summation, it can be seen that within the proximal margin the brittle continental crust is less extended than that of the whole continental crust (Figure 13). This observation corresponds to Depth-Dependent Stretching and Thinning (DDST) of continental lithosphere (e.g. Roberts et al., 1997; Driscoll and Karner, 1998; Baxter et al., 1999; Davis and Kusznir, 2004; Kusznir et al., 2004). DDST refers to the difference between the brittle continental crust extension and the whole continental crust extension at a specific location. Note that DDST does not mean and should not be confused with a discrepancy at the scale of the margin.

A rifted margin evolves from an intra-continental rift and thus typical features from early extensional lithosphere deformation are expected to exist within rifted margins.

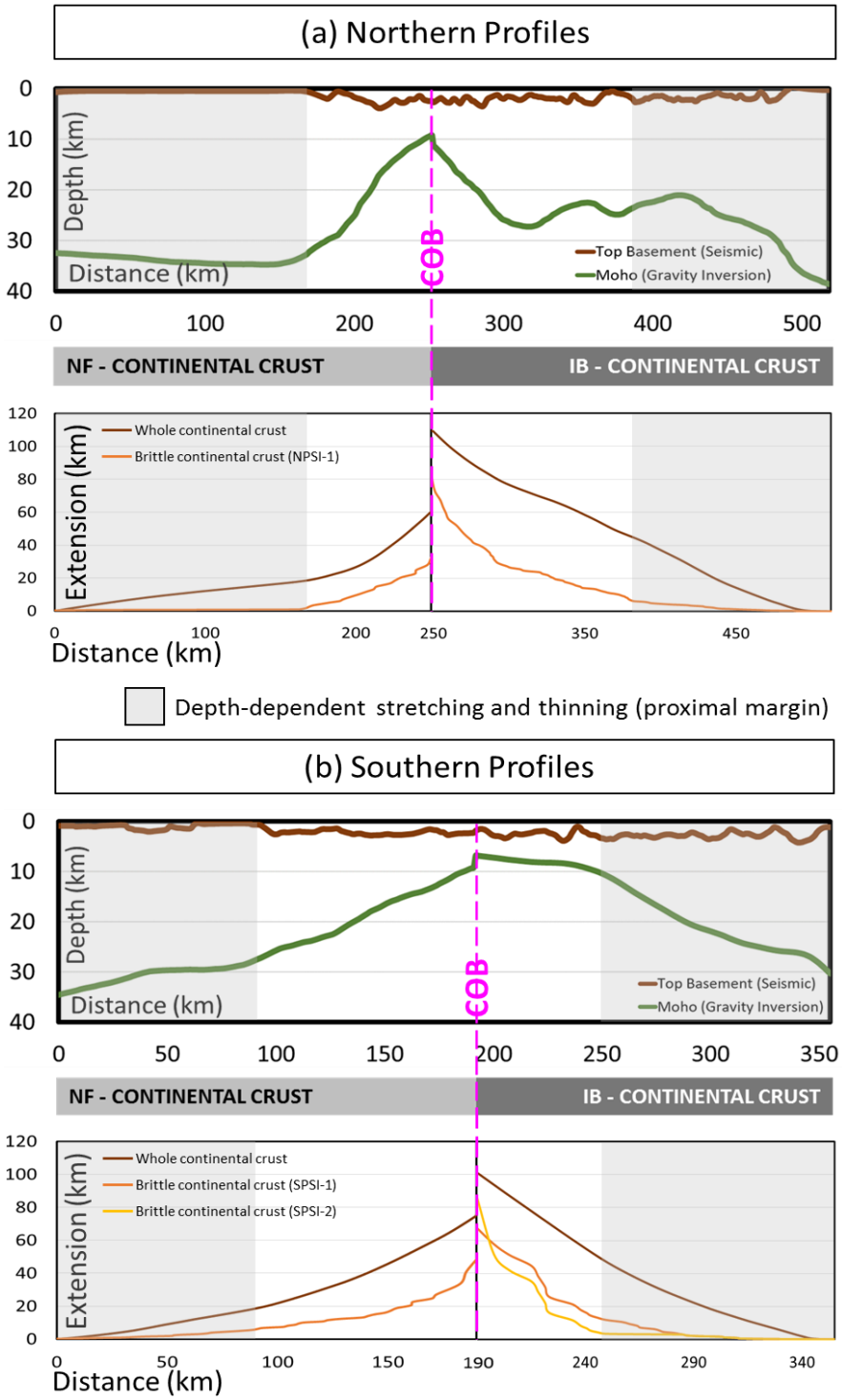

Figure 13: **a)-b)** Bathymetry and Moho depths for the Iberia and Newfoundland margins restored to the breakup time (top). Comparison between cumulative extension from proximal to COB, from integrated crustal thinning and fault heave summation (bottom).

While minor lithosphere extension may laterally extend over many 100s of km, intra-continental rift basins typically have widths of 50-75 km (Kusznir and Ziegler, 1992). Their lithosphere deformation is achieved by extensional faults within the upper crust underlain by deeper distributed deformation within the lower crust and upper mantle (Figure 14). While the upper continental crust deformation may be localized within an area of 50-75 km wide, the deeper distributed lithosphere deformation associated with an intra-continental rift is expected to be much wider (Kusznir et al., 1991).

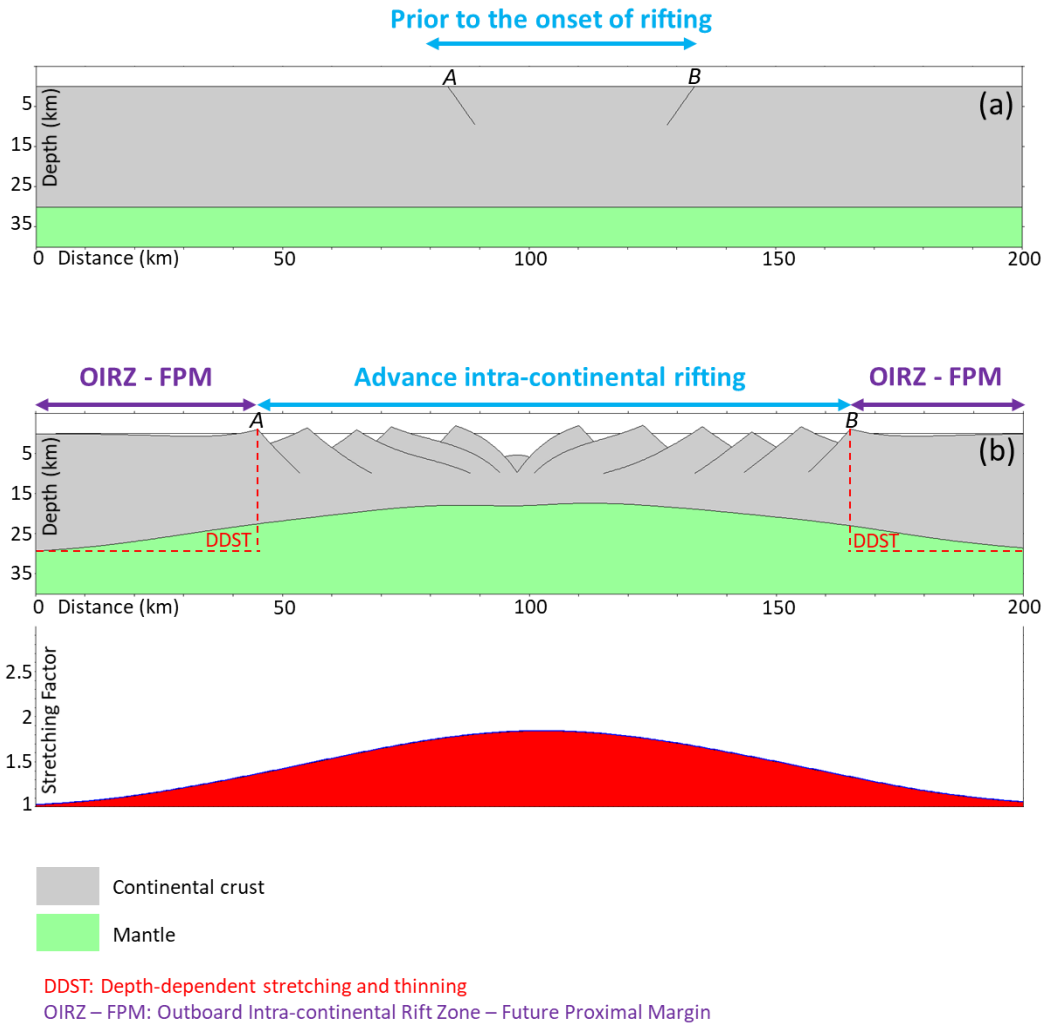

Figure 14: Stretch kinematic model showing an intra-continental rift formation. **a)** Lithosphere architecture prior to the onset of rifting. **b)** An advance stage of intra-continental rifting showing depth-dependent stretching and thinning (DDST). The stretching profiles is also shown. Note that where DDST occurs, continental crust is being thinned without any extensional fault within the upper crust.

As a consequence, within the outboard zones of an intra-continental rift, continental crust is thinned and stretched without extensional faulting within the upper crust (i.e.

DDST). This is illustrated in Figure 14b. The proximal and necking domains of rifted margins corresponds to an old outboard zone of an intra-continental rift, therefore present-day measurements of the whole continental crust extension are expected to be larger than that of the brittle continental crust extension (i.e. DDST) (Figure 13).

DDST is to be expected within the proximal and necking domains of a rifted margin and should not be confused with an extension discrepancy at the scale of the whole conjugate margin system (Roberts et al., 1997 and Davis and Kusznir, 2004 provide an example of this from mid-Norway). However, uniform stretching and thinning may occasionally be the main mechanism of the early stages of rifting as observed in the Corinth Rift (Central Greece) and the Halten Terrace (offshore mid Norway) (e.g. Bell et al., 2011; Bell et al., 2014 and references therein).

7.3. Uncertainties on determining brittle fault extension

When determining whether a discrepancy between the observed fault heave summation and lithosphere/crust extension at the scale of the whole conjugate system exists or not, two uncertainties should be addressed; (i) fault geometries and (ii) the COB location.

Fault geometries

Interpretation of seismic data is often non-unique and therefore it may lead to more than one interpreted geological scenario. For the southern profiles of Iberia and Newfoundland conjugate margins, two seismic interpretations have been proposed. Indeed, results from fault heave summation using only planar faults (SPSI-1) or a large rolling-hinge fault and planar faults (SPSI-2) provide substantially different amounts of observed brittle crustal extension (Figure 12). Note that usually rolling-hinge faults increase the amount of brittle crustal extension and therefore failing to recognize them may lead to an apparent extension discrepancy at the scale of the whole conjugate margin system. Our preferred seismic interpretation is SPSI-2, as pointed out above, and emphasizes the importance of rolling-hinge extensional faults within the necking zones of rifted margins where continental crust is thinned from 25 km thick to less than 10 km. How this extreme thinning occurs is a current debated topic but the

presence of rolling-hinge faults may play an important role during the necking rifting stage.

Results from the fault population analysis, show that the overall trend of faults sampled, along the southern profiles, appear to fit with a power-law frequency curve however, an unexpected pattern at large fault heaves for data censoring is observed. This unexpected pattern where censored data clearly plots above rather than below the extrapolated power-law line, may indicate the presence of two or more fault populations. These populations could correspond to; (i) the presence of two types of fault geometries (planar and rolling-hinge) and/or (ii) two different fault coupling levels (faults decoupled from and coupled into the mantle).

The fault population statistics for the northern profiles, cannot be represented with a unique frequency curve which may indicate the presence of two or more fault populations. Faulting within the older Galicia Interior Basin is expected to be decoupled from the mantle while the younger faulting associate with breakup is expected to be both decoupled and coupled into the mantle.

COB location

To determine the location of the distalmost continental crust is ambiguous and as a consequence two possible COB positions have been proposed in this study which in turn out correspond to the boundaries of a zone in which the COB location could be placed anywhere within it. To measure lithosphere and crust extension as well as fault heave summation from seismic data we use the COB-1 location as the distal end of continental crust. The difference between the observed cumulative fault heave summation and the integrated extension from crustal thinning decreases towards the COB-1 location (Figure 13). This is expected because if volume is conserved then we would assume the brittle continental crust extension (i.e. extensional faulting) and the whole continental crust extension (i.e. extensional faulting and deeper distributed pure-shear deformation) to be the same. From our fault population analysis, we show that this applies when sub-seismic faulting is considered and included.

Along the Newfoundland margin, the difference between the observed cumulative fault heave summation and the extension from integrated crustal thinning is higher than along the Iberia margin (Figure 13). This may indicate that the distal end of

continental crust on the Newfoundland margin may be more distal than the COB location used in this study. Note that a more distal COB location would increase both the fault heave summation as well as the whole continental crust extension.

7.4. Alternative processes that may occasionally generate an apparent extension discrepancy

Alternative processes that might generate an apparent extension discrepancy at the scale of the whole conjugate margin are non-brittle extension and continued thinning of continental crust after continental crustal breakup occurs.

Non-brittle extension might be achieved through either dyking (extremely rare at magma-poor rifted margins) or non-brittle plastic deformation (Davis and Kusznir, 2004), but it has been suggested that the majority of upper continental crust deformation is accommodated by seismic slip on faults (Jackson and McKenzie, 1983; Jackson, 1987). An alternative possibility is that continental crust may be extended after continental crustal breakup occurs. This would be achieved by deeper lithosphere deformation associated with extensional faulting within exhumed continental mantle, however how this could be recognized is uncertain. Polyphase faulting has been proposed consisting of new faults cutting across existing back-rotated and abandoned fault systems leading to complex fault geometries which are difficult to recognize on seismic data (e.g. Reston 2005; Reston and Dermott, 2014). Re-faulting of exhumed fault footwall however can be observed and is accounted for in the fault heave summation. Measured fault extension corrected for sub-seismic resolution faulting suggests that these additional mechanisms are not required to match extension from crustal and lithosphere thinning.

8. Conclusions

This study focuses on determining the extension that the whole-lithosphere, whole-continental crust and the brittle continental crust have undergone to produce continental crustal breakup. The key conclusions are the following:

1- To achieve continental crustal breakup, approximately 181 km of extension are required. This value may be applied to other conjugate rifted margins with similar crustal inheritance and rheology, obliquity and margin width, magmatic

additions and extension rate to the Iberia-Newfoundland conjugate rifted margins.

2- An apparent extension discrepancy at the scale of the whole conjugate margin system is seen when observed fault heave summation is compared with extension from crust and lithosphere thinning.
3- Allowing for fault extension at sub-seismic resolution (up to 35%), an extension discrepancy at the scale of the whole conjugate margin system does not exist. In addition to sub-seismic faulting, fault geometries and the location of the distalmost continental crust are important issues that need to be carefully considered when comparing fault heave summation and extension from crust and lithosphere thinning.
4- Failing to recognize rolling-hinge faults may lead to an under-estimate of fault extension.
5- Depth-dependent stretching and thinning (DDST) is observed and expected within the proximal and necking domains of rifted margin. DDST should not be confused with an extension discrepancy at the scale of the whole conjugate margin system.

We believe that our results are not exclusive for the Iberia-Newfoundland conjugate margins example and should be considered to better understand continental crustal breakup of any other pair of conjugate rifted margins.

Acknowledgments

We acknowledge the MM4 (Margin Modelling Phase 4) industry partners (BP, Conoco Phillips, Statoil, Petrobras, Total, Shell, BHP-Billiton, and BG) for financial support and discussions.

REFERENCES

Ackermann, R. V, Schlische, R.W., Withjack, M.O., 2001. The geometric and statistical evolution of normal fault systems: an experimental study of the effects of mechanical layer thickness on scaling laws. J. Struct. Geol. 23, 1803–1819.

Alvey, A., Gaina, C., Kusznir, N.J., Torsvik, T.H., 2008. Integrated crustal thickness mapping and plate reconstructions for the high Arctic. Earth Planet. Sci. Lett. 274, 310–321. https://doi.org/10.1016/j.epsl.2008.07.036.

Baxter, K., Cooper, G.T., Hill, K.C., O'Brien, G.W., 1999. Late Jurassic subsidence and passive margin evolution in the Vulcan Sub-basin, north-west Australia: Constraints from basin modelling. Basin Res. 11, 97–111. https://doi.org/10.1046/j.1365-2117.1999.00088.

Bell, R.E., Mcneill, L.C., Henstock, T.J., Bull, J.M., 2011. Comparing extension on multiple time and depth scales in the Corinth Rift , Central Greece. Geophys. J. Int. 186, 463–470. https://doi.org/10.1111/j.1365-246X.2011.05077.Bell, R.E., Jackson, C.A., Elliott, G.M., Gawthorpe, R.L., Sharp, I.R., Michelsen, L., 2014. Insights into the development of major rift-related unconformities from geologically constrained subsidence modelling: HaltenTerrace, offshore mid Norway. Basin Res. 26, 203–224. https://doi.org/10.1111/bre.12049.

Beslier, M.O., 1996. Data report: Seismic line LG12 in the Iberia Abyssal Plain in Whitmarsh, R.B., Sawyer, D.S., Klaus, A., and Masson, D.G. (Eds.). Proc. Ocean Drill. Program, Sci. Results 149, 737–739.

Bronner, A., Sauter, D., Manatschal, G., Péron-Pinvidic, G., Munschy, M., 2011. Magmatic breakup as an explanation for magnetic anomalies at magma-poor rifted margins. Nat. Geosci. 4, 461–461.

Buck, W.R., 1988. Flexural Rotation of Normal Faults. Tectonics 7, 959–973.

Carlson, R.L., Herrick, C.N., 1990. Densities and porosities in the oceanic crust and their variations with depth and age. J. Geophys. Res. 95, 9153–9170. https://doi.org/10.1029/JB095iB06p09153.

Chappell, A.R., Kusznir, N.J., 2008. Three-dimensional gravity inversion for Moho

depth at rifted continental margins incorporating a lithosphere thermal gravity anomaly correction. Geophys. J. Int. 174, 1–13. https://doi.org/10.1111/j.1365-246X.2008.03803.

Christensen, N.I., Mooney, W.D., 1995. Seismic velocity structure and composition of the continental crust: a global view. J. Geophys. Res. 100, 9761–9788. https://doi.org/10.1029/95JB00259.

Cowie, L., Kusznir, N., Manatschal, G., 2015. Determining the COB location along the Iberian margin and Galicia Bank from gravity anomaly inversion, residual depth anomaly and subsidence analysis. Geophys. J. Int. 203, 1355–1372. https://doi.org/10.1093/gji/ggv367

Crosby, A., White, N., Edwards, G., Shillington, D.J., 2008. Evolution of the Newfoundland – Iberia conjugate rifted margins. Earth Planet. Sci. Lett. 273, 214–226. https://doi.org/10.1016/j.epsl.2008.06.039.

Davis, M., Kusznir, N., 2004. Depth-dependent lithospheric stretching at rifted continental margins. In: Karner, G.D. (ed). Proc. NSF Rift. Margins Theor. Institute. Columbia Univ. Press. New York 92–136. https://doi.org/10.7312/karn12738-005.

Driscoll, N.W., Karner, G.D., 1998. Lower crustal extension across the Northern Carnarvon basin, Australia: Evidence for an eastward dipping detachment. J. Geophys. Res. 103, 4975–4991.

Funck, T., Hopper, J.R., Larsen, H.C., Louden, K.E., Tucholke, B.E., Holbrook, W.S., 2003. Crustal structure of the ocean-continent transition at Flemish Cap : Seismic refraction results. J. Geophys. Res. 108, 2531. https://doi.org/10.1029/2003JB002434.

Gauthier, B.D.M., Lake, S.D., 1993. Probabilistic modeling of faults below the limit of seismic resolution if Pelican Field, North Sea, Offshore United Kingdom. Am. Assoc. Pet. Geol. Bull. 77, 761–777.

Gozzard, S., Kusznir, N., Franke, D., Cullen, A., Reemst, P., Henstra, G., 2018. South China Sea crustal thickness and oceanic lithosphere distribution from satellite gravity inversion. Pet. Geosci.

https://doi.org/https://doi.org/10.1144/petgeo2016-162.

Greenhalgh, E.E., Kusznir, N.J., 2007. Evidence for thin oceanic crust on the extinct Aegir Ridge, Norwegian Basin, NE atlantic derived from satellite gravity inversion. Geophys. Res. Lett. 34, 1–5. https://doi.org/10.1029/2007GL029440.

Jackson, J., McKenzie, D., 1983. The geometrical evolution of normal fault systems. J. Struct. Geol. 5, 471–482. https://doi.org/10.1016/0191-8141(83)90053-6.

Jackson, J., 1987. Active normal faulting and crustal extension. Geol. Soc. London, Spec. Publ. 28, 3–17. https://doi.org/10.1144/GSL.SP.1987.028.01.02.

Jeanniot, L., Kusznir, N., Mohn, G., Manatschal, G., Cowie, L., 2016. Constraining lithosphere deformation modes during continental breakup for the Iberia-Newfoundland conjugate rifted margins. Tectonophysics 680, 28–49. https://doi.org/10.1016/j.tecto.2016.05.006.

Jordan, T.H., Anderson, D.L., 1974. Earth Structure from Free Oscillations and Travel Times. Geophys. J. R. Astron. Soc. 36, 411–459. https://doi.org/10.1111/j.1365-246X.1974.tb03648.

Kusznir, N.J., Marsden, G., Egan, S.S., 1991. A flexural-cantilever simple-shear/pure-shear model of continental lithosphere extension: applications to the Jeanne d'Arc Basin, Grand Banks and Viking Graben, North Sea. Geol. Soc. London, Spec. Publ. 56, 41–60. https://doi.org/10.1144/gsl.sp.1991.056.01.04.

Kusznir, N.J., Ziegler, P.A., 1992. The mechanics of continental extension and sedimentary basin formation : A simple-shear / pure-shear flexural cantilever model. Tectonophysics 215, 117–131.

Kusznir, N.J., Roberts, A.M., Morley, C.K., 1995. Forward and reverse modelling of rift basin formation. Geol. Soc. London, Spec. Publ. 80, 33–56. https://doi.org/10.1144/gsl.sp.1995.080.01.02.

Kusznir, N.J., Hunsdale, R., Roberts, A.M., 2004. Timing of depth-dependent lithosphere stretching on the S. Lofoten rifted margin offshore mid-Norway: Pre-breakup or post-breakup? Basin Res. 16, 279–296. https://doi.org/10.1111/j.1365-2117.2004.00233.

Kusznir, N.J., Karner, G.D., 2007. Continental lithospheric thinning and breakup in response to upwelling divergent mantle flow: application to the Woodlark, Newfoundland and Iberia margins. Geol. Soc. London, Spec. Publ. 282, 389–419. https://doi.org/10.1144/SP282.16.

Kusznir, N.J., Roberts, A.M., Alvey, A.D., 2018. Crustal structure of the conjugate Equatorial Atlantic Margins, derived by gravity anomaly inversion. Geol. Soc. London, Spec. Publ. SP476.5. https://doi.org/10.1144/sp476.5.

Manatschal, G., 2004. New models for evolution of magma-poor rifted margins based on a review of data and concepts from West Iberia and the Alps. Int. J. Earth Sci. 93, 432–466. https://doi.org/10.1007/s00531-004-0394-7.

Marrett, R., Allmendinger, R.W., 1992. Amount of extension on "small'' faults: an example from the Viking graben." Geology 20, 47–50.

Mckenzie, D., 1978. Some Remarks on Development of Sedimentary Basins. Earth Planet. Sci. Lett. 40, 25–32.

Mohn, G., Karner, G., Manatschal, G., Johnson, C., 2015. Structural and stratigraphic evolution of the Iberia and Newfoundland hyper-extended rifted margins: A quantitative modeling approach. Sediment. Basin Crustal Process. Cont. Margins From Mod. Hyper-extended Margins to Deform. Anc. Analog. 16, 9156. https://doi.org/10.1144/SP413.9.

Müller, R.D., Roest, W.R., Royer, J.-Y., Gahagan, L.M., Sclater, J.G., 1997. Digital isochrons of the world's ocean floor. J. Geophys. Res. 52, 3211–3214. https://doi.org/10.2337/diabetes.52.7.1655.

Parker, R.L., 1972. The rapid calculation of potential anomalies. Geophys. J. R. Astron. Soc. 31, 447–455.

Péron-Pinvidic, G., Manatschal, G., Minshull, T.A., Sawyer, D.S., 2007. Tectonosedimentary evolution of the deep Iberia-Newfoundland margins: Evidence for a complex breakup history. Tectonics 26, 1–19. https://doi.org/10.1029/2006TC001970.

Pickering, G., Bull, J.M., Sanderson, D.J., 1995. Sampling power-law distributions.

Tectonophysics 248, 1–20. https://doi.org/10.1016/0148-9062(96)80040-4.

Pickering, G., Peacock, D.C.P., Sanderson, D.J., Bull, J.M., 1997. Modeling Tip Zones to Predict the Throw and Length Characteristics of Faults. Am. Assoc. Pet. Geol. Bull. 81.

Reston, T., Mcdermott, K., 2014. An assessment of the cause of the "extension discrepancy" with reference to the west Galicia margin. Basin Res. 26, 135–153. https://doi.org/10.1111/bre.12042.

Reston, T.J., 2005. Polyphase faulting during the development of the west Galicia rifted margin. Earth Planet. Sci. Lett. 237, 561–576. https://doi.org/10.1016/j.epsl.2005.06.019.

Roberts, A.M., Lundin, E.R., Kusznir, N.J., 1997. Subsidence of the Vøring Basin and the influence of the Atlantic continental margin. J. Geol. Soc. London 154, 551–557. https://doi.org/10.1144/gsjgs.154.3.0551.

Roberts, A.M., Kusznir, N.J., Yielding, G., Styles, P., 1998. 2D flexural backstripping of extensional basin: the need for a sideways glance. Pet. Geosci. 4, 327–338. https://doi.org/10.1144/petgeo.4.4.327.

Roberts, A.M., Kusznir, N.J., Corfield, R.I., Thompson, M., Woodfine, R., 2013. Integrated tectonic basin modelling as an aid to understanding deep-water rifted continental margin structure and location. Pet. Geosci. 19. https://doi.org/10.1144/petgeo2011-046.

Roberts, A.M., Alvey, A.D., Kusznir, N.J., 2018. Crustal structure and heat-flow history in the UK Rockall Basin , derived from backstripping and gravity-inversion analysis. Pet. Geosci. https://doi.org/https://doi.org/10.1144/petgeo2017-063.

Roberts, A.M., Kusznir, N.J., Yielding, G., Beeley, H., 2019. Mapping the bathymetric evolution of the northern North Sea: from Jurassic syn-rift archipelago through Cretaceous-Tertiary post-rift subsidence. Pet. Geosci.

Russell, S.M., Whitmarsh, R.B., 2003. Magmatism at the west Iberia non-volcanic rifted continental margin: Evidence from analyses of magnetic anomalies.

Geophys. J. Int. 154, 706–730. https://doi.org/10.1046/j.1365-246X.2003.01999.

Sandwell, D.T., Smith, W.H.F., 2009. Global marine gravity from retracked Geosat and ERS-1 altimetry: Ridge segmentation versus spreading rate. J. Geophys. Res. Solid Earth 114, 1–18. https://doi.org/10.1029/2008JB006008.

Sawyer, D.S., Whitmarsh, R.B., Klaus, A., Party, S.S., 1994. Proceedings of the Ocean Drilling Program, Initital Repts., 149,. Coll. Station. TX (Ocean Drill. Program).

Sclater, J.G., Christie, P.A.F., 1980. Continental stretching: an explanation of the post-mid-Cretaceous subsidence of the central North Sea Basin. J. Geophys. Res. 85, 3711–3739.

Shillington, D.J., Holbrook, W.S., Van Avendonk, H.J.A., Tucholke, B.E., Hopper, J.R., Louden, K.E., Larsen, H.C., Nunes, G.T., 2006. Evidence for asymmetric nonvolcanic rifting and slow incipient oceanic accretion from seismic reflection data of the Newfoudland margin. J. Geophys. Res. Solid Earth 111. https://doi.org/10.1029/2005JB003981.

Smith, R.A., 1961. A uniqueness theorem concerning gravity fields. Math. Proc. Cambridge Philos. Soc. 57, 865–870.

Smith, W.H., Sandwell, D., 1997. Global sea floor topography from satellite altimetry and ship depth soundings. Science (80-.). 277, 1956–1962.

Stein, R.-S., Barrientos, S.-E., 1985. Planar High-Angle Faulting in the Basin and Range: Geodetic Analysis of the 1983 Borah Peak, Idaho, Earthquake. J. Geophys. Res. 90, 11,355-11,366.

Steinberg, J., Roberts, A.M., Kusznir, N.J., Schafer, K., Karcz, Z., 2018. Crustal structure and post-rift evolution of the Levant Basin. Mar. Pet. Geol. 96, 522–543. https://doi.org/10.1016/j.marpetgeo.2018.05.006.

Sutra, E., Manatschal, G., 2012. How does the continental crust thin in a hyperextended rifted margin? Insights from the iberia margin. Geology 40, 139–142. https://doi.org/10.1130/G32786.1.

Sutra, E., Manatschal, G., Mohn, G., Unternehr, P., 2013. Quantification and restoration of extensional deformation along the Western Iberia and

Newfoundland rifted margins. Geochemistry, Geophys. Geosystems 14, 2575–2597.

Walsh, J., Watterson, J., Yieldingt, G., 1991. The importance of small-scale faulting in regional extension. Nature 351.

White, R., McKenzie, D., 1989. Magmatism at Rift Zones - the Generation of Volcanic Continental Margins and Flood Basalts. J. Geophys. Res. Earth Planets 94, 7685–7729.

White, R.S., 1999. The lithosphere under stress. Philos. Trans. R. Soc. A Math. Phys. Eng. Sci. 357, 901–915. https://doi.org/10.1098/rsta.1999.0357.

Whitmarsh, R.B., 1998. Proceedings of the Ocean Drilling Program, Initial Reports, vol. 173, Ocean Drill. Program, College Station, Tex.

Zelt, C.A., Sain, K., Naumenko, J. V, Sawyer, D.S., 2003. Assessment of crustal velocity models using seismic refraction and reflection tomography. Geophys. J. Int. 609–626.

CHAPTER 3

Chapter 3: in preparation for a scientific publication

The geometry and evolution of extensional faults within hyperthinned continental crust leading to mantle exhumation at magma-poor rifted margins

Júlia Gómez-Romeu[1], Nick Kusznir[1,2], Alan Roberts[2]

[1]*Department of Earth, Ocean and Ecological Sciences, University of Liverpool, Liverpool, UK*

[2]*Badley Geoscience Ltd, Spilsby, UK*

Abstract

Over the last 20 years the formation of magma-poor rifted margins has been intensively studied, however many questions still remain. In particular, what is the geometry of active extensional faulting and how does it evolve within the distal rifted margins. We examine this for continental crustal thinning within the hyperthinned domain, the formation of continental allochthon blocks within the exhumed mantle domain and the transition between the hyperthinned and exhumed mantle domains. To investigate this, we use a lithosphere deformation model (RIFTER) which includes the flexural isostatic response to extensional faulting, resulting in flexural isostatically compensated as well as balanced lithospheric cross-sections. Our numerical experiments are guided by the first-order seismic observations of the Western Iberia distal rifted margin. We do not aim to reproduce the precise present-day structural architecture of the Iberia margin but rather to examine from a general viewpoint how extensional faults control the structural architecture of distal rifted margins.

Our modelling results show that the hyperthinned domain is formed by faults with relatively low offsets that couple into the mantle. However it is uncertain whether these faults are listric or planar because both produce very similar structural topography and crustal architecture. A listric fault geometry produces a sub-horizontal structure beneath the hyperthinned crust consisting of an inactive rotated extensional fault. Both

listric and planar fault geometries produce a Moho that would be indistinguishable on seismic reflection data or from the inactive rotated extensional fault of the listric model.

Extensional faulting within the exhumed mantle domain initiation is characterized by a large offset rolling-hinge fault (i.e. a master fault) that may be followed by a set of new high-angle, short-cut faults branching from the master fault producing allochthon blocks (Buck, 1988). It is uncertain whether the master fault soles out horizontally at depth with a listric geometry or is a steep planar fault. Each allochthon block overlies a sub-horizontal inactive older fault that due to flexural isostasy substantially rotates during the development of subsequent allochthon blocks.

The transition zone between the hyperthinned and exhumed mantle domains may be characterized by; (i) a large rolling-hinge in-sequence fault leading to a sub-horizontal sea-bed or (ii) low offset out-of-sequence faults leading to a distal ridge made up of mantle and crustal rocks.

To better understand extensional faulting at magma-poor rifted margins it is crucial to consider the flexural isostatic rotation of faults.

1. Introduction

The distal part of magma-poor rifted margins is characterized by two rift domains (e.g. Péron-Pinvidic et al., 2013; Tugend et al., 2014); (i) the hyperthinned domain characterized by very thin continental crust (~ 10 km) and (ii) the exhumed mantle domain characterized by serpentinized mantle with locally triangular pieces of continental crust (i.e. allochthon blocks).

Within the hyperthinned domain, continental crust is less than 10 km thick (Manatschal et al., 2001) and fully brittle allowing faults to penetrate through the entire crust and down into the mantle (Pérez-Gussinyé et al., 2001; Manatschal, 2004; Péron-Pinvidic et al., 2007). This leads to a crustal architecture characterized by a set of oceanwards tilted continental crustal fault blocks often underlain by a low-angle sub-surface structure, imaged on seismic, the role of which has been intensively debated (e.g. Krawczyk et al., 1996; Reston et al., 1996). Within the exhumed mantle domain,

allochthon blocks are believed to be fault blocks generated by a process consistent with the rolling-hinge model of Buck (1988).

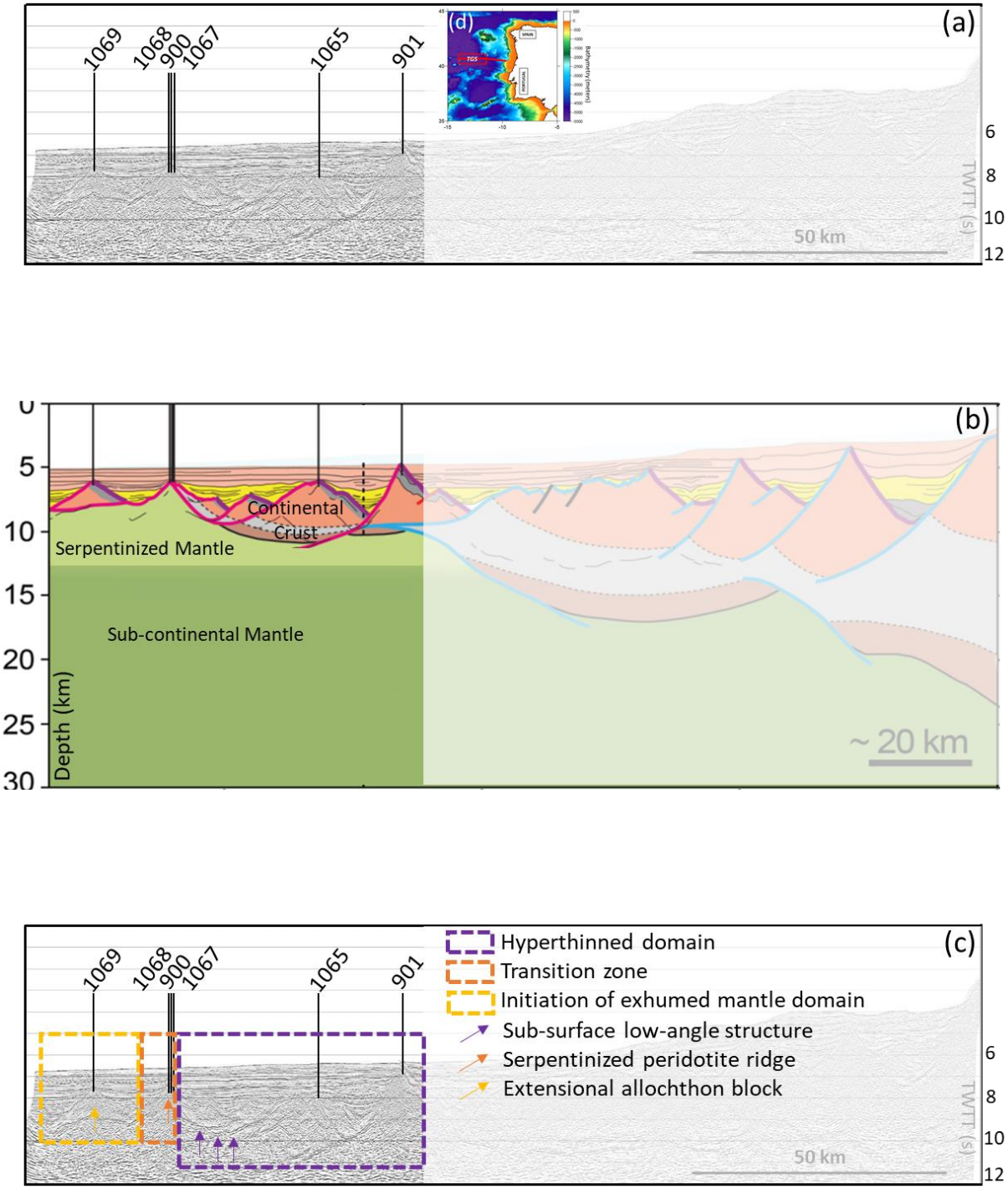

***Figure 1*: a)** The distal Western Iberia margin along the TGS seismic line (Sutra and Manatschal et al., 2012) showing the ODP wells positions (black lines). **b)** Interpretation of the seismic line shown in Figure 1a by Sutra et al., (2013). **c)** Same as shown in Figure 1a but highlighting the hyperthinned domain, transition zone and initiation of exhumed mantle domain together with the first-order seismic observations used in this study. **d)** Bathymetric map of the Iberia margin showing in red the position of TGS seismic profile.

In the transition between these hyperthinned and exhumed mantle domains, the first mantle exposed sometimes takes the form of a peridotite ridge and may be topographically higher than the fault blocks within the hyperthinned domain (e.g. Péron-Pinvidic et al., 2007; Sutra et al., 2013). Pérez-Gussinyé (2013) suggested that this occurs because the mantle rises due to its buoyancy pushing the thinned crustal blocks apart. However an alternative possibility that needs to be investigated is whether these observed uplifted ridges may be formed by extensional tectonics.

We examine the active extensional fault geometry and how it evolves during continental crustal thinning within the hyperthinned domain, during the formation of crustal allochthon blocks within the exhumed mantle domain and during the transition between the hyperthinned and exhumed mantle domains.

To achieve our aim, we use a lithosphere deformation model (RIFTER) which includes the flexural isostatic response to extensional faulting, resulting in flexural isostatically compensated as well as balanced lithosphere cross-sections. We reproduce the transition between the hyperthinned domain and the initiation of the exhumed mantle domain using the first-order seismic observations of the Western Iberia distal rifted margin (Figure 1). We do not aim to reproduce the precise present-day structural architecture of the Iberia margin but rather to examine from a general viewpoint how extensional faults control the structural architecture of distal rifted margins.

Our results show that to better understand extensional faulting at magma-poor rifted margins it is crucial to consider the flexural isostatic rotation of faults.

2. Western Iberia distal rifted margin as an example

One of the best imaged and studied distal rifted margins is the Western Iberia margin. In particular, the structural segments of the Galicia Banks area to the north and the Iberia Abyssal Plain in the centre. Both structural zones have been intensively studied using drilling and seismic data (e.g. Boillot et al., 1987; Montadert et al., 1979; Beslier et al., 1993; Whitmarsh et al., 1993 and 2001; Krawczyk et al., 1996; Reston et al., 1996; Reston, 1996 and 2005; Manatschal et al., 2001; Manatschal, 2004; Péron-Pinvidic et al., 2007; Ranero and Pérez-Gussinyé, 2010; Pérez-Gussinyé, 2013; Sutra et al., 2013; Lymer et al., 2019). The distal Iberia margin architecture in the Iberia

Abyssal Plain consists of a set of tilted fault blocks underlain by a low-angle seismic reflector, a serpentinized peridotite ridge and extensional allochthon blocks (Figure 1).

Fault blocks underlain by a low-angle seismic reflector

Fault blocks within the hyperthinned domain appear to terminate at depth at a bright sub-horizontal seismic feature called the S reflector for the Galicia margin and H reflector for the Iberia Abyssal Plain (de Charpal et al., 1978; Krawczyk et al., 1996) (Figure 1c). The interpretation of these sub-horizontal seismic reflectors has been intensively debated (e.g. Reston et al., 1996). Interpretations suggested for these structures (H and S type-reflectors) are; the brittle-ductile transition (de Charpal et al., 1978), a detachment fault (Wernicke et al., 1981; Hoffmann and Reston, 1992; Sibuet, 1992; Reston et al., 1996), the top of a mafic underplate (Horsefield, 1992), a thin igneous intrusion (Reston, 1996) and a serpentinization front (Boillot et al., 1987). Despite this wide range of possible interpretations, after the work by Reston et al., (1996) and Krawczyk et al., (1996) it has been generally accepted that the H and S reflectors are detachment faults (Manatschal et al., 2001). However, a debate about whether these seismic features (H and S) were active sub-horizontally has been ongoing (e.g. Reston et al., 1996; Pérez-Gussinyé, 2013) and as a consequence the term detachment fault may be misleading. Pérez-Gussinyé, (2013) suggested that present-day detachment fault geometry such as the S reflector were never active at such low-angles. As faults form at a smaller spacing, the rotation of an active fault modifies the deepest geometry of the previous inactive fault. This process leads to the deep segment of an inactive fault plane passively rotating to a lower angle producing an overall listric fault geometry or even a sub-horizontal appearance. This occurs as a result of a sequential fault activity within a very thin (~10 km) brittle crust (Pérez-Gussinyé, 2013).

A serpentinized peridotite ridge

Oceanwards of the sub-horizontal reflectors (H and S) on the Iberian margin, a prominent ridge made up of serpentinized peridotite is observed. On the Iberia Abyssal Plain, this was drilled at ODP sites 900, 1067 and 1068 over Hobby High (Manatschal et al., 2001) and it was suggested that the drilled rocks were exhumed along a downward concave detachment fault to the seafloor (Péron-Pinvidic et al., 2007).

Manatschal et al., (2001) suggested that, within the ocean-continent transition, sub-horizontal structures exhuming mantle at the sea-floor correspond to downward concave detachment faults with large offsets (tens of kilometres). This is consistent with the rolling-hinge model of Buck (1988) suggesting that sub-horizontal sea-bed structures are formed by an active high-angle fault at depth associated with large fault offset. This leads to the exhumation of the fault footwall becoming sub-horizontal at the sea-bed due to flexural isostatic rotation.

Allochthon blocks

On the Iberia Abyssal Plain, extensional allochthon blocks or basement highs made of continental crust were drilled (Figure 1). Manatschal et al., (2001) suggested that these extensional allochthon blocks may be formed by the rolling-hinge model of Buck (1988).

We examine the active extensional fault geometry and how it evolves in these three distinct structural zones at the distal magma-poor rifted margins using RIFTER model.

3. RIFTER model

We use a numerical model (RIFTER) to reproduce the fault blocks geometry within the hyperthinned domain, the formation of crustal allochthon blocks within the exhumed mantle domain and the transition between the hyperthinned and exhumed mantle domains. RIFTER is a kinematic forward lithosphere deformation model that allows the production of flexural isostatically compensated as well as balanced cross-sections. Within RIFTER, lithosphere is deformed by faulting in the upper crust with underlying distributed pure-shear deformation in the lower crust and mantle. A key attribute of RIFTER is that it incorporates the flexural isostatic response to extensional faulting and crustal thinning. Therefore, RIFTER can be used to model and predict the structural development of extensional tectonic settings. The model is kinematically controlled with fault geometry and displacement and pure-shear distribution given as model inputs as a function of time. Lithosphere flexural strength, parameterised as lithosphere effective elastic thickness, is also defined. Model outputs are geological cross-sections which are flexural isostatically compensated as well as structurally balanced. The kinematic formulation of RIFTER represents an advantage over

dynamic modelling because the input data given to RIFTER can be constrained by observed geology. In addition, RIFTER provides for the isostatic testing of palinspastic cross-sections and can also be used to explore different kinematic scenarios. A more detailed description of the model formulation (originally called OROGENY) is given by Toth et al., (1996), Ford et al., (1999) and Jácome et al., (2003). These studies show the model formulation applied to compressional tectonics however similar physical principles apply for an extensional tectonics scenario.

3.1. Lithosphere effective elastic thickness

Within RIFTER, loads resulting from extensional lithosphere deformation are assumed to be compensated by flexural isostasy. These loads are generated by faulting, crustal thinning, sedimentation, erosion and lithosphere thermal perturbation and re-equilibration (Kusznir et al., 1991). For the purposes of calculating the flexural isostatic response, the lithosphere is represented as an elastic plate of effective elastic thickness (Te) floating on a fluid substratum.

The lithosphere effective elastic thickness (Te) is defined as the equivalent thickness of a perfectly elastic plate which has the same flexural strength as the lithosphere. Extension on major basement faults produces flexure which, as well as generating footwall uplift and hangingwall subsidence, gives rise to substantial bending stresses. Magnavita et al., (1994) showed the flexural bending stresses for a perfectly elastic plate of 20 km thick and how these are reduced by combined brittle and plastic failure. Therefore the flexural bending moment and the flexural strength of a perfectly elastic layer 20 km thick are reduced by an increase in brittle and plastic failure with extension so that the elastic thickness of this plate (T) is reduced to an effective elastic thickness (Te) that decreases with increase in extension (Magnavita et al., 1994).

It has been shown that the effective elastic thickness (Te) of extended lithosphere is less than 5 km assuming a brittle/seismogenic layer thickness governed by earthquake focal depths of approximately 15 km (e.g. Magnavita et al., 1994). The most geologically satisfactory results of lithospheric flexural models for continental rifting scenarios use Te values that range between 1.5 and 3 km (Roberts et al., 1998; White, 1999; Roberts et al., 2019). During more advanced rifting stages (e.g. hyperthinned continental crust) the lithosphere bending stresses are reduced due to high lithosphere

extension leading to a decrease of the flexural lithosphere strength. Therefore, in these tectonic settings, a low effective elastic thickness (Te) is expected and required to reproduce the consequences of lithosphere deformation due to extensional faulting.

We use a Te value of 0.5 km associated to each fault for the development of the transition between the hyperthinned domain and the initiation of exhumed mantle domain. This value is consistent to those calculated at slow-spreading ocean ridges ranging between 0.5 and 1 km (e.g. Smith et al., 2008; Schouten et al., 2010) where a similar lithosphere flexural strength to that of the distal rifted margins is expected.

The lithosphere flexural strength must be considered to understand the flexural rotation of faults and therefore to investigate their geometric evolution.

4. Modelling experiments: distal rifted margins

We use RIFTER model to constrain a set of 2D crustal cross-sections that show the evolution between the hyperthinned domain and the initiation of exhumed mantle domain formation.

The initial RIFTER model setup consists of horizontal layers with uniform thickness representing 25 km thick continental crust underlain by mantle (Figure 2a). We model the end of the necking rifting stage characterized by a rift basin of 100 km width showing substantial continental crust thinning and stretching (Figure 2b). How continental crust thins to ~10 km thick during the necking rifting stage is a different question out of the scope of this study. The extensional deformation during the necking rifting stage is achieved by extensional faults soling out at mid or lower crustal levels (Pérez-Gussinyé et al., 2001; Sutra et al., 2013). Figure 2b shows the resultant crustal thinning of this deformation stage achieved by depth-dependent stretching and thinning rather than by extensional faulting and deeper distributed deformation. This is a simplified model template that allows to explore the distal magma-poor rifted margin formation avoiding the complexity given by the earlier extensional faulting structures from continental and necking rifting stages. Figures 2c-e are different model templates showing the progressive formation of a distal rifted margin. The detail of these numerical experiments is shown below for the formation of the hyperthinned

domain, the initiation of the exhumed mantle domain and the transition between these two domains.

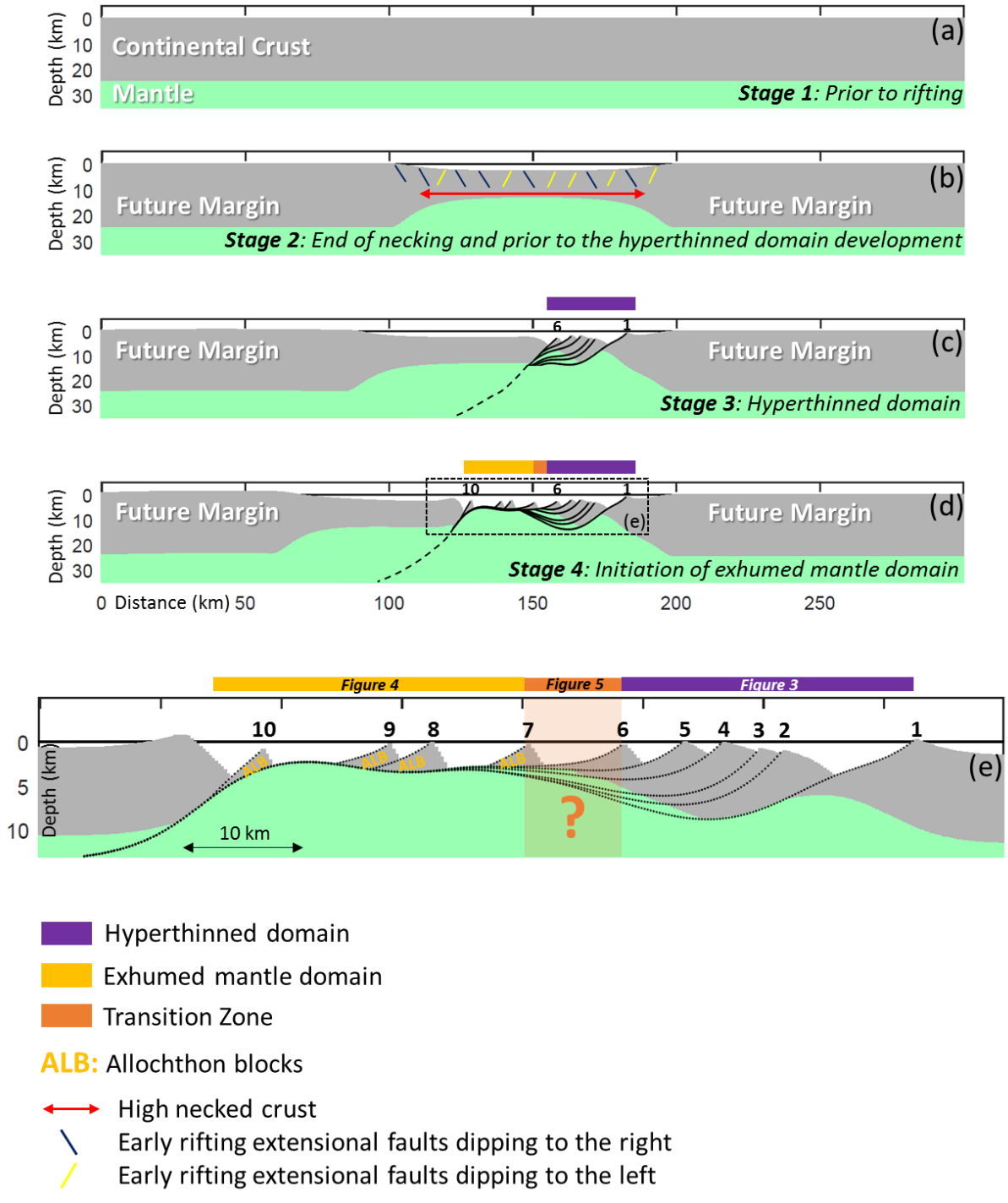

Figure 2: A generalized evolutionary RIFTER model showing how a distal rifted margin forms. **a)** Lithosphere architecture prior to rifting. **b)** Lithosphere architecture prior to the formation of hyper-extended domain (i.e. end of necking domain). **c)** Formation of hyperthinned domain. **d)** Transition zone and the initiation of exhumed mantle domain form. **e)** A zoom in on Figure 2d.

For simplicity purposes we only model the formation of a distal rifted margin and consider its distal conjugate as undeformed thin continental crust (~10 km) during our modelling experiment.

4.1. Uncertainties in deep fault geometry

Magma-poor rifted margins are formed by progressive lithosphere stretching and thinning leading to lithospheric breakup. This is achieved by brittle fault deformation within the upper lithosphere with distributed pure-shear deformation below. A key question is how faults connect to the deep distributed lithosphere deformation. Two possible scenarios may be; (i) through a sub-horizontal shear zone where faults sole out and beneath which distributed deformation occurs or (ii) through a diffusive process by which faults connect to the deep distributed deformation.

We use RIFTER to explore the structural consequences of these two tectonic scenarios during the formation of the hyperthinned and exhumed mantle domains assuming a brittle-ductile transition depth at 15 km (Figure 3). To reproduce a sub-horizontal shear zone we use a listric fault geometry characterized by an initial surface fault dipping 60° soling out horizontally at 15 km depth (Figures 3a-b). In contrast, to reproduce a diffusive evolution between extensional faults and the deep distributed deformation we use a listric fault geometry with an initial surface fault dipping 60° soling out horizontally in the deeper mantle (60 km depth for our case) allowing to simulate a planar fault geometry (Figures 3d-e). Our numerical results show that both a listric and planar fault geometry produce very similar structural topography and crustal architecture within the distal rifted margin but very different sub-surface fault geometries (Figures 3c and f). A listric fault geometry produces a sub-horizontal structure beneath the hyperthinned crust consisting of an inactive rotated extensional fault. Both listric and planar fault geometries produce a Moho that would be indistinguishable on seismic reflection data or from the inactive rotated extensional fault of the listric model.

4.2. Hyperthinned domain formation

The hyperthinned domain is characterized by a set of fault-continental blocks dipping oceanwards which appear to terminate at depth at a bright sub-horizontal seismic reflector (de Charpal et al., 1978; Krawczyk et al., 1996) (Figure 1).

Within this domain, continental crust is fully brittle and as a consequence faults penetrate through the entire crust and down into the mantle (Pérez-Gussinyé et al., 2001; Manatschal, 2004; Péron-Pinvidic et al., 2007). Therefore, to reproduce the hyperthinned and exhumed mantle domains using RIFTER we use extensional faults coupled into the mantle (Figures 4-5).

The initial RIFTER template used to reproduce the hyperthinned domain consists of 10 km horizontal and uniform thick continental crust underlain by mantle (central part of Figure 2b). To reproduce the hyperthinned domain we use a listric geometry for all modelled faults characterized by an initial surface fault dipping 60° soling out horizontally at 15 km depth. In addition we define the footwall break-away position and the horizontal displacement of each fault to reproduce the hyperthinned domain.

We first activate fault 1 with a horizontal displacement of 7 km. This deformation leads to an intense rotation and uplift of the footwall block resulting in the Moho dipping continentwards while the hangingwall block subsides (Figure 4a). We then generate faults 2, 3 and 4 with low fault offsets (0.5, 0.5 and 1.5 km respectively) and as a consequence the footwall block uplift and hangingwall subsidence is less (Figures 4b-d). Figure 4e shows the deformation consequence of activating fault 5 which has a displacement of 4 km. Interestingly at this stage, an inactive sub-horizontal fault is developed beneath the hyperthinned crust. Figure 4e shows the end of the hyperthinned domain formation characterized by a set of crustal fault-blocks dipping continentwards.

Often at the distal edge of the hyperthinned domain at rifted margins, a sub-horizontal sea-bed consisting of exhumed mantle is observed (e.g. Manatschal et al., 2001). We develop an additional model stage to reproduce this by using fault 6 with a horizontal displacement of 13 km (Figure 4f). Large fault offsets, such as fault 6, produce the exhumation of the fault footwall becoming sub-horizontal at the sea-bed due to flexural isostatic rotation (i.e. the rolling-hinge model of Buck, 1988). Fault 6 extends very thin

continental crust and due to its high offset leads to continental crus separation and consequent mantle exhumation (Figure 4f).

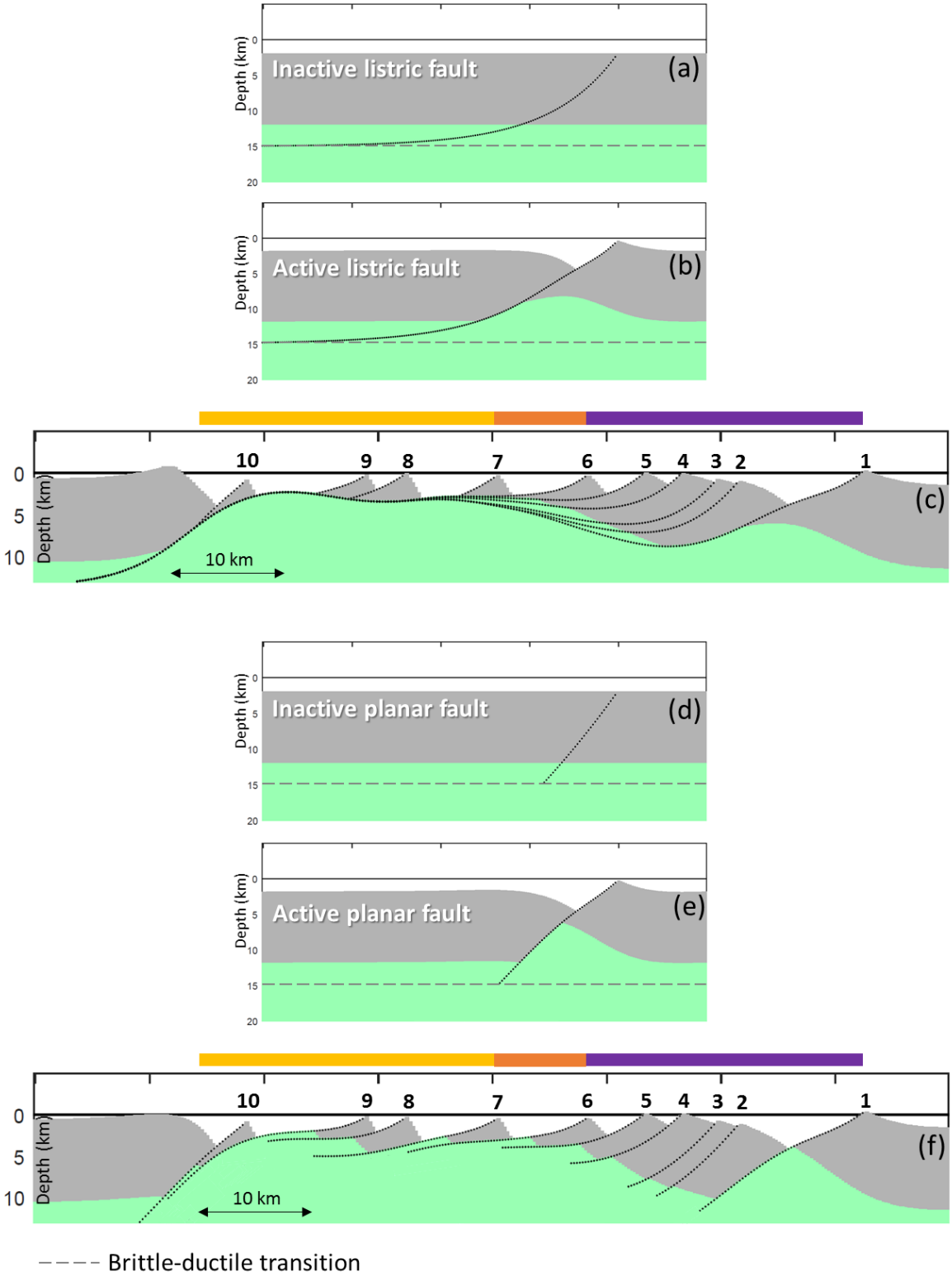

Figure 3: **a-c)** Formation of a distal rifted margin using listric faults (same as shown in Figure 2e) and **d-f)** formation of a distal rifted margin using simulated planar faults (see text for further detail). See Figure 2 for the legend of the models.

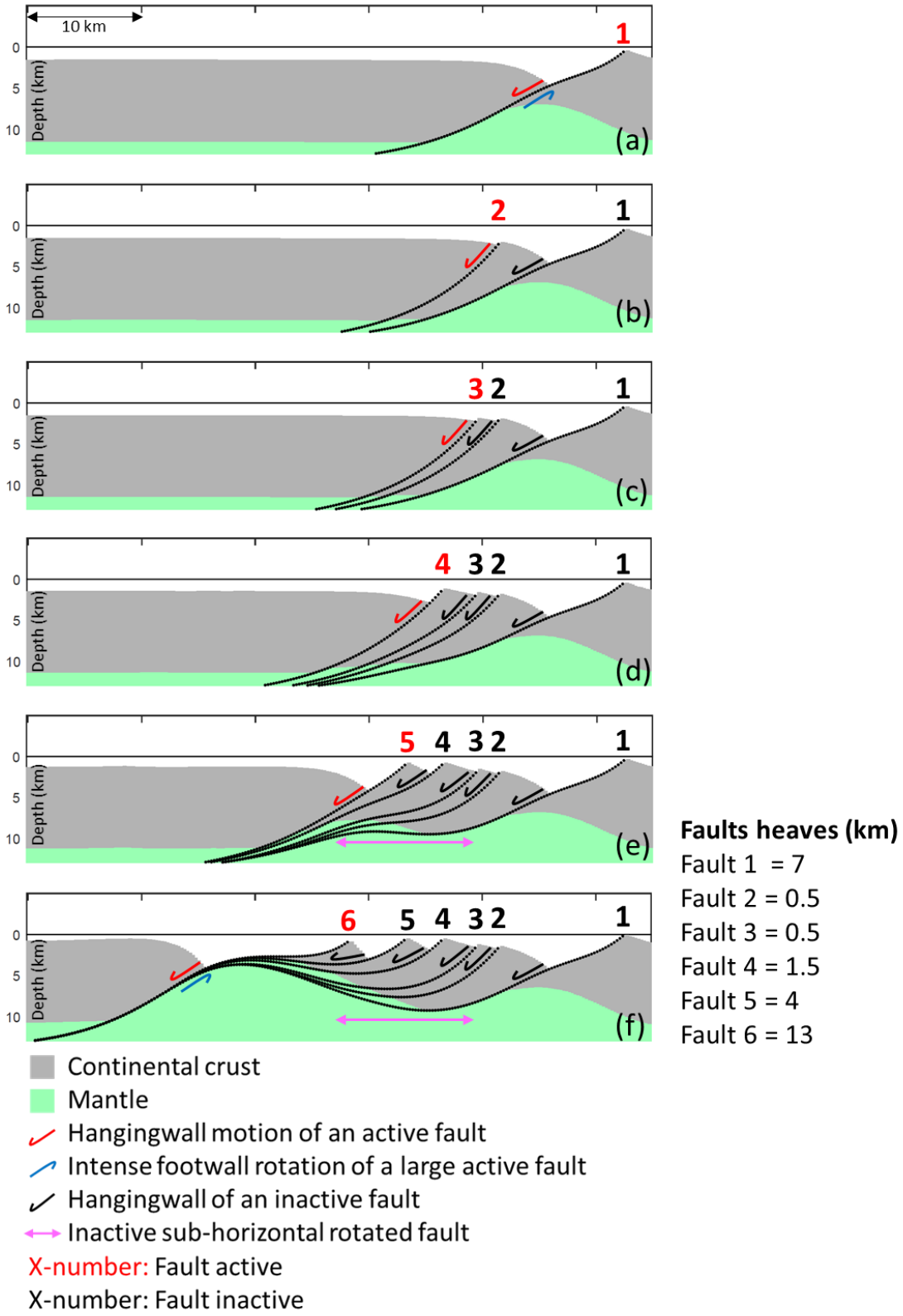

Figure 4: **a-e)** A generalized evolutionary RIFTER model showing the hyperthinned domain formation. **f)** Produces continental crustal breakup using a rolling-hinge type fault.

4.3. Initiation of exhumed mantle domain formation

The initiation of the exhumed mantle domain may be characterized by extensional crustal allochthon blocks underlain by a sub-horizontal seismic reflector beneath which mantle is assumed to be present (Figure 1). Manatschal et al., (2001) suggested that these extensional allochthon blocks may be formed by the rolling-hinge model of Buck (1988).

We use RIFTER to show the formation of four extensional allochthon blocks formed by extensional faults with different offsets (Figure 5). This allows us to examine the role of fault offsets on the present-day architecture of the exhumed mantle domain initiation.

The initial RIFTER template used to reproduce the exhumed mantle domain consists of a 10 km horizontal and uniform thick continental crust underlain by mantle (central part of Figure 2b). As for the development of the hyperthinned domain, we use listric geometries for all modelled faults characterized by an initial surface fault dipping 60° soling out horizontally at 15 km depth. Three fault types are labelled in Figure 5; (i) an active fault, (ii) a non-active fault already moved and (iii) the initial position and geometry of a fault that will be moved in the next model stage.

We first generate fault 6 coupled into the mantle at 15 km depth and with a horizontal offset of 13 km. This deformation leads to the breakup of 10 km thick continental crust and mantle exhumation (Figure 5a). Allochthon blocks are produced by extensional faults cutting through the hangingwall block of fault 6 (i.e. master fault) and pulling out pieces of crust (i.e. the rolling hinge model of Buck, 1988). These faults are short-cuts of the master fault and depending on which depth they initiate at and their break-away position, the size of the crustal allochthon block generated will vary (Figure 5). The intersection depth between the master fault and the new extensional faults is different in each model stage but it ranges between 5 and 10 km depth consistent with deMartin et al., (2007).

We produce the first allochthon block by using fault 7 with a displacement of 7 km and as a consequence a triangular piece of crust is pulled out from the hangingwall of fault 6. Note that the crustal block formed is strongly rotated and overlies part of the inactive fault 6 which is sub-horizontal at the sea-bed at this stage (Figures 5a-b). This

process is repeated when faults 8, 9 and 10 are generated, however the distance between the allochthon blocks varies depending on the fault offsets (Figure 5b-e). A small fault offset will not generate exhumed mantle between two allochthon blocks as shown in Figures 5c-d where fault 8 is only moved by 3 km. In contrast, a large fault offset will generate exhumed mantle and a sub-horizontal sea-bed geometry between two allochthon blocks as shown in Figures 5d-e where fault 9 is moved by 7 km.

Note that each allochthon block overlies a sub-horizontal structure consisting of an inactive older fault that due to flexural isostasy substantially rotates during the development of subsequent allochthon blocks (Figure 5).

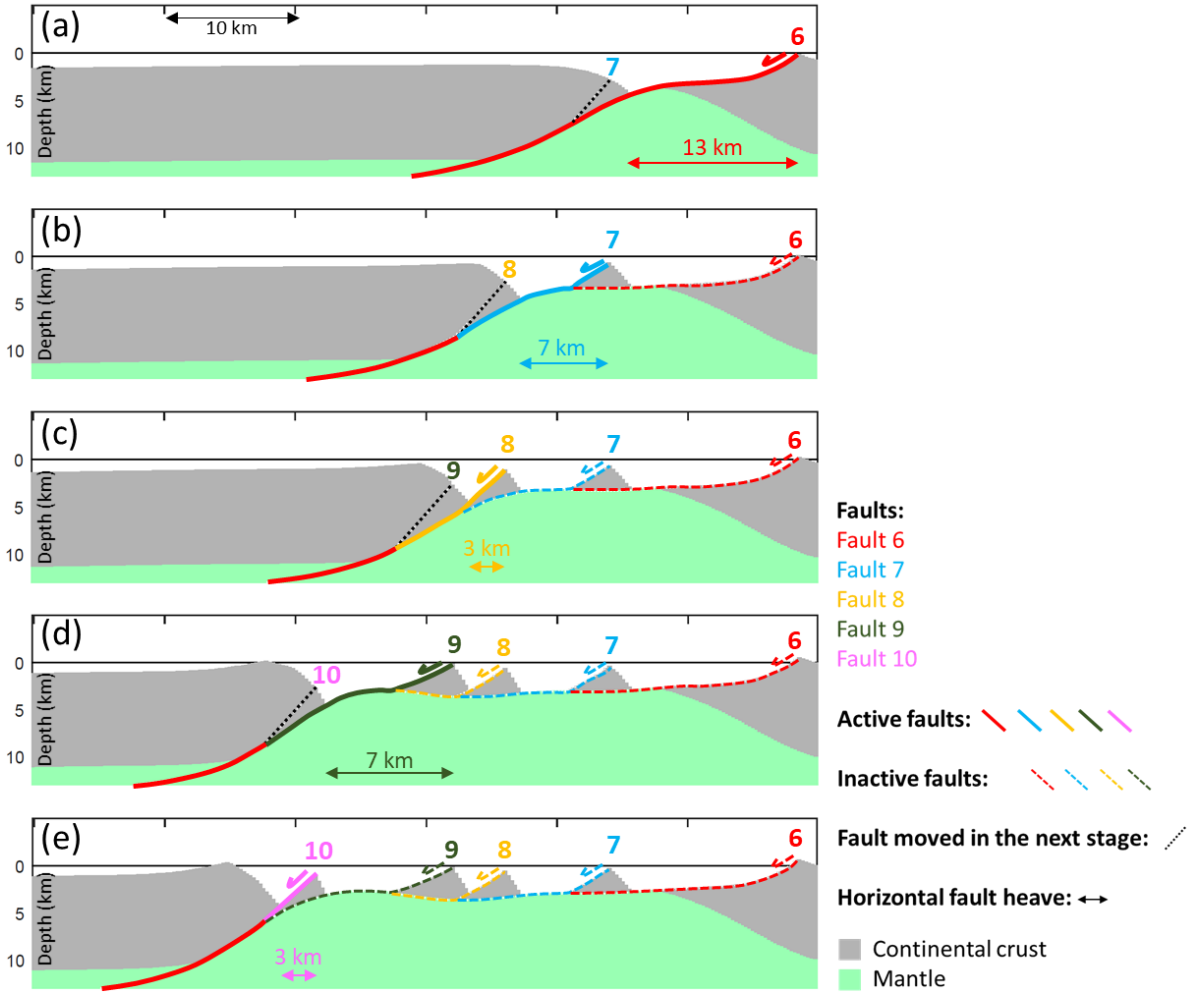

***Figure 5*: a-e)** A generalized evolutionary RIFTER model showing the initiation of exhumed mantle domain characterized by exhumed mantle and four allochthon blocks.

4.4. Transition zone formation

The transition zone between the hyperthinned and exhumed mantle domains may be characterized by a distal ridge made up of serpentinized peridotite on its oceanward edge and crustal rocks on its continentward edge as shown in the distal Iberia margin (Manatschal et al., 2001) (Figure 1). We use our modelling approach to explore whether a distal ridge at magma-poor rifted margins may be formed by extensional tectonics.

The initial RIFTER template (Figure 6a) consists of a set of fault blocks belonging to the hyperthinned domain and four allochthon blocks within the exhumed mantle domain previously shown in Figures 4 and 5 respectively. Note that in Figure 6a continental crustal separation does not occur in the transition zone and instead takes place within the exhumed mantle domain. Three tectonic scenarios are explored; (i) in-sequence faulting, (ii) out-of-sequence faulting with an oceanward dipping fault and (iii) out-of-sequence faulting with an oceanward and a continentward dipping faults (Figures 6b-d).

In-sequence faulting

We develop an in-sequence faulting scenario consisting of first the formation of the hyperthinned domain characterized by extensional faults 1 to 5 (same as shown in Figure 4e). We then activate fault 6 consisting of a listric fault with an initial surface fault dipping 60° soling out horizontally at 15 km depth. The fault offset is 13 km and as a consequence the footwall block is exhumed and due to flexural isostatic rotation it becomes sub-horizontal at the sea-bed. In addition, continental crustal separation occurs and consequently mantle is exhumed. In this case, the architecture of the transition zone is characterized by a sub-horizontal sea-bed consisting of exhumed mantle (Figure 6b). Lastly, allochthon blocks are formed by short-cuts extensional faults 7 to 10 (same as shown in Figure 5) using fault 6 as the master fault.

Out-of-sequence faulting

We develop two out-of-sequence faulting scenarios both consisting of first the development of the hyperthinned domain followed by the exhumed mantle domain

initiation and finally the transition zone formation between these two domains (Figures 6c-d).

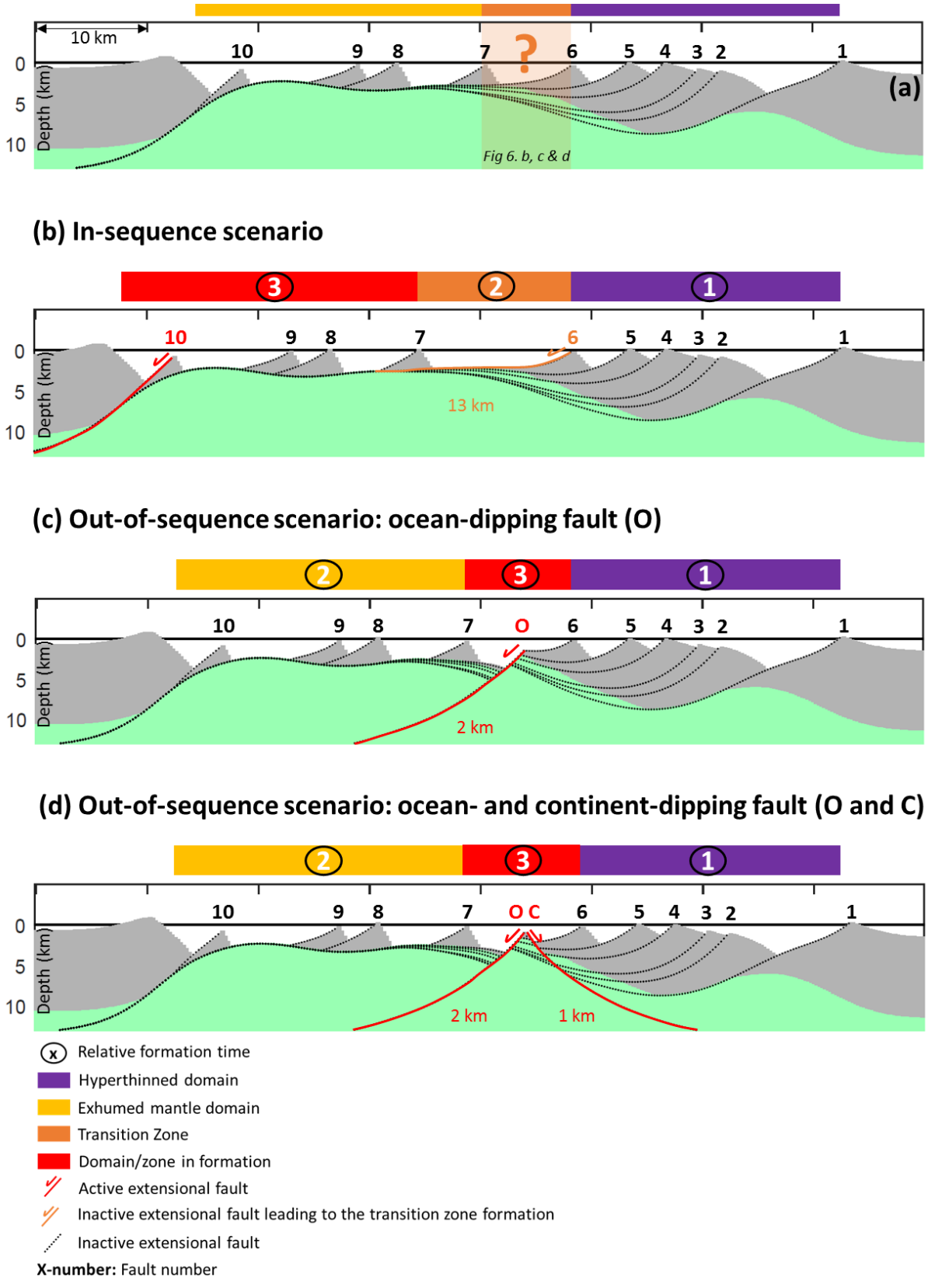

Figure 6: Exploring the transition zone formation using RIFTER. **a)** Hyperthinned and exhumed mantle domains as shown in Figures 4 and 5 respectively. This model is the initial template used to explore the scenarios shown in b-d. **b)** Transition zone formed by an in-sequence rolling-hinge fault. **c)** Transition zone formed by an ocean-dipping out-of-sequence fault. **d)** Transition zone formed by an ocean- and continent-dipping out-of-sequence faults. Grey and green are crust and mantle respectively.

The hyperthinned and exhumed mantle domains are formed using faults 1 to 5 and 7 to 10 respectively which are the same faults used to reproduce the model stage shown in Figure 6b. To explore an out-of-sequence faulting scenario, we use the same fault 6 required to produce the model shown in Figure 6b but in this case it is moved by 7 km which does not generate continental crustal separation (Figures 6c-d).

The first out-of-sequence scenario is characterized by a listric fault dipping oceanwards (fault 0) with an initial surface fault dipping 60° and soling out horizontally at 15 km depth (Figure 6c). This structure is moved by 2 km producing continental crustal separation and leading to a ridge made up of continental rocks on the continentwards-side and mantle rocks on the oceanwards-side (Figure 6c). The second out-of-sequence scenario uses two listric faults both characterized by an initial surface fault dipping 60° and soling out horizontally at 15 km depth with one dipping continentwards while the other oceanwards (faults O and C) (Figure 6d). The ocean-dipping fault is moved by 2 km while the continent-dipping fault is displaced by 1 km and both produce continental crustal separation (Figure 6d).

As a result of this tectonic episode, a ridge (similar to Hobby High) characterized by a thin package of crustal rocks on its top underline by mantle is produced. In addition, the ridge is relatively more uplifted and shows a larger accommodation space on its continentwards edge with respect of the model generated only using an oceanwards dipping fault (Figures 6c-d).

5. Discussion

This study focuses on to better understand the extensional faulting evolution during the tectonic development of the hyperthinned domain and the initiation of the exhumed mantle domain at magma-poor rifted margins. To examine this, we use a lithosphere deformation model (RIFTER) which includes the flexural isostatic response to extensional faulting, resulting in flexural isostatically compensated as well as balanced

lithosphere cross-sections. This allows us to show the geometric evolution of extensional faults and the fault offsets required to reproduce the first-order observations of the Iberia distal rifted margin (Figure 1).

5.1. Extensional faulting within the hyperthinned domain

We explore whether a listric or planar fault geometry is more likely to be expected within the hyperthinned domain of rifted margins. A listric fault is characterized by an initial surface fault dipping 60° and soling out horizontally at 15 km depth while a planar fault is steep (60°) to 15 km depth.

Results from our numerical experiment do not allow us to indicate whether a listric or planar fault geometry is more likely to be expected within the hyperthinned domain of rifted margins. Both a listric and planar fault geometry produce very similar structural topography and crustal architecture but very different sub-surface fault geometries (Figures 3c and f).

Despite of the uncertainty on the fault geometry, we show a present-day horizontal structure beneath the hyperthinned continental crust consistent with a seismic sub-horizontal reflector (S and H) observed at the distal Iberia margin (de Charpal et al., 1978; Krawczyk et al., 1996). Note that different hypothesis have been suggested for the origin of these type of sub-horizontal reflectors (e.g. Reston et al., 1996). Modelling results of this work cannot be used to rule them all out but we show that this structure, if it is tectonic in origin, was not active sub-horizontally which is consistent with the work by Pérez-Gussinyé (2013) but differs from the work by Lymer et al., (2019). Indeed, we show that this structure could be the Moho as well as an inactive rotated extensional fault (Figure 7).

We show that extensional faults within the hyperthinned domain are characterized for having low fault offsets (~less than 7 km) and being coupled into the mantle (Pérez-Gussinyé et al., 2001; Manatschal, 2004; Péron-Pinvidic et al., 2007) at a horizontal level at 15 km depth. Whether extensional faults sole out at depth into a horizontal shear zone beneath which distributed deformation occurs or diffusively connect to the deep distributed deformation is still a key remaining question.

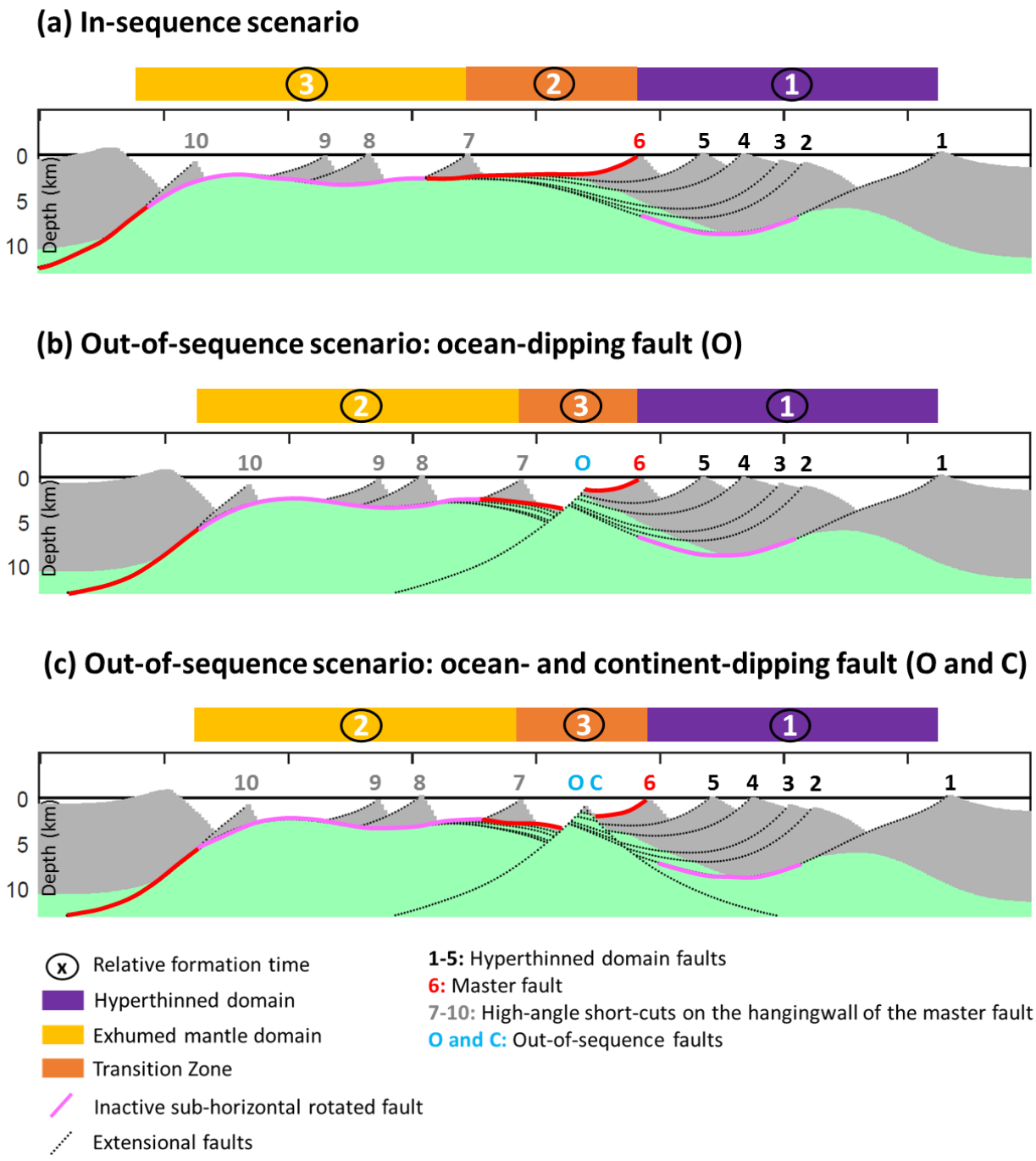

Figure 7: Same as shown in Figure 6b-d but highlighting present-day fault geometries.

5.2. Extensional faulting within the exhumed mantle domain initiation

Our results show that the extensional faults leading to the formation of the exhumed mantle domain initiation are compatible with the rolling-hinge model of Buck (1988). Exhumed mantle may or may not be overlain by extensional allochthon blocks but we consider their presence in our numerical experiments (Figure 5).

The onset of the exhumed mantle domain is characterized by a large offset rolling-hinge fault (i.e. master fault) that may produce continental crustal separation. This structure may be either a listric fault characterized by an initial surface fault dipping 60° and soling out horizontally at 15 km depth or a planar fault characterized by being steep (60°) down to 15 km. Allochthon blocks are produced by high-angle short-cut faults pulling out pieces of continental crust from the hangingwall of the master fault. These new faults form due to the rotation of the master fault leading to a surface dip too low to accommodate further extension and thus it continues through new short-cut faulting (Buck, 1988). Note that each allochthon block overlies a sub-horizontal structure consisting of an inactive older fault that due to flexural isostasy substantially rotates during the development of subsequent allochthon blocks (Figure 5). The fault offsets of the new short-cuts may vary but they strongly control the architecture of the exhumed mantle domain initiation. Large fault offsets (~more than 5 km) lead to a sub-horizontal sea-bed characterized by exhumed mantle between two allochthon blocks. In contrast, small fault offsets (~less than 3 km) do not produce mantle exhumation between two allochthon blocks (Figure 5).

We show an exhumed mantle domain architecture characterized by a sub-horizontal sea-bed geometry consisting of exhumed mantle and triangular pieces of continental crust (i.e. allochthon blocks) lying on it. This occurs due to the flexural isostatic rotation of high-angle active faults of variable offsets (Buck, 1988).

5.3. Extensional faulting within the transition between the hyperthinned and exhumed mantle domains

In the distal Iberia margin a prominent ridge (i.e. Hobby High) made up of serpentinized peridotite on its oceanward edge and crustal rocks on its continentward edge has been drilled (Manatschal et al., 2001). It has been generally assumed that the drilled rocks were exhumed along a large offset rolling-hinge fault (e.g. Péron-Pinvidic et al., 2007; Reston and McDermott, 2011; Sutra et al., 2013).

We use our modelling approach to explore whether a rolling-hinge fault is compatible with the formation of a distal ridge at magma-poor rifted margins by considering the flexural isostatic response to extensional faulting and crustal thinning. We examine the

formation of a distal ridge between the hyperthinned and exhumed mantle domains as evidenced by the distal Iberia margin observations (Figure 1).

We assume that first the hyperthinned domain is formed followed by the distal ridge and lastly the allochthon blocks within the exhumed mantle domain (Figure 7a). Our results show that using a rolling-hinge large extensional fault (13 km in our case) does not produce a ridge at the transition between the hyperthinned and exhumed mantle domains. Instead, it produces continental crustal separation and a sub-horizontal sea-bed characterized by exhumed mantle (Figure 7a). This result differs from what has been suggested up to date for the distal Iberia margin where is assumed that the Hobby High is formed by a rolling-hinge fault (e.g. Péron-Pinvidic et al., 2007; Reston and McDermott, 2011; Sutra et al., 2013).

The deformation within distal rifted margins is expected to migrate oceanwards and therefore to be characterized by in-sequence faulting (e.g. Péron-Pinvidic et al., 2007). However, the fact that an in-sequence faulting scenario using a rolling-hinge extensional fault does not produce a ridge as the Hobby High topographic high, leads us to explore whether out-of-sequence faulting may occur during the formation of distal rifted margins. The presence of out-of-sequence faulting in the transition between "true" oceanic crust and either exhumed mantle or hyperthinned continental crust has already been suggested (Gillard et al., 2016).

We assume that first the hyperthinned domain is formed followed by the allochthon blocks within the exhumed mantle domain and lastly the distal ridge between these two domains (Figures 7b-c). Note that continental crustal separation is not produced at the transition zone as we explore how this could be achieved by out-of-sequence faulting. Our results show that using this tectonic scenario (i.e. out-of-sequence faulting) a distal ridge made up of mantle on its oceanward edge and crustal rocks on its continentward edge is produced (Figures 7b-c) as observed on the Iberia distal margin (Figure 1). These out-of-sequence faults cross-cut an older rolling-hinge fault that, in our case, corresponds to the master fault leading to the formation of allochthon blocks. The out-of-sequence faulting may either consist of listric faults characterized by an initial surface fault dipping 60° and soling out horizontally at 15 km depth or planar and steep (60°) faults. In any case, we suggest that are faults with low offsets (less than 3 km). Both a fault dipping oceanwards as well as a continentwards dipping

fault together with an oceanwards dipping fault generate a distal ridge producing continental crustal separation at the transition between the hyperthinned and exhumed mantle domains (Figure 7b-c). Interestingly the second out-of-sequence faulting scenario (Figure 7c) produces a ridge which is slightly more uplifted than that produced by only an oceanwards dipping fault (Figure 7b).

A rifted margin evolves from an intra-continental rift and thus typical features from early extensional lithosphere deformation are expected to exist within rifted margins. Intra-continental rift basins consist of graben and half-grabens separated by extensional faults of different polarities between them. Therefore, continent-dipping faults as well as ocean-dipping faults are expected along rifted margins (Figures 2b and 7c).

We suggest that out-of-sequence faulting may play an important role during the development of the hyperthinned domain leading to mantle exhumation at magma-poor rifted margins consistent with the work by Gillard et al., (2016).

6. Conclusions

We use a kinematic modelling approach that includes the flexural isostatic response to extensional faulting and crustal thinning to examine the geometry of active extensional faults and how does it evolve within hyperthinned continental crust leading to mantle exhumation at magma-poor rifted margins. The key conclusions are the following:

1- Extensional faulting within the hyperthinned domain is characterized by faults with relatively low offsets that couple into the mantle. However it is uncertain whether these faults are listric or planar. A listric fault geometry produces a sub-horizontal structure beneath the hyperthinned crust consisting of an inactive rotated extensional fault while a planar geometry does not.

2- Extensional faulting within the exhumed mantle domain initiation is characterized by a large offset rolling-hinge fault (i.e. a master fault). It is uncertain whether the master fault soles out horizontally at depth with a listric geometry or is a steep planar fault.

3- Allochthon blocks within the exhumed mantle domain are formed by high-angle short-cut faults from the master fault. Each allochthon block overlies a

sub-horizontal inactive older fault that due to flexural isostasy substantially rotates during the development of subsequent allochthon blocks. This leads to an exhumed mantle domain architecture characterized by a sub-horizontal sea-bed geometry with exhumed mantle and allochthon blocks above it.

4- The transition zone between the hyperthinned and exhumed mantle domains may be characterized by; (i) a large rolling-hinge in-sequence fault leading to a sub-horizontal sea-bed or (ii) low offset out-of-sequence faults leading to a distal ridge made up of mantle and crustal rocks.

Acknowledgments

We acknowledge the MM4 (Margin Modelling Phase 4) industry partners (BP, Conoco Phillips, Statoil, Petrobras, Total, Shell, BHP-Billiton, and BG) for financial support and discussions.

REFERENCES

Beslier, M.O., Ask, M., Boillot, G., 1993. Ocean-continent boundary in the Iberia Abyssal Plain from multichannel seismic data. Tectonophysics 218, 383–393. https://doi.org/10.1016/0040-1951(93)90327.

Boillot, G., Recq, M., Winterer, E.L., Meyer, A.W., Applegate, J., Baltuck, M., Bergen, J.A., Comas, M.C., Davies, T.A., Dunham, K., Evans, C.A., Girardeau, J., Goldberg, G., Haggerty, J., Jansa, L.F., Johnson, J.A., Kasahara, J., Loreau, J.P., Luna-Sierra, E., Moullade, M., Ogg, J., Sarti, M., Thurow, J., Williamson, M., 1987. Tectonic denudation of the upper mantle along passive margins: a model based on drilling results (ODP leg 103, western Galicia margin, Spain). Tectonophysics 132, 335–342. https://doi.org/10.1016/0040-1951(87)90352-0.

Buck, W.R., 1988. Flexural Rotation of Normal Faults. Tectonics 7, 959–973.

De Charpal, O., Guennoc, P., Montadert, L., Roberts, D.G., 1978. Rifting, crustal attenuation and subsidence in the Bay of Biscay. Nature 275, 706–711. https://doi.org/10.1038/275706a0.

deMartin, B.J., Sohn, R.A., Canales, J.P., Humphris, S.E., 2007. Kinematics and geometry of active detachment faulting beneath the Trans-Atlantic geotraverse (TAG) hydrothermal field on the Mid-Atlantic Ridge. Geology 35, 711–714. https://doi.org/10.1130/G23718A.1.

Ford, M., Lickorish, W.H., Kusznir, N.J., 1999. Tertiary foreland sedimentation in the Southern Subalpine Chains, SE France: A geodynamic appraisal. Basin Res. 11, 315–336. doi:10.1046/j.1365-2117.1999.00103.

Gillard, M., Autin, J., Manatschal, G., 2016. Fault systems at hyper-extended rifted margins and embryonic oceanic crust: Structural style, evolution and relation to magma. Mar. Pet. Geol. https://doi.org/10.1016/j.marpetgeo.2016.05.013.Hoffmann, H.J., Reston, T.J., 1992. Nature of the S reflector beneath the Galicia Banks rifted margin: preliminary results from prestack depth migration. Geology 20, 1091–1094.

Horsefield, S.J., 1992. Crustal structure across the contiennt-ocean boundary [Ph.D. thesis]. Cambridge Univ.

Jácome, M.I., Kusznir, N., Audemard, F., Flint, S., 2003. Formation of the Maturín Foreland Basin, eastern Venezuela: Thrust sheet loading or subduction dynamic topography. Tectonics 22, n/a-n/a. https://doi.org/10.1029/2002tc001381.

Krawczyk, C.M., Reston, T.J., Beslier, M.O., Boillot, G., 1996. Evidence for Detachment Tectonics on the Iberia Abyssal Plain Rifted Margin 149, 1–13. https://doi.org/10.2973/odp.proc.sr.149.244.1996.

Kusznir, N.J., Marsden, G., Egan, S.S., 1991. A flexural-cantilever simple-shear/pure-shear model of continental lithosphere extension: applications to the Jeanne d'Arc Basin, Grand Banks and Viking Graben, North Sea. Geol. Soc. London, Spec. Publ. 56, 41–60. https://doi.org/10.1144/gsl.sp.1991.056.01.04.

Lymer, G., Cresswell, D.J.F., Reston, T.J., Bull, J.M., Sawyer, D.S., Morgan, J.K., Stevenson, C., Causer, A., Minshull, T.A., Shillington, D.J., 2019. 3D development of detachment faulting during continental breakup. Earth Planet. Sci. Lett. 515, 90–99. https://doi.org/10.1016/j.epsl.2019.03.018.

Magnavita, L.P., Davison, I., Kusznir, N.J., 1994. Rifting, erosion, and uplift history of the Reconcavo-Tucano-Jatoba Rift, northeast Brazil. Tectonics 13, 367–388.

Manatschal, G., Froitzheim, N., Rubenach, M., Turrin, B., 2001. The role of detachment faulting in the formation of an ocean-continent transition: insights from the Iberia Abyssal Plain from: Wilson, R.C.L., Whitmarsh, R.B., Taylor, B. & Froitzheim, N. Non-Volcaninc Rifting of Continental Margins: A Comparison of Evid. Geol. Soc. London, Spec. Publ. 187, 405–428. https://doi.org/0305-8719/01/1500.

Manatschal, G., 2004. New models for evolution of magma-poor rifted margins based on a review of data and concepts from West Iberia and the Alps. Int. J. Earth Sci. 93, 432–466. https://doi.org/10.1007/s00531-004-0394-7.

Montadert, L., De Charpal, O., Roberts, D., Guennoc, P., Sibuet, J.-C., 1979. Northeast Atlantic passive continental margins: Rifting and subsidence processes. In: Talwani, M., Hay, W. & Ryan, W. B. F. (eds) Deep Drilling Results in the Atlantic Ocean: Continental Margins and Palaeoenvironments. Am. Geophiscal Union, Washington, DC 154–186.

Pérez-Gussinyé, M., Reston, T.J., Morgan, J.., 2001. Serpentinization and magmatism during extension at non-volcanic margins: the effect of initial lithospheric structure. Geol. Soc. London, Spec. Publ. 187, 551–576. https://doi.org/10.1144/GSL.SP.2001.187.01.27.

Pérez-Gussinyé, M., 2013. A tectonic model for hyperextension at magma-poor rifted margins: an example from the West Iberia – Newfoundland conjugate margins. Geol. Soc. London, Spec. Publ. 369, 403–427. https://doi.org/10.1144/SP369.19.

Péron-Pinvidic, G., Manatschal, G., Minshull, T.A., Sawyer, D.S., 2007. Tectonosedimentary evolution of the deep Iberia-Newfoundland margins: Evidence for a complex breakup history. Tectonics 26, 1–19. https://doi.org/10.1029/2006TC001970.

Péron-Pinvidic, G., Manatschal, G., Osmundsen, P.T., 2013. Structural comparison of archetypal Atlantic rifted margins: A review of observations and concepts. Mar. Pet. Geol. 43, 21–47. https://doi.org/10.1016/j.marpetgeo.2013.02.002.

Ranero, C.R., Pérez-Gussinyé, M., 2010. Sequential faulting explains the asymmetry and extension discrepancy of conjugate margins. Nature 468, 294–299. https://doi.org/10.1038/nature09520.

Reston, T.J., 1996. The S reflector west of Galicia: The seismic signature of a detachment fault. Geophys. J. Int. 127, 230–244. https://doi.org/10.1111/j.1365-246X.1996.tb01547.

Reston, T.J., Krawczyk, C.M., Klaeschen, D., 1996. The S reflector west of Galicia (Spain): Evidence from prestack depth migration for detachment faulting during continental breakup. J. Geophys. Res. Solid Earth 101, 8075–8091. https://doi.org/10.1029/95jb03466.

Reston, T.J., 2005. Polyphase faulting during the development of the west Galicia rifted margin. Earth Planet. Sci. Lett. 237, 561–576. https://doi.org/10.1016/j.epsl.2005.06.019.

Reston, T.J., McDermott, K.G., 2011. Successive detachment faults and mantle unroofing at magma-poor rifted margins. Geology 39, 1071–1074. https://doi.org/10.1130/G32428.1.

Roberts, A.M., Kusznir, N.J., Yielding, G., Styles, P., 1998. 2D flexural backstripping of extensional basin: the need for a sideways glance. Pet. Geosci. 4, 327–338. https://doi.org/10.1144/petgeo.4.4.327.

Roberts, A.M., Kusznir, N.J., Yielding, G., Beeley, H., 2019. Mapping the bathymetric evolution of the northern North Sea: from Jurassic syn-rift archipelago through Cretaceous-Tertiary post-rift subsidence. Pet. Geosci.

Schouten, H., Smith, D.K., Cann, J.R., Escartín, J., 2010. Tectonic versus magmatic extension in the presence of core complexes at slow-spreading ridges from a visualization of faulted seafloor topography. Geology 38, 615–618. https://doi.org/10.1130/G30803.1.

Sibuet, J.-C., 1992. Formation of non-volcanic passive margins: a composite model applies to the conjugate Galicia and southeastern Flemish cap margins. Geophys. Res. Lett. 19, 769–772.

Smith, D.K., Escartín, J., Schouten, H., Cann, J.R., 2008. Fault rotation and core complex formation: Significant processes in seafloor formation at slow-spreading mid-ocean ridges (Mid-Atlantic Ridge, 13°-15°N). Geochemistry, Geophys. Geosystems 9. https://doi.org/10.1029/2007GC001699.

Sutra, E., Manatschal, G., 2012. How does the continental crust thin in a hyperextended rifted margin? Insights from the iberia margin. Geology 40, 139–142. https://doi.org/10.1130/G32786.1.

Sutra, E., Manatschal, G., Mohn, G., Unternehr, P., 2013. Quantification and restoration of extensional deformation along the Western Iberia and Newfoundland rifted margins. Geochemistry, Geophys. Geosystems 14, 2575–2597.

Toth, J., Kusznir, N.J., Flint, S.S., 1996. A flexural isostatic model of lithosphere shortening and foreland basin formation: Application to the Eastern Cordillera and Subandean belt of NW Argentina. Tectonics 15, 2–3.

Tugend, J., Manatschal, G., Kusznir, N.J., Masini, E., Mohn, G., Thinon, I., 2014. Formation and deformation of hyperextended rift systems: Insights from rift domain mapping in the Bay of Biscay-Pyrenees. Tectonics 33, 1239–1276.

Wernicke, B., 1981. Low-angle normal faults in the Basin and Range Province: nappe tectonics in an extending orogen. Nature 291, 645–648. https://doi.org/10.1038/291645a0.

White, R.S., 1999. The lithosphere under stress. Philos. Trans. R. Soc. A Math. Phys. Eng. Sci. 357, 901–915. https://doi.org/10.1098/rsta.1999.0357.

Whitmarsh, R.B., Pinheiro, L.M., Miles, P.R., Recq, M., Sibuet, J.-C., 1993. Thin crust at the western Iberia ocean-continent transition and ophiolites. Tectonics 12, 5.

Whitmarsh, R.B., Manatschal, G., Minshull, T, 2001. Evolution of magma-poor continental margins from rifting to seafloor spreading. Nature 413, 150–154. https://doi.org/10.1038/35093085.

CHAPTER 4

Chapter 4: under review for a special issue on Tectonophysics entitled: "Style of deformation and tectono-sedimentary evolution of fold-and-thrust belts and foreland basins: from nature to models"

Role of rift structural inheritance in orogeny highlighted by the Western Pyrenees case-study

Júlia Gómez-Romeu[1], Emmanuel Masini[2], Julie Tugend[2,3], Maxime Ducoux[2,4] & Nick Kusznir[1]

[1]*Department of Earth, Ocean and Ecological Sciences, University of Liverpool, Liverpool, UK*

[2]*Total SA, R&D, Pau, France*

[3]*Sorbonne Université, CNRS-INSU, Institut des Sciences de la Terre, Paris, France*

[4]*E2S-UPPA, Université de Pau et Pays Adour-CNRS-TOTAL, LFCR IPRA, UMR 5150, Pau, France*

Abstract

It is commonly accepted that many orogens form by contractional reactivation of earlier continental rifts or rifted margins. Therefore, to better understand orogenesis, it is important to also understand how rift domains and their associated structures are incorporated into orogens.

We investigate the role of rift structural inheritance during orogeny using the Western Pyrenees as a case-study. To achieve our aim, we use a kinematic forward lithosphere deformation model (RIFTER) to produce flexural isostatically compensated as well as balanced cross-sections showing the structural and stratigraphic development of both the rift and orogenic stages of the Western Pyrenees. The cross-section produced extends from the Northern to the Southern Foreland Basins and crosses the Mauléon-Arzacq Basin.

Our modelling results show how rift-domains and their faults are sequentially reactivated and incorporated into the present-day Western Pyrenees architecture. Based on the results from our case-study, we identify a sequence of tectonic stages

separated by critical events that record the transition between different tectonic styles by which lithosphere is deformed. The pre-orogenic extensional stage is characterized by a hyper-extended rift system that eventually led to exhumed mantle. This constitutes the pre-orogenic template. The subsequent contractional tectonics consists of two stages: (i) the inversion of the hyper-extended rift system reactivating extensional structures and (ii) the crustal shortening of the southern proximal rift domain.

Results of the Western Pyrenees case-study may be used to understand the development of other Alpine-type collisional systems involving the sequential reactivation and inversion of former hyper-extended rift systems.

1. Introduction

The Wilson cycle represents one of the most important concepts of the plate tectonic theory and one of its key implications is that mountain belts are built on the former site of continental rifted margins (Wilson, 1966). This implies that present-day orogens are formed by the closure of precursor rift basins or rifted margins. Many studies have shown that remnants of distal rifted margins are present within internal parts of orogens (e.g. Alps: Lemoine et al., 1987; Manatschal, 2004; Mohn et al., 2010; 2014; Masini et al., 2012, Beltrando et al., 2014 and Epin et al., 2017, Pyrenees: Lagabrielle and Bodinier, 2008; Jammes et al., 2009; Lagabrielle et al., 2010; Clerc et al., 2012; Clerc and Lagabrielle, 2014, Masini et al., 2014, Tugend et al., 2014, Mouthereau et al., 2014, Teixell et al., 2016 and 2018, Caledonides: Andersen et al., 2012). These observations demonstrate the necessity of understanding the role of the earlier extensional rift history during orogen formation.

We use the Western Pyrenees as a natural laboratory to study the influence of rift structural inheritance on collision. The Western Pyrenees underwent Late Jurassic to Cretaceous rifting (Canérot, 2008; Jammes et al., 2009, 2010a) followed by the Alpine orogeny between the Santonian and the Miocene (Garrido-Megías and Ríos, 1972; Muñoz, 1992; Vergés et al., 1995; Capote et al., 2002; Vergés and García-Senz, 2001; McClay et al., 2004; Mouthereau et al., 2014). The contractional reactivation of the Western Pyrenees enabled the partial preservation of the earlier rift history (e.g. Jammes et al., 2009; Masini et al., 2014; Tugend et al., 2014). Tugend et al., (2014) has proposed that the sequential rift domain reactivation made a large contribution to

the present-day orogen architecture of the Western Pyrenees making it an ideal case-study to study the role of rift structural inheritance during orogeny. We investigate the sequential rift domain reactivation paying particular attention to the role of pre-existing rift structures required to produce the present-day Western Pyrenees architecture.

Early work showing balanced geological sections across the Pyrenees (e.g. Roure et al., 1989; Choukroune et al., 1990; Muñoz, 1992; Teixell, 1998; Vergés et al., 2002) used pull-apart basins as the initial template for the collisional stage. However, recent published cross-sections (Jammes et al., 2009; Tugend et al., 2014; Mouthereau et al., 2014; Teixell et al., 2016) have improved the pre-orogenic template by including a hyper-extended rift architecture, consistent with observations of major crustal thinning and mantle exhumation (Lagabrielle and Bodinier, 2008; Jammes et al., 2009; Lagabrielle et al., 2010; Masini et al., 2014; Tugend et al., 2014, 2015b). A common feature of all these sections is that they are palinspastically restored but do not include the flexural isostatic compensation of the lithosphere resulting from both extensional and contractional tectonics. In this study, we use a kinematic forward lithosphere deformation model (RIFTER) that allows us to produce flexural isostatically compensated as well as balanced cross-sections.

Using RIFTER we produce a cross-section extending from the Northern (Aquitaine Basin) to the Southern Foreland Basins, that crosses the Mauléon-Arzacq Basin, and incorporates both the hyper-extended rifting and the orogenic evolution of the Western Pyrenees. Our modelling strategy consists of bringing together the shallow observed geology, seismic reflection observations and the deeper seismic tomographic structure of the Western Pyrenees into a single unified model that balances isostatically as well as structurally. Our RIFTER modelling shows that by including the earlier rift history we are able to reproduce the present-day first-order structural and stratigraphic architecture of the Western Pyrenees. We show that the present-day first-order structure of this orogen can be reproduced through the sequential reactivation of pre-existing rift domains. In addition, we bring insights on how the pre-orogenic rift-related faults may be reactivated and incorporated into the present-day Western Pyrenees architecture.

2. Geological setting

The Pyrenees is a double vergent orogen orientated east-west and located at the boundary between Spain (part of the Iberian plate) and France (part of the European plate). It is bounded to the east by the Mediterranean Sea and to the west by the Bay of Biscay (Figure 1). The Pyrenees form the central part of an orogenic system, developed subsequently to the subduction of the Iberian plate underneath the European plate.

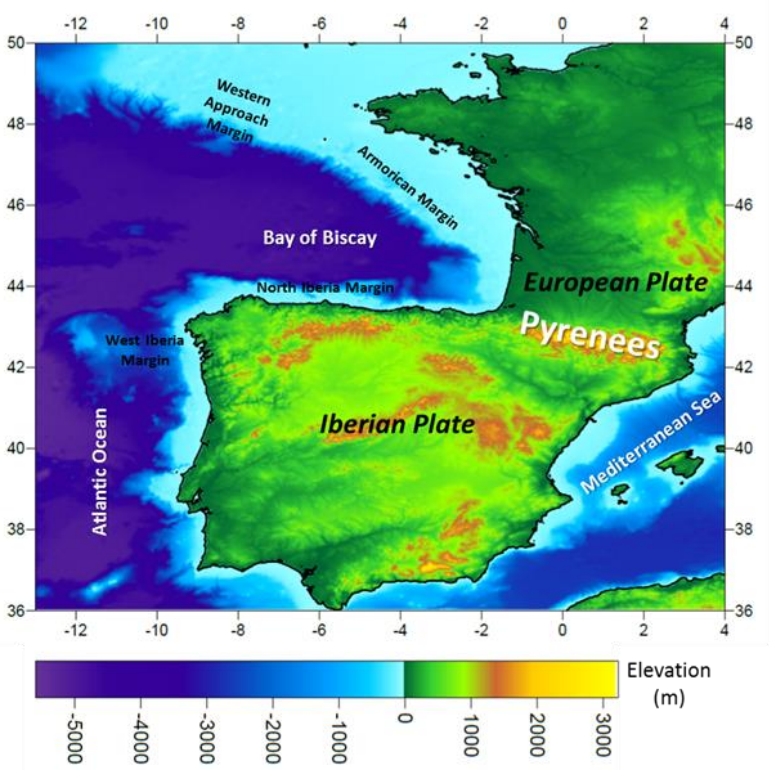

Figure 1: Bathymetric and topographic map of the Iberian and European plates, showing the location of the Bay of Biscay and Pyrenees.

2.1. Present-day structure of the Pyrenees

The Pyrenees can be divided into five main structural units. From north to south these are: (1) the Aquitaine Northern Foreland Basin, (2) the North Pyrenean Zone forming the retro-verging region of the orogenic system where Meso-Cenozoic rocks are exposed, (3) the Axial Zone made by a stack of thrust sheets involving Paleozoic basement (4) the South Pyrenean Zone forming the pro-wedge of the orogenic system

and (5) the Ebro Foreland Basin (e.g. Choukroune and Séguret, 1973; Mattauer and Henry, 1974; Teixell, 1990; Daignières et al., 1994 and references therein) (Figure 2a).

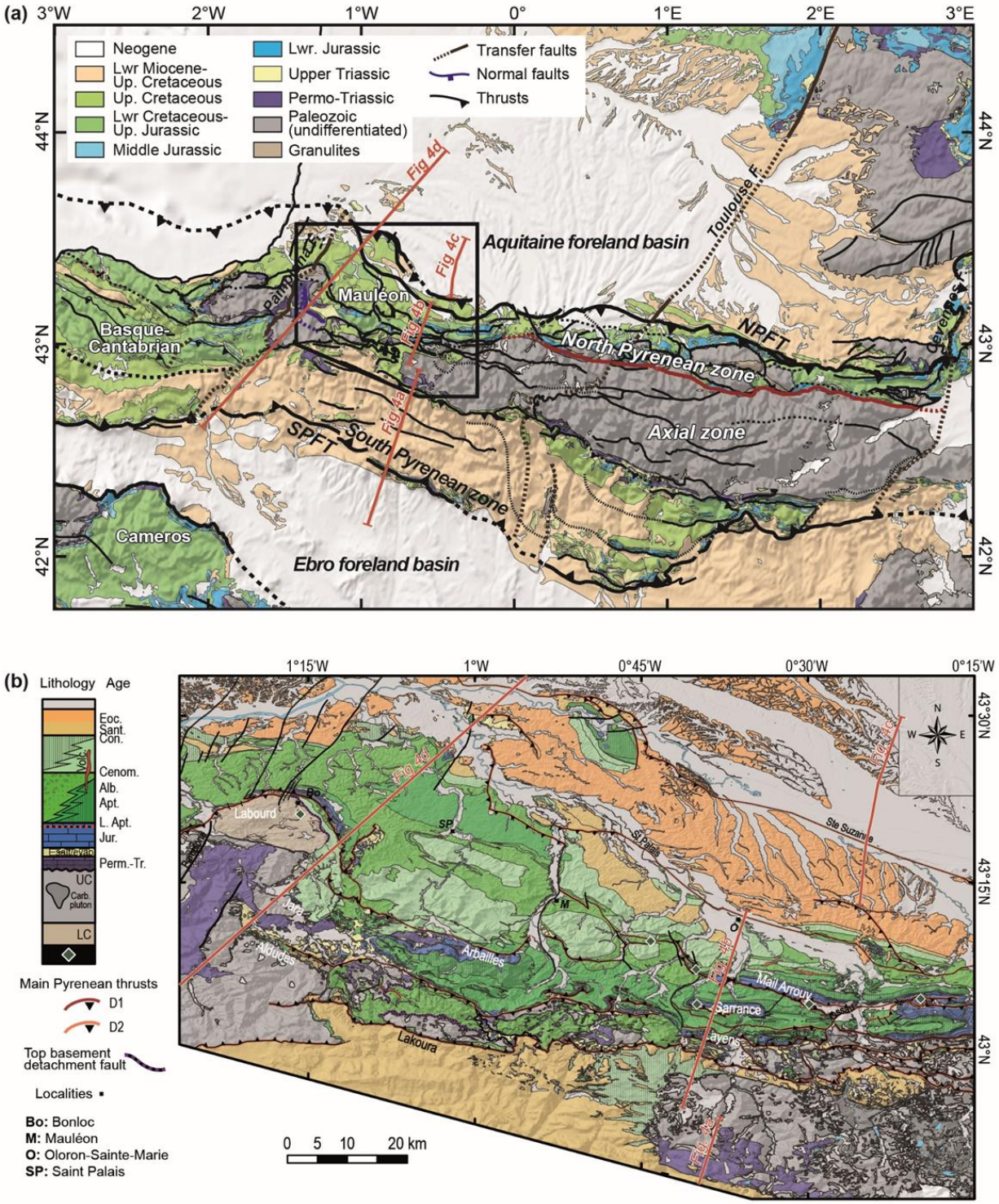

Figure 2: **a)** Geological map of the Western Pyrenean orogen. The black polygon shows the position of the Mauléon Basin map shown in **b).** This map is modified after the BRGM 1 million map. **b)** Geological map of the Mauléon basin as shown in Tugend et al., (2014 and 2015). Lithologies and age of sequences are synthetized in a log. The red lines indicate the location of the geological sections shown in Figures 4a-c and the position of the PYROPE seismic transect (Chevrot et al., 2015) shown in Figure 4d.

In the eastern and central part of the Pyrenees, the Axial Zone is well-developed exposing Palaeozoic rocks (Figure 2a). Towards the west, the Axial Zone is reduced and the Mauléon Basin, made up of Mesozoic sediments, occupies most of the western edge of the Pyrenees (Figure 2a). In the northern and southern part of the Pyrenees, a wide range of sediments ranging from Lower Triassic up to Lower Miocene are present (Figure 2a). It is important to highlight the presence of an evaporitic sequence at the bottom of the Mesozoic cover (Upper Triassic) that acts as a decollement layer and strongly controls both the extensional and compressional tectonics of the Pyrenees (Canérot, 1989; James and Canérot, 1999; Jammes et al., 2010b; Lagabrielle et al., 2010). The Aquitaine Northern and Ebro Southern Foreland Basins contain Neogene sediments deposited during the syn- to post-orogenic evolution of the Pyrenees (Figure 2a) (see Vacherat et al., 2017 and Grool et al., 2018 for a detailed tectonostratigraphy of these basins).

During the Alpine collision, the Pyrenees orogen was mainly deformed by E-W trending thrust faults such as the North Pyrenean Frontal Thrust and the South Pyrenean Frontal Thrust (Figure 2a). Additionally, present-day NE-SW trending faults (e.g. Toulouse structure) that formed in the Late Variscan (Burg, 1994) were possibly partly reactivated as transfer zones during rifting (Tugend et al., 2014). What type of Variscan faults they were and how they reactivated during the development of the Pyrenees remains uncertain.

2.2. Tectonic evolution of the Pyrenees

The opening of the North Atlantic Ocean together with the opening of the Bay of Biscay strongly controlled the relative motions of the Iberian plate with respect to the European and African plates (e.g. Olivet, 1996; Rosenbaum et al., 2002; Macchiavelli et al., 2017; Nirrengarten et al., 2018). The relative movements between these three plates are recorded through the tectonic evolution of the Pyrenees. Over the past 30 years, the formation and development of the Pyrenees have been intensively studied (e.g. Le Pichon et al., 1971; Srivastava et al., 1990; Roest and Srivastava, 1991; Sibuet and Collette, 1991; Olivet, 1996), but there is still controversies on the paleogeographic evolution prior to the Alpine collision of this orogen. As a first order simplification, the Pyrenees can be considered as the result of several extensional and

compressional tectonic events that initiated in the Palaeozoic and finalized in the Miocene. We focus on the main rift episode that occurred from latest Jurassic to early Late Cretaceous time (Schettino and Scotese, 2002; Canérot, 2008; Jammes et al., 2009, 2010a; Tugend et al., 2015b). The rifting episode was followed by the Alpine orogeny that took place between the Late Santonian and the Miocene (Garrido-Megías and Ríos, 1972; Muñoz, 1992; Vergés et al., 1995; Capote et al., 2002; Vergés and García-Senz, 2001; McClay et al., 2004; Mouthereau et al., 2014).

2.2.1. Rift evolution

The pre-Alpine evolution of the Iberian and European plate boundary was accommodated within three oblique rift systems; the Bay of Biscay-Parentis, the Pyrenean-Basque-Cantabrian and the Central Iberian Range (Salas and Casas, 1993; Vergés and García-Senz, 2001; Roca et al., 2011; Tugend et al., 2014; 2015a). The onset of the Mesozoic rifting occurred in the latest Jurassic (Figure 3a) during an overall left-lateral movement between the Iberian and European plates deduced from plate kinematic scenarios (e.g. Rosenbaum et al., 2002; Schettino and Scotese, 2002; Canérot, 2008; Jammes et al., 2010a; Nirrengarten et al., 2018). Details of the partitioning of the deformation between the different rift systems remain debated (Tugend et al., 2015a; Nirrengarten et al., 2018; Rat et al., 2019). From the Aptian up to early Late Cretaceous the relative movement between Iberia and Europe appears purely divergent as deduced from field interpretations (Jammes et al., 2010a; Tavani et al., 2018). Onset of sea-floor spreading of the western Bay of Biscay in Aptian time (Montadert et al., 1979) (Figure 3b) coincides with the main crustal thinning event and local mantle exhumation in the Pyrenean-Basque-Cantabrian rift system (Lagabrielle and Bodinier, 2008; Jammes et al., 2009; Masini et al., 2014; Tugend et al., 2014; 2015b) (Figure 3c). The identification of anomaly 34 in the Bay of Biscay and absence of anomaly 33 (Roest and Srivastava, 1991) suggest that sea-floor spreading persisted until Santonian-Early Campanian time (e.g. Montadert and Roberts, 1979, Montadert et al., 1979). This extensional deformation is not evidenced in the Pyrenean-Basque-Cantabrian rift system.

The relative movement between the Iberian and European plates resulted in a complex rift domain architecture giving the pre-Alpine setting of the Pyrenees (Figure 3c).

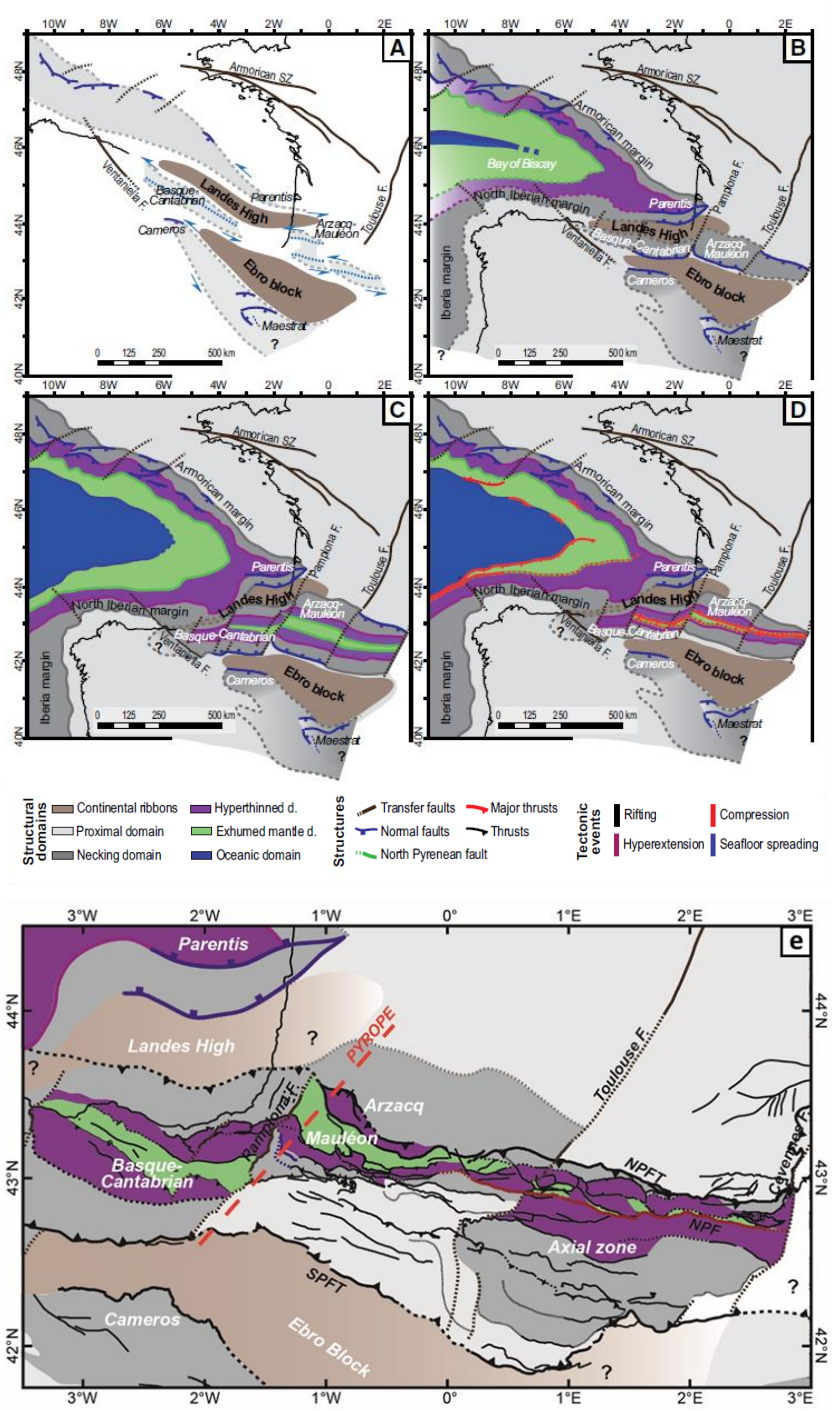

Figure 3: **a), b), c)** and **d)** Restoration showing the spatial and temporal evolution of the Iberian-European plate boundary from Tugend et al., (2015). **a)** Initiation of transtensional rifting stage (Late Jurassic). **b)** Sea-floor spreading initiation and northeast-southwest extension (Aptian-Albian). **c)** Failed tentative localization of plate boundary (before Santonian). **d)** Subduction initiation (Late Cretaceous). **e)** Rift domains map of the Pyrenean-Cantabrian rift system (after Tugend et al., 2014). The red dashed line shows the position of the PYROPE seismic transect (Chevrot et al., 2015) shown in Figure 4d.

2.2.2. Convergence evolution

Onset of the Alpine orogeny (Figure 3d) started in the late Santonian – Campanian (Garrido-Megías and Ríos 1972; Capote et al., 2002; McClay et al., 2004) and evolved up to the Late Oligocene – Early Miocene (Muñoz, 2002; Verges et al., 2002). This orogeny is related to the northward motion of Africa relative to Europe (e.g. Rosenbaum et al., 2002) leading to a north-south to northeast-southwest convergent motion between the Iberian and European plates. In the Pyrenees, this motion is characterized by the subduction of Iberia beneath Europe (Pulgar et al., 1996; Gallastegui et al., 2002; Muñoz, 1992, 2002; Pedreira et al., 2007). During this episode, Mesozoic basins were shortened and inverted leading to the formation of the present-day architecture of the Pyrenees (Capote et al., 2002).

3. Modelling constraints for the Western Pyrenees

Our modelled section includes both the Northern and the Southern Foreland Basins but we pay particular attention to the Arzacq-Mauléon Basin development. This basin initially formed during rifting and was later reactivated during the Alpine orogeny. A singular feature of this basin is that it escaped from most of the pervasive Alpine deformation and exposes part of the pre-collision history (e.g. Jammes et al., 2009; Masini et al., 2014).. We have less constraints for the rifting episode along the rest of the section but we use the available dataset to infer the rift record and how this may have been reactivated during collision.

Our modelling strategy consists of bringing together the shallow observed geology, seismic observations and the deeper structure of the Western Pyrenees into a single unified model that balances isostatically as well as structurally. In particular, we use sub-surface geology (down to a depth of 5-10 km) along the eastern Mauléon Basin (Figure 4a-c) and the deep crustal structure along the western Mauléon Basin (Figure 4d). The sub-surface observations for the Southern Foreland Basin (i.e. Ebro and Jaca Basins), the Axial Zone and the Mauléon Basin are based on the work by Teixell et al., (2016 and 2018), Tugend et al., (2014) and Lagabrielle et al., (2010) respectively (Figures 4a-b). The architecture of the Aquitaine-Arzacq Basin (Figure 4c) is revealed by the interpretation of seismic reflection line nº1325 (Appendix 1) together with well data owned by Total SA. Because no deep crustal information is available across the

eastern Mauléon Basin, we use first-order deep constraints from the western Mauléon Basin. These are obtained from a passive seismic tomography transect (PYROPE, Wang et al., 2016; Chevrot et al., 2018), whose data was acquired by Chevrot et al., (2015) and are shown in Figures 4d-e.

The RIFTER model is used to bring together sub-surface and deep observations distributed across the Western Pyrenees into a single unified model that balances isostatically as well as structurally, showing both the rifting and convergent evolution of this orogen.

3.1. Sub-surface geology

From south to north, the transect that we model consists of the sub-surface geology of; the Southern Foreland Basin, Axial Zone, Mauléon Basin, Grand Rieu Ridge and the Arzacq Basin (e.g. Casteras, 1969; BRGM, 1974; Le Pochat et al., 1976; Teixell, 1990; Daignières et al., 1994; Serrano et al., 2006; Jammes et al., 2009; Masini et al., 2014).

Southern Foreland Basin

The Southern Foreland Basin (i.e. Jaca and Ebro basins) formed as a consequence of the Axial Zone loading leading to the flexure of the Iberian lithosphere as compressional deformation was migrating southwards. Most of the calciclastic and siliciclastic sedimentation that fills up this basin is derived from the erosion of the Axial Zone during the Cenozoic. The South Pyrenean Frontal Thrusts affects the sedimentary cover of the Southern Foreland Basin leading to the last compressional deformation by early Miocene times (Teixell et al., 2016) (Figure 4a).

Axial Zone

One of the key characteristics of the Axial Zone is the deposition of post-rift sediments (Turonian and younger) on top of the eroded basement due to the occurrence of a major hiatus (Jammes et al., 2009; Masini et al., 2014) (Figures a-b).

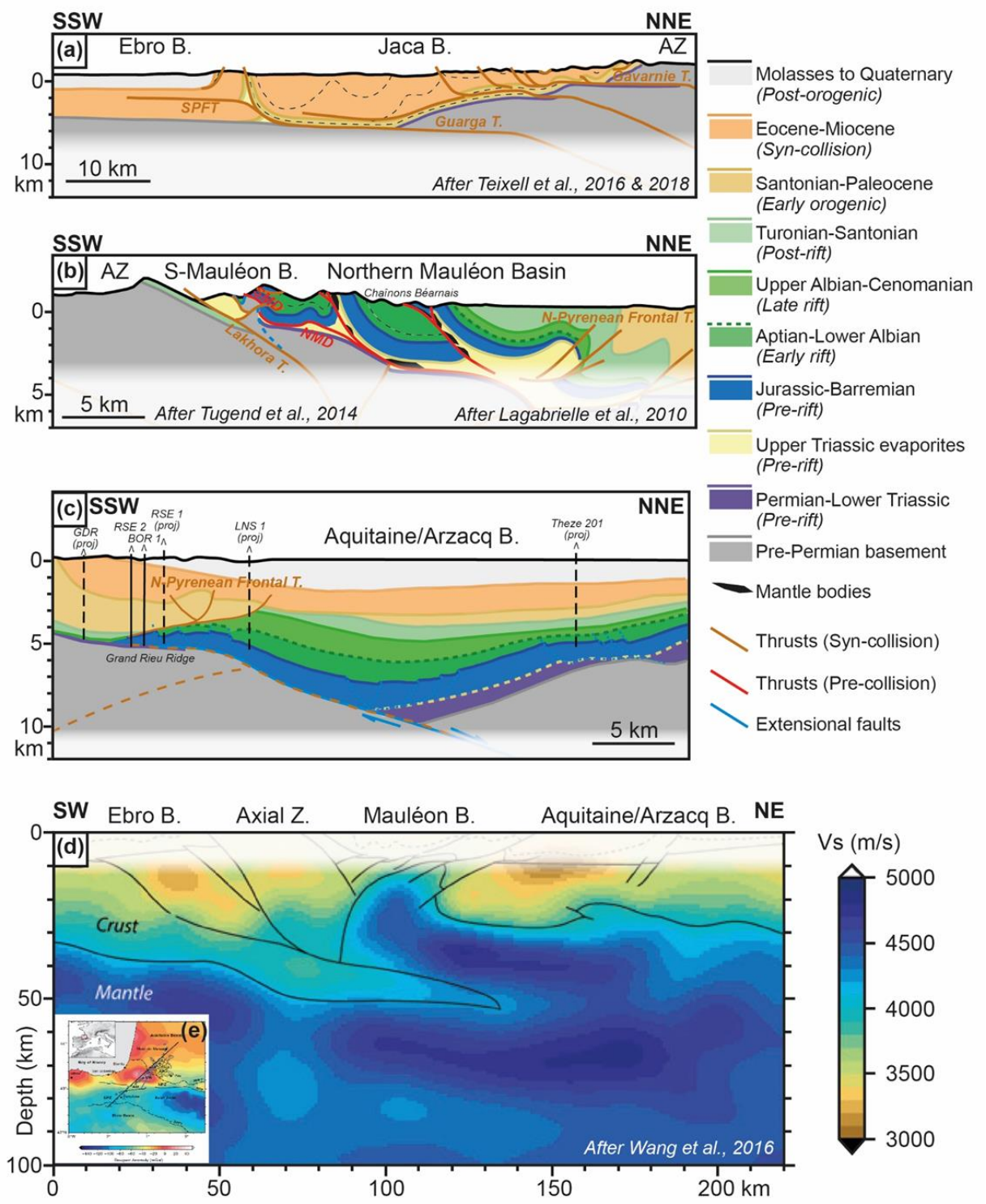

Figure 4: **a), b)** and **c)** Present-day geological cross-sections across the Western Pyrenees. **a)** and **b)** Are constrained using published cross-sections and mainly based on field observations while **c)** is constrained using seismic line nº1325 and well logs (black lines) owned by Total SA (seismic line is shown in Appendix 1). **d)** Vs seismic velocity model obtained by full waveform inversion and its interpretation along the PYROPE seismic transect located in the Western Pyrenees (Wang et al., 2016). **e)** Map of Bouguer gravity anomaly with the location of the seismic stations (blue triangles) as well as the location of the PYROPE transect (black line) (Wang et al., 2016). **AZ:** Axial Zone, **S-Mauléon B.:** Southern Mauléon Basin, **SPFT:** South Pyrenean Frontal Thrust, **SMD:** Southern Mauléon Detachment, **NMD:** Northern Mauléon Detachment; **N-Pyrenean Frontal T.:** North Pyrenean Frontal Thrust.

This hiatus argues for a major uplift and/or no deposition on the future Axial Zone during the rifting episode (Jammes et al., 2009). The Gavarnie and Guarga north-dipping thrusts are the main structures that led to the uplifting of the Axial Zone during the Late Cretaceous and Cenozoic Pyrenean collision. The overall timing of these structures is well documented by tectono-sedimentary and thermochronological data (e.g. Teixell et al., 2016 and references therein). However, the Gavarnie and Guarga thrust geometries at depth remains poorly understood as does their importance in terms of shortening (e.g. Cochelin et al., 2018).

Mauléon Basin

Former rift structures are exposed and preserved in the western Mauléon Basin enabling extensive studies of basement-sediment primary relationships (e.g. Jammes et al., 2009; Masini et al., 2014; Tugend et al., 2015b; Saspiturry et al., 2019). While preservation of these rift structures along the eastern Mauléon Basin is poor, former structural rift domains can still be identified and correlated at the scale of the entire basin (Tugend et al., 2015b).

The Mauléon Basin is squashed between the Grand Rieu Ridge to the north and the Axial Zone to the south (Lagabrielle et al., 2010; Masini et al., 2014; Tugend et al. 2014; Teixell et al., 2016) by the NPFT and the Lakhora Thrust system respectively (Figures 4b-c). A remarkable feature of this basin is that it preserves a complex rift history showing discontinuous pre-rift layers lying on top of the Upper Triassic evaporitic decollement as well as a non-uniform syn-rift sedimentary architecture (Masini et al., 2014) (Figure 4b). Studies carried out in the Mauléon Basin (e.g., Jammes et al., 2009; Lagabrielle et al., 2010; Masini et al., 2014; Tugend et al., 2014) suggest that it was formed through a hyper-extension rift episode leading to extreme crustal thinning and mantle exhumation. Field studies such as Masini et al., (2014) interpreted that this deformation was accommodated by two diachronous thick-skinned detachment systems (the Southern Mauléon Detachment and the Northern Mauléon Detachment) related to the formation of two sub-basins; the Southern Mauléon Basin and the Northern Mauléon Basin respectively. The onset of the tectonic inversion of the Mauléon Basin occurred between Santonian and Campanian times (Teixell et al., 2016 and references therein). This inversion episode led to the thrusting of the Northern Mauléon Basin over the former Grand Rieu Ridge and Arzacq Basin

(e.g. Casteras, 1969; Teixell, 1990 and 1998; Muñoz, 1992; Daignières et al., 1994) while the Southern Mauléon Basin was thrusted over the Axial Zone along the Lakhora Thrust system (Muñoz, 1992; Teixell, 1998). The presence of south-directed thrust sheets made of Mauléon Basin sediments within the former hyper-extended domain and subsequently folded and tilted during the formation of the Axial Zone located to the south, argues that the Alpine shortening began in the hyper-extended basin by Cretaceous times before migrating into the Axial Zone by Eocene times (Tugend et al., 2014; Dumont et al., 2015).

Grand Rieu Ridge

The Grand Rieu Ridge is characterized by the local absence of syn-rift sediments (e.g. Cardesse 2 drill hole; Serrano et al., 2006; Tugend et al., 2014). Post-rift sediments cover either discontinuous slivers of pre-rift cover or lay directly on top of basement (Masini et al., 2014) (Figure 4c). The north-vergent North Pyrenean Frontal Thrust system is located on this ridge that separates the Arzacq Basin in the north from the Mauléon Basin in the south (Figures 4b-c).

Arzacq Basin

The architecture of the Arzacq Basin (Figure 4c) is revealed using the seismic reflection line nº1325 (Appendix 1) together with well data owned by Total SA. It consists of a smooth 25 km wide "sag basin" syncline consisting of sediments of Permian-Lower Triassic to Quaternary age. A north-dipping extensional fault is the main observed rift structure, which bounds the southern Arzacq Basin and separates it from the Grand Rieu Ridge basement. On top of this major fault, syn-rift sediments (Aptian-Albian in age) show a growth strata development in an overall syncline-shape geometry. This indicates that the deformation of the basement was decoupled from the sedimentary cover by a major basal decollement level corresponding to the Triassic Keuper evaporitic layer (e.g. Le Pochat et al., 1978; Canérot et al., 2001; Jammes et al., 2010b; Masini et al., 2014). It can be inferred that the pre-tectonic sedimentary cover lying above the Upper Triassic decollement was dragged and gently folded above the normal fault. No important collisional structures can be identified within this basin at this location apart from a few thrusts at the southern edge of the Arzacq Basin corresponding to the North Pyrenean Frontal Thrust system (Figure 4c)

suggesting that a minor compressional tightening affected this basin (see Rocher et al., 2000 for a detailed structural analysis of this basin). The Arzacq Basin is characterized by substantial crustal thinning reaching beta values of 2 (Brunet, 1984) and consistent with the crustal architecture imaged by Wang et al., (2016). Indeed, the overall subsidence evolution of this basin can only be explained by a post-rift thermal subsidence continuing largely after the onset of shortening (Angrand et al., 2018). Masini et al., (2014) pointed out that the amount of thinning that the Arzacq Basin underwent cannot be simply provided by the observed north-dipping extensional fault located at the southern edge of the basin. They suggested that additional thinning may have been achieved by strain transfer from the Southern Mauléon Detachment in the Southern Mauléon Basin to the middle and lower crustal levels in the Arzacq Basin. This crustal decoupling structure may have generated the asymmetric rifting architecture between the Mauléon Basin (lower plate) and the Arzacq Basin (upper plate).

3.2. Deep crustal structure

Recent studies have imaged the deepest part of the Western Pyrenees, along the western Mauléon Basin, based on a tomographic model (Chevrot et al., 2015 and 2018; Wang et al., 2016). Figure 4d shows the Vs seismic velocity model obtained by full waveform inversion together with a simple interpretation of the crustal architecture suggested by Wang et al., (2016). The Vs data shows the southernmost Iberian Moho at 30 km depth which gently dips to the north reaching 50 km deep beneath the Mauléon Basin. In contrast, the geometry of the European Moho is almost horizontal beneath the Arzacq Basin at 30 km deep while beneath the Mauléon Basin it becomes shallower reaching 10 km depth. Indeed, in the western part of the Mauléon Basin, a strong positive Bouguer gravity anomaly is observed (Figure 4e) and has been interpreted as deriving from a piece of Iberian mantle (Casas et al., 1997; Jammes et al., 2010a) or lower crust (Grandjean, 1994; Vacher and Souriau, 2001; Pedreira et al., 2007). However, the work by Wang et al., (2016) shows seismic velocities beneath the western part of the Mauléon Basin (Vp ~ 7.3 km/s and Vs 4.2 km/s) that were interpreted as a body of exhumed mantle, inherited from the pre-collision hyperextended rift system. These geophysical results are consistent with many recent geological studies of the Western Pyrenees that describe remnants of a hyper-extended

rift with pre-orogenic mantle exposures (e.g., Jammes et al., 2009; Lagabrielle et al., 2010; Masini et al., 2014; Tugend et al., 2014; Tugend et al., 2015b). We use the Iberian Moho geometry as well as the geometry of the European indenter as reference observations to constrain our modelled profile. The disappearance of the main gravity anomaly towards the eastern Mauléon Basin (Figure 4e) suggests that, if the mantle body exists, then it would be of limited importance under the eastern Mauléon Basin or consist of less-dense more intensively serpentinized mantle. Masini et al., (2014) suggested that this difference in gravity anomaly between the western and eastern Mauléon Basin (Figure 4e) may result from a lateral change in the Pyrenean structure accommodated by the Saison transverse structure.

3.3. Rift domains

The repartition of former rift domains in the present-day Pyrenean orogen was recently interpreted by Tugend et al., (2014) (Figure 3e). At the scale of the Western Pyrenees, the Arzacq Basin likely recorded the necking of the European plate in an upper plate setting bounded in the south by the Northern Mauléon Detachment (Masini et al., 2014). The Northern Mauléon Basin presumably corresponded to a lower plate hyper-extended domain including (the hyperthinned and exhumed mantle domains in Tugend et al., 2014. The Southern Mauléon Basin is interpreted as the former Iberian necking domain while the former proximal domain might be eroded in the Axial Zone or buried beneath the southern Pyrenees (Figure 3e).

4. RIFTER model

We use a numerical model (RIFTER) to constrain the evolution of the Western Pyrenees. RIFTER is a kinematic forward lithosphere deformation model that allows the production of flexural isostatically compensated as well as balanced cross-sections. Within RIFTER, lithosphere is deformed by faulting in the upper crust with underlying distributed pure-shear deformation in the lower crust and mantle. A key attribute of RIFTER is that it incorporates the flexural isostatic response to extensional and/or reverse faulting, crustal thinning and/or thickening, lithosphere thermal loads, sedimentation and erosion. Therefore, RIFTER can be used to model and predict the structural and stratigraphic development of both extensional and contractional tectonic

settings. The model is kinematically controlled with fault geometry and displacement, pure-shear distribution and the amount of sedimentation and erosion given as model inputs as a function of time. Lithosphere flexural strength, parameterised as lithosphere effective elastic thickness, is also defined. The model incorporates lithosphere thermal perturbation and re-equilibration in response to lithosphere deformation. Model outputs are geological cross-sections which are flexural isostatically compensated as well as structurally balanced.

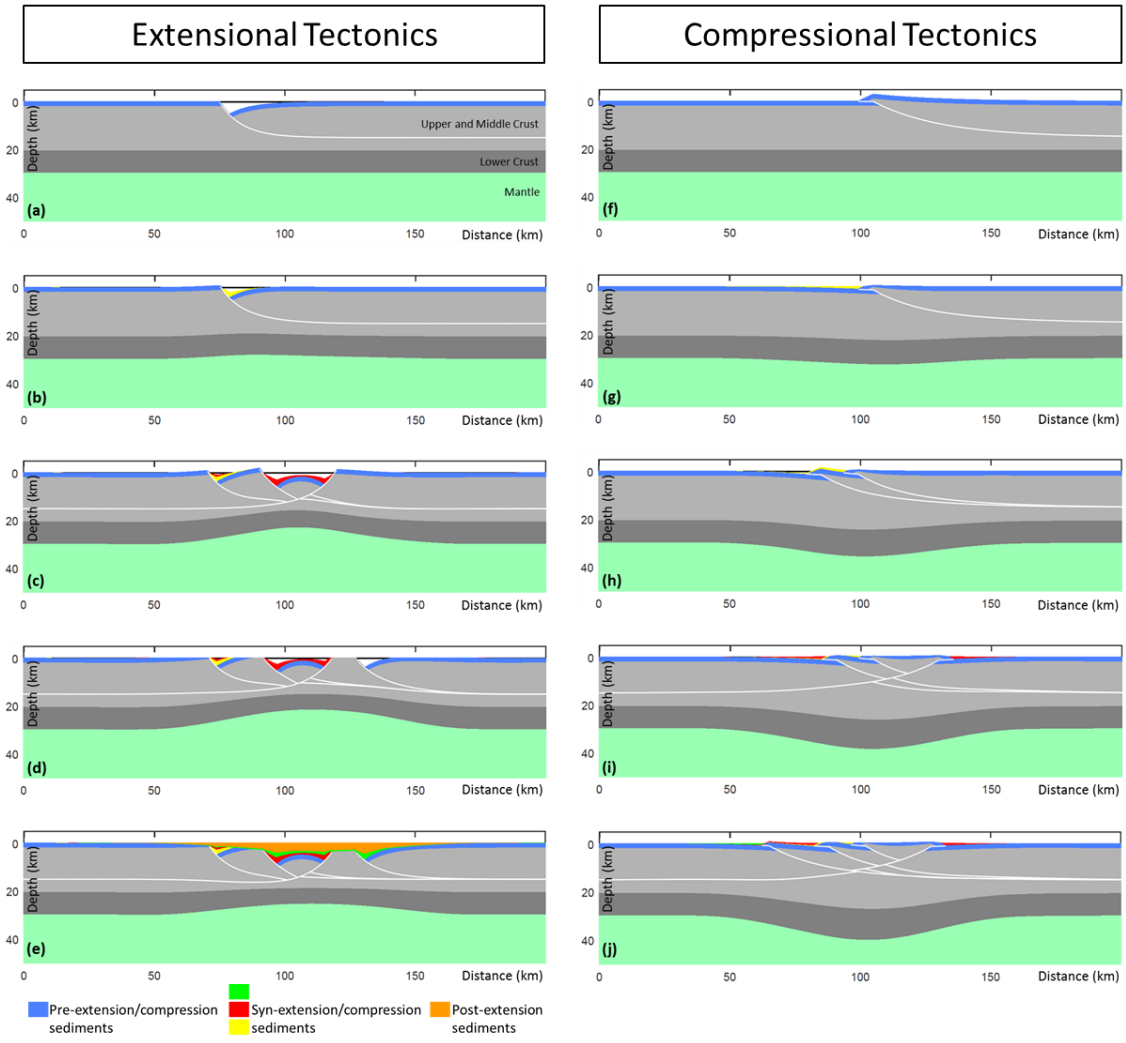

Figure 5: The RIFTER model applied to extensional (**a-e**) and contractional (**f-j**) tectonics. **a)** and **f)** show faulting alone with no deep pure-shear deformation below. **b-e)** and **g-j)** show the lithosphere response to sequential faulting, deeper lithosphere deformation giving crustal thinning or thickening, sediment loading, erosional unloading, lithosphere thermal perturbation and re-equilibration and their flexural isostatic responses. See text for more explanation**.**

The kinematic formulation of RIFTER represents an advantage over dynamic modelling because the input data given to RIFTER can be constrained by observed

geology. In addition RIFTER provides for the isostatic testing of palinspastic cross-sections and can also be used to explore different kinematic scenarios. A more detailed description of the model formulation (originally called OROGENY) is given by Toth et al., (1996), Ford et al., (1999) and Jacome et al., (2003). These studies show the model formulation applied to contractional tectonics however similar physical principles apply for an extensional tectonics scenario.

The fundamental behaviour of RIFTER and its flexural isostatic response, to sequential faulting, sedimentation and erosion, is shown in Figure 5 for both simple extensional and contractional settings. The upper lithosphere is deformed by faults whose geometry is assumed to be listric and whose response to fault displacement is calculated using the vertical shear (Chevron) construction. Faults within RIFTER detach at a defined horizontal level, below which the deeper lithosphere is deformed by pure-shear.

RIFTER also includes the deeper lithosphere deformation response during extensional and/or contractional tectonics. Failure to incorporate this deeper deformation results in an unrealistic cross-section, as shown in Figures 5a and 5f where an extensional and reverse fault respectively deform the upper lithosphere without any deep pure-shear deformation below. Any robust lithospheric model must include both the upper and lower lithosphere deformation response to extensional and/or contractional tectonics.

Model results shown in Figures 5b-e (for extension) and Figures 5g-j (for shortening) include deeper deformation and the flexural isostatic response to faulting, crustal thinning or thickening, sediment fill, erosion, lithosphere thermal perturbation and re-equilibration. Figure 5b shows half-graben formation resulting from a single extensional fault while Figure 5g shows subsidence and foreland basin formation ahead of the over-thrusting. For both extension and shortening, sediment fill and its isostatic loading generates subsidence while erosion consisting of unloading of the subaerial topography generate flexural uplift. New faults modify the earlier formed basins. For extensional tectonics, lithosphere thermal re-equilibration results in post-tectonic thermal subsidence (Figures 5c-e) while for shortening, re-equilibration results in thermal uplift (Figures 5h-j).

5. Modelling experiments applied to the Western Pyrenees

RIFTER model is used to construct the development of the Western Pyrenees across the hyper-extended Mauléon Basin including the Northern (Arzacq) and the Southern Foreland Basins. In this section, we present a set of sequential 2D crustal sections showing the rift and orogenic forward evolution of the Western Pyrenees (Figure 6).

5.1. Rifting evolution

Three main extensional events are responsible of the Arzacq-Mauléon Basin formation (Masini et al., 2014; Jammes et al., 2009). These are; (i) an early rifting event believed to be dominated by a left-lateral transtensional movement but currently highly debated (Late Jurassic – Early Cretaceous), (ii) a necking rifting event (Aptian–Albian) and (iii) a hyper-extended rifting event leading to extreme crustal thinning and locale mantle exhumation (Albian – Cenomanian). Because several studies highlighted the role of salt tectonics in this area (James and Canérot, 1999; Canérot, 1989; Jammes et al., 2010b; Lagabrielle et al., 2010; Masini et al., 2014), we tentatively include this in our modelling as a supplementary surface decollement. However, using our kinematic model, we are unable to generate diapiric structures arising from salt tectonics; this study focuses on the large crustal scale architecture.

Initial RIFTER model setup consists of horizontal layers with uniform thickness. From top to bottom they are; (i) 2 km of pre-rift sediments representing Upper Triassic to Lower Jurassic times, (ii) 28 km of continental crust representing basement consisting of pre-Triassic rocks, (iii) 90 km of continental lithospheric mantle and (iv) asthenospheric mantle.

5.1.1. Early rifting

The first extensional episode that we model is poorly constrained and understood. It has been suggested that during the Late Jurassic – Early Cretaceous a transtensional rifting episode may have occurred leading to slight crustal thinning (e.g. Jammes et al., 2009 and 2010a), however this is currently debated. Local erosion within Jurassic sediments together with Neocomian bauxitic deposits indicate sub-aerial exposures (e.g. James et al., 1996; Canérot, 2008). During the Late Jurassic – Early Cretaceous,

the Aquitaine basin recorded long wavelength vertical motions (e.g. Brunet, 1984; Biteau et al., 2006) rather than an intense localized crustal stretching and thinning which suggests that this deformation might have been controlled by lithospheric scale processes. While Canérot (2008) proposed a regional "transpression" event, recent studies have shown that this phase is coeval with the main stage of transtensional rifting in the nearby Bay of Biscay westwards and Central Iberian Range rift system southwards, both acting as the limits of a diffuse plate boundary at this time (e.g. Tugend et al., 2015a; Nirrengarten et al., 2018; Tavani et al., 2018; Rat et al., 2019). Based on these studies, we suggest that the Late Jurassic – Early Cretaceous rifting episode in the Western Pyrenees occurred due to incipient crustal stretching and thinning ahead of the propagation tip of the Bay of Biscay.

We represent this episode in RIFTER by a non-uniform minor crustal thinning (15 km of extension) followed by partial erosion (Figures 6a and 7a). This deformation affects only the southern area of the model resulting in slight uplift and partial erosion of Upper Triassic to Lower Jurassic sediments which is consistent with field observations (Figure 2).

5.1.2. Necking rifting

The second modelled extensional episode corresponds to the necking rift event that occurred between the Aptian and Albian (Jammes et al., 2009; Masini et al., 2014). The deformation that resulted from this episode is believed to be achieved by the Southern Mauléon Detachment system and an extensional fault that controls the formation of the Southern Mauléon Basin and the Arzacq Basin respectively (Masini et al., 2014). The activity of these north-directed extensional faults started in the Lower Aptian and lasted until the Lower Albian although the climax of the deformation took place between the Upper Aptian and the Lower Albian (Jammes et al., 2009; Masini et al., 2014; Tugend et al., 2014). Lower crustal thinning (boudinage) may have occurred during this stage and, in the Arzacq Basin which shows crustal thinning by a factor of 2 (e.g. Brunet, 1984), may have been more important than the upper crustal stretching.

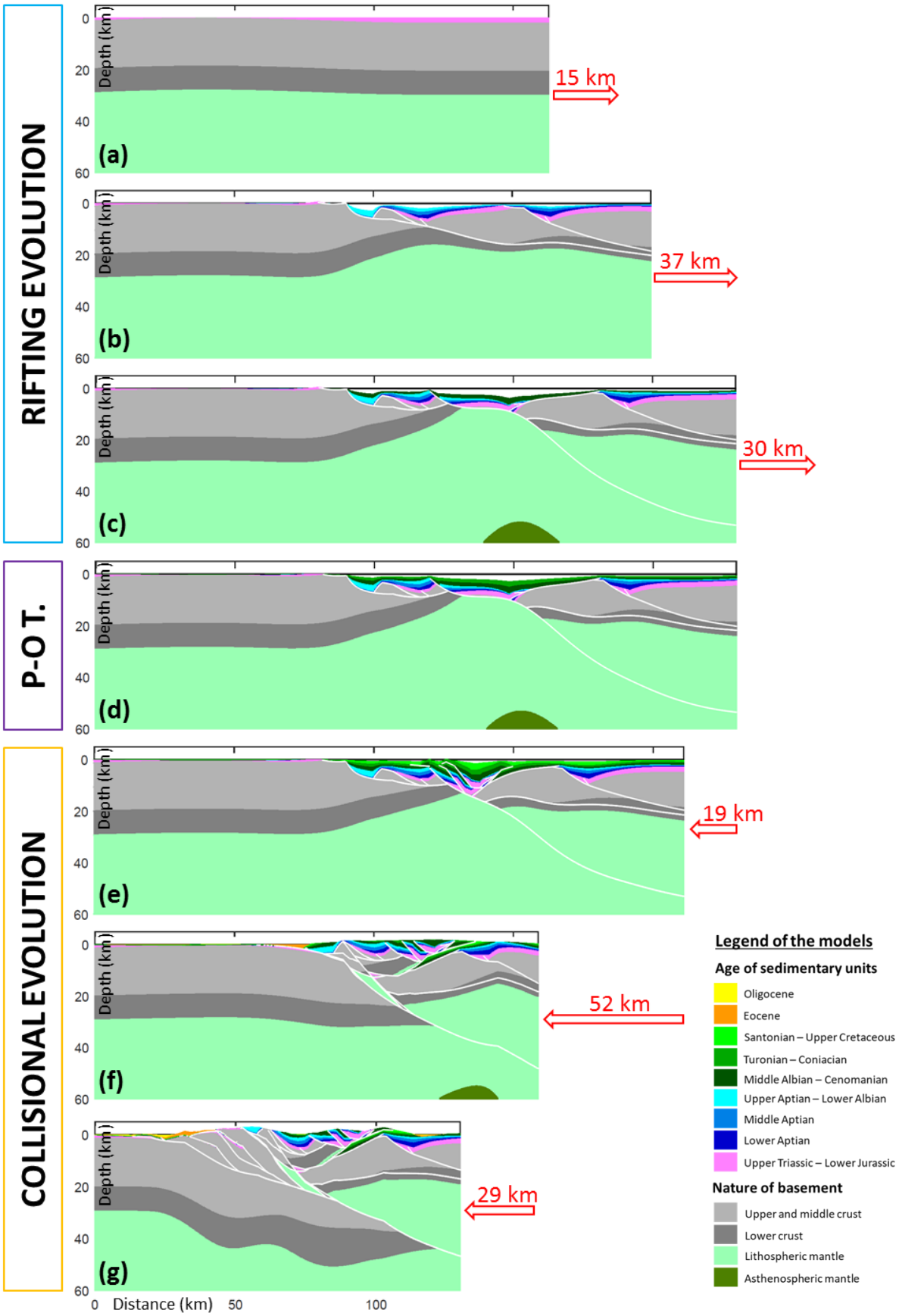
RIFTING EVOLUTION
P-O T.
COLLISIONAL EVOLUTION
Depth (km)
0
20
40
60
(a)
15 km
(b)
37 km
(c)
30 km
(d)
(e)
19 km
(f)
52 km
(g)
29 km
0
Distance (km)
50
100
Legend of the models
Age of sedimentary units
Oligocene
Eocene
Santonian – Upper Cretaceous
Turonian – Coniacian
Middle Albian – Cenomanian
Upper Aptian – Lower Albian
Middle Aptian
Lower Aptian
Upper Triassic – Lower Jurassic
Nature of basement
Upper and middle crust
Lower crust
Lithospheric mantle
Asthenospheric mantle

Figure 6: Rifting and orogenic evolution of the Western Pyrenees using a kinematic structural-stratigraphic forward model (RIFTER). The rifting evolution is shown in **a-c)**, the pre-orogenic template obtained at the end of rifting and used to start the orogenic evolution is show in **d)**, and the orogenic evolution is shown in **e-g)**. **a)** Early rifting with lithosphere extended by 15 km. **b)** Necking rifting with lithosphere extended by 37 km. **c)** Hyper-extension rifting with lithosphere extended by 30 km. **d)** Post-rifting giving the pre-orogenic template (**P-O T**.). **e)** Reactivation of hyper-extended domain with lithosphere shortened by 19 km. **f)** Reactivation of necking domain with lithosphere shortened by 52 km. **g)** Shortening of proximal domain with lithosphere shortened by 29 km. Age of sedimentary units and the nature of the basement are shown in the legend.

To reproduce the consequences of the necking rifting episode, we develop a model template that shows asymmetric crustal thinning (37 km of total extension) affecting only the northern part of the model (Figure 6b). To achieve this, we first create two north-dipping extensional faults soling out at lower crustal levels followed by Lower Aptian sedimentation (Figure 7b). These structures form the northern realm of the Southern Mauléon Detachment and the extensional fault controlling the Arzacq Basin formation (i.e. South-Arzacq fault in this study), the displacement of which is achieved using the Triassic salt layer as a decoupling horizon. We then reactivate the northern realm of the Southern Mauléon Detachment and add another sedimentary unit equivalent to Middle Aptian times (Figure 7c). The last input parameter is the formation of the southern realm of the Southern Mauléon Detachment followed by Upper Aptian to Lower Albian sedimentation and 15 Myr of thermal subsidence representing the duration of the rift event (Figure 7d). As a result of these input parameters, smooth synclines, approximately 5 km deep, consisting of pre- and syn-necking rift sediments are predicted within the Southern Mauléon Basin and the Arzacq Basin (Figures 6b and 7d). These geometries are consistent with the structural observations from the Arzacq Basin (Figure 4c and Appendix 1) as well as with the outcropping of the southern part of the Mauléon Basin located ~20 km west of the cross-section shown in Figure 4b consisting of the Arbailles massif syn-rift syncline (Canérot, 2008). The resultant deep crustal architecture of the Southern Mauléon Basin is characterized by an important crustal thinning forming the typical crustal neck shape whereas beneath the Arzacq Basin the crustal thinning is less pronounced and mainly focused within the lower crust.

5.1.3. Hyper-extension rifting

The last extensional episode modelled corresponds to the hyper-extension rift event. According to Masini et al., (2014), major crustal thinning was achieved by the Northern Mauléon Detachment between Middle Albian and Cenomanian times. This deformation led to the Northern Mauléon Basin formation located between the Southern Mauléon Basin and the Grand Rieu Ridge.

To reproduce this extensional episode, we develop a model that gives major crustal thinning (30 km of total extension) together with mantle exhumation (Figure 6c). To achieve this, we create the Northern Mauléon Detachment corresponding to a large north-dipping extensional fault crosscutting the previously thinned continental crust and coupled into the mantle (Figure 7e) and the Future North Pyrenean Frontal Thrust consisting of an extensional antithetic conjugate fault of the Northern Mauléon Detachment (Figure 7f). The fact that the Northern Mauléon Detachment cuts through a previous necking decollement and thinned crust implies that the crust ahead of the breakaway zone of the Northern Mauléon Detachment is substantially thin. This is in accordance with observations from the western Mauléon Basin where a thinned crustal section without most of the middle-lower crustal rocks is reported (Labourd massif section, Jammes et al., 2009; Masini et al., 2014).

The displacement of the Future North Pyrenean Frontal Thrust (i.e. along the southern slope of the Grand Rieu Ridge) is achieved using the Triassic salt as a decoupling horizon mimicking gravity slides into the axis of the Mauléon Basin. In particular, this tectonic event allows the movement of pre- to syn-hyper-extension sediments from the southern flank of the Grand Rieu Ridge downwards in to the Northern Mauléon Basin. We add a sedimentary unit (representing Middle-Albian to Cenomanian times) while deformation occurs followed by 15 Myr of thermal subsidence (Figure 7f). As a result of these input parameters, the Northern Mauléon Basin with its 8 km deep depocenter is formed together with the occurrence of crustal breakup and mantle exhumation (Figure 7f). The resultant crustal architecture of hyper-extension rifting is that of a typical young pair of conjugate rifted margins characterized by Iberia being the lower plate and Europe being the upper plate (Figure 6c).

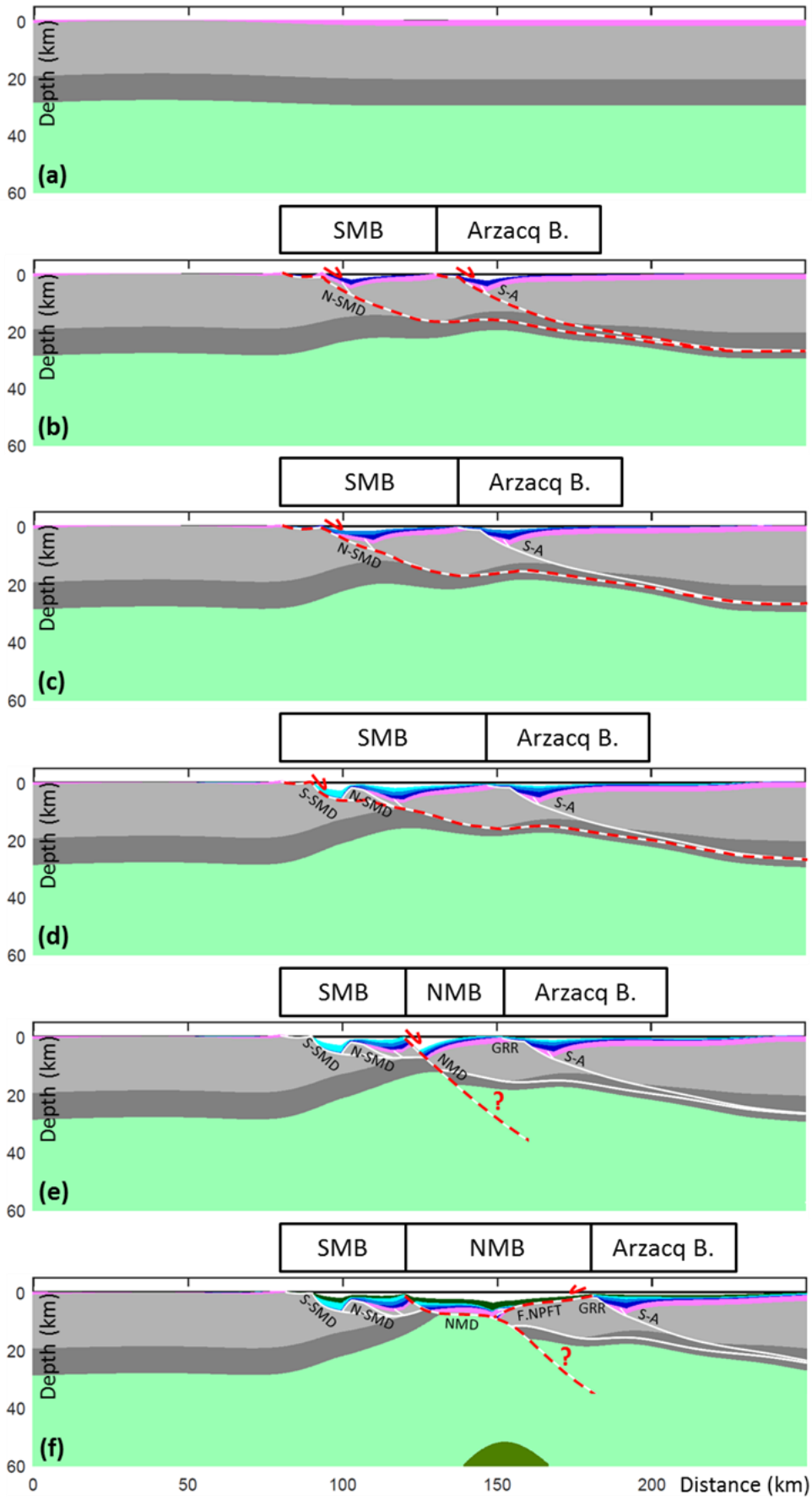
SMB
Arzacq B.
NMB
N-SMD
S-SMD
S-A
GRR
NMD
F.NPFT
Depth (km)
Distance (km)
(a)
(b)
(c)
(d)
(e)
(f)

Figure 7: Detail of the rifting evolution of the Western Pyrenees shown in Figure 6. Red dashed lines indicate active extensional faults whereas white solid lines are inactive extensional faults. **a)** Slight crustal thinning is achieved by lithosphere stretching and thinning. **b)** The N-SMD and the S-A extensional faults are moved at this stage. Sediments partly fill the SMB and the Arzacq Basin. **c)** The N-SMD extensional fault is re-activated at this stage and sediments added. **d)** The S-SMD extensional fault is active at this stage and sediments added. **e)** The NMD extensional fault is active at this stage. **f)** The F.NPFT is active at this stage and a new sedimentary unit fills the SMB, the NMB and the Arzacq Basin. See Figure 6 for the model legend. Structures are; **S-A:** South-Arzacq extensional fault, **N-SMD:** Northern realm of the Southern Mauléon Detachment, **S-SMD:** Southern realm of the Southern Mauléon Detachment, **NMD:** Northern Mauléon Detachment. **F.NPFT:** Future North Pyrenean Frontal Thrust, Basins: **SMB:** Southern Mauléon Basin, **NMB:** Northern Mauléon Basin and **GRR:** Grand Rieu Ridge.

5.2. Post-rifting

To reproduce the post-rifting stage, we first generate erosion followed by 8 Myr of thermal subsidence and partial sedimentation corresponding to post-rift sediments of Turonian to Coniacian age. As a result of this input data, regional subsidence is produced (Figure 6d).

Using RIFTER we have reproduced the development of the rift evolution of the Western Pyrenees (Figures 6a-c) using 82 km of total extension. This post-rifting stage (Figure 6d) is the initial template that we use for the subsequent collisional development of the Western Pyrenees.

5.3. Orogenic evolution

In this section, we quantitatively test a sequential reactivation of former rift domains leading to orogen formation using the Western Pyrenees case-study by reproducing the following three events; (i) reactivation of the hyper-extended domain, (ii) reactivation of the necking domain and (ii) shortening of the proximal domain.

5.3.1. Reactivation of hyper-extended domain

To reproduce the reactivation of the hyper-extended domain (i.e. the hyperthinned and exhumed mantle domains), we use RIFTER to generate a model that shows the nappe-stacking of the Northern Mauléon Basin sedimentary cover while the exhumed Iberian material is underthrusted below the Grand Rieu Ridge. This leads to the closure of the exhumed mantle domain and shortening of the hyper-thinned domain (Figure 6e) (Jammes et al., 2009; Mouthereau et al., 2014; Tugend et al., 2014; Dumont et al.,

2015; Teixell et al., 2016). The structures related to this phase are affected by the later folding and thrusting collisional phase suggesting that the reactivation of the hyper-extended domain took place between the Santonian and Upper Cretaceous (Tugend et al., 2014; Dumont et al., 2015).

To achieve this collisional stage, we reactivate the Northern Mauléon Detachment and the North Pyrenean Frontal Thrust together with minor additional shortening generated by two new north-dipping synthetic thrusts of the Northern Mauléon Detachment leading to the Chaînons Béarnais formation (Figures 8a-b). We add sedimentation while the deformation occurs followed by 6 Myr of thermal re-equilibration and partial erosion. As a consequence of 19 km of shortening during the reactivation of the hyper-extended domain, an important uplift of the Northern Mauléon Basin sedimentary cover (e.g. Chaînons Béarnais fold and thrust belt) corresponding to an accretionary wedge is formed (Figure 6e).

5.3.2. Reactivation of necking domain

For the convergent reactivation of the necking domain, we use 52 km of shortening in RIFTER which generates sub-aerial regional uplift and leads to the restoration of crustal thickness to near normal (~ 30 km) (Figure 6f). This stage is mostly accommodated by south-directed thrusting along the Lakhora-Eaux Chaudes thrust system (Teixell, 1998; Tugend et al., 2014; Dumont et al., 2015; Teixell et al. 2016). Shortening in this domain occurs between the Late Cretaceous and Early Eocene, before the deformation migrates into the subsequent main structures of the Axial Zone (i.e. Gavarnie and Guarga thrusts). The transition between the pre- and post-Palaeocene shortening remains poorly constrained during the reactivation of the necking domain due to an erosional post-Cretaceous event (Bosch et al., 2016). The reactivation of the necking domain is partly simultaneous with the reactivation of the hyper-extended domain as well as with relief initiation in the Axial Zone (Teixell et al., 2016 and 2018). This indicates that the reactivation of the necking domain is a transitional phase consistent with recent results of thermo-mechanical modelling experiments (Jourdon et al., 2019).

To achieve the reactivation of the necking domain, we use the Southern Mauléon Detachment system, the Northern Mauléon Detachment, and the North Pyrenean

Frontal Thrust consisting of an antithetic structure of the Southern Mauléon Detachment (Figures 8b-c). Note that the Northern Mauléon Detachment only acts as the underthrusting plane and therefore its shallower segment is not active. We first displace by thrusting a realm of the North Pyrenean Frontal Thrust and the southernmost realm of the Sothern Mauléon Detachment system (i.e. Lakhora Thrust), followed by partial erosion and sedimentation. The Lakhora Thrust consists of a synthetic footwall fault of the Northern Mauléon Detachment coupled into the shallow mantle enabling to carry upwards a small piece of mantle. We then thrust the northernmost realm of the Southern Mauléon Detachment system (i.e. a synthetic hangingwall fault of the Lakhora Thrust) followed by partial erosion and sedimentation. As a result of this tectonic event, the pop-up of the Southern Mauléon Basin and the Northern Mauléon Basin sedimentary cover is accomplished together with the development of the pre-indentation structure between the Iberian and European plates (Figure 6f). Note that as a consequence of this tectonic event a relatively small piece of anomalously shallow mantle is generated which is consistent with the attenuation of the gravity anomaly towards the east of the Mauléon Basin. In contrast with the western Mauléon Basin where a larger gravity anomaly is observed and interpreted as a shallow large mantle body (Wang et al., 2016). To sample and carry upwards a large piece of mantle, the Lakhora Thrust may has to be coupled into deeper mantle during the reactivation of the necking domain.

5.3.3. Shortening of proximal domain

The later collision phase is characterized by the formation of the Axial Zone together with the development of the Southern Foreland Basin (Figure 6g). This deformation phase occurred between the Eocene and Miocene times which corresponds to the climax of the Alpine orogeny of the Western Pyrenees. This phase is generally described as responsible for the creation of high relief and acceleration of crustal thickening in the Axial Zone and flexural subsidence in the foreland basin.

To reproduce this stage, we develop a set of new south-vergent thrusts crosscutting the Iberian unthinned crust (Figures 8d-e). These structures are, from north to south; Gavarnie Thrust, a minor thrust, Guarga Thrust, and the South Pyrenean Frontal Thrust (Lacombe and Bellahsen, 2016).

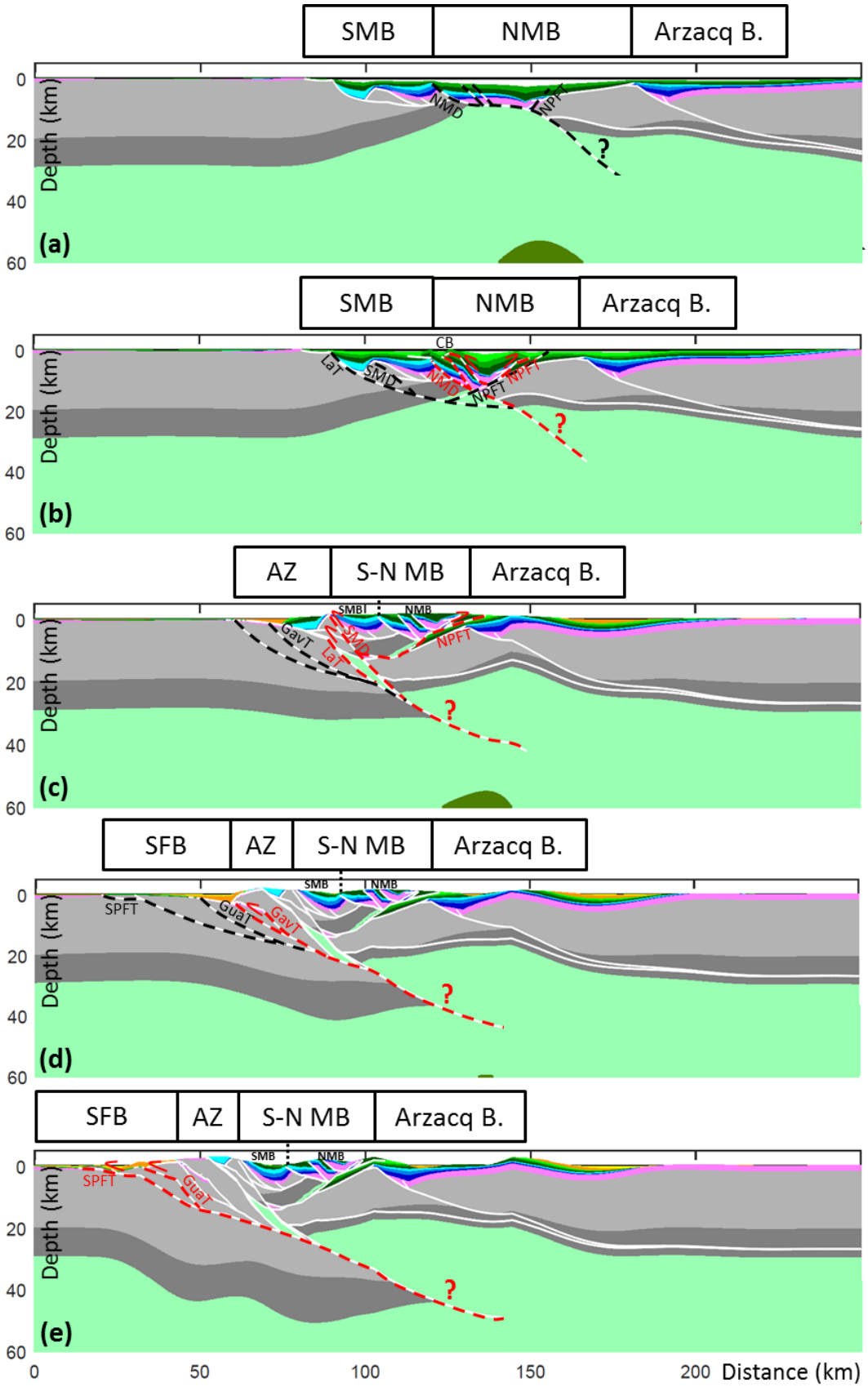
SMB
NMB
Arzacq B.
Depth (km)
0
20
40
60
NMD
NPFT
?
(a)
SMB
NMB
Arzacq B.
CB
LaT
SMD
NMD
NPFT
?
(b)
AZ
S-N MB
Arzacq B.
SMB
NMB
GavT
LaT
SMD
NPFT
?
(c)
SFB
AZ
S-N MB
Arzacq B.
SMB
NMB
SPFT
GuaT
GavT
?
(d)
SFB
AZ
S-N MB
Arzacq B.
SMB
NMB
SPFT
GuaT
?
(e)
0
50
100
150
200
Distance (km)

Figure 8: Detail of the orogenic evolution of the Western Pyrenees shown in Figure 6. Red dashed lines indicate active thrusts faults, black dash lines highlight the position and geometry of thrusts that are active in the next model stage and white solid lines indicate inactive faults. **a)** Pre-orogenic model stage resulting from earlier rifting and thermal subsidence. No thrusts are active at this stage however structures that will be active in the next model stage (**b**) are indicated as black dashed lines. **b)** The NMD, the NPFT and two thrusts within the sedimentary cover leading to the formation of CB are activated as thrusts. A sedimentary unit is added at this stage. **c)** The LaT system and a realm of the NPFT are activated as thrusts at this stage. A sedimentary unit is added at this stage. **d)** The GavT and a minor north-dipping thrust are active. A sedimentary unit is added at this stage. **e)** The GuaT and the SPFT thrusts are active at this stage. See Figure 6 for the legend of the models. Structures are; **NMD:** Northern Mauléon Detachment. **NPFT:** North Pyrenean Frontal Thrust. **SMD:** Southern Mauléon Detachment, **LaT:** Lakhora Thrust, **GavT:** Gavarnie Thrust, **GuaT:** Guarga Thrust, **SPFT:** South Pyrenean Frontal Thrust. **SMB:** Southern Mauléon Basin, **NMB:** Northern Mauléon Basin, **S-N MB:** Southern and Northern Mauléon Basin, **AZ:** Axial Zone, **SFB:** Southern Foreland Basin, **CB:** Chaînons Béarnais.

Additional intermediate second-order thrusts are sometimes discussed (e.g. Teixell et al., 2016, 2018) but are of limited importance for the total amount of shortening as well as for the overall crustal architecture. We sequentially move these thrust structures followed by partial erosion, sedimentation and 6 Myr of thermal re-equilibration. This results in the formation of high relief (using a total shortening of 29 km) together with substantial thickening of the Iberian continental crust from south to north whereas, in contrast, the European continental crust shows a relatively uniform thickness (Figure 6g).

The RIFTER model of the entire collisional evolution of the Western Pyrenees (Figures 6e-g) uses a total of 100 km of shortening including the closing of the former hyper-extended rift basins.

6. Discussion

The purpose of our investigation of the evolution of the Western Pyrenees is to better understand the role of rift structural inheritance during orogeny. We examine both rifting and orogenic histories using structural and stratigraphic modelling that produces cross-sections that are both isostatically as well as structurally balanced.

6.1. Comparison between our model and the target data

Our present-day modelled profile of the Western Pyrenees (Figure 9b) shows a very similar architecture to the target observations (Figures 9a and c).

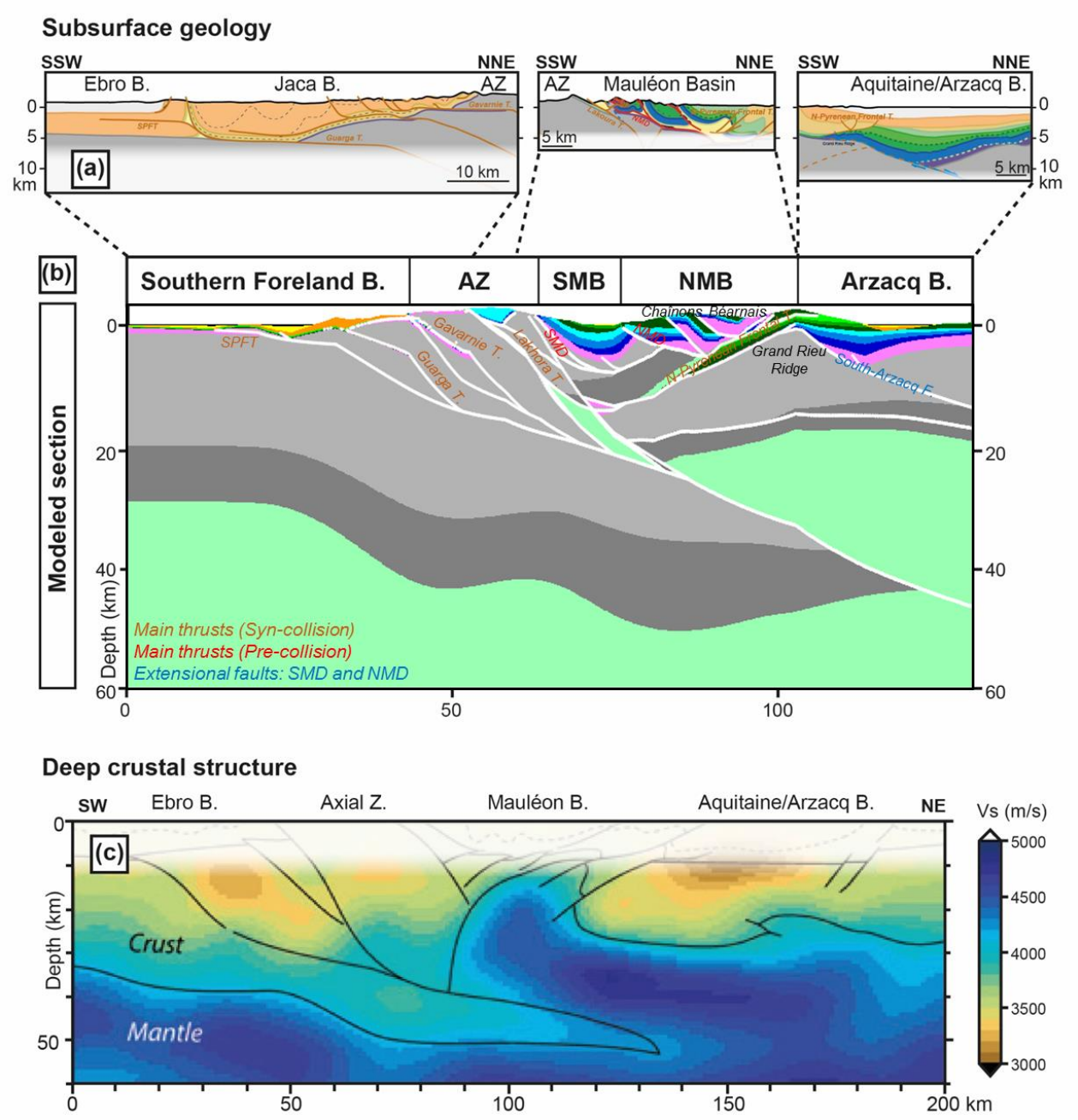

Figure 9: **a)** Present-day geological cross-sections across the Western Pyrenees (from South to North: after Teixell et al., 2016 and 2018; after Tugend et al., 2014; after Lagabrielle et al., 2010 and based on seismic and well data owned by Total) also shown in Figure 4 (their location is shown in Figure 2) and used as a target of the shallow architecture of the modelled section shown in **b)**. **b)** Present-day architecture of the Western Pyrenees generated using RIFTER model in this study (see Figure 6 for model legend). **c)** The PYROPE seismic transect located in the Western Pyrenees (Wang et al., 2016) and also shown in Figure 4 (its position is shown in Figure 2) used as a target of the deep crustal architecture of the modelled section shown in **b)**. **Arzacq B.:** Arzacq Basin, **NMB:** Northern Mauléon Basin, **SMB:** Southern Mauléon Basin, **AZ:** Axial Zone, **Southern Foreland B.:** Southern Foreland Basin (includes Ebro and Jaca Basins). **SPFT:** South Pyrenean Frontal Thrust, **SMD:** Southern Mauléon Detachment, **NMD:** Northern Mauléon Detachment.

We are able to reproduce the first-order sub-surface geology of the main domains of the Western Pyrenees across the Mauléon Basin including the Northern (Arzacq) and the Southern Foreland Basins. From north to south these are; the Arzacq Basin, the Northern Mauléon Basin, the Southern Mauléon Basin, the Axial Zone and the Southern Foreland Basin (Figure 9b). However, some parts of our modelled section using RIFTER, such as the Southern Foreland Basin and the Arzacq Basin, require more subsidence to match the target data more precisely. One of the reasons for this misfit may be the value of the effective elastic thickness (Te) used to define the flexural isostatic strength of the lithosphere. The typical Te during continental rifting ranges between 1.5 and 3 km (Roberts et al., 1998; White, 1999; Roberts et al., 2019) while during shortening tectonics this value is usually higher than that. Ford et al., (1992) explored the sensitivity of Te to the lithosphere flexure during thrust sheet emplacement and foreland basin formation and showed that a Te value of 20 km is representative of the foreland region while a lower Te is expected for the centre of the orogen. Jácome et al., (2003) showed that Te = 7.5 km provided the best fit to observations for models of the development of the Maturín Foreland Basin, Eastern Venezuela. In this study we use Te = 1.5 km to calculate the flexural isostatic response for both rifting and contractional tectonics. Not using a higher Te during the contractional history most probably explains the insufficient subsidence predicted for the Arzacq and Southern Foreland Basins (Figure 9b).

Despite this, the Southern and Northern Mauléon Basin as well as the Axial Zone are reasonably well reproduced (Figure 9b) and show the first order stratigraphic architecture as suggested by field observations (Figure 9a). Note that the Southern Mauléon Basin is not well preserved along the eastern Mauléon Basin (Figure 2) and thus we use as reference the outcropping geology ~20 km to the west (Arbailles massif syn-rift syncline, Canérot, 2008) of the target cross-section shown in Figures 4b and 9a to reproduce the Southern Mauléon Basin architecture.

The deeper part of our modelled section shows the southern Iberian Moho at about 30 km depth which gently dips towards the north reaching values of 50 km deep beneath the Mauléon-Arzacq Basin, while the European Moho is more or less horizontal at 20 km deep (Figure 9b). At the larger scale, our modelled deep crustal architecture is similar to that shown by the PYROPE seismic transect of Wang et al., (2016).

However, it differs from the seismically imaged Moho beneath the Mauléon Basin (Figure 9c). The PYROPE profile is located across the western part of the Mauléon Basin (Figure 2) where a localized strong positive Bouguer gravity anomaly has been identified (Figure 4e) and interpreted as a piece of exhumed mantle. However, this anomaly is not observed in the eastern Mauléon Basin where the majority of sub-surface geological target observations are obtained (Figure 2). The Moho beneath the Mauléon Basin of our modelled profile is more characteristic of the eastern Mauléon Basin. The overall deep crustal architecture along the Southern Foreland Basin, Axial Zone and Arzacq Basin is expected to be similar across both the eastern and western parts of the Mauléon Basin.

6.2. Uncertainties of deep fault geometry

Fault geometries used to produce our preferred model of the present-day architecture of the Western Pyrenees (Figure 9b) are relatively well constrained for the top 10 to 15 km of depth using surface geology, seismic data and boreholes. However, below these depths, there is little constraint on deep fault geometry. Our preferred model uses deeper fault geometries to give the closest possible agreement to the deep target data (Figure 9c) as well as to the shallower constraints (Figure 9c), however the deeper fault geometries that we have used are not unique. An important question that remains is whether thrust faults within the reactivated necking and proximal rift domains are coupled into the mantle or sole out within the middle-lower crust associated with distributed (pure-shear) deformation below. The evolution of the coupling-depth of faults of other orogenic systems should be investigated to better understand this.

6.3. From rifting to orogeny

Based on the Western Pyrenean example, we suggest a succession of first order tectonic stages that may be used to understand the development of other Alpine type collisional systems. These stages are separated by critical events in geological time that record the change between different tectonic styles of lithosphere deformation. In Figure 10 we show a tectonic evolutionary chart which summarises the deformation mechanism associated with these first order extensional and contractional tectonic stages. The attribution of deformation mechanisms for the rifting stage is based on

literature review, while the attribution of deformation mechanisms during the orogenic stage is based on this study.

6.3.1. Rifting evolution

The rifting evolution of the Western Pyrenean example is characterized by three different tectonic phases, each of them respectively bounded by Lower Aptian, Middle Albian and Upper Cenomanian critical events (Figures 10a-c).

During an early rifting stage, the deformation is typically wide and diffuse. This is achieved by faulting in the brittle upper crust soling out at mid-crustal levels (e.g. Stein and Barrientos, 1985, Jackson, 1987) with distributed deformation below in the lower crust and mantle. This typically leads to a slight crustal thinning (e.g. Marsden et al., 1990). In our Western Pyrenees case-study, the first early rifting stage occurred up to the Lower Aptian leading to slight crustal thinning resulting into an overall crustal doming architecture (Figure 10a). In the subsequent necking rift stage, the extensional deformation localizes although it is still achieved by faults decoupled from the mantle which sole out at mid to lower crustal levels (Pérez-Gussinyé et al., 2001; Sutra et al., 2013). During this stage more substantial crustal thinning occurs (Pérez-Gussinyé et al., 2003; Osmundsen and Redfield, 2011, Sutra et al., 2013). This second rifting stage affected the Western Pyrenees up to the Lower Albian. This resulted in high crustal thinning and deepening of the Southern Mauléon and Arzacq Basins (Figure 10b). In our study-case, the necking rifting stage was strongly asymmetric characterized by north-dipping faulting. This is evidenced by: (i) major uplift of the southern flank of the Mauléon Basin (footwall uplift of the lower plate) and (ii) an extension discrepancy between the observed rift structures and the amount of total crustal thinning in the Arzacq Basin. Note that this peculiar asymmetric necking is not always the case and can be more symmetric in other examples (e.g. Lavier and Manatschal, 2006). The third rifting stage consists of hyper-extension rifting where deformation is also localized, however in this case it is achieved by extensional faults coupled into the mantle (Pérez-Gussinyé et al., 2001; Sutra et al., 2013), the maximum penetration depth of which is unknown.

In our Western Pyrenean example, this stage lasted up to the Upper Cenomanian critical event leading to the deepening of the Northern Mauléon Basin (Figure 10c).

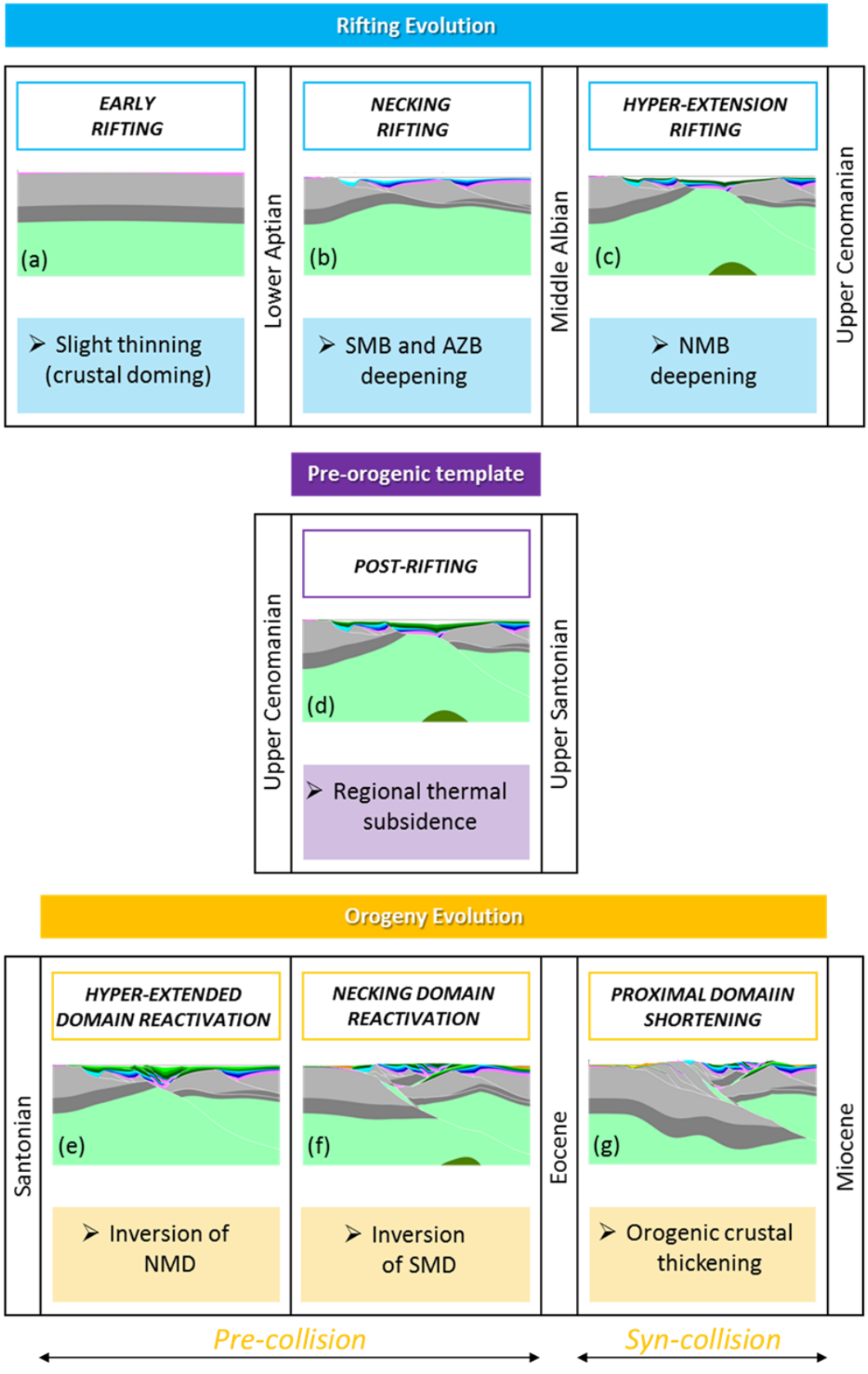

Figure 10: Evolutionary chart summarizing the rifting and orogenic evolution of the Western Pyrenees showing the different tectonic stages and their geological times. **a)** Early rifting, **b)** Necking rifting, **c)** Hyper-extension rifting), **d)** Post-rifting subsidence giving the pre-orogenic template, **e)** Hyper-extended domain reactivation, **f)** Necking domain reactivation and **g)** Proximal domain shortening. See Figures 6 models legend. Basins: **SMB:** Southern Mauléon Basin, **AZB:** Arzacq Basin, **NMB:** Northern Mauléon Basin. Structures: **NMD:** Northern Mauléon Detachment, **SMD:** Southern Mauléon Detachment.

6.3.2. Pre-orogenic template

In the Western Pyrenees, the post-rifting stage consists of a period of tectonic quiescence characterized by regional thermal subsidence (Figure 10d). This stage, spanning the Upper Cenomanian to Upper Santonian, is bounded by two critical events marking the end of rifting and the onset of orogeny respectively. It is important to point out that the end of this stage (Upper Santonian) corresponds to the pre-orogenic template.

6.3.3. Orogenic evolution

The orogenic evolution of the Western Pyrenees consists of two stages divided by critical events in the Santonian, Eocene and Miocene marking changes in deformation style (Figures 10e-g). The first stage is characterized initially by the reactivation of the hyper-extended domain (i.e. exhumed mantle and hyperthinned domains) followed by the reactivation of the necking domain. This deformation stage, involving the contractional reactivation of hyper-extended and necking rift domains, leads to the recovery of normal crustal thickness (~ 30 km). The second deformation stage is characterized by the shortening of the proximal rift domain consisting of crustal thickening as well as the development of the orogenic root.

Reactivation of hyper-extended domain

According to Péron-Pinvidic et al., (2008) the exhumed continental mantle within the hyper-extended domain corresponds to the weakest part of the margin and thus is a preferred location for the initiation of subduction. This area may become even more weaker if serpentinization of exhumed mantle takes place as suggested by Pérez-Gussinyé et al., (2001) and may consequently generate a weakness within the mantle where the contractional deformation may preferentially initiate (Péron-Pinvidic et al., 2008; Lundin and Doré, 2011; Tugend et al., 2014 and 2015a).

In the Western Pyrenees, the initiation of the reactivation of the hyper-extended domain starts in the Santonian. We show that the deformation during this stage is localized and achieved through extensional fault reactivation within the hyper-extended domain where the Northern Mauléon Detachment system is coupled into the mantle. This reactivated structure pre-configures the continental underthrusting plane and may define, in this case, the vergence of the belt (Figure 10e).

Reactivation of necking domain

How structures developed during the necking rift stage may reactivate during collision is uncertain. One possibility is that the necking-domain extensional faults are reactivated using their original geometry which corresponds to faults soling out within the crust with distributed pure-shear deformation below. However, another possibility is that the reactivated necking-domain extensional faults modify their deeper geometry and couple directly into shallow mantle towards the underthrusting plane. From a geometrical point of view, this would consist of a footwall shortcut that may sample lower crust or even mantle rocks. Whether one fault reactivation mechanism is generally more common than the other is unknown. However, to reproduce the present-day architecture of the Western Pyrenees we use the second hypothesis consisting on the reactivation of the Southern Mauléon Detachment system modifying its deeper geometry and coupling into shallow mantle. This can also explain the occurrence of shallow bodies of mantle rocks that outcrop and/or are suggested from gravity anomalies (Wang et al., 2016).

In any case, the contractional reactivation of the hyper-extended and necking domains results in the closure of the earlier rift basins and leads to the restoration of the thickness of continental crust towards normal values (~30 km) (Figure 10f).

Shortening of proximal domain

Previous geometric or model-based studies such as Teixell et al., (2016) or Jammes et al., (2014) suggested that basement involved thrusts responsible for the collisional stage may be decoupled at about 15 km. Using the Western Pyrenees as an example, we show that to achieve the shortening of the proximal domain, thrusts ramps are decoupled from the mantle by a flat decollement at 25 km depth which laterally branches within the underthrusting plane (ramp). These north-dipping thrusts may be

either new faults or reactivated extensional faults (Bellahsen et al., 2012) within the proximal rift domain. As a result of this deformation stage, significant orogenic crustal thickening is produced and hence the Axial Zone is formed (Figure 10g).

The deformation mechanism by which this final stage is achieved differs from that of the earlier convergent stage, involving reactivation of the hyper-extended and necking domains, and thus suggests a critical event between these two stages during the Eocene. The final convergent stage of the Western Pyrenees lasted until the Miocene when contractional deformation ended.

7. Conclusions

Using modelling we investigate the structural and stratigraphic evolution of both the rift and orogenic lithosphere deformation of the Western Pyrenees through a set of isostatically as well as structurally balanced cross-sections. We use this to better understand the role of rift structural inheritance during orogeny.

The key conclusions of this work on the formation of rifted margins and their subsequent development into orogens are the following:

1- The present-day structure of the Western Pyrenees orogen has been reproduced by including the extensional as well as the compressional history of lithosphere deformation.
2- The earlier extensional tectonic of the Western Pyrenees is characterized by a Cretaceous hyper-extended rift system. This is followed by contractional tectonics consisting of two sequential deformation stages: (i) the reactivation of the hyper-extended and necking rift domains and (ii) the shortening of the proximal rift domain.
3- Using the Western Pyrenees as an example, we suggest the following insights on the deeper fault geometries during orogeny, although this still needs to be compared with other orogenic systems. The contractional reactivation of the hyper-extended rift domain uses faults which are coupled into the mantle. The contractional reactivation of the necking rift domain uses faults which modify their deeper geometry and couple into shallow mantle. The shortening of the

proximal rift domain on the pro-side of the belt is achieved by thrusts ramps which laterally link into the continental underthrusting ramp plane.

We believe that the tectonic evolutionary chart derived from this study, which summarises the extensional and contractional lithosphere deformation stages, may be applied to other Alpine-type collisional systems involving the reactivation and inversion of former hyper-extended rift domains.

Acknowledgments

We acknowledge the MM4 (Margin Modelling Phase 4) industry partners (BP, Conoco Phillips, Statoil, Petrobras, Total, Shell, BHP-Billiton, and BG) for financial support and discussions. We thank Total SA and notably S. Calassou for allowing the use of seismic and well data across the Arzacq Basin and publication of proprietary seismic line nº1325. E.M. acknowledge the Orogen research program for fruitful discussions. J.G-R. thanks A. Lamur for collaborate in the development of a new MATLAB code used to display the graphics of all RIFTER models presented here. The original manuscript was improved by reviews from S. Tavani, an anonymous reviewer and by guest editors O. Lacombe and S. Mazzoli, who we thank for their helpful comments.

Appendix 1

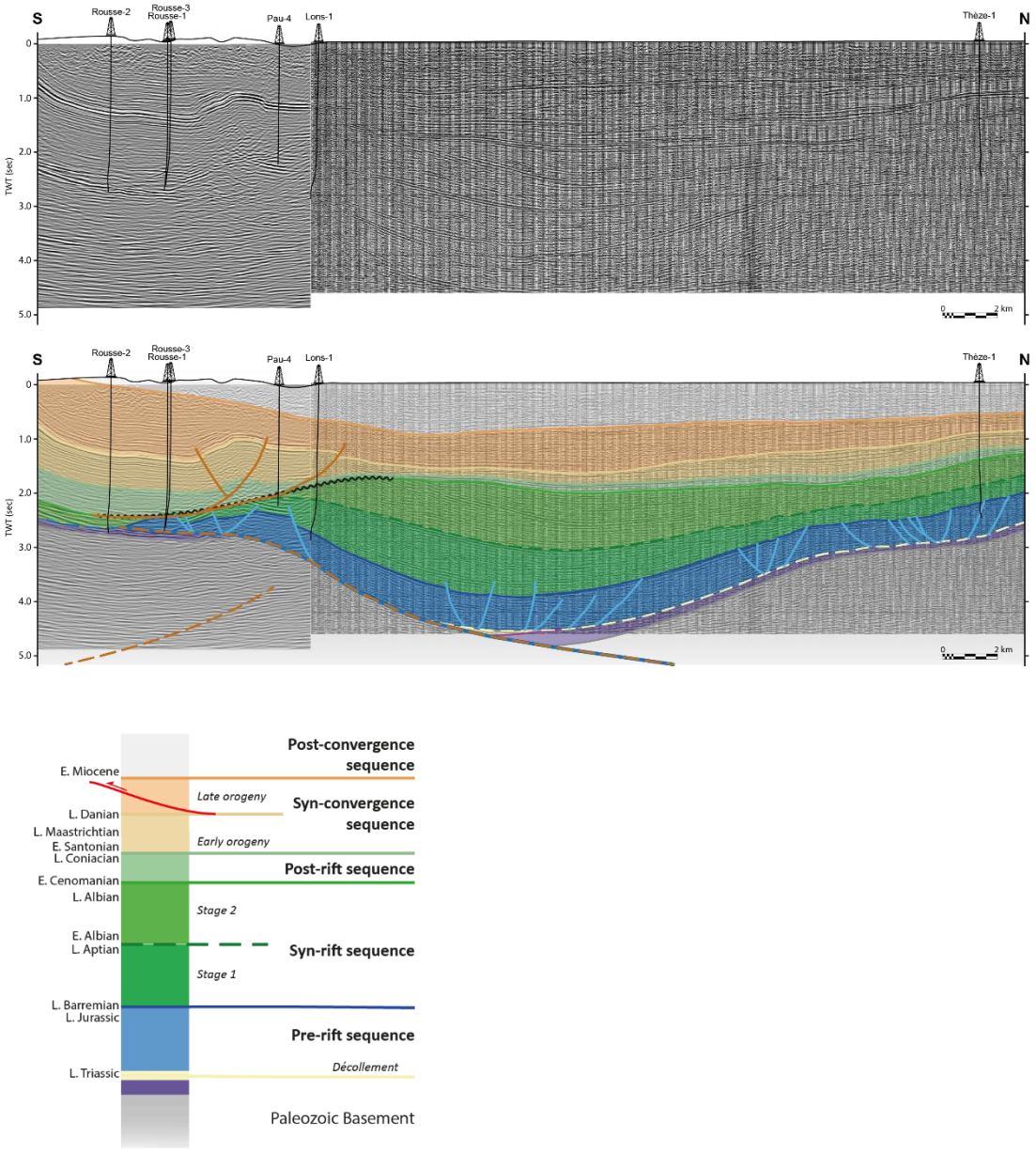

Figure 1: Seismic line nº1325 and the position of well logs owned by Total SA (above) used to constrain the first order seismic interpretation of the Arzacq Basin (below).

REFERENCES

Andersen, T.B., Corfu, F., Labrousse, L., Osmundsen, P.-T., 2012. Evidence for hyperextension along the pre-Caledonian margin of Baltica. J. Geol. Soc. London. 169, 601–612. https://doi.org/10.1144/0016-76492012-011.

Angrand, P., Ford, M., & Watts, A. B. (2018). Lateral variations in foreland flexure of a rifted continental margin: The Aquitaine Basin (SW France). Tectonics, 37(2), 430-449.

Bellahsen, N., Jolivet, L., Lacombe, O., Bellanger, M., Boutoux, A., Garcia, S., Mouthereau, F., Le Pourhiet, L., Gumiaux, C., 2012. Mechanisms of margin inversion in the external Western Alps: Implications for crustal rheology. Tectonophysics 560–561, 62–83. https://doi.org/10.1016/j.tecto.2012.06.022.

Beltrando, M., Manatschal, G., Mohn, G., Dal Piaz, G.V., Vitale Brovarone, A., Masini, E., 2014. Recognizing remnants of magma-poor rifted margins in high-pressure orogenic belts: The Alpine case study. Earth-Science Rev. 131, 88–115. doi:10.1016/j.earscirev.2014.01.001.

Biteau, J.-J., Le Marrec, A., Le Vot, M., Masset, J.-M., 2006. The Aquitaine Basin. Pet. Geosci. 12, 247–273. doi:10.1144/1354-079305-674.

Bosch, G. V., Teixell, A., Jolivet, M., Labaume, P., Stockli, D., Domènech, M., Monié, P., 2016. Timing of Eocene-Miocene thrust activity in the Western Axial Zone and Chaînons Béarnais (west-central Pyrenees) revealed by multi-method thermochronology. Comptes Rendus - Geosci. 348, 246–256. https://doi.org/10.1016/j.crte.2016.01.001.

Brgm, Esso, S., 1974. Géologie du bassin d'Aquitaine. Orléans, France.

Brunet, M.F., 1984. Subsidence history of the Aquitaine basin determined from subsidence curves. Geol. Mag. 121, 421–428. doi:10.1017/S0016756800029952.

Burg, J.-P., 1994. Syn-to post-thickening extension in the Variscan Belt of Western Europe: modes and structural consequences. Géologie la Fr. 3, 33–51.

Canérot, J., 1989. Early Cretaceous rifting and salt tectonics on the Iberian margin of the western Pyrenees (France). Structural consequences. Bull. Tech. Explor. Elf

Aquitaine 13 (1), 87–99.

Canérot, J., Majeste-Menjoulas, C., Ternet, Y., James, V., Fabre, R., Desrumaux, C., Lebourg, T., 2001. Les glissements rocheux du versant sud du Layens (Vallée d'Aspe, Pyrénées occidentales). Bull. la Société géologique Fr. 172, 779–784.

Canérot, J., 2008. Les Pyrénées: histoire géologique et itinéraires de découverte. Biarrtiz: Atlantica/BRGM éds., 2, 646 p.

Capote, R., Muñoz, J.A., Simón, J., 2002. Alpine tectonics. I: The Alpine system north of the Betic Cordillera. Geol. Soc. London, Spec. Publ. n W. Gibbo, 367–400.

Casas, A., Kearey, P., Rivero, L., Adam, C., 1997. Gravity anomaly map of the Pyrenean region and a comparison of the deep geological structure of the western and eastern Pyrenees. Earth Planet. Sci. Lett. 150, 65–78. doi:10.1016/S0012-821X(97)00087-3.

Casteras, M., 1969. Geological map sheet of Mauléon-Licharre, 1/80000. BRGM Orléans, France.

Chevrot, S., Sylvander, M., Diaz, J., Ruiz, M., Paul, A., Cougoulat, G., Péquegnat, C., Wolyniec, D., Delmas, P., Grimaud, F., Benahmed, S., Pauchet, H., de Saint Blanquat, M., Lagabrielle, Y., Manatschal, G., 2015. The Pyrenean architecture as revealed by teleseismic P-to-S converted waves recorded along two dense transects. Geophys. J. Int. 200, 1096–1107. doi:10.1093/gji/ggu400.

Chevrot, S., Sylvander, M., Diaz, J., Martin, R., Mouthereau, F., Manatschal, G., Masini, E., Calassou, S., Grimaud, F., Pauchet, H., Ruiz, M., 2018. The non-cylindrical crustal architecture of the Pyrenees 1–8. https://doi.org/10.1038/s41598-018-27889-x.

Choukroune, P., Pinet, B., Roure, F., Cazes, M., 1990. Major Hercynian thrusts along the ECORS Pyrenees and Biscay lines. Bull. la Société géologique Fr. 2, 313–320.

Clerc, C., Lagabrielle, Y., Neumaier, M., Reynaud, J.-Y., de Saint Blanquat, M., 2012. Exhumation of subcontinental mantle rocks: evidence from ultramafic-bearing clastic deposits nearby the Lherz peridotite body, French Pyrenees. Bull. la Soc.

Geol. Fr. 183, 443–459. https://doi.org/10.2113/gssgfbull.183.5.443.

Clerc, C., Lagabrielle, Y., 2014. Thermal control on the modes of crustal thinning leading to mantle exhumation: Insights from the cretaceous pyrenean hot paleomargins. Tectonics 33. https://doi.org/10.1002/2013TC003471.

Cochelin, B., Lemirre, B., Denèle, Y., de Saint Blanquat, M., Lahfid, A., & Duchêne, S. (2018). Structural inheritance in the Central Pyrenees: the Variscan to Alpine tectonometamorphic evolution of the Axial Zone. Journal of the Geological Society, 175(2), 336-351.

Daignières, M., Séguret, M., Specht, M., ECORS, T., 1994. The Arzacq-Western Pyrenees ECORS deep seismic profile. Publ. Eur. Assoc. Pet. Geol. 4, 199–208.

Dumont, T., Replumaz, A., Rouméjon, S., Briais, A., Rigo, A., Bouillin, J.P., 2015. Microseismicity of the Béarn range: Reactivation of inversion and collision structures at the northern edge of the Iberian plate. Tectonics, 34, doi:10.1002/2014TC003816.

Epin, M., 2017. Defining diagnostic criteria to describe the role of rift inheritance in collisional orogens : the case of the Err-Platta nappes (Switzerland). Swiss J Geosci, doi:10.1007/s00015-017-0271-6.

Ford, M., Lickorish, W.H., Kusznir, N.J., 1999. Tertiary foreland sedimentation in the Southern Subalpine Chains, SE France: A geodynamic appraisal. Basin Res. 11, 315–336. doi:10.1046/j.1365-2117.1999.00103.

Gallastegui, J., Pulgar, J.A., Gallart, J., 2002. Initiation of an active margin at the North Iberian continent-ocean transition. Tectonics 21, 1–14. doi:10.1029/2001TC901046.

Garrido-Megías, A., Ríos, L., 1972. Síntesis geologica del Secundario y Terciario entre los ríos Cinca y Segre (Pirineo Central de la vertiente surpirenaica, provincias de Huesca y Lerida). Bol. Geol. Min 83, 1–47.

Grandjean, G., 1994. Etude des structures crustales dans une portion de chaîne et de leur relation avec les bassins sédimentaires. Application aux Pyrenees occidentales. Bull. la Société géologique Fr. Explor. Elf-Aquitaine Prod 18, 391–

419.

Grool, A.R., Ford, M., Vergés, J., Huismans, R.S., Christophoul, F., Dielforder, A., 2018. Insights Into the Crustal-Scale Dynamics of a Doubly Vergent Orogen From a Quantitative Analysis of Its Forelands: A Case Study of the Eastern Pyrenees. Tectonics 37, 450–476. https://doi.org/10.1002/2017TC004731.

Jackson, J., 1987. Active normal faulting and crustal extension. Geol. Soc. London, Spec. Publ. 28, 3–17. doi:10.1144/GSL.SP.1987.028.01.02.

Jácome, M.I., Kusznir, N., Audemard, F., Flint, S., 2003. Formation of the Maturín Foreland Basin, eastern Venezuela: Thrust sheet loading or subduction dynamic topography. Tectonics 22, n/a-n/a. https://doi.org/10.1029/2002tc001381.

James, V., Canérot, J., Biteau, J. J., 1996. Données nouvelles sur la phase de rifting atlantique des Pyrénées occidentales au Kimméridgien: La masse glissée d'Ouzous (Hautes Pyrénées), Géol. France 3, 60–66.

James, V., Canérot, J., 1999 Diapirisme et structuration post-triasique des Pyrénées occidentales et de l'aquitaine méridionales (France). Eclogae Geol Helv 92:63–72.

Jammes, S., Manatschal, G., Lavier, L., Masini, E., 2009. Tectonosedimentary evolution related to extreme crustal thinning ahead of a propagating ocean: Example of the western Pyrenees. Tectonics, 28, TC4012, doi:10.1029/2008TC002406.

Jammes, S., Lavier, L., Manatschal, G., 2010a. Extreme crustal thinning in the Bay of Biscay and the Western Pyrenees: From observations to modeling. Geochem. Geophys. Geosyst., 11, Q10016, doi:10.1029/2010GC003218.

Jammes, S., Manatschal, G., Lavier, L., 2010b. Interaction between prerift salt and detachment faulting in hyperextended rift systems : The example of the Parentis and Mauléon basins (Bay of Biscay and western Pyrenees). AAPG Bulletin, v. 94, num 7, 957–975. doi:10.1306/12090909116.

Jammes, S., Huismans, R.S., Muñoz, J.A., 2014. Lateral variation in structural style of mountain building: Controls of rheological and rift inheritance. Terra Nova, 26, 201–207. doi:10.1111/ter.12087.

Jourdon, A., Le Pourhiet, L., Mouthereau, F., Masini, E., 2019. Role of rift maturity on the architecture and shortening distribution in mountain belts. Earth Planet. Sci. Lett. 512, 89–99. https://doi.org/S0012821X19300937.

Lacombe, O., Bellahsen, N., 2016. Thick-skinned tectonics and basement-involved fold-thrust belts: Insights from selected Cenozoic orogens, Geological Magazine. https://doi.org/10.1017/S0016756816000078.

Lagabrielle, Y., Bodinier, J., 2008. Submarine reworking of exhumed subcontinental mantle rocks : field evidence from the Lherz peridotites. French Pyrenees 11–21. doi:10.1111/j.1365-3121.2007.00781.

Lagabrielle, Y., Labaume, P., Blanquat, M.D. Saint, 2010. Mantle exhumation , crustal denudation , and gravity tectonics during Cretaceous rifting in the Pyrenean realm (SW Europe): Insights from the geological setting of the lherzolite bodies. Tectonics, 29, TC4012, doi:10.1029/2009TC002588.

Lavier, L., Manatschal, G., 2006. Mechanism to thin continental lithosphere at magma poor margins. Nature 440:324-328.

Lemoine, M., Tricart, P., Boillot, G., 1987. Ultramafic and gabbroic ocean floor of the Ligurian Tethys (Alps, Corsica, Apennines): in search of a genetic model. Geology 15, 622–625. https://doi.org/10.1130/0091-7613.

Le Pichon, X., Sibuet, J.-C., 1971. Western extension of boundary between European and Iberians plates during the Pyrenean orogeny. Earth Planet. Sci. Lett. 12, 83–88.

Le Pochat, G., Lenguin, M., Thibault, C., 1976. Carte géologique de la France à 1/50 000, feuille n^{o} XIV-45, Mauléon-Licharre, avec notice explicative. Orléans: BRGM éd, 24 p.

Le Pochat, G., Lenguin, M., Napias, J.-C., Thibaut, C., Roger, P., Bois, J.-P., 1978. Carte géologique de la France à 1/50 000, feuille n^{o} XIII-46, Saint-Jean-Pied-de-Port, avec notice explicative. Orléans: BRGM éd, 41.

Lundin, E.R., Doré, A.G., 2011. Hyperextension, serpentinization, and weakening: A new paradigm for rifted margin compressional deformation. Geology 39, 347–

350. doi:10.1130/G31499.1.

Macchiavelli, C., Vergés, J., Schettino, A., Fernàndez, M., Turco, E., Casciello, E., Tunini, L. (2017). A new southern North Atlantic isochron map: Insights into the drift of the Iberian plate since the Late Cretaceous. Journal of Geophysical Research: Solid Earth, 122(12), 9603-9626.

Manatschal, G., 2004. New models for evolution of magma-poor rifted margins based on a review of data and concepts from West Iberia and the Alps. Int. J. Earth Sci. 93, 432–466. https://doi.org/10.1007/s00531-004-0394-7.

Masini, E., Manatschal, G., Mohn, G., Unternehr, P., 2012. Anatomy and tectono-sedimentary evolution of a rift-related detachment system : The example of the Err detachment (central Alps, SE Switzerland). GSA Bull. 1535–1551. https://doi.org/10.1130/B30557.1.

Masini, E., Manatschal, G., Tugend, J., Mohn, G., Flament, J.M., 2014. The tectono-sedimentary evolution of a hyper-extended rift basin: The example of the Arzacq-Maul??on rift system (Western Pyrenees, SW France). Int. J. Earth Sci. 103, 1569–1596. doi:10.1007/s00531-014-1023-8.

Marsden, G., Yielding, G., Roberts, A., Kusznir, N., 1990. Application of a flexural cantilever simple-shear/pure-shear model of continental lithosphere extension to the formation of the northern North Sea basin. In: D.J. Blundell and A.D. Gibbs (Editors), Tectonic Evolution of the North Sea Rifts. Oxford Univ, Press 236–257.

Mattauer, M., Henry, J., 1974. The Pyrenees, in Mesozoic-Cenozoic Orogenic Belts. Data for orogenic Studies: Alpine-Himalayan Orogens, edited by A. M. Spencer. Geol. Soc. London Spec. Publ 4,3-21.

McClay, K., Muñoz, J.A., García-Senz, J., 2004. Extensional salt tectonics in a contractional orogen : A newly identified tectonic event in the Spanish Pyrenees. Geology, v.4, 737–740. https://doi.org/10.1130/G20565.1.

Mohn, G., Manatschal, G., Müntener, O., Beltrando, M., Masini, E., 2010. Unravelling the interaction between tectonic and sedimentary processes during lithospheric thinning in the Alpine Tethys margins. Int. J. Earth Sci. 99, 75–101.

https://doi.org/10.1007/s00531-010-0566-6.

Mohn, G., Manatschal, G., Beltrando, M., Haupert, I., 2014. The role of rift-inherited hyper-extension in Alpine-type orogens. Terra Nov. 26, 347–353. https://doi.org/10.1111/ter.12104.

Montadert, L., Roberts, D.G., 1979. Initial Reports of the Deep Sea Drilling Project, 48 pp., US Governmment Printing Office, Washington, D.C.

Montadert, L., De Charpal, O., Roberts, D., Guennoc, P., Sibuet, J.-C., 1979. Northeast Atlantic passive continental margins: Rifting and subsidence processes. In: Talwani, M., Hay, W. & Ryan, W. B. F. (eds) Deep Drilling Results in the Atlantic Ocean: Continental Margins and Palaeoenvironments. Am. Geophiscal Union, Washington, DC 154–186.

Mouthereau, F., Filleaudeau, P.-Y., Vacherat, A., Pik, R., Lacombe, O., Guiditta-Fellin, M., Castelltort, S., Christophoul, F., Masini, E., 2014. Placing limits to shortening evolution in the Pyrenees: Role of margin architecture and implications for the Iberia/Europe convergence. Tectonics, 33, doi:10.1002/2014TC003663.

Muñoz, J.A., 1992. Evolution of a continental collision belt: ECORS-Pyrenees crustal balanced section, in Thrust Tectonics edited by K.R. McClay 235–246.

Muñoz, J.A., 2002. The Pyrenees. Gibbons W., Moreno, T. 370–385.

Nirrengarten, M., Manatschal, G., Tugend, J., Kusznir, N., Sauter, D., 2018. Kinematic Evolution of the Southern North Atlantic: Implications for the Formation of Hyperextended Rift Systems. Tectonics, 37, 89–118.doi:10.1002/2017TC004495.

Olivet, J.L., 1996. La cinématique de la plaque Ibérique. Bull. Cent. Rech. Explor. Prod. Elf Aquitaine 20, 131–195.

Osmundsen, P.T., Redfield, T.F., 2011. Crustal taper and topography at passive continental margins. Terra Nova, 23, 349-361. doi:10.1111/j.1365-3121.2011.01014.

Pedreira, D., Pulgar, J.A., Gallart, J., Torné, M., 2007. Three-dimensional gravity and

magnetic modeling of crustal indentation and wedging in the western Pyrenees-Cantabrian Mountains. J. Geophys. Res. Solid Earth 112, 1–19. doi:10.1029/2007JB005021.

Pérez-Gussinyé, M., Reston, T.J., Phipps Morgan, J., 2001. Serpentinization and magmatism during extension at non-volcanic margins: the effect of initial lithospheric structure. Geol. Soc. London, Spec. Publ. 187, 551–576. doi:10.1144/GSL.SP.2001.187.01.27.

Pérez-Gussinyé, M., Ranero, C., Reston, T., Sawyer, D., 2003. Mechanisms of extension at nonvolcanic margins: Evidence from the Galicia interior basin, west of Iberia. J. Geophys. Res. 108, 1–19. doi:10.1029/2001JB000901.

Péron-Pinvidic, G., Manatschal, G., Dean, S.M., Minshull, T.A., 2008. Compressional structures on the West Iberia rifted margin: Controls on their distribution, in Johnson, H., et al., eds., The nature and origin of compression in passive margins. Geol. Soc. London, Spec. Publ. 306, 169–183. doi:10.1144/SP306.8.

Pulgar, J.A., Gallart, J., Fernandez-Viejo, G., Perez-Estaun, A., Alvarez-Marron, J., Alonso, J.L., Gallastegui, J., Marcos, A., Bastida, F., Aller, J., Farias, P., Marín, J., García-Espina, R., Martínez-Catalán, J.R., Comas, M.C., Banda, E., Dañobeitia, J.J., Córdoba, D., Heredia, N., Rodríguez, R., 1996. Seismic image of the Cantabrian Mountains in the western extension of the Pyrenees from integrated ESCIN reflection and refraction data. Tectonophysics 264, 1–19. https://doi.org/10.1016/S0040-1951(96)00114-X.

Rat, J., Mouthereau, F., Brichau, S., Crémades, A., Bernet, M., Balvay, M., Ganne, J., Lahfid, A., Gautheron, C., 2019. Tectonothermal Evolution of the Cameros Basin: Implications for Tectonics of North Iberia. Tectonics. https://doi.org/10.1029/2018TC005294.

Roberts, A.M., Kusznir, N.J., Yielding, G., Styles, P., 1998. 2D flexural backstripping of extensional basins; the need for a sideways glance. Pet. Geosci. 4, 327–338. https://doi.org/10.1144/petgeo.4.4.327.

Roberts, A.M., Kusznir, N.J., Yielding, G., Beeley, H., 2019. Mapping the bathymetric evolution of the northern North Sea: from Jurassic syn-rift archipelago through

Cretaceous-Tertiary post-rift subsidence. Pet. Geosci.

Roca, E., Muñoz, J.A., Ferrer, O., Ellouz, N., 2011. The role of the Bay of Biscay Mesozoic extensional structure in the configuration of the Pyrenean orogen: Constraints from the MARCONI deep seismic reflection survey. Tectonics, 30, 1–33. doi:10.1029/2010TC002735.

Rocher, M., Lacombe, O., Angelier, J., Deffontaines, B., Verdier, F., 2000. Cenozoic folding and faulting in the south Aquitaine Basin (France): Insights from combined structural and paleostress analyses. J. Struct. Geol. 22, 627–645. https://doi.org/10.1016/S0191-8141(99)00181-9.

Roest, W.R., Srivastava, S.P., 1991. Kinematics of the plate boundaries between Eurasia, Iberia, and Africa in the North Atlantic from the Late Cretaceous to the present. Geology, 19, 613–616. doi:10.1130/0091-7613.

Rosenbaum, G., Lister, G.S., Duboz, C., 2002. Relative motions of Africa, Iberia and Europe during Alpine orogeny. Tectonophysics 359, 117–129. doi:10.1016/S0040-1951(02)00442-0.

Roure, F., Choukroune, P., Mu, J.A., Camara, P., Researcher, I., Iberian, S.W., Tethys, L., 1989. ECORS Deep seismic data and balanced cross- section ; geometric constraints on the evolution of the Pyrenees. Tectonics, vol 8, num 1. doi:10.1029/TC008i001p00041.

Salas, R., Casas, A., 1993. Mesozoic extensional tectonics, stratigraphy and crustal evolution during the Alpine cycle of the eastern Iberian basin. Tectonophysics 228, 33–55. doi:10.1016/0040-1951(93)90213-4.

Saspiturry, N., Razin, P., Baudin, T., Serrano, O., Issautier, B., Lasseur, E., Allanic, C., Thinon, I., Leleu, S., 2019. Symmetry vs. asymmetry of a hyper-thinned rift: Example of the Mauléon Basin (Western Pyrenees, France). Mar. Pet. Geol. 104, 86–105. https://doi.org/10.1016/j.marpetgeo.2019.03.031.

Schettino, A., Scotese, C.R., 2002. Global kinematic constraints to the tectonic history of the Mediterranean region and surrounding areas during the Jurassic and cretaceous. J. Virtual Explor. 8. doi:10.3809/jvirtex.2002.00056.

Serrano, O., Delmas, J., Hanot, F., Vially, R., Herbin, J.P., Houel, P., Tourlière, B., 2006. Le bassin d'Aquitaine: Valorisation des données sismiques, cartographie structurale et potentiel pétrolier. Rapp. Régional d'Evaluation Pétrolière. Bur. la Rech. Géologique Minière, Orléans, Fr. 245.

Sibuet, J.-C., Collette, B.J., 1991. Triple junctions of Bay of Biscay and North Atlantic: New constraints on the kinematic evolution. Geol. 19E. Banda, 525.

Srivastava, S.P., Roest, W.R., Kovacs, L.C., Oakey, G., Lévesque, S., Verhoef, J., Macnab, R., 1990. Motion of Iberia since the Late Jurassic: Results from detailed aeromagnetic measurements in the Newfoundland Basin. Tectonophysics 184, 229–260. doi:10.1016/0040-1951(90)90442-B.

Stein, R.-S., Barrientos, S.-E., 1985. Planar High-Angle Faulting in the Basin and Range: Geodetic Analysis of the 1983 Borah Peak, Idaho, Earthquake. J. Geophys. Res. 90, 11,355-11,366.

Sutra, E., Manatschal, G., Mohn, G., Unternehr, P., 2013. Quantification and restoration of extensional deformation along the Western Iberia and Newfoundland rifted margins. Geochemistry, Geophys. Geosystems 14, 2575–2597. doi:10.1002/ggge.20135.

Tavani, S., Bertok, C., Granado, P., Piana, F., Salas, R., Vigna, B., Muñoz, J.A., 2018. The Iberia-Eurasia plate boundary east of the Pyrenees. Earth-Science Rev. 187, 314–337. https://doi.org/10.1016/j.earscirev.2018.10.008.

Teixell, A., 1990. Alpine thrusts at the western termination of the Pyrenean Axial Zone. Bull. la Société géologique Fr. 8(6), 241–249.

Teixell, A., 1998. Crustal structure and orogenic material budget in the west central Pyrenees. Tectonics, vol 17, num 3, 395–406.

Teixell, A., Labaume, P., Lagabrielle, Y., 2016. The crustal evolution of the west-central Pyrenees revisited: Inferences from a new kinematic scenario. Comptes Rendus - Geosci. 348, 257–267. doi:10.1016/j.crte.2015.10.010.

Teixell, A., Labaume, P., Ayarza, P., Espurt, N., de Saint Blanquat, M., Lagabrielle, Y., 2018. Crustal structure and evolution of the Pyrenean-Cantabrian belt: A

review and new interpretations from recent concepts and data. Tectonophysics 724–725, 146–170. https://doi.org/10.1016/j.tecto.2018.01.009.

Toth, J., Kusznir, N.J., Flint, S.S., 1996. A flexural isostatic model of lithosphere shortening and foreland basin formation: Application to the Eastern Cordillera and Subandean belt of NW Argentina. Tectonics 15, 2–3.

Tugend, J., Manatschal, G., Kusznir, N.J., Masini, E., Mohn, G., Thinon, I., 2014. Formation and deformation of hyperextended rift systems: Insights from rift domain mapping in the Bay of Biscay-Pyrenees, Tectonics, 33, 1239-1276, doi:10.1002/2014TC003529.

Tugend, J., Manatschal, G., Kusznir, N.J., 2015a. Spatial and temporal evolution of hyperextended rift systems: Implication for the nature, kinematics, and timing of the Iberian- European plate boundary. Geology, 15–18. doi:10.1130/G36072.1.

Tugend, J., Manatschal, G., Kusznir, N.J., Masini, E., 2015b. Characterizing and identifying structural domains at rifted continental margins: application to the Bay of Biscay margins and its Western Pyrenean fossil remnants. Geological Society, London, Special Publications, 413.10.1144/SP413.3.

Vacher, P., Souriau, A., 2001. A three-dimensional model of the Pyrenean deep structure based on gravity modelling, seismic images and petrological constraints. Geophys. J. Int. 145, 460–470.

Vacherat, A., Mouthereau, F., Pik, R., Huyghe, D., Paquette, J.L., Christophoul, F., Loget, N., Tibari, B., 2017. Rift-to-collision sediment routing in the Pyrenees: A synthesis from sedimentological, geochronological and kinematic constraints. Earth-Science Rev. 172, 43–74. https://doi.org/10.1016/j.earscirev.2017.07.004.

Vergés, J., Millán, H., Roca, E., Muñoz, J.A., Marzo, M., Cirés, J., Bezemer, T. Den, Zoetemeijer, R., Cloetingh, S., 1995. Eastern Pyrenees and related foreland basins: pre-, syn- and post-collisional crustal-scale cross-sections. Mar. Pet. Geol. 12, 903–915. https://doi.org/10.1016/0264-8172(95)98854-X.

Vergés, J., García-Senz, J., 2001. Mesozoic evolution and Cainozoic inversion of the Pyrenean rift. Peri-Tethys Mem. 6 Peri-Tethyan Rift. Mém. Mus. natn. Hist, nat. 186, 187–212.

Vergés, J., Fernàndez, M., Martìnez, A., 2002. The Pyrenean orogen: Pre-, syn-, and post-collisional evolution. J. Virtual Explor. 8. doi:10.3809/jvirtex.2002.00058.

Wang, Y., Chevrot, S., Monteiller, V., Komatitsch, D., Mouthereau, F., Manatschal, G., Sylvander, M., Diaz, J., Ruiz, M., Grimaud, F., Benahmed, S., Pauchet, H., Martin, R., 2016. The deep roots of the western Pyrenees revealed by full waveform inversion of teleseismic P waves. Geology 44. doi:10.1130/G37812.1.

White, R.S., 1999. The lithosphere under stress. Philos. Trans. R. Soc. A Math. Phys. Eng. Sci. 357, 901–915. https://doi.org/10.1098/rsta.1999.0357.

Wilson, J., 1966. Did the atlantic close and then reopen?. Nature 211, 286. doi:10.12789/geocanj.2016.43.109.

CHAPTER 5
DISCUSSION-CONCLUSIONS

1. How much extension is required to produce continental crustal breakup?

(Chapter 2: Measurements of the extension required for continental breakup)

Rifted margins have been extensively studied, however there are still important unknowns related to their formation process. In this thesis, the Iberia-Newfoundland conjugate rifted margins are used as a natural laboratory to investigate how much extension is required to produce continental crustal breakup. Previous studies using geometric restoration techniques (e.g. Sutra et al., 2013) or extension rate histories (e.g. Jeanniot et al., 2016) have made extension estimates required to produce crustal breakup at the Iberia-Newfoundland conjugate rifted margins. In this thesis, subsidence analysis and gravity inversion are applied along two conjugate profiles (northern and southern) of the Iberia and Newfoundland margins to determine continental lithosphere extension and continental crust extension respectively. These measurements have been made between the proximal continental crust and the distal end of continental crust (i.e. COB-1 location defined in this study). Results from these two quantitative techniques are very similar and suggest that on average continental lithosphere and continental crust are required to be extended by 181 km to produce continental crustal breakup (Figure 1a). This is comparable with extension estimates obtained by Jeanniot et al., (2016) (~168 km), however, it is substantially lower than that suggested by Sutra et al., (2013) (~242 km).

2. How does extension by faulting compare with extension from crustal and lithosphere thinning at conjugate rifted margins?

(Chapter 2: Measurements of the extension required for continental breakup)

Subsidence analysis, gravity inversion and fault heave summation from seismic observations have been used to determine whole continental lithosphere extension, whole continental crust extension and brittle continental crust extension respectively required to produce continental crustal breakup (Figure 1a). These results show that the observed brittle fault extension is less than that of the whole continental crust and lithosphere. If material is conserved then we would expect the thinning and stretching of the brittle continental crust by extensional faulting, and that of the whole continental crust and lithosphere, by combined extensional faulting and deeper distributed deformation, to be the same. Therefore, an apparent extension discrepancy at the scale of the whole conjugate margin system is observed when fault heave summation is compared with lithosphere and crust extension (Figure 1a).

Comparing the cumulative extension from proximal to COB-1, from integrated crustal thinning and fault heave summation, highlights the apparent extension discrepancy at the COB-1 location (Figure 1b). In addition, it shows depth-dependent stretching and thinning (DDST) (e.g. Driscoll and Karner, 1998; Roberts et al., 1997; Baxter et al., 1999; Davis and Kusznir, 2004; Kusznir and Karner, 2007) within the proximal margin where the brittle continental crust is less extended than that of the whole continental crust (Figure 1b). DDST should not be confused with an extension discrepancy at the scale of the whole conjugate margin system. Interestingly, the difference between the observed cumulative fault heave summation and the extension integrated from crustal thinning decreases towards the COB-1 location (Figure 1b).

Fault population analysis carried out in this thesis indicate that between 20-35% (e.g. Walsh et al., 1991; Ackermann et al., 2001) of faulting extension is not being seen on the seismic reflection data. This result leads to suggest that, allowing for fault extension at sub-seismic resolution (up to 35%), an extension discrepancy at the scale of the whole conjugate system does not exist along the southern profiles using the SPSI-2 seismic interpretation (Figure 1a). In contrast, the faults sampled along the northern profiles cannot be represented with a unique frequency curve therefore we

consider these profiles inconclusive for comparing fault extension with extension from crust and lithosphere thinning.

When determining whether a discrepancy between the observed fault heave summation and lithosphere/crust extension at the scale of the whole conjugate system exists, two issues should be addressed; (i) fault geometries and (ii) the COB location.

Interpretation of seismic data is often non-unique and hence leads to more than one possible geological scenario. For the southern profiles of Iberia and Newfoundland conjugate margins, two seismic interpretations have been proposed. Indeed, results from fault heave summation using only planar faults (SPSI-1) or a large rolling-hinge fault and planar faults (SPSI-2) provide substantially different amounts of observed brittle crustal extension (Figure 1a). Note that usually rolling-hinge faults increase the amount of brittle crustal extension and therefore failing to recognize them may lead to an apparent extension discrepancy at the scale of the whole conjugate margin system.

Results from the fault population analysis, show that the overall trend of faults sampled, along the southern profiles, appear to fit with a power-law frequency curve however, an unexpected pattern at large fault heaves for data censoring is observed. The fault population statistics for the northern profiles, as pointed out above, cannot be represented with a unique frequency curve. This and the unexpected pattern observed on the southern profiles may indicate the presence of two or more fault populations along both profiles. These populations could correspond to; (i) the presence of two types of fault geometries (planar and rolling-hinge) and/or (ii) two different fault coupling levels (faults decoupled from and coupled into the mantle).

To determine the location of the distalmost continental crust is ambiguous and as a consequence two possible COB positions have been proposed in this study which in turn out correspond to the boundaries of a zone in which the COB location could be placed anywhere within it. To measure lithosphere and crust extension as well as fault heave summation from seismic data we define the distal end of continental crust at the COB-1 location. Note that a more distal COB location would increase both the fault heave summation as well as the whole continental crust extension (Figure 1b).

Alternative processes that might generate an apparent extension discrepancy at the scale of the whole conjugate margin are non-brittle extension and continued thinning of continental crust after continental crustal breakup occurs.

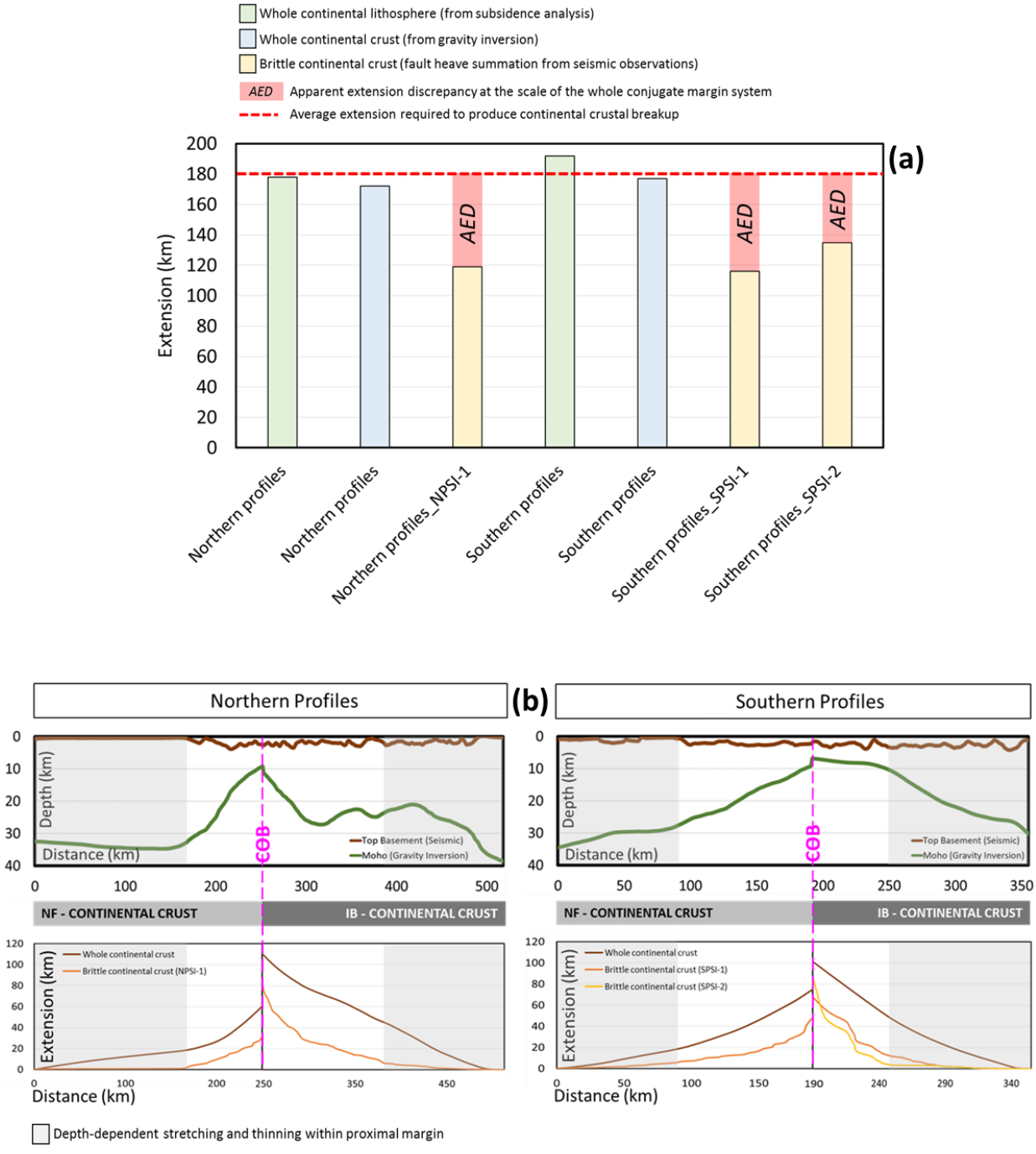

Figure 1: **a)** Summary of the extension estimates required to produce continental crustal breakup along the southern and northern profiles. **b)** Paleobathymetry and paleo-Moho depth for Iberia and Newfoundland at continental crustal breakup time (top). Comparison between cumulative extension from proximal to COB, from integrated crustal thinning and fault heave summation (bottom).

3. What is the geometric evolution of extensional faults within distal magma-poor rifted margins?

(Chapter 3: Geometric evolution of faults)

The geometric evolution of extensional faults at rifted margins are studied by examining present-day datasets (e.g. seismic and field data) which provide the post-extensional structural configuration. Therefore, these datasets do not directly indicate the initial and active fault geometry. This has led to an ongoing debate about how faults form and evolve especially within the distal part of rifted margins (e.g. Manatschal et al., 2001; Pérez-Gussinyé et al., 2001; Manatschal, 2004; Péron-Pinvidic et al., 2007; Reston and McDermott, 2011; Pérez-Gussinyé et al., 2013; Lymer et al., 2019). In this thesis, a lithosphere deformation model (RIFTER) which includes the flexural isostatic response to extensional faulting is used to investigate the geometry of active extensional faults and how it evolves within distal rifted margins. In particular, this is examined for continental crustal thinning within the hyperthinned domain, the formation of continental allochthon blocks within the exhumed mantle domain and the transition between the hyperthinned and exhumed mantle domains (Figure 2a).

Modelling results show that the hyperthinned domain is formed by faults with relatively low offsets that couple into the mantle (Figure 2b). However it is uncertain whether these faults are listric or planar. A listric fault geometry produces a sub-horizontal structure beneath the hyperthinned crust consisting of an inactive rotated extensional fault while a planar fault geometry does not. Both listric and planar fault geometries produce a Moho that would be indistinguishable on seismic reflection data or from the inactive rotated extensional fault of the listric model.

The initiation of the exhumed mantle domain is characterized by extensional faults compatible with the rolling-hinge model of Buck (1988). The onset of this domain is achieved by a large offset rolling-hinge fault (i.e. master fault) that may produce continental crustal separation. Allochthon blocks are formed by high-angle short-cut faults, of variable offsets, from the master fault pulling out pieces of continental crust from the hangingwall of the master fault. Each allochthon block overlies a sub-horizontal inactive older fault that due to flexural isostasy substantially rotates during the development of subsequent allochthon blocks (Figure 2c).

The transition zone between the hyperthinned and exhumed mantle domains may be characterized by; (i) a large rolling-hinge in-sequence fault leading to a sub-horizontal sea-bed (Figure 2d) or (ii) low offset out-of-sequence faults leading to a distal ridge made up of mantle and crustal rocks (Figures 2e-f). These results indicate that out-of-sequence faulting may play an important role during the development of the hyperthinned domain leading to mantle exhumation at magma-poor rifted margins.

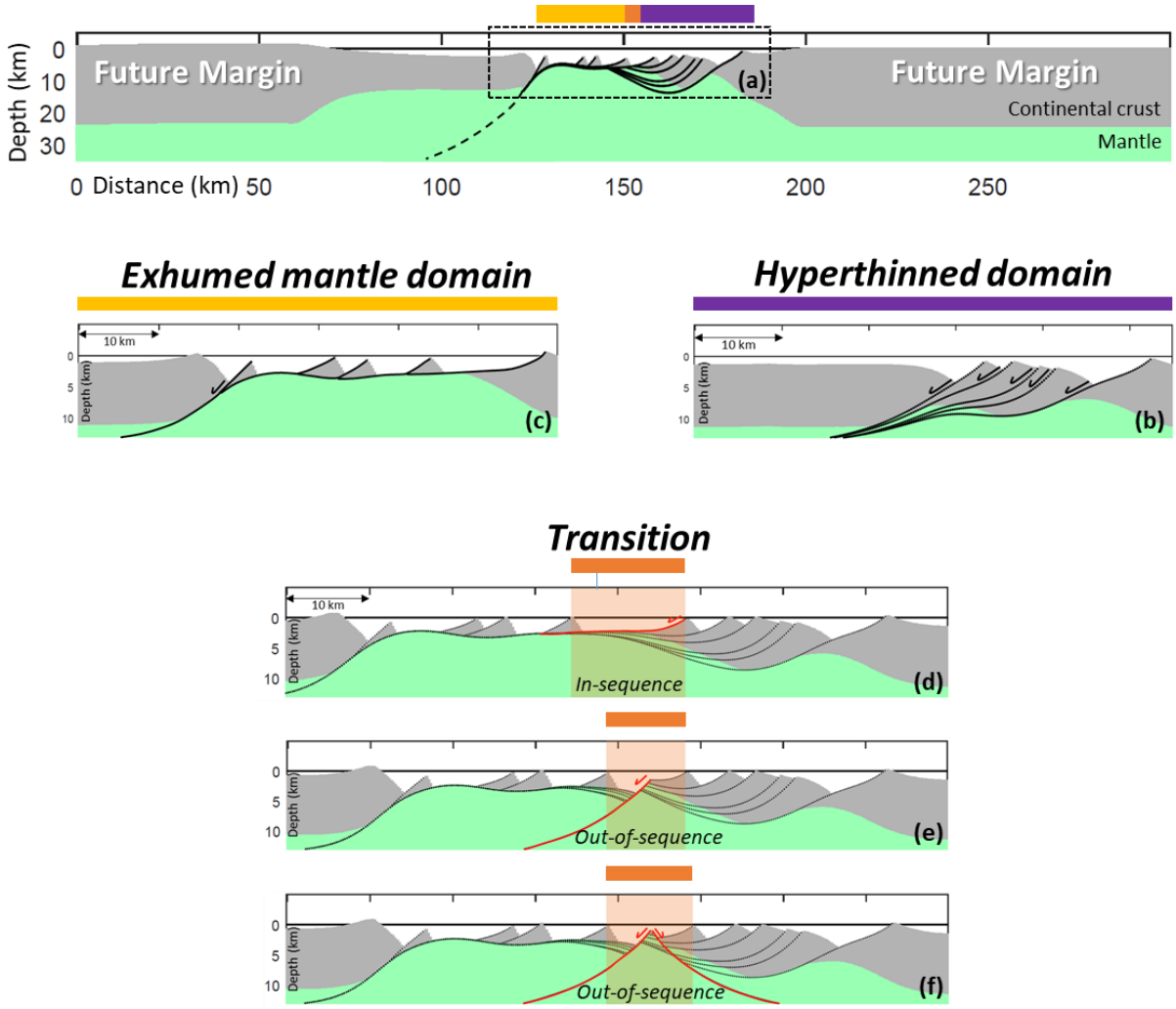

Figure 2: **a)** Structural architecture of the hyperthinned domain (purple), initiation of exhumed mantle domain (yellow) and the transition between these two domains (orange) along a rifted margin using RIFTER. **b)** Present-day fault geometries within the hyperthinned domain. **c)** Present-day fault geometries within the initiation of exhumed mantle domain. **d-f)** Three different faulting scenarios by which the transition between the hyperthinned and exhumed mantle domains may occur.

4. How do rift domains and their extensional structures reactivate during compression leading to orogen formation?

(Chapter 4: Rift structural inheritance in orogeny)

The Wilson cycle represents one of the most important concepts of the plate tectonic theory and one of its key implications is that mountain belts are built on the former site of continental rifted margins (Wilson, 1966). This implies that present-day orogens are formed by the closure of precursor rift basins or rifted margins. Therefore, to better understand orogen formation it is crucial to also understand the earlier extensional rift history. In the Western Pyrenees evidence for a reactivated hyper-extended basin formed before collision has been shown (e.g. Masini et al., 2014; Tugend et al., 2015). The Western Pyrenees is used as a case-study to examine the reactivation of rift domains and their rift-related faults during collision using a lithosphere deformation model (RIFTER) that allows the production of flexural isostatically compensated as well as balanced cross-sections. RIFTER model is used to bring together shallow observed geology, seismic observations and deep observations into a single unified profile.

Modelling results show the first order structural and stratigraphic architecture development of the Western Pyrenees and indeed highlight that this orogen can only be reproduced by including the extensional as well as the compressional history of lithosphere deformation (Figure 3). The earlier extensional stage of the Western Pyrenees is modelled by producing a Cretaceous hyper-extended rift (Canérot, 2008; Jammes et al., 2009, 2010) followed by a compressional Alpine stage between the Santonian and the Miocene (Garrido-Megías and Ríos, 1972; Muñoz, 1992; Vergés et al., 1995; Capote et al., 2002; Vergés and García-Senz, 2001; McClay et al., 2004; Mouthereau et al., 2014). Tugend et al., (2014) suggested that orogens are formed by sequential rift domain reactivation. The Western Pyrenees is used to demonstrate the flexural isostatic testing of Tugend et al., (2014) hypothesis by developing two sequential deformation phases; (i) the reactivation stage of the hyper-extended (Figure 3e) and necking (Figure 3f) domains and (ii) the shortening stage of the proximal rift domain (Figure 3g). These two phases correspond to the pre-collision and syn-collision stages respectively. In addition to this, results from the Western Pyrenees modelling provide insights on the deeper fault geometries during orogeny (Figure 4). The

reactivation of the hyper-extended rift domain is achieved by faults coupled into the mantle (Figure 4a) while the reactivation of the necking rift domain uses faults which modify their deeper geometry and couple into shallow mantle (Figure 4b). The shortening of the proximal rift domain is developed by thrusts ramps of the pro-side of the belt soling out into a crustal decollement level at 25 km depth that laterally branches within the continental underthrusting ramp plane (Figure 4c).

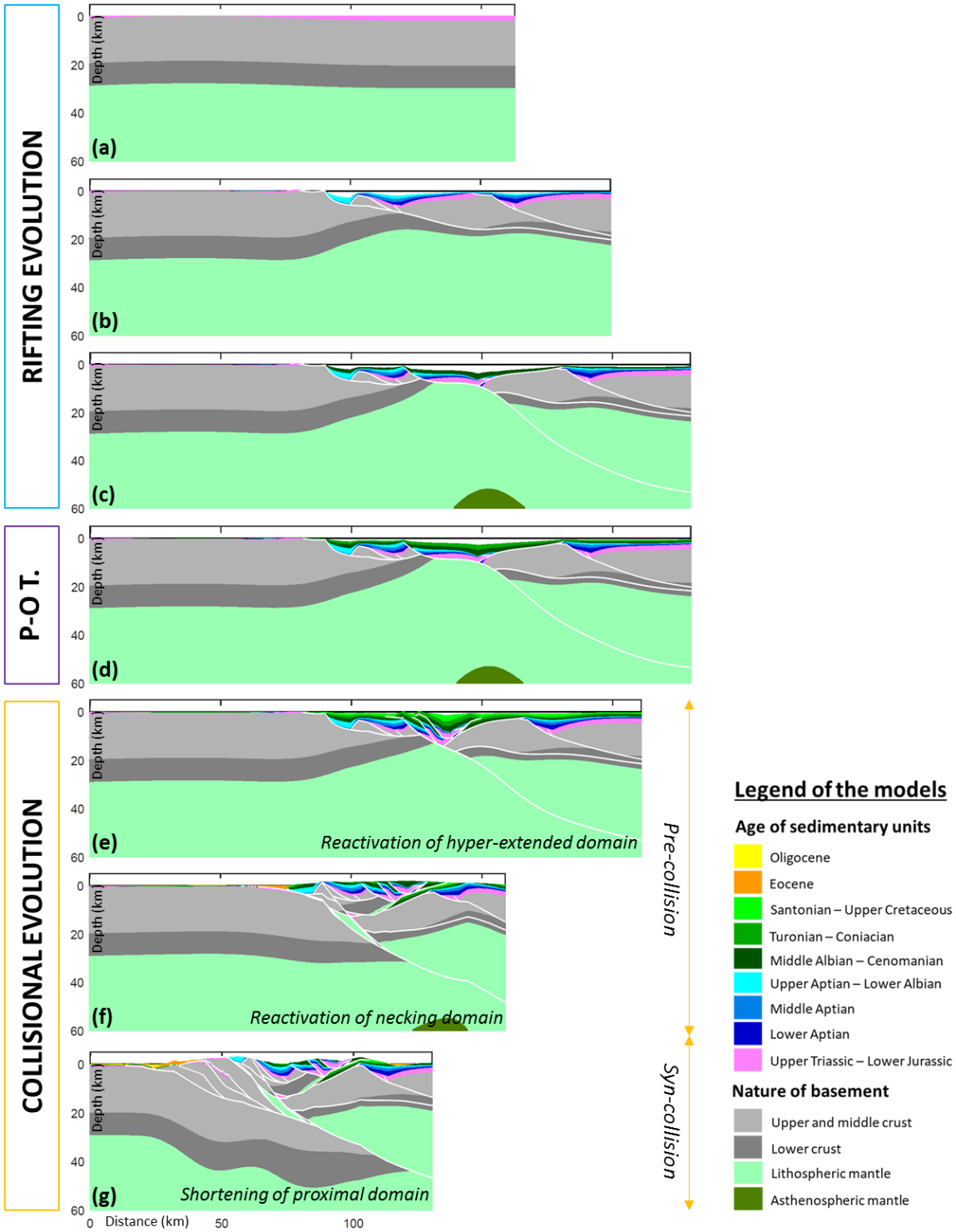

Figure 3: Rifting and collisional evolution of the Western Pyrenees using RIFTER. The rifting evolution is shown in **a-c)**, the pre-orogenic template (P-O T.) obtained at the end of rifting and used to start the collisional evolution is show in **d)**, and the collisional evolution is shown in **e-g)**. Age of sedimentary units and the nature of the basement are shown in the legend.

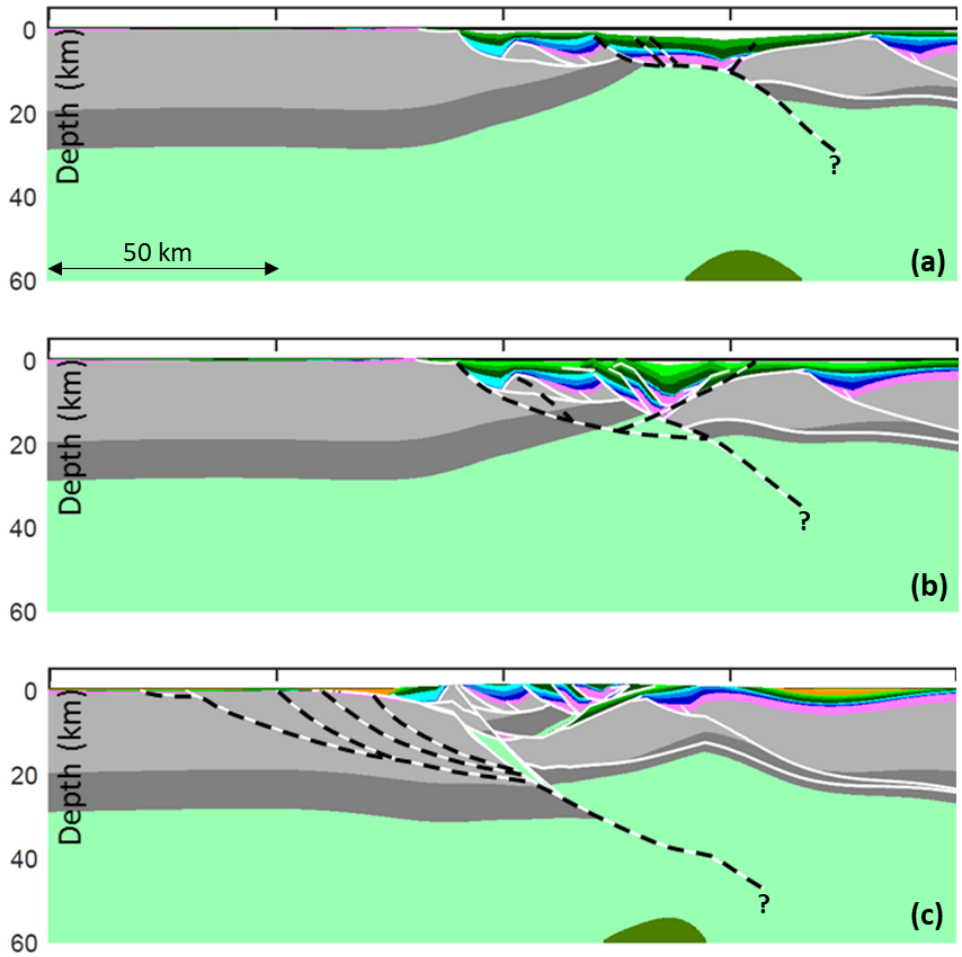

Figure 4: Fault geometries prior to be active (black dashed lines) during orogeny using the Western Pyrenees as a case-study. **a)** Reactivated faults used to reactivate the hyper-extended rift domain. **b)** Reactivated faults used to reactivate the necking domain. **c)** New thrusts used for the shortening of the proximal rift domain. See Figure 3 for the legend of the models.

5. What is the extensional fault geometry at magma-poor rifted margins and how these faults reactivate during orogeny?

(General discussion: Chapter 2, Chapter 3 and Chapter 4)

Results from the three scientific chapters of this thesis provide new insights on the extensional faulting at magma-poor rifted margins and how these faults reactivate during orogeny.

Rifted margins are the transition, and thus record the evolution, from continental rifting to slow spreading ocean ridges. Active high-angle planar faults are the dominant mechanism by which the upper brittle continental lithosphere extends during early continental rifting (Stein and Barrientos, 1985; Jackson, 1987; Bell et al., 2017) leading to the formation of the proximal domain at rifted margins (Figure 5a). At slow spreading ocean ridges, lithosphere extension is mostly achieved by rolling-hinge extensional faults (Buck, 1988). These consist of an active high-angle planar fault segment below sea-floor with typically large fault offsets leading to exhumed footwall that due to flexural isostatic rotation becomes sub-horizontal at the sea-bed. Within the oceanic domain at magma-poor rifted margins, these fault geometries are expected during lithosphere extension (Figure 5b). The main difference between extensional faulting within continental rifting (i.e. proximal domain) and slow spreading ocean ridges (i.e. oceanic domain) is the fault offset which is often less than 10 km and more than 15 km respectively.

Results from chapters 2 and 3 of this thesis allow a better understanding of the active extensional fault geometries as well as the typical fault offsets within the necking, hyperthinned and exhumed mantle initiation domains at rifted margins. Within the necking domain extensional faults are active at high-angles but their offsets may vary. Large faults offsets (i.e. rolling-hinge faults) lead to a sub-horizontal sea-bed while low faults offsets (i.e. planar faults) to a horst-graben geometry (Figure 5c). Often, it is difficult to distinguish between these two fault types because the exhumed sub-horizontal footwall of a rolling-hinge fault may be re-faulted by planar faults and this would lead to a sub-horizontal sea-bed with small topographic variations. This geometry may difficulty the recognition of an older exhumed footwall block of a rolling-hinge fault.

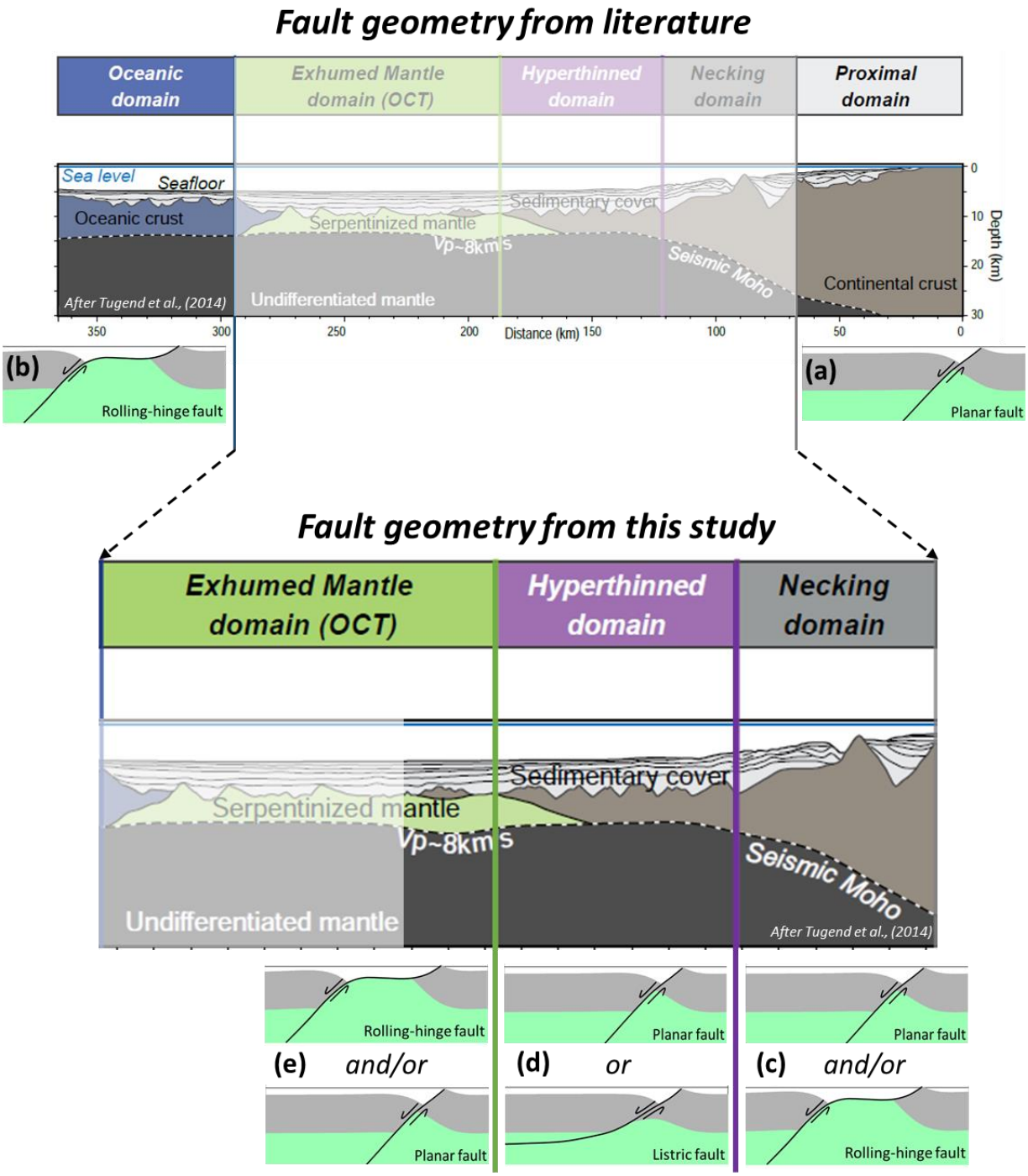

Figure 5: Extensional fault geometries at magma-poor rifted margins. **a-b)** Based on literature and **c-e)** Based on the results from this study. See text for more explanation.

Seismic observations together with modelling experiments focused on the hyperthinned domain of rifted margins do not allow to distinguish between these two low offset fault types; (i) steep planar faults characterized by an initial surface fault dipping 60° soling out horizontally at 15 km depth or (ii) listric faults characterized by dipping 60° down to 15 km depth (Figure 5d). A listric fault geometry produces a sub-

horizontal structure beneath the hyperthinned crust consisting of an inactive rotated extensional fault while a planar fault geometry does not. Both listric and planar fault geometries produce a Moho that would be indistinguishable on seismic reflection data or from the inactive rotated extensional fault of the listric model. Despite of the uncertainty on the fault geometry, the exhumed mantle domain is characterized by a large offset rolling-hinge fault (i.e. master fault) and may be followed by a set of new high-angle short-cut faults, of variable offsets, from the master fault producing allochthon blocks (Buck, 1988). Out-of-sequence faults with low offsets may as well be present and cross-cut the footwall of the master fault leading to topographic highs (Figure 5e).

Orogens are often the result of the closure of precursor oceanic basins, rifted margins or rift basins. Therefore, it is crucial to first investigate extensional fault geometries at magma-poor rifted margins prior to examine how the pre-orogenic rift structures may reactivate during collision. At magma-poor rifted margins, extensional faults within the proximal domain are restricted within the topmost brittle upper crust soling out at approximately 15 km depth (e.g. Stein and Barrientos, 1985, Jackson, 1987) (Figure 6a) while extensional faults within the necking domain are still decoupled from the mantle but sole out at mid or lower crustal levels (Pérez-Gussinyé et al., 2001; Sutra et al., 2013) (Figure 6b). In contrast, extensional faults within the hyper-extended domain are coupled into the mantle (Pérez-Gussinyé et al., 2001; Sutra et al., 2013) (Figure 6c).

In chapter 4 of this thesis, listric fault geometries are used to reproduce the formation and evolution of a hyper-extended rift basin that is reactivated during collision. These faults are characterized by an initial surface fault dipping 60° soling out horizontally at depth (i.e. the vertical shear construction). This fault geometry allows to provide insights on whether faults may be decoupled from or coupled into the mantle during orogeny (Figure 6d-f).

Orogen formation consists of sequential rift domain reactivation as suggested by Tugend et al., (2014) and shown by the modelling of the Western Pyrenees in this thesis. The reactivation of the hyper-extended rift domain is achieved through extensional fault reactivation coupled into the mantle (Figure 6d). This reactivated structure prefigures the continental underthrusting plane and may define the vergence

of the belt. How necking-domain rift structures reactivate during collision is uncertain. One possibility is that the necking-domain extensional faults are reactivated using their original geometry which corresponds to faults soling out within the crust with distributed pure-shear deformation below. However, another possibility is that the reactivated necking-domain extensional faults modify their deeper geometry and couple directly into shallow mantle towards the former underthrusting plane. Whether one fault reactivation mechanism is generally more common than the other is unknown. However, to reproduce the present-day architecture of the Western Pyrenees the second hypothesis is used (Figure 6e). Note that this faulting scenario allows for carrying upwards shallow mantle rocks while reactivation of extensional faults soled out within the crust would not. The shortening of the proximal rift domain is achieved by thrusts ramps that sole out into a crustal decollement level at 25 km depth (for the Western Pyrenees example) that laterally branches within the underthrusting ramp plane and therefore these thrusts are coupled into the mantle (Figure 6f).

Therefore, results from the Western Pyrenees modelling suggest that to reactivate the necking domain and shorten the proximal domain, faults are coupled into the mantle (Figures 6e-f). This is contrasting with the pre-orogenic rift structures of these domains which are soled out within crustal levels (Figures 6a-b). A key remaining question is whether this evolution on the coupling-depth of faults during a Wilson cycle may be applicable to other orogenic systems or not (Figure 6).

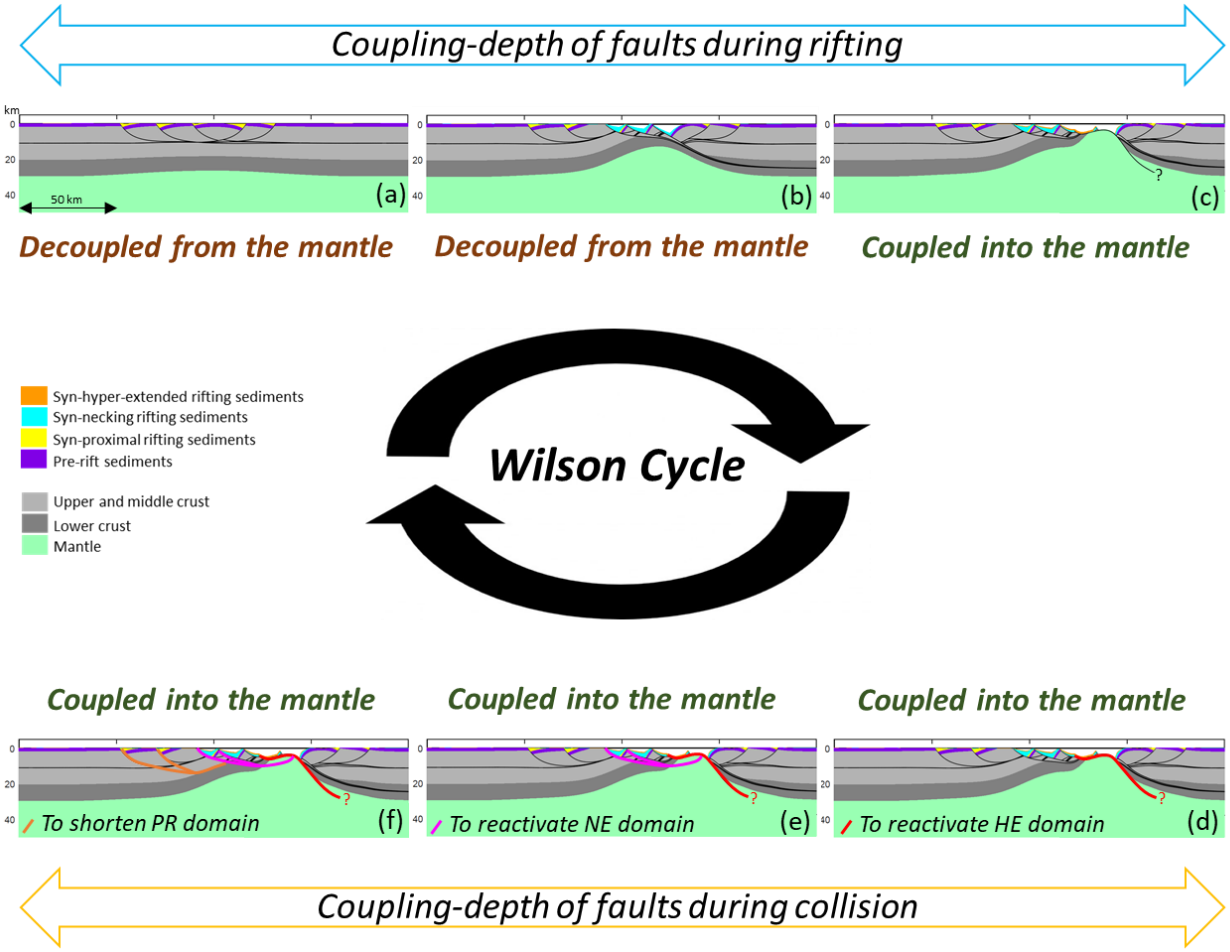

Figure 6: Coupling-depth of faults throughout a complete Wilson cycle based on literature review (**a-c**) and the Western Pyrenees case-study (**d-f**). RIFTER models showing the lithosphere deformation during rifting, the active extensional faults and their coupling-depth (**a-c**). **a)** Formation of the proximal rift domain. **b)** Necking domain formation. **c)** Hyper-extended domain formation (includes hyperthinned crust and exhumed mantle). RIFTER models showing the evolution of the coupling-depth of faults (inactive) during orogeny (**d-f**). **d-f)** Show the same lithosphere template consisting of a hyper-extended rift basin. **d)** Reactivated red fault leads to the reactivation of the hyper-extended (HE) domain. **e)** Reactivated pink faults lead to the reactivation of the necking (NE) domain. **f)** Orange thrusts lead to the shortening of the proximal (PR) domain.

CONCLUSIONS

The aim of this thesis is to investigate extensional faulting at magma-poor rifted margins as well as to examine how extensional structures formed during rifted margin development are reactivated during orogeny. To achieve this, the Iberia-Newfoundland conjugate rifted margins and the Western Pyrenees are used as natural laboratories. The main conclusions of this thesis are:

- To achieve continental crustal breakup, approximately 181 km of extension are required. This value may be applied to other conjugate rifted margins with similar crustal inheritance and rheology, obliquity and margin width, magmatic additions and extension rate to the Iberia-Newfoundland conjugate rifted margins.
- An apparent extension discrepancy at the scale of the whole conjugate margin system is seen when observed fault heave summation is compared with extension from crust and lithosphere thinning.
- Allowing for fault extension at sub-seismic resolution (up to 35%), an extension discrepancy at the scale of the whole conjugate margin system does not exist. In addition to sub-seismic faulting, fault geometries and the location of the distalmost continental crust are important issues that need to be carefully considered when comparing fault heave summation and extension from crust and lithosphere thinning.
- Failing to recognize rolling-hinge faults may lead to an under-estimate of fault extension.
- Depth-dependent stretching and thinning (DDST) is observed and expected within the proximal and necking domains of rifted margins. DDST should not be confused with an extension discrepancy at the scale of the whole conjugate margin system.
- Extensional faults within the necking domain are active at high-angle and may be rolling-hinge faults (large offset) and/or planar faults (low offset).
- Extensional faulting within the hyperthinned domain is characterized by faults with relatively low offsets that couple into the mantle. However it is uncertain whether these faults are listric or planar. A listric fault geometry produces a sub-horizontal structure beneath the hyperthinned crust consisting of an inactive rotated extensional fault while a planar geometry does not.

- Extensional faulting within the exhumed mantle domain initiation is characterized by a large offset rolling-hinge fault (i.e. a master fault). It is uncertain whether the master fault soles out horizontally at depth with a listric geometry or is a steep planar fault.
- Allochthon blocks within the exhumed mantle domain are formed by high-angle short-cut faults from the master fault. Each allochthon block overlies a sub-horizontal inactive older fault that due to flexural isostasy substantially rotates during the development of subsequent allochthon blocks. This leads to an exhumed mantle domain architecture characterized by a sub-horizontal sea-bed geometry with exhumed mantle and allochthon blocks above it.
- The transition zone between the hyperthinned and exhumed mantle domains may be characterized by; (i) a large rolling-hinge in-sequence fault leading to a sub-horizontal sea-bed or (ii) low offset out-of-sequence faults leading to a distal ridge made up of mantle and crustal rocks.
- The formation of the Western Pyrenees can only be understood by including the extensional as well as the compressional history of lithosphere deformation. This may be applicable to other orogenic systems.
- The earlier extensional stage of the Western Pyrenees is characterized by a Cretaceous hyper-extended rift system followed by a compressional stage consisting of two sequential deformation phases; (i) the reactivation stage of the hyper-extended and necking domains and (ii) the shortening stage of the proximal rift domain. These two phases correspond to the pre-collision and syn-collision stages respectively.
- The Western Pyrenees modelling results provide insights on the deeper fault geometries during orogeny, although this should be compared with other orogenic systems. The compressional reactivation of the hyper-extended rift domain uses faults coupled into the mantle. The compressional reactivation of the necking rift domain uses faults which modify their deeper geometry and couple into shallow mantle allowing for carrying upwards deep crustal and/or mantle rocks. The shortening of the proximal rift domain is developed by thrusts ramps of the pro-side of the belt soling out into a crustal decollement level at 25 km depth that laterally branches within the continental underthrusting ramp plane.

Future work

The focus of this thesis is to better understand lithosphere extension at magma-poor rifted margins. Three particular aspects are examined; extensional fault contribution required to produce continental crustal breakup, geometric evolution of extensional faults within distal rifted margins and the reactivation of extensional faults during orogenesis. While the results of these topics are presented in chapters 2, 3 and 4 respectively, a set of suggestions for future studies are listed below:

- To obtain a representative average value of how much extension is required to produce continental crustal breakup, the same or similar methodology of chapter 2 should be applied to other conjugate rifted margins. Results of the Iberia-Newfoundland fault population statistics indicate that allowing for fault extension at sub-seismic resolution increases the brittle extension up to 35%. Whether this value is applicable or not to other rifted margins is unknown and therefore future studies should investigate if 35% of sub-seismic fault resolution exists in other conjugate rifted margins.

- To better understand the deep geometric evolution of extensional faults during the formation of distal rifted margins, future studies should focus on understanding how brittle faulting evolves into the deep distributed lithosphere deformation. Results from chapter 3 do not allow to distinguish whether this may be achieved either (i) through a sub-horizontal shear zone where faults sole out and beneath which deformation occurs or (ii) through a diffusive process by which faults connect to the deep distributed deformation.

- The suggested evolution of the deeper fault geometries during collision is obtained from the Western Pyrenees case-study and therefore it should be compared with other orogenic systems. By doing so, a better understanding of the lithosphere strength during collision may be achieved.

REFERENCES

Ackermann, R. V, Schlische, R.W., Withjack, M.O., 2001. The geometric and statistical evolution of normal fault systems: an experimental study of the effects of mechanical layer thickness on scaling laws. J. Struct. Geol. 23, 1803–1819.

Baxter, K., Cooper, G.T., Hill, K.C., O'Brien, G.W., 1999. Late Jurassic subsidence and passive margin evolution in the Vulcan Sub-basin, north-west Australia: Constraints from basin modelling. Basin Res. 11, 97–111. https://doi.org/10.1046/j.1365-2117.1999.00088.

Bell, R.E., Duclaux, G., Nixon, C.W., Gawthorpe, R.L., McNeill, L.C., 2017. High-angle, not low-angle, normal faults dominate early rift extension in the Corinth Rift, central Greece. Geology 46, 115–118. https://doi.org/10.1130/g39560.1.

Buck, W.R., 1988. Flexural Rotation of Normal Faults. Tectonics 7, 959–973.

Canérot, J., 2008. Les Pyrénées: histoire géologique et itinéraires de découverte. Biarrtiz: Atlantica/BRGM éds., 2, 646 p.

Capote, R., Muñoz, J.A., Simón, J.., 2002. Apine tectonics. I: The Alpine system north of the Betic Cordillera. Geol. Soc. London, Spec. Publ. n W. Gibbo, 367–400.

Davis, M., Kusznir, N., 2004. Depth-dependent lithospheric stretching at rifted continental margins. In: Karner, G.D. (ed). Proc. NSF Rift. Margins Theor. Institute. Columbia Univ. Press. New York 92–136. https://doi.org/10.7312/karn12738-005.

Driscoll, N.W., Karner, G.D., 1998. Lower crustal extension across the Northern Carnarvon basin, Australia: Evidence for an eastward dipping detachment. J. Geophys. Res. 103, 4975–4991.

Garrido-Megías, A., Ríos, L., 1972. Síntesis geologica del Secundario y Terciario entre los ríos Cinca y Segre (Pirineo Central de la vertiente surpirenaica, provincias de Huesca y Lerida). Bol. Geol. Min 83, 1–47.

Jackson, J. a., 1987. Active normal faulting and crustal extension. Geol. Soc. London, Spec. Publ. 28, 3–17. https://doi.org/10.1144/GSL.SP.1987.028.01.02.

Jammes, S., Manatschal, G., Lavier, L., Masini, E., 2009. Tectonosedimentary

evolution related to extreme crustal thinning ahead of a propagating ocean: Example of the western Pyrenees. Tectonics 28. https://doi.org/10.1029/2008TC002406.

Jammes, S., Lavier, L., Manatschal, G., 2010. Extreme crustal thinning in the Bay of Biscay and the Western Pyrenees: From observations to modeling.

Jeanniot, L., Kusznir, N., Mohn, G., Manatschal, G., Cowie, L., 2016. Constraining lithosphere deformation modes during continental breakup for the Iberia-Newfoundland conjugate rifted margins. Tectonophysics 680, 28–49. https://doi.org/10.1016/j.tecto.2016.05.006.

Kusznir, N.J., Karner, G.D., 2007. Continental lithospheric thinning and breakup in response to upwelling divergent mantle flow: application to the Woodlark, Newfoundland and Iberia margins. Geol. Soc. London, Spec. Publ. 282, 389–419. https://doi.org/10.1144/SP282.16.

Lymer, G., Cresswell, D.J.F., Reston, T.J., Bull, J.M., Sawyer, D.S., Morgan, J.K., Stevenson, C., Causer, A., Minshull, T.A., Shillington, D.J., 2019. 3D development of detachment faulting during continental breakup. Earth Planet. Sci. Lett. 515, 90–99. https://doi.org/10.1016/j.epsl.2019.03.018.

Manatschal, G., Froitzheim, N., Rubenach, M., Turrin, B., 2001. The role of detachment faulting in the formation of an ocean-continent transition: insights from the Iberia Abyssal Plain from: Wilson, R.C.L., Whitmarsh, R.B., Taylor, B. & Froitzheim, N. Non-Volcaninc Rifting of Continental Margins: A Comparison of Evid. Geol. Soc. London, Spec. Publ. 187, 405–428. https://doi.org/0305-8719/01/1500.

Manatschal, G., 2004. New models for evolution of magma-poor rifted margins based on a review of data and concepts from West Iberia and the Alps. Int. J. Earth Sci. 93, 432–466. https://doi.org/10.1007/s00531-004-0394-7.

Masini, E., Manatschal, G., Tugend, J., Mohn, G., Flament, J.M., 2014. The tectono-sedimentary evolution of a hyper-extended rift basin: The example of the Arzacq-Maul??on rift system (Western Pyrenees, SW France). Int. J. Earth Sci. 103, 1569–1596. https://doi.org/10.1007/s00531-014-1023-8.

Mcclay, K., Dynamics, F., Holloway, R., Garcıa, J., 2004. Extensional salt tectonics in a contractional orogen : A newly identified tectonic event in the Spanish Pyrenees 737–740. https://doi.org/10.1130/G20565.1.

Mouthereau, F., Fellin, M.G., 2014. Placing limits to shortening evolution in the Pyrenees : Role of margin architecture and implications for the Iberia / Europe convergence. Tectonics. https://doi.org/10.1002/2014TC003663.

Muñoz, J.A., 1992. Evolution of a continental collision belt: ECORS-Pyrenees crustal balanced section, in Thrust Tectonics edited by K.R. McClay 235–246.

Pérez-Gussinyé, M., Reston, T.J., Morgan, J., 2001. Serpentinization and magmatism during extension at non-volcanic margins: the effect of initial lithospheric structure. Geol. Soc. London, Spec. Publ. 187, 551–576. https://doi.org/10.1144/GSL.SP.2001.187.01.27.

Pérez-Gussinyé, M., 2013. A tectonic model for hyperextension at magma-poor rifted margins: an example from the West Iberia – Newfoundland conjugate margins. Geol. Soc. London, Spec. Publ. 369, 403–427. https://doi.org/10.1144/SP369.19.

Péron-Pinvidic, G., Manatschal, G., Minshull, T.A., Sawyer, D.S., 2007. Tectonosedimentary evolution of the deep Iberia-Newfoundland margins: Evidence for a complex breakup history. Tectonics 26, 1–19. https://doi.org/10.1029/2006TC001970.

Reston, T.J., McDermott, K.G., 2011. Successive detachment faults and mantle unroofing at magma-poor rifted margins. Geology 39, 1071–1074. https://doi.org/10.1130/G32428.1.

Roberts, A.M., Lundin, E.R., Kusznir, N.J., 1997. Subsidence of the Vøring Basin and the influence of the Atlantic continental margin. J. Geol. Soc. London 154, 551–557. https://doi.org/10.1144/gsjgs.154.3.0551.

Stein, R.-S., Barrientos, S.-E., 1985. Planar High-Angle Faulting in the Basin and Range: Geodetic Analysis of the 1983 Borah Peak, Idaho, Earthquake. J. Geophys. Res. 90, 11,355-11,366.

Sutra, E., Manatschal, G., Mohn, G., Unternehr, P., 2013. Quantification and restoration of extensional deformation along the Western Iberia and

Newfoundland rifted margins. Geochemistry, Geophys. Geosystems 14, 2575–2597.

Tugend, J., Manatschal, G., Kusznir, N.J., Masini, E., Mohn, G., Thinon, I., 2014. Formation and deformation of hyperextended rift systems: Insights from rift domain mapping in the Bay of Biscay-Pyrenees. Tectonics 33, 1239–1276.

Tugend, J., Manatschal, G., Kusznir, N.J., Masini, E., 2015. Characterizing and identifying structural domains at rifted continental margins: application to the Bay of Biscay margins and its Western Pyrenean fossil remnants. From Gibson, G.M, Roure, F. & Manatschal, G. (eds). Sedimentary basins and crustal processe. Geol. Soc. London, Spec. Publ. 413. https://doi.org/10.1144/SP413.3.

Vergés, J., Millán, H., Roca, E., Muñoz, J.A., Marzo, M., Cirés, J., Bezemer, T. Den, Zoetemeijer, R., Cloetingh, S., 1995. Eastern Pyrenees and related foreland basins: pre-, syn- and post-collisional crustal-scale cross-sections. Mar. Pet. Geol. 12, 903–915. https://doi.org/10.1016/0264-8172(95)98854.

Vergés, J., García-Senz, J., 2001. Mesozoic evolution and Cainozoic inversion of the Pyrenean rift. Peri-Tethys Mem. 6 Peri-Tethyan Rift. Basins Passiv. Margins 186, 187–212.

Walsh, J., Watterson, J., Yieldingt, G., 1991. The importance of small-scale faulting in regional extension. Nature 351.

Wilson, J., 1966. Did the atlantic close and then reopen?. Nature 211, 286. https://doi.org/10.12789/geocanj.2016.43.109.

APPENDICES

Appendix 1: Gravity anomaly inversion

To understand rifted margins structure is important to know the Moho depth and hence total crustal thickness along the margin. Seismic data is one of the most used datasets when studying rifted margins, however, the Moho is often not imaged and/or ambiguous. To overcome this problem, geophysical techniques have been extensively used.

In this thesis I use a gravity anomaly inversion (Greenhalgh and Kusznir, 2007; Alvey et al., 2008; Chappell and Kusznir, 2008; Roberts et al., 2013; Cowie et al., 2015; Kusznir et al., 2018) to unravel the depth to the Moho (Output 1), crustal thickness (Output 2) and continental crustal thinning (Output 3) along the Iberia and Newfoundland conjugate rifted margins. Input data used for the gravity anomaly inversion are; (i) satellite derived free-air gravity from Sandwell and Smith (2009) (V27.1), (ii) bathymetry/topography data from Smith and Sandwell (1997) (V19.2), (iii) 2D sediment thickness obtained from both the northern (SCREECH1 – ISE01) and the southern (SCREECH2 – TGS/LG12) Iberia and Newfoundland seismic profiles and (iv) age of ocean isochrons are taken from Müller et al., (1997). The gravity anomaly inversion method is carried out using an iterative approach consisting of the following steps (Figure 1):

1) Calculate the mantle residual gravity anomaly (g_{mra})
2) Calculate Moho topography (Δr) using the scheme of Parker (1972)
3) Obtain Moho depth (md) and crustal thickness (ct) → Outputs 1 and 2
4) Obtain gravity lithosphere thinning factor (γ) → Output 3

Step 1: Calculate the mantle residual gravity anomaly (g_{mra})

The mantle residual gravity anomaly (g_{mra}) is given by:

$$g_{mra} = g_{fag} - g_b - g_s - g_t$$

g_{fag} = observed free-air gravity anomaly.

g_b = bathymetry gravity anomaly.

g_s = sediment thickness gravity anomaly can be obtained either from public data or specific seismic lines of an area (the second case gives a more accurate result).

g_t = lithosphere thermal gravity anomaly. This is obtained from thinning factor determined in Stage 4 so the first iteration of the gravity anomaly inversion is run with zero for this parameter.

Step 2: Calculate Moho topography (Δr) using the scheme of Parker (1972)

Moho topography (Δr) is calculated from the g_{mra} using the mathematical scheme of Parker (1972). It is assumed that the signal produced by the mantle residual gravity anomaly is only caused by the variations in the depth to the Moho. Prior to apply the Parker's scheme, the g_{mra} must be filtered to remove the high frequency components within the data. To achieve this, a Butterworth low-pass filter with a cut-off wavelength of 100 km is used (Chappell and Kusznir, 2008). The method of Parker (1972) is carried out in a 3-D spectral domain and applies Smith's theorem (Smith, 1961) to provide a unique solution for the assumptions made. Using a constant crustal density (2850 kg m^{-3}) and knowing the bathymetry, only one solution for the base of the mass can predict the observed gravity anomaly.

Step 3: Obtain Moho depth (md) and crustal thickness (ct) → Outputs 1 and 2

To determine Moho depth (md) from gravity inversion, a reference Moho depth (d_{ref}) is needed and requires calibration against seismic refraction Moho depths (see Cowie et al., 2015 for a detailed discussion). We use a reference Moho depth of 40 km for the Iberia margin (Cowie et al., 2015) while 37.5 km for the Newfoundland margin (Jeanniot et al., 2016). The depth to the Moho (md) and crustal thickness (ct) is obtained as following:

$$md = d_{ref} + \Delta r$$

$$ct = md - b$$

Δr = Moho topography

b = bathymetry

Step 4: Obtain gravity lithosphere thinning factor (γ) → Output 3

Key to the success of the gravity anomaly inversion method is a correction for the lithosphere thermal gravity anomaly (Chappell and Kusznir, 2008) associated with the elevated geotherm resulting from rifting/breakup of the margin. The lithosphere thermal gravity anomaly is obtained from the gravity lithosphere thinning factor (γ).

$$\gamma = 1\text{-}1/\beta$$

β = lithosphere stretching factor (McKenzie, 1978)

For ocean lithosphere γ = 1 while for continental lithosphere the γ is obtained from the stretching lithosphere factor defined by the difference between the initial crustal thickness (ct_{ini}) respect to the present-day crustal thickness (ct_{now}). A key assumption is that lithosphere thinning and crustal thinning are equivalent as depth-uniform stretching and thinning is assumed. During rifting and breakup there can be a significant amount of magmatic addition which would contribute to the total thickness of the crust. A correction for the thickness of volcanic additions resulting from decompression melting is also included:

$$\beta = ct_{ini}/(ct_{now} - ct_{mag})$$

Ct_{ini}= initial crustal thickness

ct_{now} = present-day crustal thickness

ct_{mag} = thickness of volcanic additions from decompression melting

The critical thinning factor at which decompression melting starts is obtained from the decompression melting model predicted by White and McKenzie (1989). In addition, the maximum thickness of volcanic additions when γ = 1 is defined. This corresponds to the thickness of oceanic crust produced.

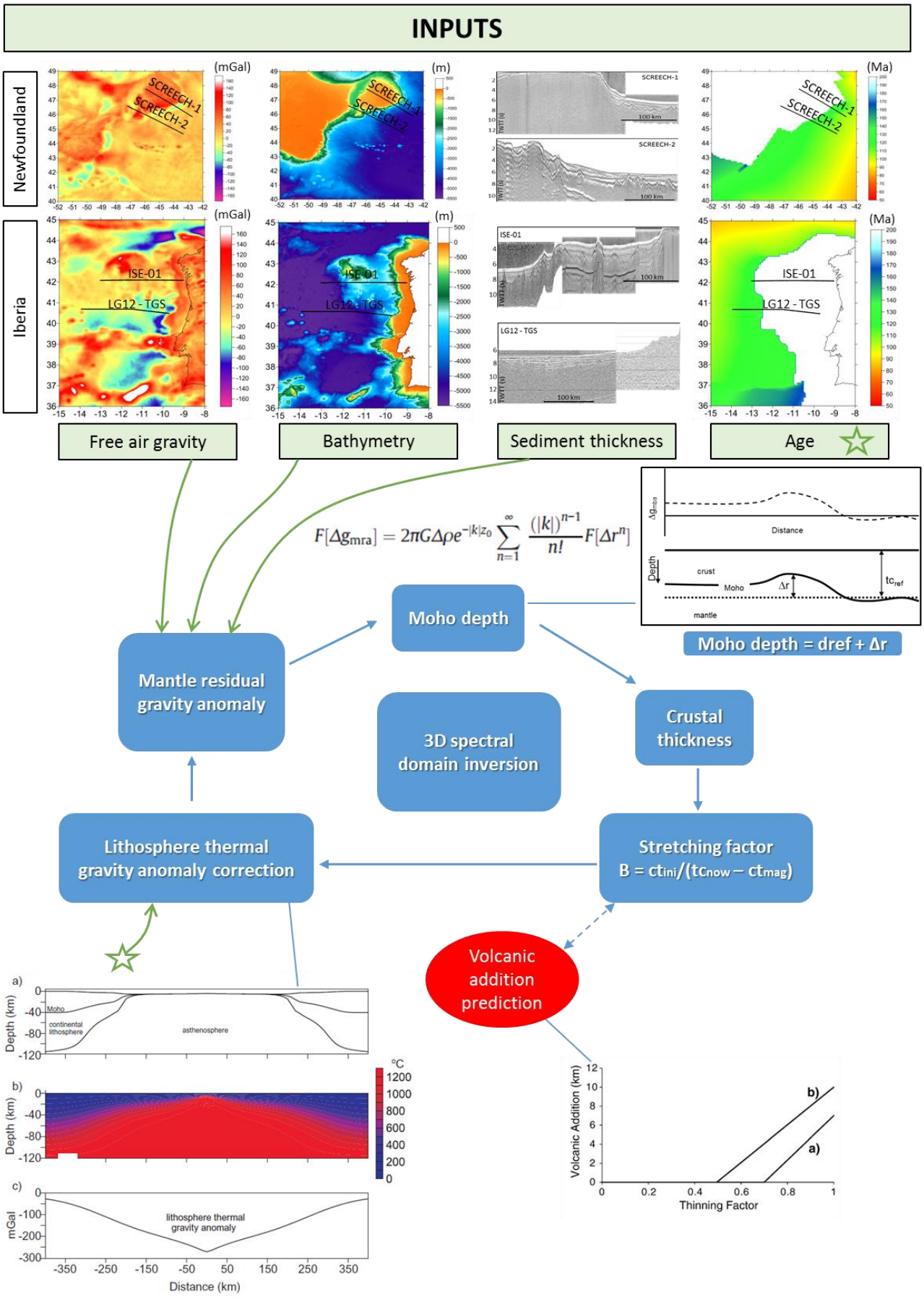

Figure 1: Cartoon showing the iterative approach of the gravity anomaly inversion.

Appendix 2: Subsidence analysis

We use a subsidence analysis technique (Roberts et al., 2013; Cowie et al., 2015) to obtain lithosphere thinning factor which we compare against the crustal thinning factor from gravity anomaly inversion. This technique involves converting water loaded subsidence into lithosphere thinning factor assuming McKenzie (1978). Flexural backstripping and decompaction assuming shaly-sand parameters (Sclater and Christie, 1980) is used to remove sedimentary layers and loading to the top of pre-rift sequence and top of oceanic crust. This gives a sediment-corrected bathymetry which we equate to water-loaded subsidence assuming that top of pre-rift sequence was at sea-level prior rifting. Water loaded subsidence is interpreted as the sum of initial and thermal subsidence in the context of McKenzie (1978). We convert water-loaded subsidence into lithosphere thinning factor including a correction for magmatic addition from decompression melting (White and McKenzie, 1989). Figure 2 summarizes the relationship between water loaded subsidence and lithosphere thinning factor (γ) assuming McKenzie (1978) for three different solutions; magma-poor where no magmatic addition is generated (Figure 2a), normal magmatic generating 7 km of volcanic addition starting at $\gamma = 0.7$ (Figure 2b) and serpentinized mantle starting at $\gamma = 0.7$ (corresponding to approximately 10 km thick crust) and at $\gamma = 1.0$ producing a serpentinized mantle with a mass deficiency with respect to mantle equivalent to a crustal basement 3 km thick (Figure 2c) (see Cowie et al., 2015 for further detail).

A breakup age of 120 Ma, an initial crustal thickness of 37.5 km and a crustal density of 2.85 g cm^{-3} are used for the three magmatic solutions for the Iberia and Newfoundland margins. Note that in the subsidence analysis method, lithosphere thinning and crustal thinning are assumed to be the same (i.e. depth-uniform stretching and thinning is assumed). Further detail of the subsidence analysis technique is given by Roberts et al., (2013) and Cowie et al., (2015).

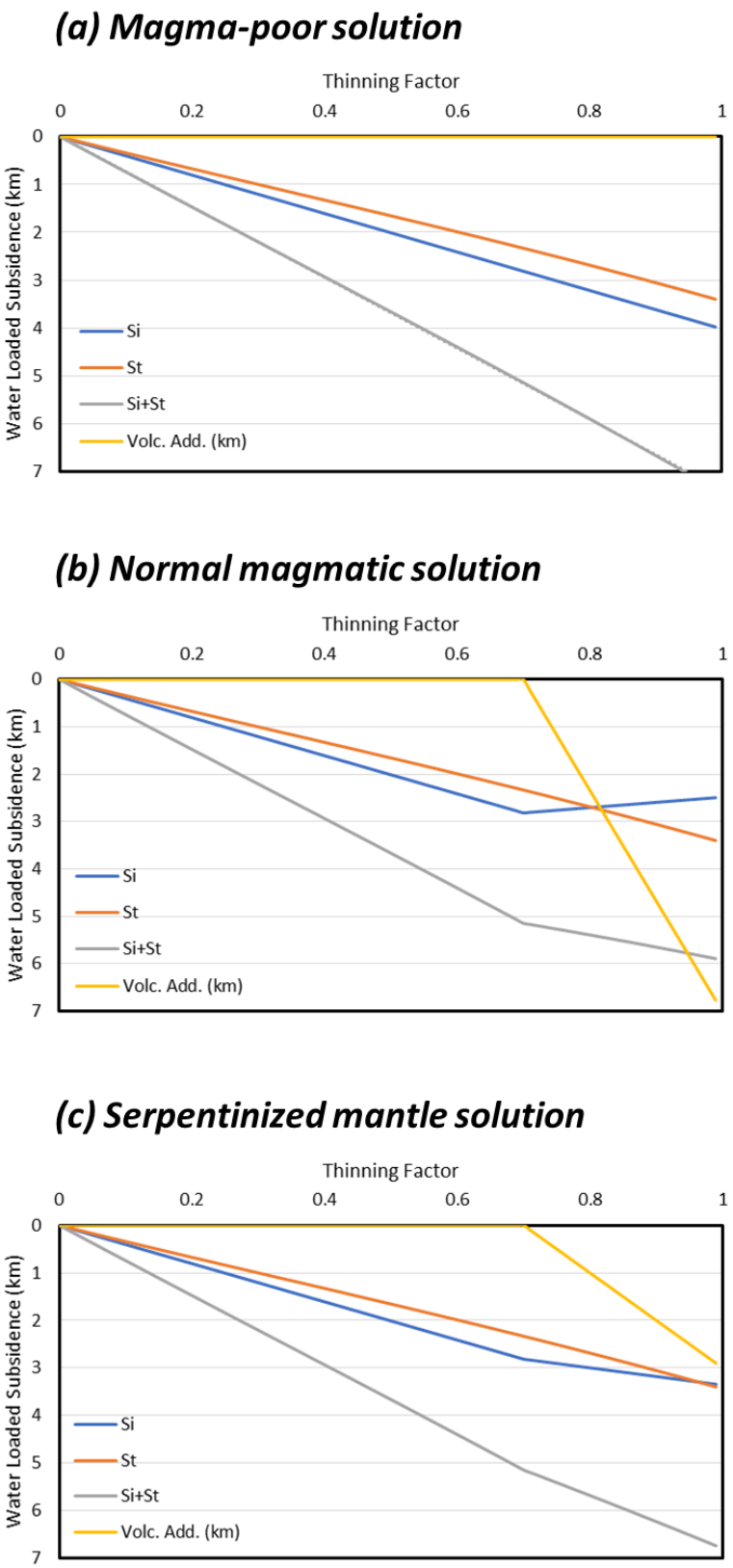

Figure 2: Water loaded subsidence as a function of lithosphere thinning factor (γ). Initial subsidence (Si) is shown in blue, the thermal subsidence (St) is shown in orange, the combined total subsidence (Si+St) is shown in grey and the sensitivity to magmatic addition (magma-poor, normal and serpentinized mantle) is shown in yellow.

Appendix 3: Numerical kinematic model (RIFTER)

A summary of the model formulation of RIFTER (originally called OROGENY) developed by Nick Kusznir is shown below. Further mathematical detail is given by Toth et al., (1996), Ford et al., (1999) and Jácome et al., (2003). These studies show the model formulation applied to compressional tectonics (same as shown below) however similar physical principles apply for an extensional tectonics scenario.

Structural response

Lithosphere shortening is assumed to occur by thrusting in the upper crust and by distributed pure-shear deformation in the lower crust and lithospheric mantle. These two deformation types (i.e. faulting and pure-shear) are kinematically defined but their consequences are dynamically calculated.

The geometry of the thrust fault is defined by its surface position and dip angle as well as its detachment depth. The fault geometry used is that of a listric fault (i.e. the vertical-shear construction) soling into a horizontal detachment for simplicity purposes. Toth et al., (1996) described a mathematical equation that simulates the shape of the thrust given by:

$$D(x) = Z_d\,(1 - \exp\,(-x \tan\theta / Z_d)$$

where D(x) is the fault depth, Z_d is the horizontal fault detachment depth, x is the horizontal distance from fault cutoff and θ is the surface dip of the fault.

Once the geometry of the fault has been defined, the amount of upper crustal thickening (T_{uc}) due to thrust faulting is given by:

$$T_{uc}\,(x) = D\,(x + S) - D(x)$$

where S is the amount of shortening and $D(x) = 0$ for $x < 0$. This is the mathematical description of a simple geometric construction in which the hangingwall block is picked up, moved horizontally and collapsed by vertical shear onto the footwall.

The corresponding load produced by the thrust (l_{uc}) is given by:

$$l_{uc}\,(x) = T_{uc}\,(x)\,\rho_c\,g$$

where ρ_c is the crustal density (2800 kg m^{-3}) and g is the gravitational acceleration.

The distributed pure-shear deformation beneath the detachment depth (Z_d) is localised and can be represented at any point by a compressional shortening factor β (McKenzie, 1978) described by:

$$\beta = sl_{fin}/sl_{ori}$$

where sl_{fin} is the final section length while the sl_{ori} is the original section length. The β shortening factor is represented by a sinusoidal envelope such that:

$$\beta(x) = 1 + C \sin\left(\frac{\pi x}{W}\right)$$

where β = 1 represents no shortening and c is negative. The distance from the boundary of the upper pure-shear region is defined by x and w represents the precompressional width of the pure-shear region. Upper crustal shortening (S) by faulting is balanced at depth by distributed deformation (β). Hence, the following assumption is made:

$$S = -\int_0^W (\beta(x)-1)\,dx = -\int_0^W C \sin\left(\frac{\pi x}{W}\right) dx$$

The corresponding load produced by the thickening of the lower crust (l_{lc}) is given by:

$$l_{lc}(x) = -T_{lc}(x)(\rho_m - \rho_c)\,g$$

where T_{lc} is the amount of lower crustal thickening, ρ_m is the mantle density (3300 kg m^{-3}), ρ_c is the crustal density (2800 kg m^{-3}) and g is the gravitational acceleration.

Sedimentation and erosion

Loading due to sedimentation is included in the model by iteratively filling any available accommodation space below a specified depositional base level. Erosion is also included by removing a percentage of topography above a specified erosional base level (Toth et al., 1996). Both sedimentation and erosion produce an isostatic response characterized by loading and unloading respectively.

REFERENCES

Alvey, A., Gaina, C., Kusznir, N.J., Torsvik, T.H., 2008. Integrated crustal thickness mapping and plate reconstructions for the high Arctic. Earth Planet. Sci. Lett. 274, 310–321. https://doi.org/10.1016/j.epsl.2008.07.036.

Chappell, A.R., Kusznir, N.J., 2008. Three-dimensional gravity inversion for Moho depth at rifted continental margins incorporating a lithosphere thermal gravity anomaly correction. Geophys. J. Int. 174, 1–13. https://doi.org/10.1111/j.1365-246X.2008.03803.

Cowie, L., Kusznir, N., Manatschal, G., 2015. Determining the COB location along the Iberian margin and Galicia Bank from gravity anomaly inversion, residual depth anomaly and subsidence analysis. Geophys. J. Int. 203, 1355–1372. https://doi.org/10.1093/gji/ggv367.

Ford, M., Lickorish, W.H., Kusznir, N.J., 1999. Tertiary foreland sedimentation in the Southern Subalpine Chains, SE France: A geodynamic appraisal. Basin Res. 11, 315–336. https://doi.org/10.1046/j.1365-2117.1999.00103.

Greenhalgh, E.E., Kusznir, N.J., 2007. Evidence for thin oceanic crust on the extinct Aegir Ridge, Norwegian Basin, NE atlantic derived from satellite gravity inversion. Geophys. Res. Lett. 34, 1–5. https://doi.org/10.1029/2007GL029440.

Jácome, M.I., Kusznir, N., Audemard, F., Flint, S., 2003. Formation of the Maturín Foreland Basin, eastern Venezuela: Thrust sheet loading or subduction dynamic topography. Tectonics 22, n/a-n/a. https://doi.org/10.1029/2002tc001381.

Jeanniot, L., Kusznir, N., Mohn, G., Manatschal, G., Cowie, L., 2016. Constraining lithosphere deformation modes during continental breakup for the Iberia-Newfoundland conjugate rifted margins. Tectonophysics 680, 28–49. https://doi.org/10.1016/j.tecto.2016.05.006.

Kusznir, N.J., Roberts, A.M., Alvey, A.D., 2018. Crustal structure of the conjugate Equatorial Atlantic Margins, derived by gravity anomaly inversion. Geol. Soc. London, Spec. Publ. SP476.5. https://doi.org/10.1144/sp476.5.

Mckenzie, D., 1978. Some Remarks on Development of Sedimentary Basins. Earth Planet. Sci. Lett. 40, 25–32.

Müller, R.D., Roest, W.R., Royer, J.-Y., Gahagan, L.M., Sclater, J.G., 1997. Digital isochrons of the world's ocean floor. J. Geophys. Res. 52, 3211–3214.

Parker, R.L., 1972. The rapid calculation of potential anomalies. Geophys. J. R. Astron. Soc. 31, 447–455.

Roberts, A.M., Kusznir, N.J., Corfield, R.I., Thompson, M., Woodfine, R., 2013. Integrated tectonic basin modelling as an aid to understanding deep-water rifted continental margin structure and location. Pet. Geosci. 19. https://doi.org/10.1144/petgeo2011-046.

Sandwell, D.T., Smith, W.H.F., 2009. Global marine gravity from retracked Geosat and ERS-1 altimetry: Ridge segmentation versus spreading rate. J. Geophys. Res. Solid Earth 114, 1–18. https://doi.org/10.1029/2008JB006008.

Sclater, J.G., Christie, P.A.F., 1980. Continental stretching: an explanation of the post-mid-Cretaceous subsidence of the central North Sea Basin. J. Geophys. Res. 85, 3711–3739.

Smith, R.A., 1961. A uniqueness theorem concerning gravity fields. Math. Proc. Cambridge Philos. Soc. 57, 865–870. https://doi.org/10.1017/S030500410003601.

Smith, W.H., Sandwell, D., 1997. Global sea floor topography from satellite altimetry and ship depth soundings. Science (80). 277, 1956–1962.

Toth, J., Kusznir, N.J., Flint, S.S., 1996. A flexural isostatic model of lithosphere shortening and foreland basin formation: Application to the Eastern Cordillera and Subandean belt of NW Argentina. Tectonics 15, 2–3.

White, R., McKenzie, D., 1989. Magmatism at Rift Zones - the Generation of Volcanic Continental Margins and Flood Basalts. J. Geophys. Res. Earth Planets 94, 7685–7729.